Crystallisation Behaviour of Buffalo Milk Fat

Yoga Pratama

Submitted in accordance with the requirements for the degree of

Doctor of Philosophy

The University of Leeds

School of Food Science and Nutrition

May, 2023

The candidate confirms that the work submitted is his own, except where work has formed part of jointly-authored publications. The candidate confirms that appropriate credit has been given within the thesis where reference has been made to the work of others. Details of the jointly-authored publications and the contributions of each author are outlined on the pages ii and iii.

Details of jointly-authored publications and corresponding thesis chapter

Chapter 3

Pratama, Y., Simone, E. and Rappolt, M. 2021. The unique crystallisation behaviour of buffalo milk fat. Crystal Growth and Design. 21(4), pp.2113-2127.

Chapter 4

Pratama, Y., Burholt, S., Baker, D.L., Sadeghpour, A., Simone, E. and Rappolt, M. 2022. Polymorphism of a highly asymmetrical triacylglycerol in milk fat: 1-butyryl 2-stearoyl 3-palmitoyl-glycerol. Crystal Growth and Design. 22(10), pp.6120-6130.

Chapter 5

Pratama, Y., Seilert, J., Sadeghpour, A., Simone, E. and Rappolt, M. 2023. Decoding the role of triacylglycerol composition in the milk fat crystallisation behaviour: a study using buffalo milk fat fractions. LWT - Food Science and Technology. 186, 115274.

Details of authorship contributions

The Unique Crystallisation Behaviour of Buffalo Milk Fat.

Yoga Pratama designed and conducted the experimental work. Whereas the data analyses were mainly executed by Yoga, Michael Rappolt contributed on the peak fitting and electron density calculations. The manuscript was prepared by Yoga Pratama and commented/revised by all co-authors.

Polymorphism of a Highly Asymmetrical Triacylglycerol in Milk Fat: 1-Butyryl 2-Stearoyl 3-Palmitoyl-Glycerol.

Yoga Pratama designed the experiment and analysed the data. The synchrotron beamtime was carried out by Yoga Pratama and Michael Rappolt. Sam Burholt is acknowledged for his help during the offline synchrotron beamtime and its data processing. Dan Baker helped during the DSC data collection. Amin Sadeghpour contributed on the analysis of pre-crystallisation structure of the triacylglycerol molten phase. The manuscript was prepared by Yoga Pratama and commented/revised by all co-authors.

Decoding the Role of Triacylglycerol Composition in the Milk Fat Crystallisation Behaviour: a Study Using Buffalo Milk Fat Fractions.

Yoga Pratama designed, carried out the experimental work and analysed the data. The manuscript was prepared by Yoga Pratama whereas other co-authors provided important insights during the data analysis and interpretation. The manuscript has been commented and revised by all authors.

List of accepted conference abstracts and awards

Poster presentations

Pratama, Y., Simone, E. and Rappolt, M. 2019. Comparative analysis of buffalo and cow milk fat crystallisation behaviour. 6th Food Science and Nutrition PhD conference - Leeds, UK (poster)

Pratama, Y., Simone, E. and Rappolt, M. 2021. Highlighting differences in buffalo and cow milk fat crystallisation behaviour for optimal design of dairy food products. 35th The European Federation of Food Science and Technology (EFFoST) International Conference - Lausanne, Switzerland (poster).

Pratama, Y., Simone, E. and Rappolt, M. 2022. Towards more diverse dairy products: highlighting differences in buffalo and cow milk fat crystallisation behaviour. 7th European Crystallisation School - Lisbon, Portugal (poster).

Oral presentations

Pratama, Y., Simone, E. and Rappolt, M. 2020. Understanding the role of triacylglycerols in complex fat crystallisation behaviour. 7th Food Science and Nutrition PhD conference - online

Pratama, Y., Simone, E. and Rappolt, M. 2021. Towards tailored crystallisation of buffalo milk fat. 2021. 18th Euro Fed Lipid Congress and Expo - online

Pratama, Y., Simone, E. and Rappolt, M. 2022. Towards more diverse dairy products: highlighting differences in buffalo and cow milk fat crystallisation behaviour. 21st The International Union of Food Science and Technology World Congress - Singapore

Pratama, Y., Sadeghpour, A, Simone, E. and Rappolt, M. 2023. Understanding and tailoring milk fat crystallisation. 9th Food Science and Nutrition PhD conference - Leeds, UK

Awards

Beamtime grant for experiments at the Diamond Leeds SAXS Facility: Proposal number SM29590 - Crystallisation behaviour of milk fat unsymmetrical triacylglycerol (2021).

Beamtime and travel grant for experiments at the Diamond Leeds SAXS Facility: Proposal number SM31079 - The kinetics of β-polymorph formation in milk fat as affected by triacylglycerol composition and crystallisation temperatures (2022).

Shortlisted for Outstanding Student Award, Faculty Partnership Awards 2022, given by The Faculty of Environment and Leeds University Union.

Acknowledgements

I could not have undertaken this journey without my supervisors, Prof. Michael Rappolt and Dr Elena Simone who have guided me from the day 1, giving me moral support, encouragement and also constructive challenges. Deciding to take my PhD in Leeds and having them as my mentors is the best decision I took in my PhD life. I am able to say that my PhD journey was dominated by excitement and joy, with very infrequent pressure and stress, all because of them, whom I am most indebted to.

I am also highly thankful to Dr. Amin Sadeghpour, who joined my supervisory team in my 3rd year. His insightful comments, and advice have helped me tremendously in my research and the writing of my paper and this thesis.

My heartfelt gratitude goes to Dr Arwen Tyler and Dr Elke Scholten (Wageningen University and Research, Netherlands) who have provided constructive feedbacks during and after thesis examination. These have further improved my thesis.

I would like to express my deepest gratitude to the “The Indonesia Endowment Funds for Education (LPDP)” for granting me the PhD scholarship and financial support for me and my family during my study in the UK. Their support has made my dream, to pursue a PhD degree in a reputable university, comes true.

I would like to extend my sincere thanks to all technical staffs in the School of Food Science and Nutrition who helped me directly or indirectly throughout my research: Sara Viney, Ian Hardy, Miles Ratcliffe, Neil Rigby, Joanna Sier, Natalie for their invaluable technical support during my PhD.

I had the pleasure of working with other PhD students, my colleagues: Lorenzo, Liam, Panayiotis, Bradley, Gerome, Elisabeth, Janine, Aygul, Jessica, Dorothy, Lujin, Kristina who made my PhD journey a wonderful and enjoyable. I wish you guys have successful career ahead.

I would be remiss in not mentioning my Indonesian community who colour my days in Leeds. My gratitude goes to the Indonesian PhD group for their valuable supports and sharing that have helped me tremendously, especially during my first year PhD. I am also grateful to my riding buddies, Goweser in Leeds, whom I share many wonderful adventures, pain, sweat and laughter with. I wish I can etch those beautiful moments eternally in my memory. I am sorry to not mention your names one by one, but you know who you are. My

thanks also go to Kibar and PPI Greater Leeds for their endeavours to make Indonesian community flourish in Leeds.

I dedicate this work to my parents, Yuli Wintarno and Supanti, whom I know always mention my name in every prayer. They are my source of motivation to pursue a higher education. I sincerely wish that this work will make them proud. This is also for you, my love, my partner in crime, Gading Inayah Avianisa, who always be by my side in this roller coaster of life. I hope my achievement could also inspire my three sons, Hafizh, Khaleef and Zayn. I am so blessed to spend this chapter of life together with my family. I also extend my gratitude to my other family members, brother, sister, especially my in law Bunda, for their continuous supports during my study.

Finally, all praises and gratitudes belong to Allah, the most merciful. I humbly pray that this work will bring benefits to humankind.

Abstract

Milk fat is one of the key natural fats. It is used widely in the food industry such as in butter, cheese, ice cream, whipped cream and confectionary products. The quality attributes of those products are greatly influenced by the crystallisation behaviour of milk fat.

Buffalo milk has gained increasing popularity for the last few decades and has become the second most consumed milk globally. Its high fat content (6-15%) is particularly suitable for fat-based food products with buffalo mozzarella being the most popular one. However, the crystallisation behaviour of buffalo milk fat, which may explain the unique characteristics of buffalo milk-based products, is poorly understood. Therefore, this thesis aims to evaluate the key compositional differences of buffalo milk fat, as compared to the globally leading cow milk fat, and examines the compositional effects on the crystallisation behaviour. Further, the role of different triacylglycerols (TAGs) in milk fat crystallisation is analysed in great detail using a new proposed method using a chemical grouping approach.

The TAGs composition of cow and buffalo milk fat was measured using liquid chromatography and mass spectrophotometry. Whereas, the crystallisation behaviour of milk fat was investigated using small and wide-angle X-ray scattering, differential scanning calorimetry and polarised light microscopy techniques.

The results show that buffalo milk fat has similar TAGs species, but in significantly different proportions as compared to cow milk fat. This leads to a different crystallisation behaviour, where buffalo milk fat showed a higher melting point, but with slower α → β' polymorphic transformation kinetics. In-depth analysis of the crystallisation of pure asymmetrical TAGs, which are abundantly present in milk fat, revealed a possible crystallisation inhibiting mechanism, which slows the polymorphic transformation and most-likely is also responsible for the dominant β'-polymorph appearance in milk fat crystals.

A new approach in the analysis of the TAG's role in milk fat classified the complex milk fat TAGs into four different groups based on their chemical properties. This way, a direct association of two main crystal structures in milk fat - the high melting double-layered and the low melting triple-layered crystals - with fully saturated TAGs and TAGs containing unsaturated fatty acid(s), respectively, was demonstrated. This approach can be universally applied to other complex mixture of TAGs, and will be useful for future crystallisation studies involving modified TAGs compositions.

Table of Contents

List of Tables

List of Figures

List of Abbreviations

BM	Buffalo milk
BMF	Buffalo milk fat
BuSP	1-butyryl-2-stearoyl-3-palmitoyl-glycerol
CB	Cocoa butter
CM	Cow milk
CMF	Cow milk fat
CNT	Classical nucleation theory
CVD	Cardiovascular disease
DAG	Diacylglycerol
DCL	Double chain length
DSC	Differential scanning calorimetry
DPPE	1,2- dipalmitoyl-sn-glycero-3-phosphoethanolamine
EDP	Electron density profile
ESI	Electrospray ionisation
FA	Fatty acid
HCL	Hexa chain length
HMF	High melting fraction
LCMS	Liquid chromatography and mass spectrophotometry
LMF	Low melting fraction
MMF	Medium melting fraction
PLM	Polarised light microscopy
POP	1,3-dipalmitoyl-2-oleoyl-*sn*-glycerol
POPE	1-palmitoyl-2-oleoyl-sn-glycero-3-phosphoethanolamine
QCL	Quatro chain length
SAXS	Small-angle X-ray scattering
SDD	Sample to detector distance
SFA	Saturated fatty acid

SFC	Solid fat content
SOS	1,3-distearoyl-2-oleoyl-*sn*-glycerol
SR-XRD	Synchrotron radiation X-ray diffraction
TAG	Triacylglycerol
TCL	Triple chain length
UFA	Unsaturated fatty acid
WAXS	Wide-angle X-ray scattering
XRD	X-ray diffraction

Chapter 1 Introduction

Milk is a biological liquid secreted from the mammary glands of female mammals. It is highly nutritious and provides energy that is necessary for the growth of newborns or young mammals. In the food industry, milk is an economically important commodity. It is consumed not only in fresh/liquid form but also in many other dairy products such as cream, butter, cheese, and ice cream. In 2022, the milk production is forecast at around 930 million tonnes globally (FAO, 2022a). Main mammal species whose milk is utilised commercially include cow, buffalo, goat, sheep, and camel.

Milk consumption in developed countries has been decreasing over the last few decades. One of the reasons is the presence of a high content of saturated fatty acids (SFAs) in milk fat, which has been linked to cardiovascular diseases (CVDs). This view has been prominent from the ‘80s to around 2000 (Mohan et al., 2021). On the contrary, new evidence suggests that there is no direct association between SFA intake and the incidence of CVDs (Mente et al., 2009; Micha and Mozaffarian, 2010). Furthermore, these studies argued that a reduction in the consumption of SFA-containing foods, such as milk, without proper nutrient replacement would cause missing the essential health benefits related with dairy food sources.

Another important reason for the decline in milk consumption is the rising concern about livestock contribution to global warming and climate change. Livestock production has been estimated to generate 14.5% of the total greenhouse gas emissions (Cheng et al., 2022). Although, this is not true for African or developing countries. The role of livestock in these areas’ agriculture is critical, as it not only produces meat and/or milk but is also important in other aspects of farming, such as ploughing land, production of manure, and the disposal of agricultural leftover as feed (Nouala, 2022). Taking these into account, assessing the impact of livestock on climate change in poor regions may not be as straightforward as in the area where livestock is produced intensively. Despite the decline in consumption in the developed regions, the global milk production actually increased by 27% from 2010 to 2020. The main growth is observed in Asian countries such as India and Pakistan (FAO, 2022b).

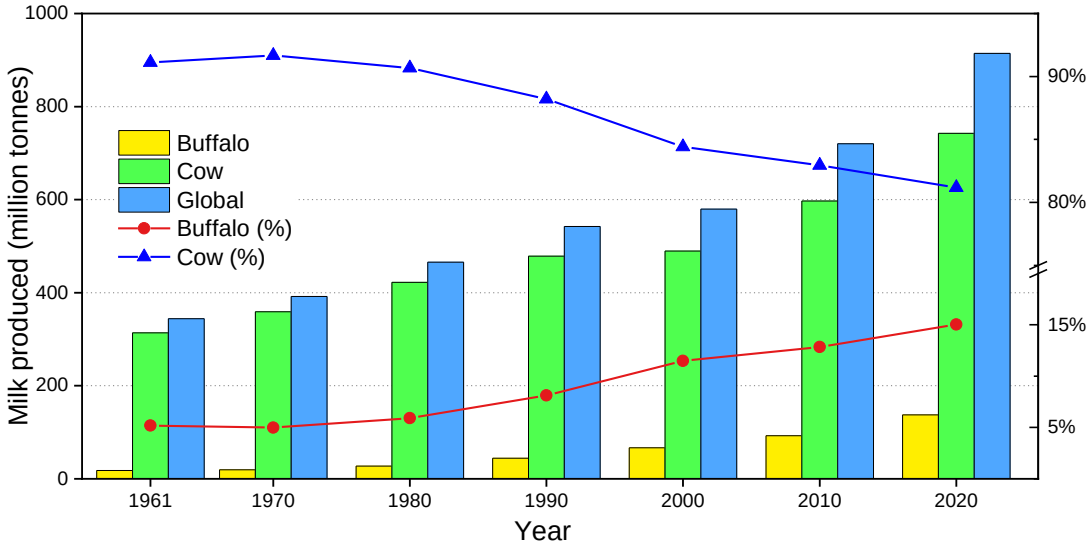

Figure 1.1 Trend of buffalo milk production and its global contribution (FAO, 2022b).

As it can be seen in **Figure 1.1**, buffalo milk (BM) contributed to about 15 % of the total global milk production in 2020, placing it as the second most produced milk after cow milk (CM). The BM production volume has increased significantly in the last few decades, starting from 17.8 million tonnes in 1961 to 137.4 in 2020, indicating the rise of its popularity.

BM is characterised by higher level of milk solids than CM (5.3-15% compared to 3.3-6.4%) (Gantner et al., 2015). Therefore, it can produce more cream and thus has high potential to be processed for milk fat-based products (i.e., butter and ice cream), and in other milk solid-based products such as cheese. In particular, the Italian buffalo mozzarella cheese (*mozzarella di bufala campana*) has been a sought-after dairy product due to its wide use as pizza topping, and its meltability properties (Angelis and Gobbetti, 2011). The BM is also considered to have better quality than CM in terms of its superior whitening effect in coffee and tea (Murtaza et al., 2017b).

As an important edible fat source, milk fat is highly regarded for its unique flavour profiles (Mohan et al., 2021). It is not only utilised in dairy based products, but also in processed food such as confectionery and bakery. More importantly, milk fat has an important role in the texture and structural development of ice cream, cheese, whipped cream and especially butter. Upon cooling from the melt, milk fat crystallizes and forms a crystal network. The crystallisation profile defines the crystal size and also the crystal network, which subsequently influences the physical properties of the final product such

as melting point, spreadability, texture, rheological properties, and overall stability (Martini and Marangoni, 2007; Wright et al., 2011).

1.1 Rationale and Overall Research Aims

Over the years, there are numerous studies on the crystallisation behaviour and the polymorphism of milk fat (Grotenhuis et al., 1999; Campos et al., 2002; Lopez, 2018). However, the majority of these employed CM fat or unspecified anhydrous milk fat (which most likely is CM). Only very limited studies specifically focused on BM fat (Patel and Frede., 1991). It has been suggested that BM fat contains higher saturated fatty acids and lower mono-unsaturated fatty acids than CM (Ménard et al., 2010; Abd El-Salam and El-Shibiny, 2011). These differences in the fatty acid composition likely lead to different crystallisation behaviour as compared to that of CM, which ultimately affects product quality attributes. Therefore, based on BM's potential for fat processing (high yield - superior quality) but limited available knowledge thereabout, the current study aims to evaluate more closely the BM fat characteristics, such as its triacylglycerol (TAG) composition, crystallisation behaviour and its polymorphism.

In addition to specific BM-oriented objectives, the current doctoral project also aims to elucidate further the effects of different TAGs composition on fat crystallisation. The variation in milk fat composition is related not only to the different milking species such as buffalo and cow, but it is also the result of different feeds, lactation period, seasons and geographical areas (Grummer, 1991; Palmquist et al., 1993; Soyeurt et al., 2006; Stoop et al., 2009; Huppertz et al., 2009; Maurice-Van Eijndhoven et al., 2011; Tzompa-Sosa et al., 2018). Particular interest is given to asymmetric TAGs in milk fat, specifically those containing the short chained butyric acid. It is worth mentioning that TAGs are considered to be asymmetrical when the difference among fatty acids chain length is more than two carbon atoms (Sato, 2001). The asymmetrical TAGs are present in high quantity in milk fat (Gresti et al., 1993) and their specific role in the crystallisation has not been elucidated yet. The existing view suggests that high concentration of asymmetrical TAGs may influence the crystallisation behaviour of the abundant β'-polymorph in milk fat (Grotenhuis et al., 1999). Importantly, BM has higher butyric acid content than CM (Ménard et al., 2010; Abd El-Salam and El-Shibiny, 2011), thus the effects of asymmetrical TAGs should be more clearly observable in this material.

1.2 Research Questions

This thesis focuses on the following research questions:

1. What is the difference between CM and BM fat in terms of TAGs composition, crystallisation behaviour, polymorphic landscape and melting range?
2. What is the role of different types of TAGs in the crystallisation behaviour of milk fat? Specifically, how do asymmetrical TAGs behave?
3. How do the differences in TAGs composition and processing condition affect the kinetics of milk fat crystallisation?

1.3 Thesis Outline

The current thesis consists of six chapters and three appendices. In **Chapter 1** “Introduction”, the background of the doctoral project, the key research questions and aims are put forward. Whereas in **Chapter 2** “Literature Review” the existing knowledge on milk fat and its crystallisation is elaborated. This includes, but is not limited to, the differences in milk fat composition from various milking species, the basic concepts of fat crystallisation, any recent advance on the theory and application of milk fat crystallisation and some of the common characterisation techniques used in the study of fat crystallisation.

Chapter 3, 4 and 5 are result chapters. As this thesis is presented as a “thesis by publication”, each of these chapters have their own introduction with a brief literature review, materials and methods, discussion and conclusion. **Chapter 3** “The unique crystallisation behaviour of buffalo milk fat” highlights the key compositional differences between buffalo and cow milk fat and discusses how these affect the crystallisation behaviour of both milk fats.

Chapter 4 “Polymorphism of a highly asymmetrical triacylglycerol in milk fat: 1-butyryl 2-stearoyl 3-palmitoyl-glycerol” examines closely the crystallisation behaviour of asymmetrical TAGs, which are present in milk fat in substantial quantity, by using a pure TAG compound. This evaluation shed light onto the role of the asymmetrical TAGs group, which is important in the milk fat polymorphism transition kinetics. Finally, **Chapter 5** “Decoding the role of triacylglycerol composition in the milk fat crystallisation behaviour: a study using buffalo milk fat fractions” builds on the results obtained from the previous chapters; this section discusses the overall role of TAGs in the crystallisation

of milk fat. Here, the effects of varying TAGs composition are evaluated using milk fat fractions obtained from a two-step dry fractionation of BM fat.

The final **Chapter 6** “General Discussion” presents an extensive critical discussion and general conclusions. This last chapter also outlines the direction of future works, which would build on the presented results. Lastly, **Appendices A, B and C** provide the supplementary information for Chapter 3, 4, and 5, respectively.

1.4 References

Abd El-Salam, M.H. and El-Shibiny, S. 2011. A comprehensive review on the composition and properties of buffalo milk. *Dairy Science & Technology*. **91**(6), pp.663-699.

Angelis, M. De and Gobbetti, M. 2011. Pasta-Filata Cheeses: Traditional Pasta-Filata Cheese *In*: J. W. Fuquay, P. F. Fox and P. L. H. McSweeney, eds. *Encyclopedia of Dairy Sciences: Second Edition*. Oxford: Academic Press, 1:745-752.

Campos, R., Narine, S.S. and Marangoni, A.G. 2002. Effect of cooling rate on the structure and mechanical properties of milk fat and lard. *Food Research International*. **35**(10), pp.971-981.

Cheng, M., McCarl, B. and Fei, C. 2022. Climate Change and Livestock Production: A Literature Review. *Atmosphere*. **13**(1), p.140.

FAO 2022a. *Dairy Market Review: Emerging trends and outlook 2022* [Online]. Rome. Available from: https://www.fao.org/3/cc3418en/cc3418en.pdf.

FAO 2022b. FAOSTAT Statistical Database. [Accessed 27 January 2023]. Available from: https://www.fao.org/faostat/en/#data/QCL.

Gantner, V., Mijić, P., Baban, M., Škrtić, Z. and Turalija, A. 2015. The overall and fat composition of milk of various species. *Mljekarstvo*. **65**(4), pp.223-231.

Gresti, J., Bugaut, M., Maniongui, C. and Bezard, J. 1993. Composition of Molecular Species of Triacylglycerols in Bovine Milk Fat. *Journal of Dairy Science*. **76**(7), pp.1850-1869.

Grotenhuis, E. Ten, Van Aken, G.A., Van Malssen, K.F. and Schenk, H. 1999. Polymorphism of milk fat studied by differential scanning calorimetry and

real-time X-ray powder diffraction. *JAOCS, Journal of the American Oil Chemists' Society*. **76**(9), pp.1031-1039.

Grummer, R.R. 1991. Effect of Feed on the Composition of Milk Fat. *Journal of Dairy Science*. **74**(9), pp.3244-3257.

Huppertz, T., Kelly, A.L. and Fox, P.F. 2009. Milk Lipids - Composition, Origin and Properties *In*: A. Y. Tamime, ed. *Dairy Fats and Related Products*. Chichester, UK: Blackwell Publishing Ltd, pp.1-27.

Lopez, C. 2018. Crystallization Properties of Milk Fats *In*: *Crystallization of Lipids: Fundamentals and Applications in Food, Cosmetics and Pharmaceuticals*. Chichester, UK: John Wiley & Sons, Ltd, pp.283-321.

Martini, S. and Marangoni, A.G. 2007. Microstructure of Dairy Fat Products *In*: A. Tamime, ed. *Structure of Dairy Products*. Oxford: Blackwell Publishing Ltd, pp.72-103.

Maurice-Van Eijndhoven, M.H.T., Hiemstra, S.J. and Calus, M.P.L. 2011. Short communication: Milk fat composition of 4 cattle breeds in the Netherlands. *Journal of Dairy Science*. **94**(2), pp.1021-1025.

Ménard, O., Ahmad, S., Rousseau, F., Briard-Bion, V., Gaucheron, F. and Lopez, C. 2010. Buffalo vs. cow milk fat globules: Size distribution, zeta-potential, compositions in total fatty acids and in polar lipids from the milk fat globule membrane. *Food Chemistry*. **120**(2), pp.544-551.

Mente, A., De Koning, L., Shannon, H.S. and Anand, S.S. 2009. A systematic review of the evidence supporting a causal link between dietary factors and coronary heart disease. *Archives of Internal Medicine*. **169**(7), pp.659-669.

Micha, R. and Mozaffarian, D. 2010. Saturated fat and cardiometabolic risk factors, coronary heart disease, stroke, and diabetes: A fresh look at the evidence. *Lipids*. **45**(10), pp.893-905.

Mohan, M.S., O'Callaghan, T.F., Kelly, P. and Hogan, S.A. 2021. Milk fat: opportunities, challenges and innovation. *Critical Reviews in Food Science and Nutrition*. **61**(14), pp.2411-2433.

Murtaza, M.A., Pandya, A.J. and Khan, M.H.M. 2017. Buffalo milk: Buffalo milk utilization for dairy products *In*: Y. W. Park, G. F. W. Haenlein and W. L. Wendorff, eds. *Handbook of Milk of Non-Bovine Mammals: Second Edition*. Oxford, UK: Wiley Blackwell, pp.284-342.

Nouala, S. 2022. Livestock is a form of climate justice in the Global South. *AlJazeera*. [Online]. [Accessed 6 February 2023]. Available from: https://www.aljazeera.com/opinions/2022/11/10/livestock-is-a-form-of-climate-justice-in-the-global-south.

Palmquist, D.L., Denise Beaulieu, A. and Barbano, D.M. 1993. Feed and Animal Factors Influencing Milk Fat Composition. *Journal of Dairy Science*. **76**(6), pp.1753-1771.

Patel, A.A. and Frede., E. 1991. Studies on thermal properties of cow and buffalo milk fats. *Lebensmittel-Wissenschaft & Technologie*. **24**(4), pp.323-327.

Sato, K. 2001. Molecular Aspects in Fat Polymorphism *In*: N. Widlak, R. Hartel and S. Narine, eds. *Crystallization and Solidification Properties of Lipids*. Champaign, Illinois, Illinois: AOCS Press, pp.1-17.

Soyeurt, H., Dardenne, P., Gillon, A., Croquet, C., Vanderick, S., Mayeres, P., Bertozzi, C. and Gengler, N. 2006. Variation in Fatty Acid Contents of Milk and Milk Fat Within and Across Breeds. *Journal of Dairy Science*. **89**(12), pp.4858-4865.

Stoop, W.M., Bovenhuis, H., Heck, J.M.L. and van Arendonk, J.A.M. 2009. Effect of lactation stage and energy status on milk fat composition of Holstein-Friesian cows. *Journal of Dairy Science*. **92**(4), pp.1469-1478.

Tzompa-Sosa, D.A., Meurs, P.P. and van Valenberg, H.J.F. 2018. Triacylglycerol Profile of Summer and Winter Bovine Milk Fat and the Feasibility of Triacylglycerol Fragmentation. *European Journal of Lipid Science and Technology*. **120**(3), p.1700291.

Wright, A.J., Marangoni, A.G. and Harte, R.W. 2011. Milk Lipids - Rheological Properties and Their Modification *In*: J. W. Fuquay, P. F. Fox and P. L. H. McSweeney, eds. *Encyclopedia of Dairy Sciences*. Oxford: Academic Press, 3:704-710.

Chapter 2 Literature Review

2.1 Buffalo Milk

Domesticated buffaloes (*Bubalus bubalis*) are predominant dairy animals in some Asian countries, contributing to 68% and 57% of the total milk production in Pakistan and India, respectively. Approximately 97% of buffaloes are found in Asia and 3% are scattered in the rest of the world (Wanapat and Chanthakhoun, 2015). Buffaloes can be classified into river and swamp types. River buffaloes are usually black in colour with sickle-shaped horns, whose habitats are river valleys with clean water. They are found in India, Pakistan, South-West Asia and South-East Europe. Swamp buffaloes instead vary in colour and their natural habitats are the swamp or marshland in South-East Asia. Commercial buffalo milk (BM) is obtained from river buffaloes as they have dairy character and produce high yield of milk. On the other hand, swamp buffaloes are primarily work animals in rice-growing areas and are poor in milk yield (Murtaza et al., 2017a).

BM is priced higher than cow milk (CM). It is paid 3.5-4 times CM's price in Italy, where most of BM is processed into mozzarella cheese (*mozzarella di bufala campana*) (Zicarelli, 2020). BM mozzarella cheese has good meltability and is widely used as pizza topping (Angelis and Gobbetti, 2011), thus it can be sold at a premium price. As a consequence, many researchers have developed ways to test the authenticity of BM mozzarella, in order to prevent any fraud or mislabelling (Cozzolino et al., 2002; Czerwenka et al., 2010; Gunning et al., 2019). Whereas in India and Pakistan, BM is priced at 1.3-1.6 times the cost of CM (Zicarelli, 2020). Indian consumers prefer the BM thick cream layer and its higher milk viscosity. It is also known to impart a distinct whitening effect to tea and coffee because of the greater content of casein and whey protein compared to CM (Murtaza et al., 2017b).

The higher market pricing for BM is reasonable as this product has almost twice the fat content as CM, with a range of 5.3-15% (BM) compared to 3.3-6.4% (CM) (Gantner et al., 2015). Indeed, the price of milk is dictated by its milk solids content, especially protein and fat, since the solids determine the yield of processed dairy products, such as butter and cheese. **Table 2.1** shows the overview of milk solids composition from different mammal species.

Table 2.1. Composition of milk solid in average from different types of mammals (Bylund, 1995). Values in % (w/w).

Mammal	Protein Total	Casein	Whey	Fat	Carbohydrate	Ash
Human	1.2	0.5	0.7	3.8	7	0.2
Cow	3.5	2.8	0.7	3.7	4.8	0.7
Buffalo	4	3.5	0.5	7.5	4.8	0.7
Goat	3.6	2.7	0.9	4.1	4.7	0.8
Sheep	5.8	4.9	0.9	7.9	4.5	0.8
Horse	2.2	1.3	0.9	1.7	6.2	0.5

Fat-rich dairy products made from BM include butter and ghee (clarified butterfat). Buffalo butter contains at least 82% of fat according to the European legislation (Lee et al., 2018) and is white in colour. The butter is typically processed from pasteurised cream followed by churning and working at 14-17 and 15-16 °C, respectively (Murtaza et al., 2017b). The BM cream churns more readily than CM cream because of the higher fat content and larger sized fat globules. In the biggest BM market, India, buffalo ghee is a prominent product. Ghee utilizes about 28% of the BM produced in the country. Chemically, ghee contains at least 99.5% milk fat, which consist of a complex mixture of triglycerides, free fatty acids, phospholipids, sterols, vitamins, minerals, and a small amount of casein (Murtaza et al., 2017b). Ghee making by the creamery butter method is the usual industrial practice. In this process, the milk is first heated to around 40 °C and water is separated through a centrifugal cream separator. The cream is pasteurised, cooled, aged and converted into butter. Butter is then heat clarified at temperatures ranging from 110 to 140 °C and residues are removed by filtration or through a clarifier.

In addition to the difference in total fat content in the whole raw milk, BM fat presents different fatty acids composition than CM fat. It has been reported that BM contains a higher portion of total saturated fatty acids and displays less unsaturated fatty acids than CM, resulting in a relatively higher melting point (Murtaza et al., 2017a). **Table 2.2** presents a complete comparison of the fatty acids composition of BM and CM.

Table 2.2. Average fatty acids (%w/w) of buffalo and cow milk fat, and its melting properties (Murtaza et al., 2017a).

Fatty acids/ constituents		Buffalo milk fat	Cow milk fat
C4:0	butyric	4.4	3.2
C6:0	caproic	1.5	2.1
C8:0	caprylic	0.8	1.2
C10:0	capric	1.3	2.6
C10:1	caproleic	Trace	0.3
C12:0	lauric	1.8	2.8
C14:0	myristic	10.8	11.9
C14:1	myristoleic	1.3	2.1
C15:0	pentadecanoic	1.3	1.2
C16:0	branched	0.2	0.3
C16:0	palmitic	33.1	30
C16:1	palmitoleic	2	2.2
C17:0	margaric	0.6	0.3
C18:0	stearic	12	10.1
C18:1	oleic	27.2	27.4
C18:2	linoleic	1.6	1.5
C18:3	linolenic	0.5	0.6
C20:4	arachidonic	0.2	0.2
Monounsaturated		29.1	34.6
Total unsaturated		31.6	40.7
Total saturated		63.8	57.3
Softening point (°C)		34.3-36.3	33.5-35.9
Melting point (°C)		33.4-46.4	31.5-35.2

2.2 Fat Crystallisation Fundamentals

A crystal is defined as an orderly array of symmetrically arranged molecules. The fundamental building block of a crystal is referred to as the unit cell, and a repetition of the unit cell make a crystal (Marangoni and Wesdorp, 2013;

Idziak, 2018). Fat crystallisation is important in the structural development of fat-based products such as butter, margarine, ice cream and chocolate. It has been associated with product quality attributes such as hardness, melting points, spreadability, emulsion stability, oral smoothness/mouthfeel, and surface glossiness. The structural hierarchy from the nano-scale of fat crystals into the macro-scale of food products is given in **Figure 2.1**.

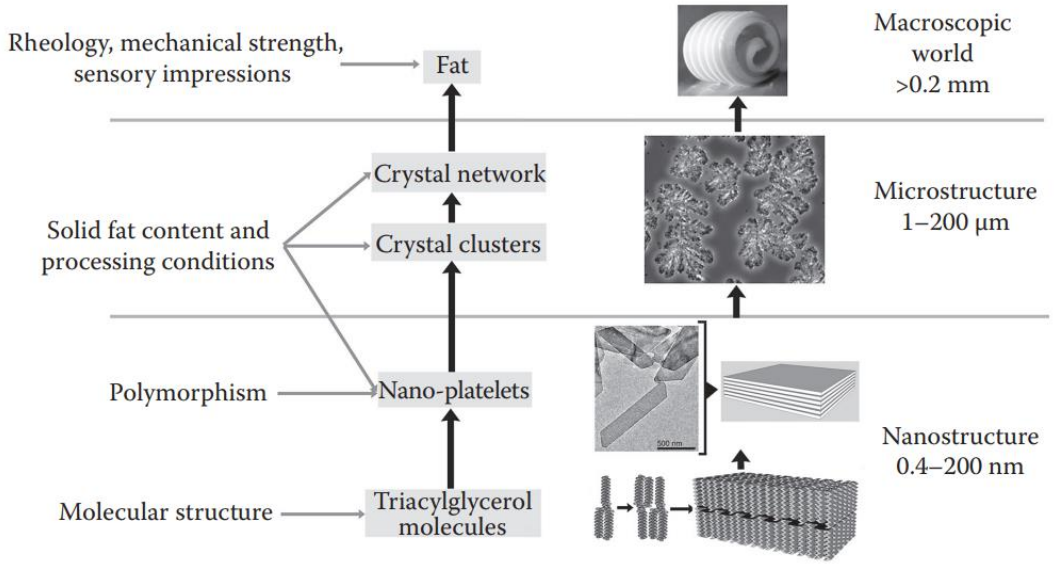

Figure 2.1 Nano to macro scale hierarchy of fat crystal structure (Marangoni and Wesdorp, 2013).

Typically, natural fat contains at least 95% of TAGs, with the rest being diacyl- and mono-acylglycerols, free fatty acids, and other minor components such as sterols and phospholipids (Huppertz et al., 2009). Therefore, fat crystallisation can also be viewed mainly as the crystallisation of complex mixtures of TAGs. When TAGs molecules crystallise, the three acyl chains are arranged either in a “fork” configuration, where the acyl chain at positions *sn*-1 and *sn*-2 are opposite to each other and the acyl chain *sn*-3 is parallel to *sn*-1; or the “chair” configuration, where the *sn*-1 and *sn*-2 acyl chains are parallel and acyl chain at *sn*-3 is at the opposite position (**Figure 2.2**). Generally, TAGs molecules align side by side in a leaflet in order to maximize the Van der Waal’s interactions. One molecular pair from two opposite leaflets form the unit cell of a triglyceride crystal (Marangoni and Wesdorp, 2013). A continuous repeat of such leaflet pair forms the lamellar structure of a fat crystal. Stacks of these lamellae construct instead nano platelet-like crystals (**Figure 2.1**), whose thickness has been estimated to be around 30 nm (Acevedo and Marangoni, 2010).

Moving to the micro scale, nano-platelets aggregate into crystal clusters and form a crystal network (1-200 μm), which can be observed with optical microscopy (e.g., polarised light microscopy). The micrograph of the fat crystals are often described according to morphological features such as spherulitic or needle-like shaped. The fat crystal network is highly important in an emulsion system such as milk. It provides bulk stabilisation, while crystals at water/fat interfaces can further stabilise the system via the Pickering effect (Green and Rousseau, 2018). Similar stabilisation effect is also observed in fat based foams (edible air-in-oil system, also called oleofoams) such as whipped cream. The incorporation of air in the product may reduce the amount of fats (particularly saturated) in high calorific food, offering a healthier product formulation (Metilli et al., 2021). Finally, at the macro scale, the properties of fat crystals are translated into quality attributes, such as textural properties and oral perception.

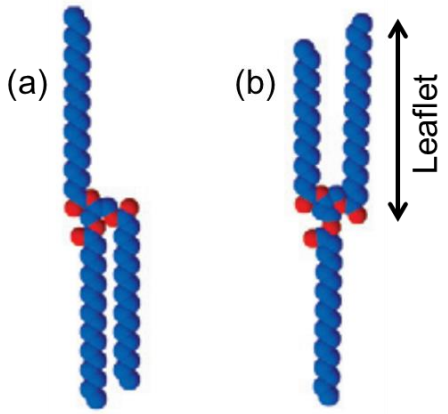

Figure 2.2. The two acyl chains conformations in triglyceride molecule found in TAG crystals. (a) “Chair”, and (b) “fork” conformation (Acevedo and Marangoni, 2015).

TAGs can crystallise in more than one crystalline structure, which is known as polymorphism. Different polymorphs display different physical properties, such as melting point, solubility, and crystal morphologies. There are three well known fat crystals polymorphs, named α, β’, and β, in the order of increasing stability. The identification of these polymorphs is based on the differences in “sub-cell”, the cross-sectional (lateral) packing modes of the zigzag aliphatic acyl chain (Abrahamsson et al., 1978; Small, 1984; Sato, 2001), and as mentioned above, TAGs stack in layers forming smectic crystals (Larsson, 1972; Callaghan, 1977; Hondoh et al., 2018). Depending on the number of leaflets per stacking unit, the smectic forms of TAGs are defined as

double chain length (DCL structures, triple chain length (TCL) structure, quatro (QCL) and hexa chain length structures (HCL) (Sato and Ueno, 2005). As a general rule, TAGs with same or similar fatty acid moieties form DCL structures, for example, monoacid TAGs like tripalmitin and tristearin. Whereas, TCL structures are preferred when one or two of the three chains are largely different in length or saturation, which promotes a chain sorting mechanism. As an example, this is observed in 1,3-dipalmitoyl-2-oleoyl-*sn*-glycerol (POP), where the bent oleic chains phase separate from the straight palmitic bilayer region into a distinct monolayer plane, thus forming a triple-layered structure (TCL) (Sato, 2018b). The DCL and TCL are the most commonly reported stacking geometries in the fat crystallisation studies. On the other hand, only a small number of QCL and HCL structures have been reported for TAGs containing asymmetric fatty acid moieties (Kodali et al., 1990).

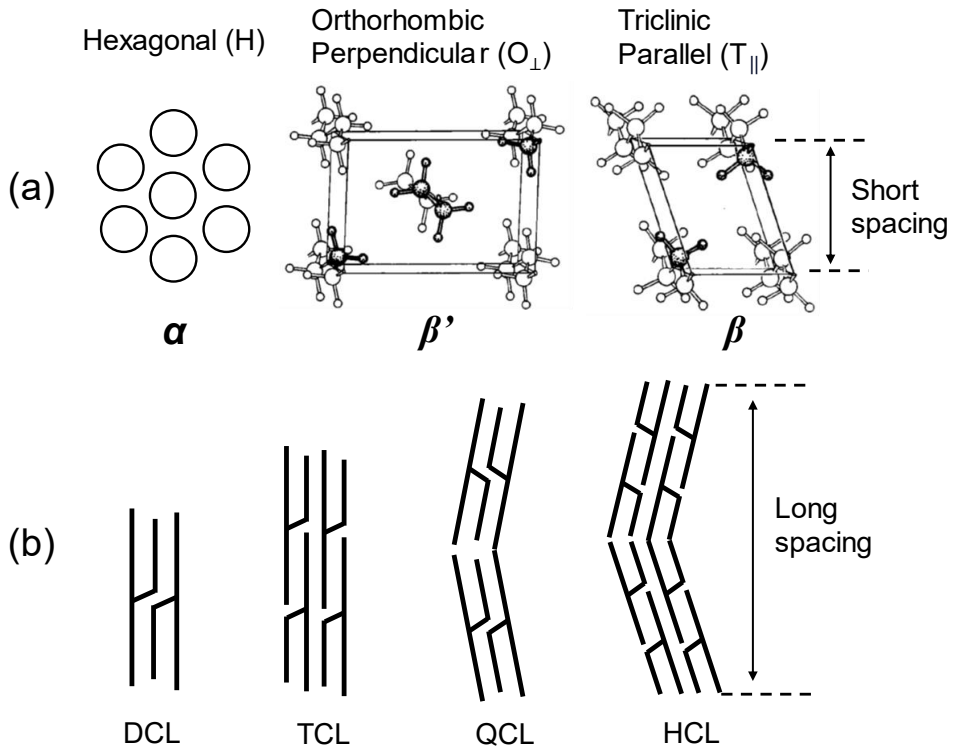

Figure 2.3. Hydrocarbon chain packing in three different types 3D sub-cells (a), four different multilayered chain-stacking modes (b) formed with TAGs molecules. Adapted from (Abrahamsson et al., 1978; Sato and Ueno, 2005).

Figure 2.3 illustrates the different chain packing (sub-cell) and stacking structures of various TAGs crystals. In order to identify these structures, X-ray scattering is utilised as a standard technique. The periodicity of crystal

structures gives rise to X-ray diffraction patterns, which can be observed in the wide and small angle regions, corresponding to the short and long spacings, respectively. The short spacings indicate the fat crystal sub-cell geometry (**Table 2.3**), while the long spacings corresponds to their stacking repeat, displaying mostly two (2L) or three leaflet (3L) structures (Idziak, 2018). Further discussion on X-ray scattering is provided in the section **2.5.1**.

In addition to three basic polymorphs, a fourth chain packing structure has been put forward, that is termed as the γ-form. This form has also been termed as sub-α phase, because it has a lower melting point than the α-form. Its chain packing is structurally related to the β′-form (Grotenhuis et al., 1999), since the hydrocarbons pack in a orthogonal fashion. The characteristic short-spacings of all mentioned polymorphs are summarised in **Table 2.3**.

Table 2.3. Characteristic of short spacing associated with different fat polymorphs and sub-cell types (D'Souza et al., 1990; Grotenhuis et al., 1999; Idziak, 2018).

Polymorph	2D sub-cell (3D sub-cell)	Short spacing (Å)
α	Hexagonal (hexagonal H)	Single at ca. 4.15
β'	Centered rectangular (orthorhombic $O_{\perp}$)	4.2 and 3.8 or 4.27, 3.97, and 3.71
β	Oblique (triclinic $T_{\parallel}$)	4.6 (often strongest reflection)
γ (low-melting β'-modification)	Centered rectangular (orthorhombic $O_{\perp}$)	4.2 and 3.7

It is worth pointing out that the 3D sub-cell concept (Table 2.3) refers to the geometrical arrangement of the hydrocarbon packing and one repetition along the chain axis, which is different to the given 3D unit cell of the fat crystals. This has led to some confusion among the food scientist community (Marangoni, 2011). Both the 3D sub-cell and 3D unit cell can have similar geometry, such as reported for orthorhombic latticed β'-polymorph of $C_nC_{n+2}C_n$-type TAGs (n=even) (Van Langevelde et al., 2000). But they can also differ, such as in the β'-polymorph of 1,2-dipalmitoyl-3-myristoyl-*sn*-glycerol which is reported to have a monoclinic unit cell despite having an orthorhombic sub-cell (Sato et al., 2001). Noteworthy, some TAGs crystals have been reported to exhibit uncommon sub-cell geometry (**Table 2.3**), such

as the β-polymorph of mono-unsaturated TAGs, POP and 1,3-distearoyl-2-oleoyl-*sn*-glycerol (SOS), which are reported to have a monoclinic unit cell as well as monoclinic sub-cell, in contrast to the common triclinic sub-cell (Van Mechelen et al., 2006). Nonetheless, the current thesis applies the widely accepted 3D sub-cell categorisation in **Table 2.3** for the milk fat polymorph identification, but also lists the 2D sub-cell lattices (Small, 1984), that are universal for the given polymorphs of food fats.

2.3 Crystallisation Process and Thermodynamics

Fat crystallisation occurs in several steps: cluster formation → nucleation → crystal growth (Sato, 2018a; Hondoh et al., 2018). The dynamics of each of these crystallisation mechanisms depend on many factors such as TAGs composition and processing conditions (temperature, pressure, shear, etc) (Hondoh et al., 2018). The thermodynamic driving force of crystallisation is the difference in the chemical potential (Δμ) between the solid crystalline phase (μ_S) and the liquid (or solution phase) (μ_L). The chemical potential can be calculated as the Gibb free energy (G) per molecule of each phase. As fat is normally crystallised from its melt, the driving force for crystallisation is proportional to the supercooling (ΔT) divided by the melting temperature (T_m) shown by **Eq. (2.1),** where ΔH_m is the enthalpy of melting of the fat (Himawan et al., 2006; Hondoh et al., 2018).

$$\boldsymbol{\Delta\mu = \mu_L - \mu_S = \Delta H_m \Delta T / T_m}$$

Eq. (2.1)

The equation above refers to the case of the crystallisation of a pure TAG molecule, or of a mixture of TAGs with similar melting points and molecular structure (e.g., fully miscible). However, natural, edible fats are normally mixtures of different, partly immiscible TAGs where the higher melting TAGs can be considered as the solute whilst the lower melting TAGs act as solvent. In this case the driving force is the supersaturation of the high melting TAGs in respect to the lower melting ones (Himawan et al., 2006). When the temperature of a molten fat is decreased below the melting point of the highest melting TAG, the melt becomes supercooled and thus ‘supersaturated’ for these particular TAGs. This so called supercooling phenomenon represents the thermodynamic driving force for a phase change from liquid to solid (Marangoni and Wesdorp, 2013).

Fats usually have to be supercooled by at least 5-10°C before they begin to crystallise. For a few degrees below the melting point, prior to nucleation, the melt is metastable, where molecules begin to aggregate into small metastable clusters called embryos (Marangoni and Wesdorp, 2013). Several structural models have been put forward to explain the TAG clustering formation (Figure 2.4). The latest model, core-shell (Figure 2.4d) (Sadeghpour et al., 2018), show particular similarities to previously proposed models and view the clustering formation as back-to-back TAGs arrangement with a bilayered geometry as the 'core' (cp. smectic model in Figure 2.4a). To this core TAGs loosely attached in nematic fashion in a second 'shell' (Figure 2.4b). Whereas, the propeller-like conformation of the TAGs as proposed in the discotic model (Figure 2.4c) are likely to accumulate in the highly curved end-points of the recently proposed cluster model (Figure 2.4d).

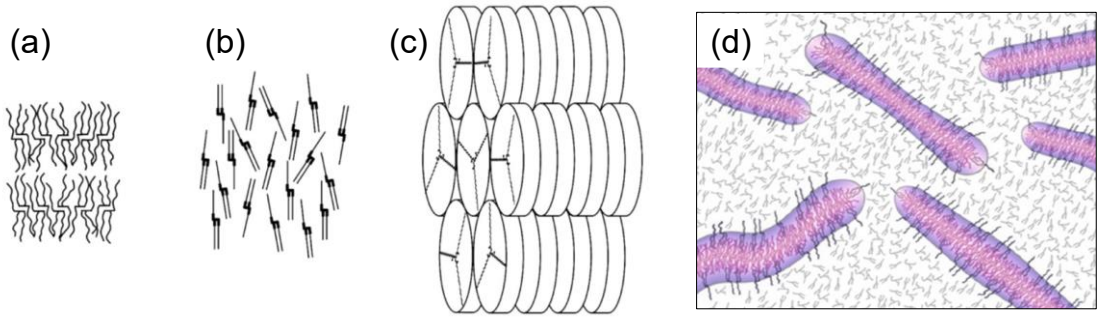

Figure 2.4 Proposed models of TAGs arrangement in the molten state, (a) smectic (Larsson, 1994), (b) nematic (Cebula et al., 1990), (c) discotic (Pink et al., 2010) and (d) core-shell models. Adapted from (Sadeghpour et al., 2018).

According to the classical nucleation theory (CNT), the metastable clusters or embryos will have to surpass a critical nucleus size at which the stable nucleus is formed and capable of growth (Povey, 2014). This stochastic process is determined by the nucleation activation energy, which is largely affected by the level of supercooling as well as the crystal/liquid or crystal/solution interfacial energy (Hondoh et al., 2018). With higher supercooling (higher $\Delta\mu$), the critical nucleus size is smaller, thus increasing the nucleation rate (Kashchiev, 2000; Povey, 2014).

Next, there are two type of nucleation, homogenous and heterogeneous nucleation. Homogenous nucleation occurs when there is no foreign particle in the system and only the crystallising substance exists. Foreign particles can interact with the crystallising substance and cause heterogeneous nucleation,

which occurs with a lower driving force, when compared to homogenous nucleation. Both homogenous and heterogeneous nucleation are considered as primary nucleation, whereas secondary nucleation occurs when crystals of the crystallising material already exist in the system and act as 'seed' (Hondoh et al., 2018).

The CNT describes the thermodynamic of nucleation event as the function of the Gibbs free energy of the system (ΔG_{hom}) changes due to the decrease of free energy per unit volume arising from the enthalpy of fusion, $-\Delta G_V$, and the increase of the surface energy due to the surface tension, ΔG_S. In a homogenous nucleation of spherical nuclei, this can be expressed as

$$\boldsymbol{\Delta G_{hom} = -\Delta G_V V + \Delta G_S S = -\frac{4}{3}\pi r^3 \Delta G_V + 4\pi r^2 \sigma}$$

Eq. (2.2)

where *V*, *S* and *r* are the volume, surface and radius of the cluster, respectively; σ is the surface energy. According to **Eq. 2.2**, ΔG_{hom} increases with the increasing cluster size *r,* until a critical size *r** is reached. ΔG_{hom}* (the critical free energy or the activation energy barrier) is obtained, when $d\Delta G_{hom}/dr = 0$, resulting in any clusters larger than $r^* = 2\sigma/\Delta G_V$ to decrease the free energy, and thus form stable nuclei (Himawan et al., 2006).

Once a stable nucleus is formed, a crystal will grow. The speed of this step is affected by a variety of factors, of which the fatty acid chain length and mass transfer rate are the most relevant. In terms of chain length, the longer triglycerides present slower growth rates than those with shorter chain lengths. Regarding mass transfer, as the solid fat content starts to increase, so does the viscosity, thus hindering the molecular diffusion of additional TAGs to the growing crystals (Himawan et al., 2006), which in turn decreases the growth rate.

The polymorphism of fat crystals can be observed even during nucleation and crystal growth, which is largely governed by the thermodynamics of the crystallisation process. The relative stability of different polymorphs is shown by their Gibbs free energies (*G*), where a lower Gibbs free energy is associated to the more stable polymorph, at given temperature and pressure (Himawan et al., 2006). As shown in **Figure 2.5a**, fat polymorphism is monotropic, meaning that there is a polymorph (β-phase) that is stable at all conditions, whereas the other forms are always metastable. Polymorphic transformations of monotropic systems occur from metastable polymorphs into the more stable one in an irreversible manner. **Figure 2.5b** illustrates the

mechanism of these transformation, which are typically α → β' → β or direct α → β polymorph changes. It is important to note, that each polymorph can also directly be nucleated from the melt, depending on the crystallisation conditions. This different polymorphic nucleation can be better explained by their free energy barriers shown in **Figure 2.5c**. The least stable α-polymorph encounters the lowest energy barrier (free activation energy), thus it will nucleate first even though its melting point is lower than the more stable forms β' and β polymorphs (Himawan et al., 2006; Marangoni and Wesdorp, 2013). Later on, the metastable form will transform into a more stable one. This phenomenon is termed 'Ostwald rule of stages'. Empirically, a higher supercooling will give preference to the nucleation of a less stable (α-polymorph) structure, whereas a lower undercooling can result in the direct nucleation of either the β' or β polymorph from melt (**Figure 2.5b)**.

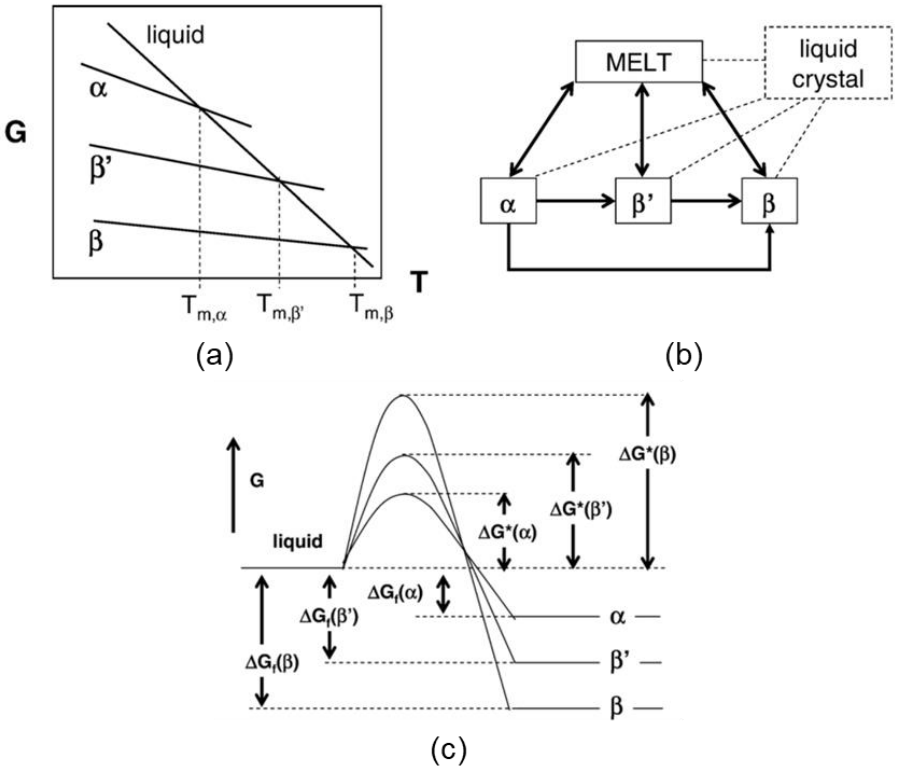

Figure 2.5 (a) Gibbs free energy of fat monotropic polymorphism, (b) fat polymorphic transformation pathways, (c) schematic of energy activation barriers for three fat crystal polymorphs. T_m denotes the equilibration melting point temperatures, G*: Gibbs free energy at the nucleation barrier, G_f: Gibbs free energy after crystal formation of α, β', and β polymorph (Rousset, 2002; Himawan et al., 2006).

External forces can be applied to override the Ostwald rule of stages, and in order to obtain specific polymorphs. As an example, chocolate tempering involves a certain temperature profile to speed up the transformation into a stable polymorph. After the initial nucleation of different polymorphs has taken place (mainly β'- and β-forms), the initial hold-temperature is increased above the metastable form's melting point, and thus removing them, leaving only the stable polymorph to grow further (Himawan et al., 2006; Ghazani and Marangoni, 2021). Shearing is also found to speed up the crystal growth process. It is argued that the shearing provokes the alignment of less stable polymorph, thus inducing faster polymorphic change into more stable forms (Mazzanti et al., 2005).

Polymorphic transformations can be classified into melt-mediated and solid-solid transformation. Melt-mediated transformations occur at a temperature above the metastable crystal melting point. Whereas, solid-solid transformation occurs at temperatures below the melting point of the least stable polymorph. However, it should be noted that lower temperatures hinder polymorphic transformation (slower kinetics of growth) (Marangoni and Wesdorp, 2013). Apart from changes in temperature, polymorphic transformations can also be facilitated by the presence of a solvent, in a process named solution-mediated transformation (Sato et al., 1989).

After the production of fat-based food products, these are often left in storage at optimal temperature range before releasing them into the markets. During this process called 'aging', the fat crystal is further stabilised through polymorphic transformations and crystal growth, which promotes the formation of lipid crystal networks (Hondoh et al., 2018). The crystal network defines many sensory attributes of fat-based products, such as mouthfeel and texture, and it is also important in maintaining the stability against coalescence in emulsion products such as margarine or butter. From a thermodynamic point of view, many fat-based products are actually metastable when they retain their functional properties. For example, a margarine is designed to have β'-polymorph instead of the most stable β-polymorph because the latter would lead to margarine with too large crystals in it, giving rise to a 'sandy' mouthfeel. Therefore, conversions into thermodynamically most stable forms might lead to a degradation of their functionality (Hondoh et al., 2018). Coarsening of the crystals can also be the result of Ostwald ripening, where the big crystals grow larger in the expense of smaller crystals during long storage (Sato, 2018a).

2.4 Milk Fat Crystallisation

A comprehensive review of milk fat crystallisation has been provided by Lopez (2018). I note that most studies are related to cow milk. Therefore, in the current sub-section (**2.4**), the term 'milk fat' is attributed to 'cow milk fat'.

Milk fat is a very complex fat found in nature with more than 400 fatty acids and 200 different triglycerides. Milk fat contains many asymmetrical triglycerides, defined as triglycerides with combination of UUS or SSU fatty acids, in which the solitary unsaturated (U) or saturated (S) fatty acid resides on either the *sn*-1 or *sn*-3 position or triglycerides with acyl chain length differences greater than 2 carbon atoms, for example BPP (B: butyric acid C4:0, P: palmitic acid C16:0) (Grotenhuis et al., 1999; Sato, 2001; Lopez, 2018).

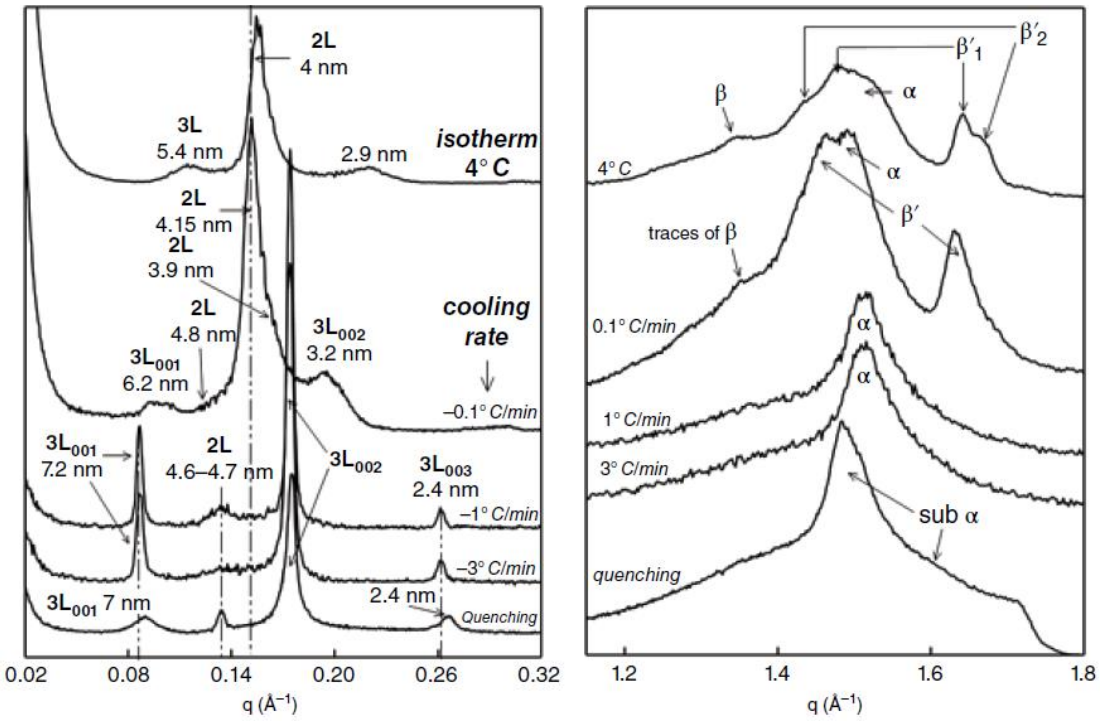

Figure 2.6. Synchrotron radiation X-ray diffraction (SR-XRD) patterns recorded at -8 °C (left) at small angles and (right) at wide angles after either cooling of anhydrous milk fat at different rates as indicated on the figure, or isothermal conditioning at 4 °C for 5 days. Adapted from (Lopez et al., 2005).

Milk fat displays a complex polymorphism. Depending on the cooling rate, six different types of crystals have been identified, with lamellar structures with DCL (4-4.8 nm) and TCL (5.4-7.2 nm) organisations of TAGs (**Figure 2.6**, left side). At least five crystalline sub-cell types have been identified, as observed

with wide angle scattering methods: α and sub-α, two β' and one β type polymorphs (**Figure 2.6**, right side). All these crystalline structures coexist with a liquid phase even at low temperature (i.e., 4 °C) (Lopez et al., 2005).

Among all chain packing geometries, the α- and β'-polymorph are the most commonly reported in the literature, while few studies reported on the sub-α and β-polymorph. The sub-α (γ-form) appeared, when a very fast cooling rate and at low crystallisation temperature (< -8 °C) was applied (Grotenhuis et al., 1999). Meanwhile, the nucleation and growth kinetics of the β-polymorph was found to be dependent on the TAGs composition, where unsaturated TAGs with a total carbon number of 52-54 were shown to promote its formation (Tzompa-Sosa et al., 2016). While the β-polymorph is occasionally found, the β'-polymorph is the dominant form in most cases. This could be attributed to the fact that milk fat contains many asymmetrical triglycerides which crystallise in orthorhombic ($O_{\perp}$) 3D sub-cell (β'-polymorph), while the β-polymorphs do crystallise in a structurally different triclinic ($T_{\parallel}$) 3D sub-cell (Sato, 2001). Note, they differ both in geometry and quite significantly differ in size in stacking direction.

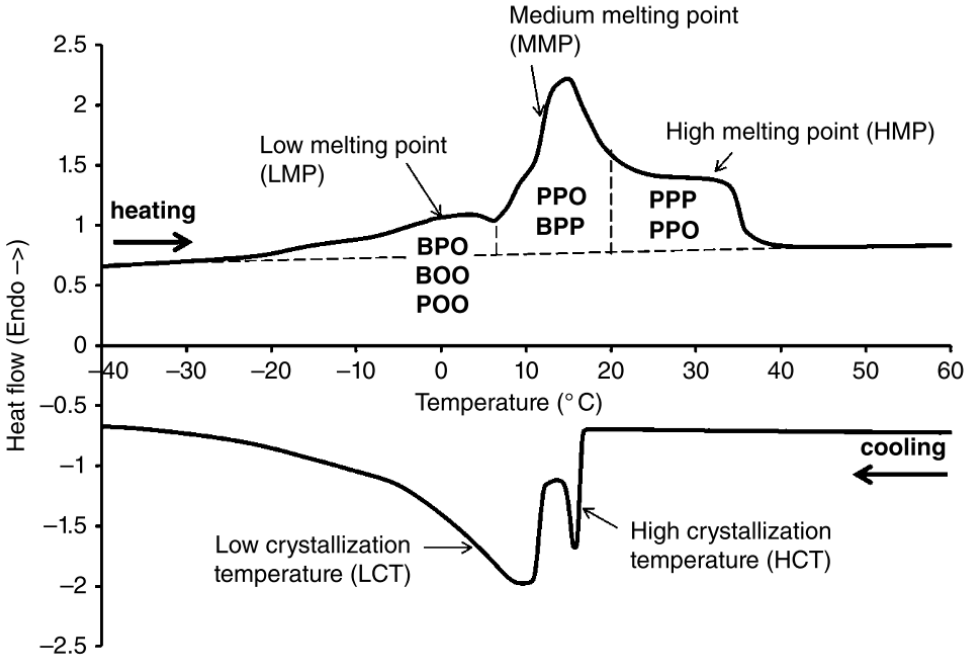

Figure 2.7 Thermal behaviour of milk fat upon cooling and heating at 2 °C/min. B: butyric, O: oleic, P: palmitic (Lopez, 2018).

The thermal behaviour of milk fat during cooling or heating is typically studied using differential scanning calorimetry (DSC). **Figure 2.7** shows the thermogram of milk fat when subjected to cooling at -2 °C/min from the melt, followed by heating at the same rate. The milk fat exhibits two main

exothermic events during cooling, associated to the crystallisation of TAGs molecules at high and low temperature. The broad exothermic peak indicates that milk fat might not be fully solid even at -40 °C (Lopez, 2018). Upon heating, milk fat is observed to melt in three steps, as shown by the three broad endothermic peaks in the thermogram of **Figure 2.7**. These peaks correspond to a large number of milk fat TAGs that melt separately, which further classify as (1) lower melting point TAGs, containing short chain and/or unsaturated fatty acids such as BPO, BOO and POO; (2) medium melting point TAGs, with TAGs predominantly containing short chain and/or single unsaturated fatty acid such as PPO and BPP; and (3) high melting point TAGs which are rich in fully saturated TAGs such as PPP (Timms, 1980). It is worth noting that the shape of a DSC thermogram largely depends on the applied heating and cooling rates. For instance, the cooling rate significantly affects the onset of the crystallisation/nucleation temperature (Tomaszewska-Gras, 2013).

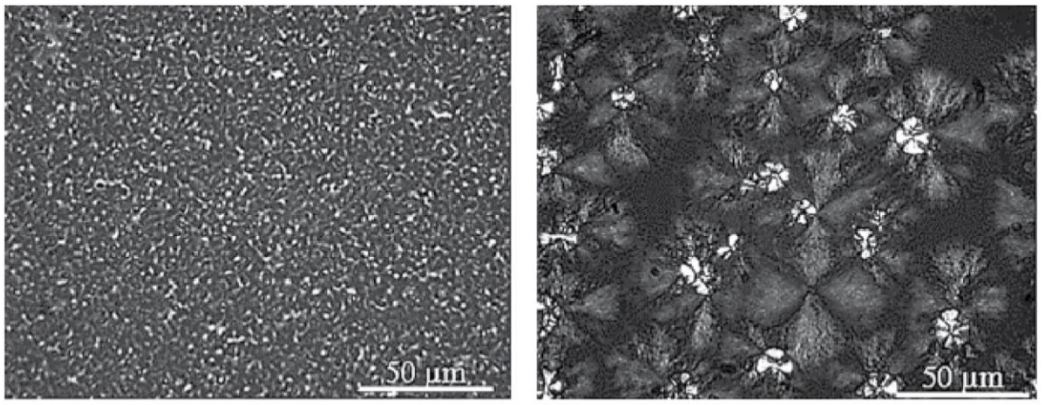

Figure 2.8 Microstructure of milk fat crystals after (a) fast cooling and (b) slow cooling. Adapted from Lopez et al. (2005).

The structure of milk fat crystals at the microscale can be observed using polarised light microscopy. There are two main types of morphologies for the crystal network. The first one is granular with small but numerous nuclei as resulting from fast cooling (**Figure 2.8a**). Whereas, the second morphology is characterised by the presence of spherulites, with larger but less nuclei, which are produced by slowly cooling the milk fat (**Figure 2.8b**). In a slow cooling process, nucleation happens at low undercooling, allowing the crystals to grow further. On the other hand, fast cooling favours higher nucleation rates over crystal growth. The rapid drop in temperature can also increase the viscosity,

which in turn reduces TAGs diffusivity and hinder crystal growth (Himawan et al., 2006).

2.5 Experimental Techniques for Crystallisation Study

2.5.1 Polymorphism by X-ray Diffraction

Much of our current knowledge on fat crystallisation is obtained from X-ray diffraction (XRD) studies. X-rays are electromagnetic waves with wavelengths around 1 Å. A typical benchtop X-ray diffractometer uses a copper X-ray tube which produces a wavelength of 1.54 Å. This wavelength corresponds roughly to the smallest crystalline lattices size found in edible fats, and thus very suitable for crystal characterisation studies (Idziak, 2018). As shown in **Figure 2.9a**, there are four basic elements in an X-ray scattering instrument: an X-ray generating source, a collimation system through which the beam size is shaped, the sample holder, and a beam stop with a detector.

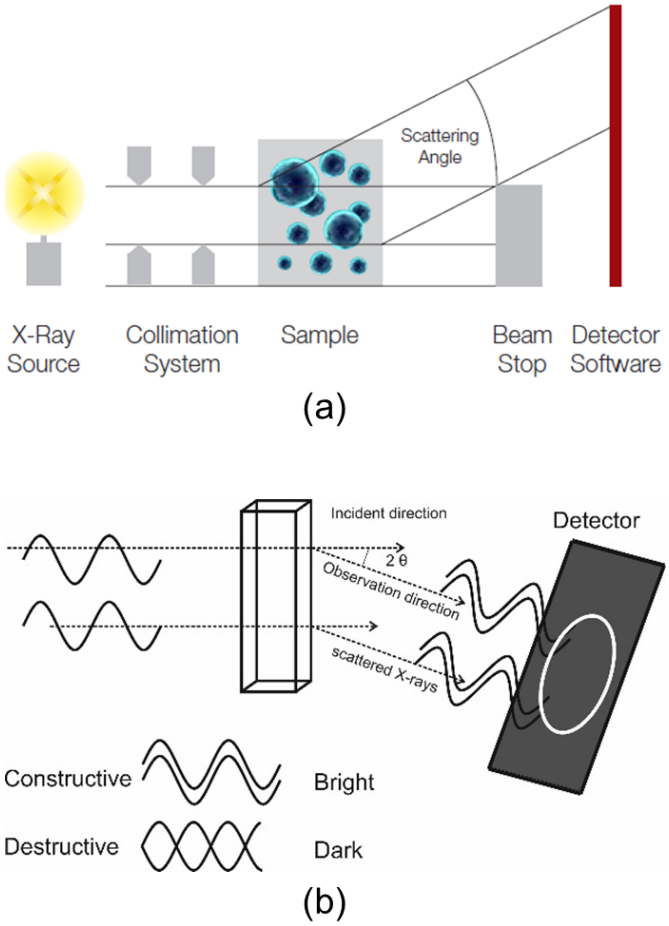

Figure 2.9. (a) Basic components of an X-ray scattering instrument. (b) Diffraction of X-rays illustrated by incident of X-rays being scattered from a sample, where constructively interfering waves are detected at the detector as a diffraction peak (white ring). Adapted from Schnablegger and Singh (2013).

X-rays are scattered by electrons in the sample, which produce scattered waves of the same wavelength (elastic scattering). Note, inelastic scattering contributions are insignificant in my carried out experiments and are not further considered. Further, two extreme cases of scattering might occur, that is, constructive or destructive interference of the scattered waves, depending on whether the waves are in or out of phase with each other when exiting the sample (**Figure 2.9b**). Only constructive interference results in diffraction peaks (Bragg and Bragg, 1913; Idziak, 2018). If the incident X-rays strike the crystal at an angle θ and the distance between adjacent crystal planes is given by d (the d-spacing of the planes), then constructive interference will occur following Bragg's law:

$$n\lambda = 2d\,sin\theta$$

Eq. (2.3)

where n is an integer and λ is the wavelength of the incident X-rays. The angle between the incident and reflected X-ray beams (2θ in the **Figure 2.9b**) is measured in an XRD experiment by calibrating the detector, e.g., with silver-behenate, which has a known d-spacing of 58.4 Å (Blanton et al., 1995). Consequently, the d-spacing of particular reflection angle is determined as:

$$d = \frac{\lambda}{2\,sin\theta}$$

Eq. (2.4)

$$q = \frac{4\pi}{\lambda}\,sin(\theta) = \frac{2\pi}{d}$$

Eq. (2.5)

However, the scattering angle 2θ has the disadvantage that it depends on the wavelength, which varies between X-ray instruments. Because of this, it is common practice to represent the scattering patterns as a function of q, which is the scattering vector modulus (**Eq. 2.4**). This allows a universal deduction of real-space distances, d (Schnablegger and Singh, 2013).

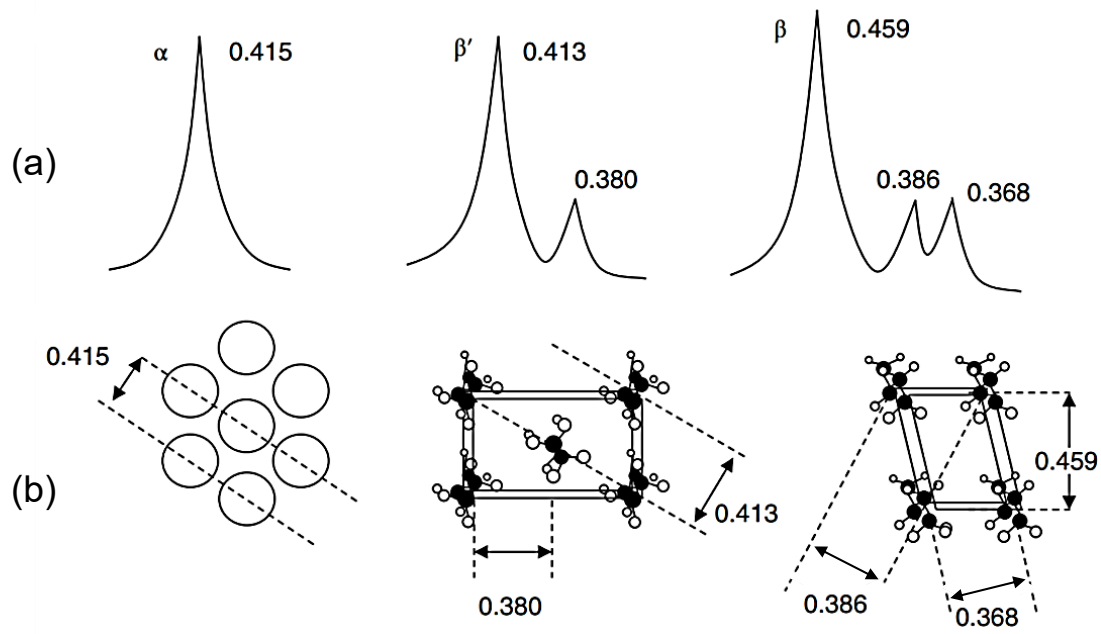

Figure 2.10. (a) XRD short spacing patterns and (b) chain packing structures of α, β', and β polymorphs of triglyceride crystals. Distance are given here in unit of nanometres (nm). Adapted from Sato (2018b).

Small-angle X-ray scattering (SAXS) and wide-angle X-ray scattering (WAXS) provide information of the lamellar (long spacings) and the chain packing structure (short spacings) of fat crystals, respectively. **Figure 2.10a** shows the typical WAXS patterns (short spacings) and its corresponding sub-cell (**Figure 2.10b**) for three basic fat polymorphs. The summary table for these values has been provided in **Table 2.3**.

Modern XRD instruments allow to perform real-time (*in situ*) observations of polymorphic transition, with precise temperature control and even under external stimuli such as shear or ultrasonication. A combination of XRD and DSC can be a powerful tool to clarify the kinetics of the polymorphic transitions of pure TAGs and their mixtures (Sato and Ueno, 2005). Apart from XRD benchtop instruments, XRD can also be performed using high-intensity sources such as synchrotron light, which allows higher resolution and faster measurement (high throughput in terms of samples analysed and fast dynamics). Most importantly, time-resolved experiments with millisecond time-resolution are only able to be carried out at synchrotron light sources.

2.5.2 Differential Scanning Calorimetry

Crystallisation of fats is an endothermic event, while the melting of a crystal is exothermic. Thermal behaviour observation can thus be very useful in a

crystallisation study. In differential scanning calorimetry (DSC), a sample and reference are subjected to the same thermal (time-temperature) profile, in which the difference between the heat/energy that must be added or withdrawn from the sample and reference is recorded. As a result, the endothermic and exothermic events can be obtained (Rigolle et al., 2018). There are two types of DSC based on its method of operation, heat-flux DSCs and power compensated DSCs. In heat-flux DSCs, both sample and reference are enclosed in pans and heated inside a single furnace. The heat flow is measured from the temperature difference of the sample and the reference. Whereas in power compensated DSCs, sample and reference pans are placed in two separate furnaces, thus heated separately. The heat flow is measured from the difference in thermal power required to keep both furnaces at the same temperature. In general, heat-flux DSCs have better (flat) baselines, whilst the power compensated DSCs benefit from more responsive and higher thermal scanning rates (Hemminger and Sarge, 1998; Gill et al., 2010).

DSC provides temperature, enthalpy and entropy values of melting, crystallisation and polymorphic transitions in fats (Sato and Ueno, 2005). DSC can also be used to indicate solid fat content (SFC) by integrating the melting peaks and the indirect stop-return method can give insight on the crystallisation mechanism (Foubert et al., 2008). The amount of sample used in DSC is typically small (5-20 mg), which allows a precise control of the temperature within the entire specimen. However, the measurement cannot normally be coupled with mechanical action, which is a disadvantage in a process-oriented crystallisation study (Rigolle et al., 2018).

2.5.3 Polarised Light Microscopy

Polarised light microscopy (PLM) is useful to evaluate the crystallisation growth (induction time, growth rate), microstructure (crystal size/shape, number of crystalline aggregates) and fractal dimension of the crystal (Marangoni and Wesdorp, 2013). Polarised light makes birefringent materials to appear bright, whilst non-birefringent samples appear dark. The crystalline fats are birefringent, whereas the liquid fats are not. Thus, the development of the crystal can be observed directly in the PLM as bright features against a dark background. A standard bright-field microscope can be converted to PLM by adding polarised filters in the light path (Rigolle et al., 2018).

By coupling PLM with a temperature and shear stage, it is possible to investigate closely the crystallisation behaviour of crystallising mixtures of fat, with and without shearing (Wright et al., 2000). PLM is useful to observe the early crystallisation, which can be expressed as induction time, i.e., the time required for the crystals to reach critical size to be visible. Because of PLM lower sensitivity compared to other techniques such as SAXS and DSC, the appearance of the crystals should be understood as early crystallisation events rather than nucleation events (Campos, 2013). The main advantage of the technique is the sample preparation; in fact, a drop of molten fat can be directly observed without further preparation. On the other hand, the major drawback comes from the fact that the samples must be adequately thin in order to allow light to pass through. Hence, the microstructures observed may be different from that of bulk samples (Rigolle et al., 2018).

2.5.4 Liquid Chromatography and Mass Spectrometry

Milk fat is mainly composed by mixture of TAGs. Therefore, identification of milk fat TAGs composition is essential in an endeavour to understand milk fat crystallisation. Liquid chromatography and mass spectrometry (LCMS) is a practical technique to characterise the TAG composition and structure, providing exact chain length of the acyl groups, the degree of saturation as well as the regio-specific location of each acyl chain. These TAG chemical properties are pivotal to the physical characteristics of fat, such as melting point, crystal structure and polymorphism (Foubert et al., 2007; Zeb and Murkovic, 2010).

As an example, Zeb and Murkovic (2010) employed a reversed phase liquid chromatography, utilising non-polar stationary phase and polar solvent as mobile phase, for the separation of TAGs in oils and fats. Whereas, the TAGs regio-isomers were analysed using electrospray ionisation mass spectrometry (ESI-MS). The ionisation causes minimal fragmentation, producing diacylglycerols (DAG) ions, whose molecular weight are analysed with mass spectrometry. The characterisation of these ions allows accurate identification of TAGs and their exact acyl chain position. This determination is possible due to 1,2-diacylglycerols ions being more dominantly formed than 1,3-diacylglycerols, because of the steric hindrance at the *sn*-2 position. For instance, a 1-butyryl 2-stearoyl 3-palmitoyl-glycerol (Bu-S-P) TAG, which is exposed to the above process will produce more intense Bu-S and S-P DAG ion bands as compared to Bu-P DAG ion band. Hence, the specific regio-isomer can be identified.

2.5.5 Electron Density Profile Analysis

Advances in fat crystal studies using the X-ray diffraction technique allow us to obtain structural characteristics. That is, the packing (short spacing) of the crystal, which is important to determine the TAGs crystal polymorphic type as well as the stacking (long spacing), which denote the TAGs lamellar thickness, can be determined. It is possible to examine further the 'inner' structure of the TAGs lamellae, using electron density profile (EDP) analysis. It is based on the fact, that TAGs contain functional groups with different electron density, i.e., carboxyl (high) and methyl (low). Because carboxyl groups are located adjacent to glycerol backbone, fine structural information of TAGs crystal can be inferred from the obtained EDP. For instance, the peak-to-peak distance in an EDP of a three-layered TAG crystal can be used to indicate the monolayer and bilayer regime thicknesses, as well as to approximate the contributing TAG species (Pratama et al., 2021; Pratama et al., 2022).

Step-wise instruction to determine an EDP has been provided by Li et al. (2017). There are three key pieces of information required to carry out an EDP determination using a Fourier transform, i.e. (1) *d*-spacing, (2) peak intensity, and (3) phase factors, α_h. The (1) and (2) are readily obtainable from X-ray scattering data. Each peak intensity, *I(h)*, corresponds to electron density contrast (*F(h)*) with respect to its corresponding lattice periodicity. Note, the amplitudes *F(h)* are given by the square root of the Lorentz-corrected intensities, *I(h)* (Li et al., 2017). For example, the first amplitude, *F(1)*, (h = 1) probes the electron density contrast with the periodicity of *d*. Further, the second, third, and fourth, amplitudes correspond to the electron density contrast with the periodicity of *d*/2, *d*/3, *d*/4, respectively. **Figure 2.11** shows the EDP example obtained from four order peaks of 1-palmitoyl-2-oleoyl-sn-glycero-3-phosphoethanolamine (POPE) with 3 mol % 1,2- dipalmitoyl-sn-glycero-3-phosphoethanolamine (DPPE).

It is important to note that the phase factors α_h are not directly obtainable from X-ray scattering experiments, but have been solved for a number of cases, such as for 2L- and 3L-stacked TAG crystals, and thus, can be taken from literature. Further calculation details are provided in the subsection **3.3.5** and **4.3.6**.

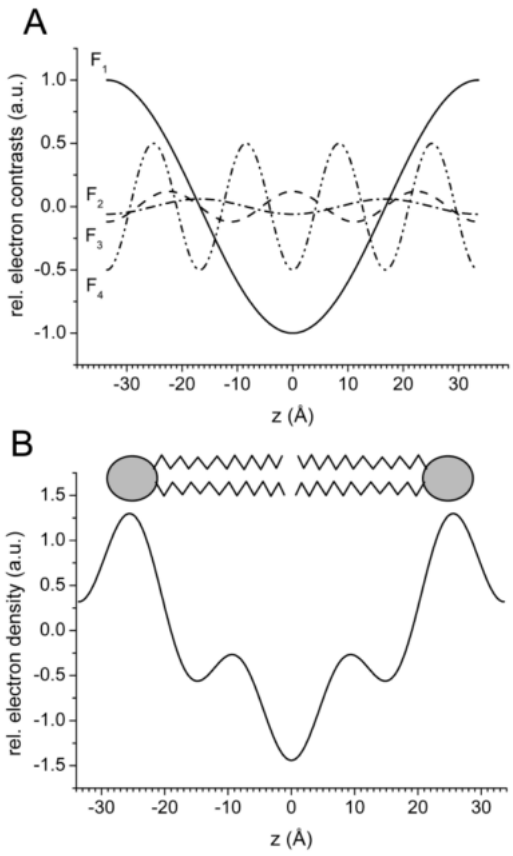

Figure 2.11. (A) Electron density contrast obtained from four peak periodicity and (B) The total and final EDP of POPE and DPPE (3 mol%) at room temperature. Adapted from Li et al.(2017).

2.6 References

Abrahamsson, S., Dahlen, B., Löfgren, H. and Pascher, I. 1978. Lateral packing of hydrocarbon chains. *Progress in the Chemistry of Fats and other Lipids*. **16**, pp.125-143.

Acevedo, N.C. and Marangoni, A.G. 2010. Characterisation of the nanoscale in triacylglycerol crystal networks. *Crystal Growth and Design*. **10**(8), pp.3327-3333.

Acevedo, N.C. and Marangoni, A.G. 2015. Nanostructured Fat Crystal Systems. *Annual Review of Food Science and Technology*. **6**(1), pp.71-96.

Angelis, M. De and Gobbetti, M. 2011. Pasta-Filata Cheeses: Traditional Pasta-Filata Cheese *In*: J. W. Fuquay, P. F. Fox and P. L. H. McSweeney, eds. *Encyclopedia of Dairy Sciences: Second Edition*. Oxford: Academic Press, 1:745-752.

Blanton, T.N., Huang, T.C., Toraya, H., Hubbard, C.R., Robie, S.B., Louër, D., Göbel, H.E., Will, G., Gilles, R. and Raftery, T. 1995. JCPDS-International Centre for Diffraction Data Round Robin Study of Silver Behenate. A Possible Low-Angle X-Ray Diffraction Calibration Standard. *Powder Diffraction*. **10**(2), pp.91-95.

Bragg, W.H. and Bragg, W.L. 1913. The reflection of X-rays by crystals. *Proceedings of the Royal Society of London. Series A, Containing Papers of a Mathematical and Physical Character*. **88**(605), pp.428-438.

Bylund, G. 1995. *Dairy Processing Handbook*. Lund: Tetra Pak Processing Systems AB.

Callaghan, P.T. 1977. The use of 13C spin relaxation to investigate molecular motion in liquid tristearin. *Chemistry and Physics of Lipids*. **19**(1), pp.56-73.

Campos, R. 2013. Experimental Methodology In: A. G. Marangoni and L. H. Wesdorp, eds. *Structure and Properties of Fat Crystal Networks Second Edition*. Boca Raton, FL: CRC Press, Taylor & Francis Group, pp.419–487.

Cebula, D.J., McClements, D.J. and Povey, M.J.W. 1990. Small angle neutron scattering from voids in crystalline trilaurin. *Journal of the American Oil Chemists' Society*. **67**(2), pp.76–78.

Cozzolino, R., Passalacqua, S., Salemi, S. and Garozzo, D. 2002. Identification of adulteration in water buffalo mozzarella and in ewe cheese by using whey proteins as biomarkers and matrix-assisted laser desorption/ionization mass spectrometry. *Journal of Mass Spectrometry*. **37**(9), pp.985-991.

Czerwenka, C., Muller, L. and Lindner, W. 2010. Detection of the adulteration of water buffalo milk and mozzarella with cow's milk by liquid chromatography-mass spectrometry analysis of β-lactoglobulin variants. *Food Chemistry*. **122**(3), pp.901-908.

D'Souza, V., deMan, J.M. and deMan, L. 1990. Short spacings and polymorphic forms of natural and commercial solid fats: A review. *Journal of the American Oil Chemists' Society*. **67**(11), pp.835-843.

Foubert, I., Dewettinck, K., Van de Walle, D., Dijkstra, A.J. and Quinn, P.J. 2007. Physical Properties: Structural And Physical Characteristics *In*: F. D. Gunstone, J. L. Harwood and A. J. Dijkstra, eds. *The Lipid Handbook*,

3rd ed. Boca Raton, FL: CRC Press, Taylor & Francis Group, pp.535–590.

Foubert, I., Fredrick, E., Vereecken, J., Sichien, M. and Dewettinck, K. 2008. Stop-and-return DSC method to study fat crystallization. *Thermochimica Acta*. **471**(1-2), pp.7-13.

Gantner, V., Mijić, P., Baban, M., Škrtić, Z. and Turalija, A. 2015. The overall and fat composition of milk of various species. *Mljekarstvo*. **65**(4), pp.223-231.

Ghazani, S.M. and Marangoni, A.G. 2021. Molecular Origins of Polymorphism in Cocoa Butter. *Annual Review of Food Science and Technology*. **12**, pp.567-590.

Gill, P., Moghadam, T.T. and Ranjbar, B. 2010. Differential scanning calorimetry techniques: Applications in biology and nanoscience. *Journal of Biomolecular Techniques*. **21**(4), pp.167–193.

Green, N.L. and Rousseau, D. 2018. Lipid Crystallization in Water-in-Oil Emulsions *In*: K. Sato, ed. *Crystallization of Lipids: Fundamentals and Applications in Food, Cosmetics and Pharmaceuticals*. Hoboken, NJ: Wiley Blackwell, pp.405-429.

Grotenhuis, E. Ten, Van Aken, G.A., Van Malssen, K.F. and Schenk, H. 1999. Polymorphism of milk fat studied by differential scanning calorimetry and real-time X-ray powder diffraction. *JAOCS, Journal of the American Oil Chemists' Society*. **76**(9), pp.1031-1039.

Gunning, Y., Fong, L.K.W., Watson, A.D., Philo, M. and Kemsley, E.K. 2019. Quantitative authenticity testing of buffalo mozzarella via α s1 -Casein using multiple reaction monitoring mass spectrometry. *Food Control*. **101**, pp.189-197.

Hemminger, W. and Sarge, S.M. 1998. Chapter 1 Definitions, Nomenclature, Terms and Literature *In: Handbook of Thermal Analysis and Calorimetry*. Elsevier Science B.V., pp.1–73.

Himawan, C., Starov, V.M. and Stapley, A.G.F. 2006. Thermodynamic and kinetic aspects of fat crystallization. *Advances in Colloid and Interface Science*. **122**(1-3), pp.3-33.

Hondoh, H., Ueno, S. and Sato, K. 2018. Fundamental Aspects of Crystallization of Lipids *In*: K. Sato, ed. *Crystallization of Lipids: Fundamentals and Applications in Food, Cosmetics and Pharmaceuticals*. Hoboken, NJ: Wiley Blackwell, pp.105-141.

Huppertz, T., Kelly, A.L. and Fox, P.F. 2009. Milk Lipids - Composition, Origin and Properties *In*: A. Y. Tamime, ed. *Dairy Fats and Related Products*. Chichester, UK: Blackwell Publishing Ltd, pp.1-27.

Idziak, S.H.J. 2018. Powder X-ray Diffraction of Triglycerides in the Study of Polymorphism *In*: A. G. Marangoni, ed. *Structure-Function Analysis of Edible Fats Second Edition*. AOAC Press, pp.73-99.

Kashchiev, D. 2000. *Nucleation: Basic Theory with Applications*. Oxford: Butterworth-Heinemann.

Kodali, D.R., Atkinson, D. and Small, D.M. 1990. Polymorphic behavior of 1,2-dipalmitoyl-3-lauroyl(PP12)- and 3-myristoyl(PP14)-sn-glycerols. *Journal of Lipid Research*. **31**(10), pp.1853-1864.

Van Langevelde, A., Van Malssen, K., Driessen, R., Goubitz, K., Hollander, F., Peschar, R., Zwart, P. and Schenk, H. 2000. Structure of CnCn+2Cn-type (n = even) β′-triacylglycerols. *Acta Crystallographica Section B: Structural Science*. **56**(6), pp.1103-1111.

Larsson, K. 1972. Molecular Arrangement in Glycerides. *Fette, Seifen, Anstrichmittel*. **74**(3), pp.136-142.

Larsson, K. 1994. The Liquid State *In: Lipids-Molecular Organisation, Physical Functions and Technical Applications*. Scotland: The Oily Press, L.T.D., pp.75–80.

Lee, C.L., Liao, H.L., Lee, W.C., Hsu, C.K., Hsueh, F.C., Pan, J.Q., Chu, C.H., Wei, C.T. and Chen, M.J. 2018. Standards and labeling of milk fat and spread products in different countries. *Journal of Food and Drug Analysis*. **26**(2), pp.469-480.

Li, N.Y.D., Perutková, Š., Iglič, A. and Rappolt, M. 2017. My first electron density map: A beginner's guide to small angle X-ray diffraction. *Elektrotehniski Vestnik/Electrotechnical Review*. **84**(3), pp.69–75.

Lopez, C. 2018. Crystallization Properties of Milk Fats *In*: K. Sato, ed. *Crystallization of Lipids: Fundamentals and Applications in Food, Cosmetics and Pharmaceuticals*. Hoboken, NJ: Wiley Blackwell, pp.283-321.

Lopez, C., Lesieur, P., Bourgaux, C. and Ollivon, M. 2005. Thermal and structural behavior of anhydrous milk fat. 3. Influence of cooling rate. *Journal of Dairy Science*. **88**(2), pp.511-526.

Marangoni, A. 2011. The trouble with crystal polymorphism. *INFORM - International News on Fats, Oils and Related Materials*. **22**(6).

Marangoni, A.G. and Wesdorp, L.H. 2013. *Structure and Properties of Fat Crystal Networks: Second Edition*. Boca Raton, FL: CRC Press.

Mazzanti, G., Marangoni, A.G. and Idziak, S.H.J. 2005. Modeling phase transitions during the crystallization of a multicomponent fat under shear. *Physical Review E - Statistical, Nonlinear, and Soft Matter Physics*. **71**(4).

Van Mechelen, J.B., Peschar, R. and Schenk, H. 2006. Structures of mono-unsaturated triacylglycerols. I. The β1 polymorph. *Acta Crystallographica Section B: Structural Science*. **62**(6), pp.1121-1130.

Metilli, L., Lazidis, A., Francis, M., Marty-Terrade, S., Ray, J. and Simone, E. 2021. The Effect of Crystallization Conditions on the Structural Properties of Oleofoams Made of Cocoa Butter Crystals and High Oleic Sunflower Oil. *Crystal Growth and Design*. **21**(3), pp.1562-1575.

Murtaza, M.A., Pandya, A.J. and Khan, M.H.M. 2017a. Buffalo milk: Buffalo milk production *In*: Young W. Park, George F. W. Haenlein and William L. Wendorff, eds. *Handbook of Milk of Non-Bovine Mammals: Second Edition*. Oxford, UK: Wiley Blackwell, pp.261-283.

Murtaza, M.A., Pandya, A.J. and Khan, M.H.M. 2017b. Buffalo milk: Buffalo milk utilization for dairy products *In*: Y. W. Park, G. F. W. Haenlein and W. L. Wendorff, eds. *Handbook of Milk of Non-Bovine Mammals: Second Edition*. Oxford, UK: Wiley Blackwell, pp.284-342.

Pink, D.A., Hanna, C.B., Sandt, C., MacDonald, A.J., MacEachern, R., Corkery, R. and Rousseau, D. 2010. Modeling the solid-liquid phase transition in saturated triglycerides. *Journal of Chemical Physics*. 132(054502).

Povey, M.J.W. 2014. Crystal nucleation in food colloids. *Food Hydrocolloids*. **42**, pp.118-129.

Rigolle, A., Van Den Abeele, K. and Foubert, I. 2018. Conventional and New Techniques to Monitor Lipid Crystallization *In*: K. Sato, ed. *Crystallization of Lipids: Fundamentals and Applications in Food, Cosmetics and Pharmaceuticals*. Hoboken, NJ: Wiley Blackwell, pp.465-492.

Rousset, P. 2002. Modeling Crystallization Kinetics of Triacylglycerols *In*: A. G. Marangoni and S. S. Narine, eds. *Physical Properties of Lipids*. New York: Marcel Dekker.

Sadeghpour, A., Ladd Parada, M., Vieira, J.J., Povey, M., Rappolt, M., Parada, M.L., Vieira, J.J., Povey, M. and Rappolt, M. 2018. Global Small-Angle X-ray Scattering Data Analysis of Triacylglycerols in the Molten State (Part I). *J. Phys. Chem. B*. **122**(45), pp.10320-10329.

Sato, K. 2018a. Introduction: Relationships of Structures, Properties, and Functionality *In*: K. Sato, ed. *Crystallization of Lipids: Fundamentals and Applications in Food, Cosmetics and Pharmaceuticals*. Hoboken, NJ: Wiley Blackwell, pp.1-15.

Sato, K. 2001. Molecular Aspects in Fat Polymorphism *In*: N. Widlak, R. Hartel and S. Narine, eds. *Crystallization and Solidification Properties of Lipids*. Champaign, Illinois, Illinois: AOCS Press, pp.1-17.

Sato, K. 2018b. Polymorphism of Lipid Crystals *In*: K. Sato, ed. *Crystallization of Lipids: Fundamentals and Applications in Food, Cosmetics and Pharmaceuticals*. Hoboken, NJ: Wiley Blackwell, pp.17-60.

Sato, K., Goto, M., Yano, J., Honda, K., Kodali, D.R. and Small, D.M. 2001. Atomic resolution structure analysis of β′ polymorph crystal of a triacylglycerol: 1,2-dipalmitoyl-3-myristoyl-sn-glycerol. *Journal of Lipid Research*. **42**(3), pp.338-345.

Sato, K. and Ueno, S. 2005. Polymorphism in Fats and Oils *In*: F. Shahidi, ed. *Bailey's Industrial Oil and Fat Products Sixth Edition*. Wiley-Interscience., 1:77-120.

Sato, K., Yoshimoto, N. and Arishima, T. 1989. Crystallization phenomena in fats and lipids. *Journal of Dispersion Science and Technology*. **10**(4-5), pp.363-392.

Schnablegger, H. and Singh, Y. 2013. *The SAXS Guide: Getting acquainted with the principles* 3rd ed. Graz: Anton Paar GmbH.

Small, D.M. 1984. Lateral chain packing in lipids and membranes. *Journal of Lipid Research*. **25**(13), pp.1490-1500.

Timms, R.E. 1980. The phase behaviour and polymorphism of milk fat, milf fat fractions and fully hardened milk fat. *The Australian Journal of Dairy Technology*. **35**, pp.47-52.

Tomaszewska-Gras, J. 2013. Melting and crystallization DSC profiles of milk fat depending on selected factors. *Journal of Thermal Analysis and Calorimetry*. **113**(1), pp.199-208.

Tzompa-Sosa, D.A., Ramel, P.R., Van Valenberg, H.J.F. and Van Aken, G.A. 2016. Formation of β Polymorphs in Milk Fats with Large Differences in Triacylglycerol Profiles. *Journal of Agricultural and Food Chemistry*. **64**(20), pp.4152-4157.

Wanapat, M. and Chanthakhoun, V. 2015. Buffalo production for emerging market as a potential animal protein source for global population. *Buffalo Bulletin*. **34**(2), pp.169-180.

Wright, A.J., Narine, S.S. and Marangoni, A.G. 2000. Comparison of experimental techniques used in lipid crystallization studies. *JAOCS, Journal of the American Oil Chemists' Society*. **77**(12), pp.1239-1242.

Zicarelli, L. 2020. Current trends in buffalo milk production. *Journal of Buffalo Science*. **9**, pp.121-132.

Chapter 3 The Unique Crystallisation Behaviour of Buffalo Milk Fat

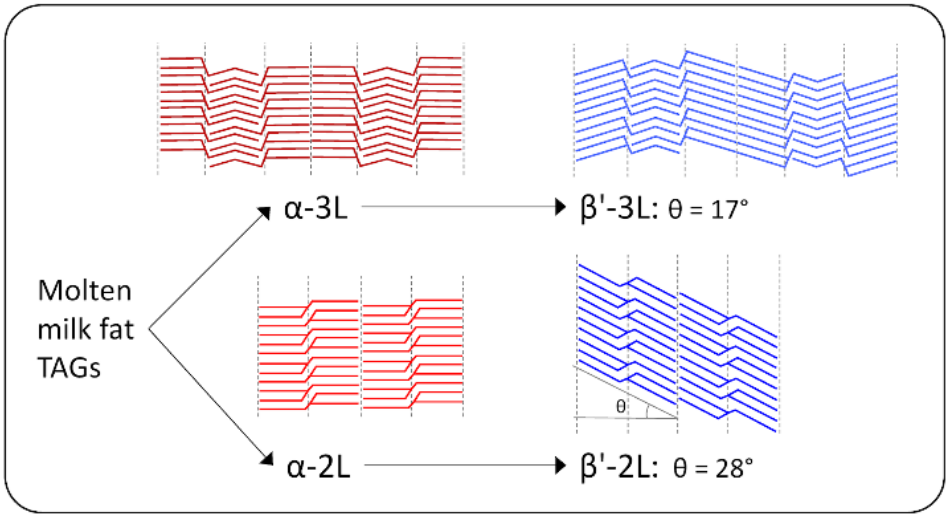

3.1 Abstract

Full comprehension of milk fat crystallisation is important for the structural development of dairy products such as butter, ice cream and cheese. The influence of triacylglycerols (TAGs) composition on the dynamics of milk fat crystallisation and the nanostructure of the formed crystals was investigated using two chemically different types of milk fat, namely buffalo and cow milk fat (BMF; CMF). TAG composition was determined using liquid chromatography and mass spectrometry (LCMS) whereas differential scanning calorimetry (DSC), small and wide-angle X-ray scattering (SAXS and WAXS) and polarised light microscopy (PLM) were used to characterise the crystallisation behaviour of the two milk fats. 37 TAG species were identified in both, BMF and CMF, but in different proportions. In particular, BMF was found to have a higher amount of low molecular weight TAGs compared to CMF. This difference in chemical composition explains the different kinetics of polymorphic transformation in the two samples. Specifically, it clarifies the delay in the nucleation of the β'-polymorph in BMF compared to CMF. BMF also showed higher nucleation rate due to its higher proportion of saturated TAGs and higher melting range. Finally, this work presents a novel interpretation for the mechanism of formation of the β-polymorph (53 Å), which has recently become subject of a vivid debate in milk fat crystallisation studies.

Keywords: buffalo milk fat, crystallisation, polymorph and triacylglycerols

3.2 Introduction

Buffalo milk (BM) is the second most produced type of milk, comprising 15% of the global milk production in 2018. Furthermore, the production of BM is increasing while cow milk (CM) has decreased its presence on the market from 83 to 81 % between 2014 and 2018 (FAO, 2022b). BM is usually considered a premium product due to its greater whitening effect to tea and coffee (Murtaza et al., 2017b) and due to its distinct melting properties that allow its use for the manufacturing of a type of mozzarella cheese known as *Mozzarella di Bufala* (Angelis and Gobbetti, 2011). Most importantly, BM contains a higher level of milk solids when compared to CM (**Table 3.1**); therefore, generating higher yield of solid-based dairy products such as cheese during processing.

Table 3.1 Buffalo and cow milk solids composition.

Component	**Buffalo** (Abd El-Salam and El-Shibiny, 2011)	**Buffalo** (Gantner et al., 2015)	**Buffalo** (Zhou et al., 2018)	**Cow** (Gantner et al., 2015)
Total solids (g/100g)	16.3-18.4	16-17	17.74-19.03	12-13
Fat (g/100g)	6.6 - 9.6	5.3-15.0	6.77-7.82	3.3-6.4
Protein (g/100g)	2.7-5.2	2.7-4.7	4.54-4.92	3.0-4.0
Lactose (g/100g)	4.51-5.24	3.2-4.9	5.13-5.28	4.5-5.6
Ash (g/100g)	0.71-0.85	0.8-0.9	ND	0.7-0.8

ND: not defined.

Milk solids hold an important role in the structure development of dairy products. In particular, the structure, stability and overall quality of fat-based products such as butter and ice cream are largely influenced by the milk fat crystallisation behaviour. In fact, the way milk fat crystallises defines the size and shape distribution of crystals within the product and also their internal nanostructure (polymorphism). All these crystal properties dictate important quality attributes of dairy products, such as mouthfeel, melting point, spread-ability, texture, and rheological properties (Martini and Marangoni, 2007).

Milk fat is a complex fat comprising of a wide variety of different TAGs. Identification of fat polymorphism is commonly investigated with X-ray scattering techniques. The periodicity of crystal structures give rise to X-ray diffraction patterns which can be observed in the small and wide angle regions, which correspond to the long and short spacings, respectively (Idziak, 2018). The long spacings correspond to the longitudinal, lamellar stacking of TAG molecules, displaying mostly two (2L) or three (3L) chain length repeating planar structures. On the molecular level, the short spacings indicate the fat crystal sub-cell or lateral packing structure, which commonly denoted as sub-α (γ), α, β' and β polymorph, in the order of increasing stability (D'Souza et al., 1990; Grotenhuis et al., 1999).

For advancing our understanding on the unique crystallisation behaviour of BMF in this study, we will discuss our findings in relation to other, mainly CMF investigations, that were focussed on the crystallisation behaviour, determining the role of TAGs and fatty acids composition (Shi et al., 2001; Lopez et al., 2006; Tzompa-Sosa et al., 2016), fractionation process (Marangoni and Lencki, 1998; Van Aken et al., 1999), cooling rates (Grotenhuis et al., 1999; Campos et al., 2002; Lopez et al., 2005), shear rate (Mazzanti et al., 2009), the presence of minor components (Amanda J. Wright, Hartel, et al., 2000), solvent addition (Amanda J. Wright, McGauley, et al., 2000), and other processing conditions (Van-Aken and Visser, 2000). At least five crystalline sub-cell species have been observed in milk fat: α and sub-α, two β' and one β type polymorphs, several of them were found in coexistence, depending on the thermal profile applied to generate milk fat crystals. Lamellar structures with 2L-architecture were found to display thicknesses between 4 to 4.8 nm and 3L-lamellar organizations of TAG are reported to have thicknesses from 5.4 to 7.2 nm (Lopez, 2018). All these crystalline structures always appear to coexist with the isotropic liquid phase, even at low temperature (e.g., 4 °C) (Lopez et al., 2005).

Among all sub-cell species, the α- and β'-polymorph of milk fat are the most common, while sub-α and β-polymorph are only rarely observed (Grotenhuis et al., 1999; Lopez et al., 2005; Ramel and Marangoni, 2017). The polymorphism of milk fat was found to be strongly affected by TAGs and fatty acids composition. In particular, the olein-rich fraction of milk fat can crystallise only in the α-polymorph, while both α- and β'-polymorph can form in the stearin-rich fractions upon cooling at 1 °C/min (Lopez et al., 2006). The sub-α (γ) form was only reported to appear upon fast cooling below -8 °C (Grotenhuis et al., 1999; Lopez et al., 2005). On the bases of WAXS

measurements, this polymorph was described as a low-melting β′-modification with orthorhombic chain packing. The presence of a β-polymorph in milk fat has been subject of debate, as this structure was not found in milk fat (Grotenhuis et al., 1999), or forming only via applying a fast cooling rate followed by an isothermal hold for a long time (Mazzanti et al., 2004). Further, experimental evidence suggests that the stability and kinetics of crystallisation of these crystal structures are affected by the TAGs and fatty acids composition of milk fat. Tzompa-Sosa, et al. (2016) studied the crystallisation behaviour of different milk fat samples of varying TAGs composition and found that the nucleation of the β-polymorph was promoted by the presence of unsaturated TAGs with carbon numbers around 52-54. Nevertheless, the same study showed that the β'-polymorph was the dominant structure in most samples at ambient conditions.

The TAG' configurational symmetry has been linked with polymorphic outcome during crystal formation (Sato, 2001). In general, TAGs containing uniform or symmetrical fatty acids follow the typical α → β'→ β transformation. Whilst, asymmetrical TAGs, i.e., TAGs with combination of UUS or SSU, in which the solitary unsaturated (U) or saturated (S) fatty acid resides on either the sn-1 or sn-3 position or TAG with acyl chain length differences greater than 2 carbon atoms, are more prevalent in the β'-polymorph. A previous study also showed that milk fat comprise of many asymmetrical TAGs, which contain short chain butyric acid (Lopez et al., 2006).

The types of TAGs and fatty acids in milk fat depends on the season and the geographical regions where cows are grown (Shi et al., 2001; Tzompa-Sosa et al., 2018); and these variations, albeit small, can strongly affect crystallisation behaviour (Shi et al., 2001; Larsen et al., 2014). Compositional differences in milk fats obtained from different animals (e.g., buffalo *vs.* cow) are more significant than variation within the same species (Ménard et al., 2010; Gantner et al., 2015). Those differences are currently not fully characterised, but they could have a significant impact on the crystallisation and melting behaviour of milk fat; as shown by a small number of crystallisation studies carried out on non-bovine milk fat, such as goat and camel (Karray et al., 2004; Amara-Dali et al., 2005; Karray et al., 2005; Amara-Dali et al., 2007).

The TAGs composition of milk fat can be investigated using various chromatography techniques, combined with molecular mass identification analysis (Mottram and Evershed, 2001; Gastaldi et al., 2011; Zhou et al., 2014; Ten-Doménech et al., 2015). Previous studies (Arumughan and

Narayanan, 1982; Ménard et al., 2010; Abd El-Salam and El-Shibiny, 2011; Smiddy et al., 2012; Penchev et al., 2016) only determined the fatty acids composition and total carbon number of each TAG forming buffalo milk fat, indicating that buffalo milk fat has a higher content of saturated fatty acids (SFA) compared to cow milk fat (Ménard et al., 2010; Abd El-Salam and El-Shibiny, 2011; Murtaza et al., 2017b). To the best of our knowledge, the current work is the first to determine exactly the TAGs composition of buffalo milk fat, and to investigate how the individual, structural configuration of TAGs in this type of fat affect its crystallisation and melting behaviour. The aim of our study is to compare the crystallisation behaviour of buffalo and cow milk fat, particularly the dynamics of α, β', and β -polymorph formation, and understand the role played by the TAG compositional differences.

The results presented here will allow a more rational design of novel dairy products for targeted applications (e.g., products with higher crystallinity or more stable polymorphs for tropical countries' markets) as well as promote a more widespread use of buffalo milk fat.

3.3 Materials and Methods

3.3.1 Sample Preparation

Milk fat (ghee) was prepared from unsalted butter following the heat clarification method (Ganguli and Jain, 1973). Unsalted La Marchesa buffalo butter was purchased from La Marchesa (Terevola-Italy) and unsalted Lurpak cow butter (Arla Foods, Denmark) was obtained from a local grocery store. The two types of butter contain approximately 82% of milk fat. 250 g of butter was heated to a temperature of 110-120 °C for at least 15 minutes, under constant stirring in order to remove the moisture. Heating was stopped when no more water vapour bubbles were observed (indicating complete removal of water), and the molten butter turned clear with visible suspended solid (milk protein) at the bottom. The milk fat was separated by the precipitated solids by filtering the molten butter it through three layers of fine muslin cheese cloth (Homestead Farm Supplies, Banbury-UK). The resulted milk fat contained ≥ 99.5% of fat, as confirmed in a total fat analysis using the Soxhlet method. Resulted milk fat was then kept in amber bottle at chill temperature for further analysis.

3.3.2 Analysis of Milk Fat TAG Composition

LCMS grade isopropanol, acetic acid and ammonium acetate (Optima LC/MS) were obtained from Fisher Chemical (USA). LCMS grade methanol (LichroSolv) was obtained from Merck (Germany). Lipid standards: a standard TAG mixture (17811-1AMP) was obtained from Sigma-Aldrich (Merck KGaA, Darmstadt, Germany). Acetone was obtained from VWR Chemicals. Nylon syringe filter 0.22µm was purchased from Gilson Scientific Ltd (Dunstable-UK).

25 mg of milk fat was added to 2 ml of acetone and 2 ml of 18% (v/v) isopropanol in methanol (IPA/MeOH). Further dilution was carried out using acetone and IPA/MeOH 1:1 (v/v) until the final concentration of 250 µg/ml. For complete dissolution, the sample was subsequently heated in a water bath at 70 °C for 5 minutes to avoid the reprecipitation of solid milk fat in the cold solvent. The mixture was then filtered using a nylon syringe filter and inserted into the injection vial. A TAG mixture standard was prepared with the same procedure.

Milk fat TAG composition measurements were performed according to the procedure described by Zeb and Murkovic (2010) using a Shimadzu LCMS 2020 (Japan) and processed with the LabSolutions software (version 5.97). A separation column Phenomenex Luna 3u C18(2) 100A LC Column 150 x 3.0 mm was used. The mobile phase consisted of 18% (v/v) isopropanol in methanol (0.1% (v/v) acetic acid) plus 0.05% (v/v) of ammonium acetate. The samples were eluted in an isocratic system with flow rate of 0.6 ml/min. The spectrometric conditions were: positive ESI mode, fragmentor potential of 150 V, drying gas temperature of 350 °C and capillary voltage of 4000 V. The column oven and autosampler chamber temperature were maintained at 40 °C in order to ensure dissolution of the fat samples. The mass spectra were obtained at an m/z range of 200 to 1000 with an elution time of 50 minutes. Each sample was measured in 4 replicates. The TAG mixture standard was used as a control of the method efficiency and as an internal standard.

The identification of chromatogram peak was achieved by mass spectra analysis where main spectra corresponds to the TAG molecular weight (Zeb and Murkovic, 2010). Whilst the fragments spectra could be used to identify the TAG configuration because fatty acid at sn-2 position tended to be easier to be lost than that at sn-1/3 positions (Zeb and Murkovic, 2010; Zhou et al., 2014). However, the present study fragments spectra intensity were not strong enough to make a justifiable positional isomer identification. Hence the

present TAG configuration is based on existing literature with similar spectra profiles (Zhou et al., 2014) with possibility of other isomer configuration.

Perpendicular separation (Norman Dyson, 1998) was uniformly applied to less-resolved peaks. Relative concentration of each TAG is calculated as the ratio between a specific peak area and the total area resulting from the sum of all the recorded peaks (including the non-TAG-identified peak areas). Statistical analysis of the data was carried out using the *t-Test* routine in Microsoft Excel Analysis ToolPak, where a p-value <0.05 indicates a statistical significance. OriginPro 2018 (OriginLab, Massachusetts, USA) was used for data pre-processing, including baseline correction and peak intensity normalisation using the highest-intensity peak.

3.3.3 Differential scanning calorimetry (DSC) measurements

Samples of molten milk fat (10±3 mg) were weighed and sealed hermetically in aluminium pans (Tzero, TA Instruments, Elstree-UK). The exact weight of each sample was used to normalise the acquired heat flow data and an empty pan was used as a reference. Heat flow measurements were performed in a DSC Q-20 (TA Instruments, Elstree-UK) following a cooling and heating cycle with three different scan rates, i.e., 0.5, 2 and 10 °C/min. The samples were brought to 60 °C and held at such temperature for 10 minutes, to erase any crystal memory before being cooled down to -40 °C with the aforementioned rates. The samples were held at -40 °C for 5 minutes, before being subjected to a heating ramp back to 60 °C using the same scan rate as before. The data analysis was performed using TA Universal Analysis 2000 software (version 4.5A). Subsequent baseline correction, plotting and integration of the peaks were carried out using the OriginPro 2018 software. All measurements were performed in four replicates and data were presented as average value ± standard deviation. *t-Test* analysis on the relative concentration of each milk fat fraction was performed in Microsoft Excel Analysis.

3.3.4 X-ray scattering measurements and analysis

Small angle X-ray scattering (SAXS) and wide-angle X-ray scattering (WAXS) measurements were carried out with a SAXSpace instrument (Anton Paar GmbH, Graz, Austria). The instrument uses a Cu-anode (λ = 0.154 nm) and operates at 40 kV and 50 mA. The sample chamber is equipped with a TCstage 150 Peltier element (Anton Paar GmbH, Graz, Austria), which provides a temperature control in a range of -30 to 150 °C (± 0.1 °C).

Simultaneous SAXS/WAXS measurements were performed at a sample-detector distance (SDD) of 130 mm, which cover a *q*-range from 0.01 to 1.76 $Å^{-1}$ ($q = 4\pi \sin\theta/\lambda$ with 2θ being the scattering angle). The 1D scattering patterns were recorded with a Mythen micro-strip X-ray detector (Dectris Ltd, Baden, Switzerland).

Milk fat samples were molten on a hot plate prior to injection into quartz disposable capillaries (Capillary Tube Supplies Ltd., Cornwall-UK) of outside diameter of 1.5 mm. The capillaries were subsequently sealed with wax and epoxy glue.

SAXS/WAXS measurements were carried out using three thermal protocols. First, milk fat samples were heated to 60 °C and equilibrated for 10 minutes in order to completely melt and erase any crystal memory. This was followed by cooling at 2 °C/min to -10 °C and final isothermal conditions for 5 hours. A 60 s exposure time was used to collect X-ray patterns every 30 minutes during isothermal conditions. The second thermal protocol included the melting procedure previously described followed by cooling at three different rates, i.e., 0.5, 2 and 4 °C/min down to -10 °C. A 30 s exposure time was used to collect measurements every minute during the cooling ramp. In the third protocol, the capillaries were stored in a freezer (*ca*. -18 °C) for three weeks and subsequently transferred into the SAXSpace sample chamber. The samples were equilibrated at -10 °C for 15 minutes, followed by heating at 2 °C/min to 60 °C. X-ray patterns were collected every minute with an exposure time of 30 s.

The position of the primary beam of all diffraction patterns was set to zero using the SAXSTreat software (Anton Paar GmbH, Graz, Austria). Using the SAXSQuant software (Anton Paar GmbH, Graz, Austria), all recorded scattering patterns were normalised for their transmission, i.e., divided by their measured transmitted direct beam intensity. From each normalised sample pattern, the normalised empty capillary scattering was then subtracted. The resulting patterns are smeared in the small angle regime, approximately from $q = 0$ to $q = 0.25$ $Å^{-1}$, due to the line collimation focus of the X-ray camera. In few cases (as indicated in the results section), the scattering contribution from molten TAG was also subtracted from the total pattern. OriginPro 2018 was used for plotting the patterns and for carrying out peak fit analysis.

3.3.5 Electron Density Profile (EDP) determination by classical Fourier analysis

EDPs of the α-, β'- and β-phases were determined by standard procedures (Li et al., 2017; Ladd Parada et al., 2018). In brief, the Bragg diffraction peaks were fitted by a Lorentzian distribution function and additionally fitting the diffuse scattering contributions with second degree polynomials. The intensities were Lorentz corrected (note, for our quasi line-focus set-up with 20 mm width by 0.2 mm height, an experimentally determined correction factor of $h^{1.5}$ was applied; this compares to a Lorentz correction for an ideal point focus of h^2 and for an ideal line focus of h, respectively), and finally, the square root of the corrected intensities resulted in the form factor values, F_h. Note, in case of centrosymmetric EDPs, the Fourier transform is obtained by the summation of cosine terms only:

$$\Delta\rho(z) = \sum_{h=1}^{h_{max}} \alpha_h F_h \cos\left(\frac{2\pi z h}{d}\right)$$

Eq. (3.1)

where $\Delta\rho$ is the electron density contrast, h the Miller index (diffraction order), α_h the phases (note, α_h is fixed to -1 for h = 1 and ±1 for h > 1), z is the real space variable, i.e., describing the real-space axis perpendicular to the lamellae, and d denotes the lattice spacing. The phases α_h for h > 1 were taken from literature (Mykhaylyk and Hamley, 2004) (determined F_h and applied phases are listed in **Table A.2** and **A.3**).

3.3.6 Polarised Light Microscopy (PLM) measurements

Milk fat crystals formed during cooling crystallisation experiments were observed using a Leitz Dialux 22 microscope (Leitz, Wetzlar, Germany) at 40x magnification, coupled with a Canon EOS 7D Mark II (Canon, Japan) digital camera. A Linkam CSS 450 hot stage (Linkam Instruments, Tadworth-UK) and the Linksys 32 software data capture system (Linkam Instruments, Tadworth-UK) were used to control the temperature profile during the crystallisation. 50 µL of milk fat sample was placed in the hot stage sample chamber with the thickness (gap) set to 100 µm. The sample was brought to 60 °C for 10 minutes in order to melt any crystal present. Subsequently, the samples were cooled at 0.5 or 2 °C/min. Images (4864 x 3648 pixel) were collected during the crystallisation process and scaled using 1 mm graticule at the same resolution. The image contrast was enhanced for publication

purpose and the area, *A*, of each crystalline object was measured individually using the freehand tool of ImageJ 1.53a software (NIH, USA). The crystal size is expressed with its diameter, *D*, assuming a nearly circular section of the crystals with $D = \sqrt{(4A/\pi)}$.

3.4 Results and Discussion

3.4.1 TAG composition of BMF and CMF

As shown in **Figure 3.1** and **Table 3.2**, 38 different TAGs from BMF and CMF were separated in the present work, and 37 of them have been successfully identified. **Figure A.1** and **Table A.1** in supplementary information present details on the peak identification procedure.

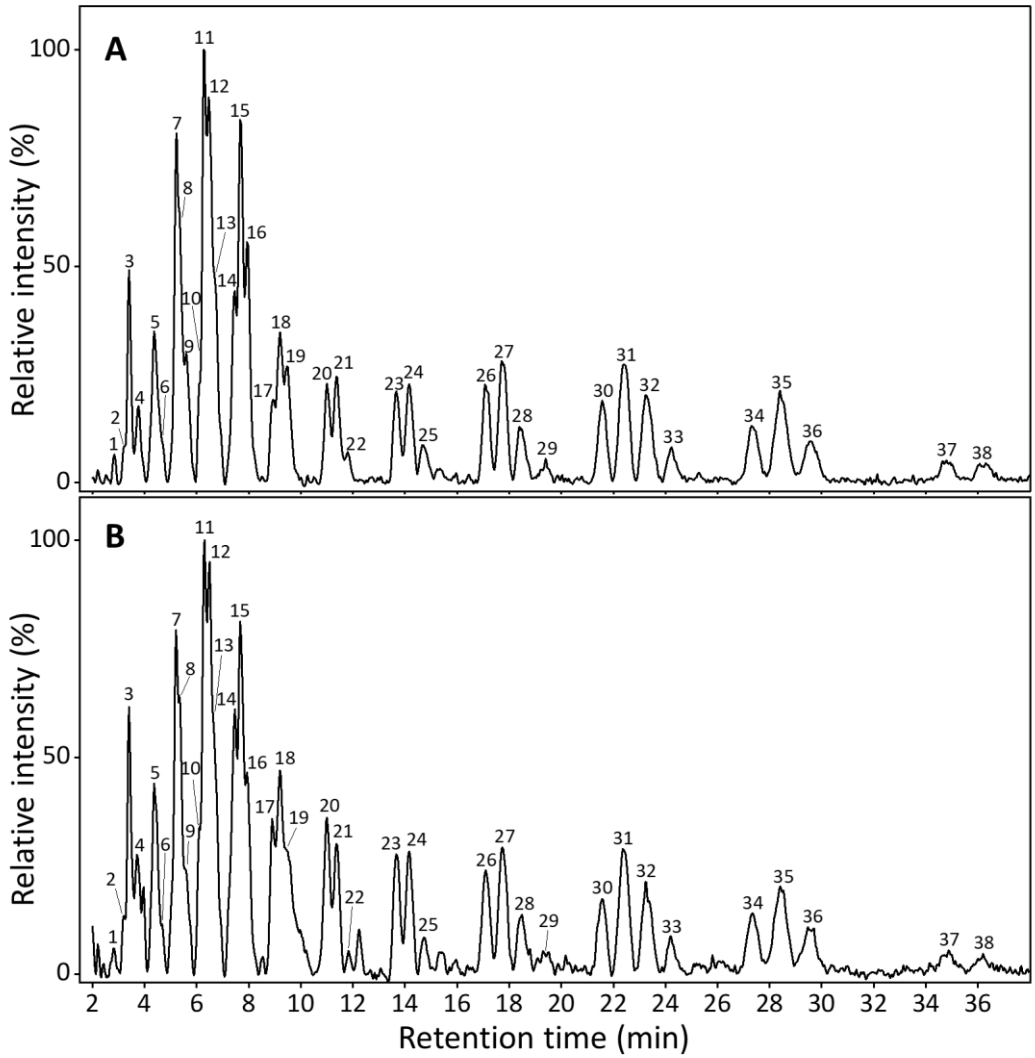

Figure 3.1 Baseline-corrected chromatograms of (A) buffalo milk fat and (B) cow milk fat triacylglycerol composition. For the identified triacylglycerol 1 to 38 refer to Table 3.2.

Table 3.2 Compositional characterisation of buffalo milk fat and cow milk fat.

Peak #	RT (min)	TAG Structure*	$[M+ NH_4]^+$	TAG weight fraction (% w/w) (mean ± SD) *n=4*		
				BMF	CMF	*p*
1	2.8	Bu-Co-P	516.4	1.10±0.18	1.23±0.22	0.400
2	3.2	Bu-C-M	544.5	1.27±0.39	0.77±0.10	0.087
3	3.4	n/i	750.5	2.98±0.26	2.70±0.19	0.147
4	3.8	Bu-C-P	572.5	2.08±0.26	1.72±0.22	0.084
5	**4.4**	**Bu-La-P**	**600.5**	**2.61±0.15**	**2.32±0.15**	**0.038**
6	4.5	Bu-La-O	626.5	2.14±0.34	2.01±0.11	0.491
7	5.2	Bu-M-P	628.5	4.28±0.31	4.16±0.17	0.514
8	**5.3**	**Bu-M-O**	**654.5**	**3.12±0.44**	**2.42±0.21**	**0.045**
9	**5.6**	**Bu-P-L**	**680.5**	**2.91±0.27**	**2.44±0.20**	**0.031**
10	6.1	Co-M-P	656.6	1.65±0.22	2.03±0.25	0.059
11	**6.3**	**Bu-P-P**	**656.6**	**5.32±0.24**	**4.27±0.22**	**0.001**
12	**6.5**	**Bu-P-O**	**682.6**	**4.49±0.35**	**3.54±0.28**	**0.005**
13	**6.7**	**Bu-O-O**	**708.6**	**3.69±0.18**	**3.18±0.29**	**0.031**
14	**7.5**	**Co-P-P**	**684.6**	**3.11±0.08**	**3.74±0.22**	**0.006**
15	**7.7**	**Bu-P-S**	**684.6**	**4.57±0.36**	**3.93±0.24**	**0.032**
16	**7.9**	**Bu-S-O**	**710.6**	**3.48±0.17**	**2.62±0.19**	**0.001**
17	**8.9**	**P-P-Cy**	**712.6**	**1.33±0.14**	**1.92±0.02**	**0.003**
18	9.2	Co-S-P	712.6	2.44±0.14	2.75±0.21	0.055
19	9.5	P-Cy-O	738.7	2.28±0.28	2.63±1.01	0.550
20	**11.0**	**P-P-C**	**740.7**	**1.74±0.05**	**2.62±0.18**	**0.002**
21	**11.4**	**P-C-O**	**766.7**	**1.90±0.06**	**2.40±0.07**	**<0.001**
22	**11.8**	**C-O-O**	**792.7**	**0.82±0.09**	**1.14±0.08**	**0.002**
23	**13.7**	**La-P-P**	**768.7**	**1.72±0.09**	**2.09±0.08**	**0.001**
24	**14.2**	**P-La-O**	**794.7**	**2.01±0.08**	**2.38±0.08**	**0.001**
25	**14.7**	**P-M-L**	**820.7**	**1.36±0.06**	**1.62±0.09**	**0.005**
26	17.1	M-P-P	796.7	2.08±0.12	2.11±0.09	0.732
27	17.7	P-M-O	822.7	2.95±0.18	2.91±0.04	0.682
28	18.4	O-M-O	848.7	2.39±0.02	2.43±0.11	0.550
29	19.4	O-P-L	874.7	1.80±0.12	1.78±0.14	0.858
30	**21.6**	**P-P-P**	**824.7**	**2.09±0.12**	**1.86±0.11**	**0.034**
31	22.4	O-P-P	850.7	3.65±0.20	3.35±0.12	0.055
32	23.2	P-O-O	876.8	3.42±0.24	3.31±0.14	0.467
33	24.2	O-O-O	902.7	1.72±0.12	1.71±0.13	0.925
34	**27.3**	**P-P-S**	**852.8**	**1.67±0.08**	**1.39±0.12**	**0.015**
35	**28.4**	**S-P-O**	**878.8**	**2.66±0.15**	**2.27±0.07**	**0.010**
36	29.6	O-O-S	904.8	1.50±0.04	1.43±0.17	0.442
37	34.8	S-P-S	880.8	0.72±0.07	0.64±0.10	0.242
38	**36.3**	**S-S-O**	**906.8**	**0.66±0.06**	**0.56±0.02**	**0.036**
Non-identified molecules				**8.30**	**11.59**	
Total				**100**	**100**	

RT: retention-time; TAG: triacylglicerols; $[M+NH_4]^+$: molecular mass of TAG + ammonium ion; BMF: buffalo milk fat; CMF: cow milk fat; *n*: number of measurements; SD: standard deviation; *p*: value of ≤ 0.5 indicate statistical significance; Bu: butyric (C4), Co: caproic (C6), Cy: caprylic (C8), C: capric

(C10), La: lauric (C12), M: myristic (C14), P: palmitic (C16), S: stearic (C18), O: oleic (C18:1), L: linoleic (C18:2) fatty acid. Results in bold show significant difference between BMF and CMF weight fraction (p<0.05). *TAG configuration includes possible positional isomers, e.g., OOS and OSO.

Figure 3.1 shows that BMF and CMF present similar TAG species. Out of 37 identified TAG, 13 were asymmetrical (fatty acids with acyl chain length difference greater than two carbon atoms) (Sato, 2001), where the low carbon number butyric acid is attached to longer chained fatty acids like palmitic or oleic acid. 17 of the TAGs identified were fully saturated, 13 contained one unsaturated fatty acid and 7 were contained more than one. The weight fractions of each CMF TAG in this work are in agreement with a previous study, where BuPP, BuMP, BuPO, OPP, and POO were among the most abundant TAGs (Lopez et al., 2006). The most abundant TAGs in BMF are BuPP, BuPS, BuPO and BuMP.

Notwithstanding the similarity in TAG species, BMF has 20 out of 37 TAGs whose weight fractions are significantly different from CMF. This includes BuMO, BuPP, BuPO, BuOO, CoPP, BuPS, and BuSO, which were found to be present in BMF in weight fraction >3%. BMF is known to have a higher amount of saturated fatty acids compared to CMF (Abd El-Salam and El-Shibiny, 2011). This was confirmed by the results present here, which show that fully saturated TAGs such as PPP and PPS are more abundant in BMF compared to CMF (significantly different ratios, p<0.05). PPP and PPS weight fractions are 2.09% and 1.67% in BMF versus 1.86% and 1.39% in CMF. Another fully saturated TAG, SPS was also found in higher concentration in BMF compared CMF, albeit the difference was statistically insignificant (**Table 3.2**).

A complete comparison of BMF and CMF in terms of weight fractions of TAG is shown in **Figure 3.2**. BMF had a higher number of TAG exiting the chromatographic column at early and late retention-time compared to CMF. In contrast, CMF had more TAG exiting at medium retention-times.

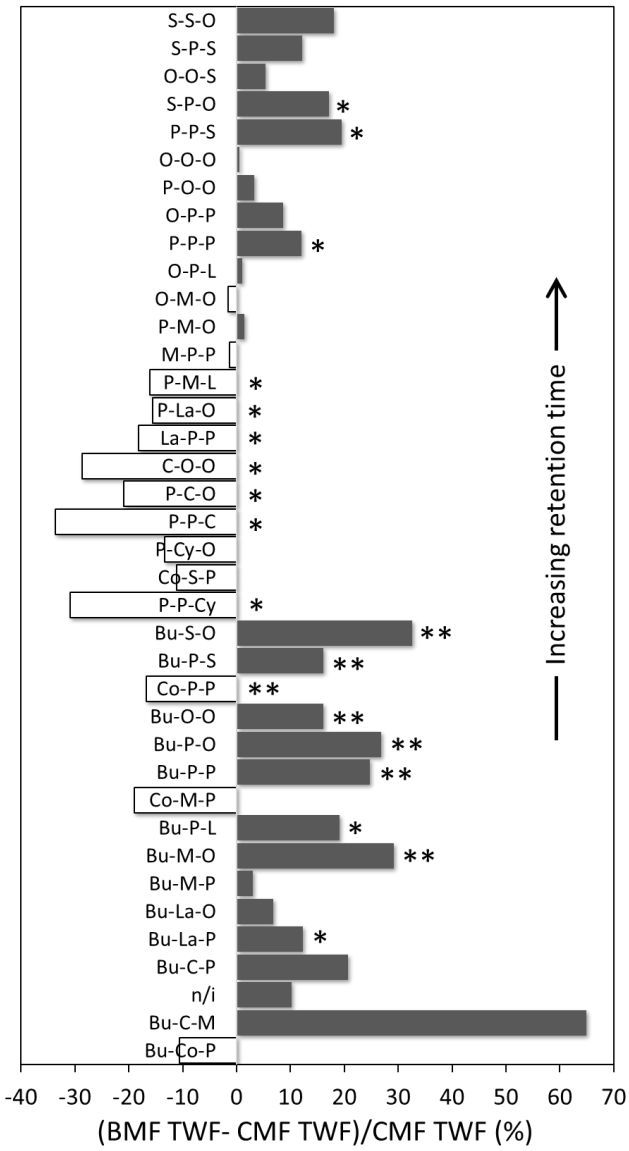

Figure 3.2 Percentage difference of buffalo milk fat (BMF) compared to cow milk fat (CMF) triacylglycerol (TAG) composition. Positive values indicate higher relative TAG concentration in BMF. TWF: triacylglycerol weight fraction, for other abbreviations refer to Table 1. TAG configuration includes possible positional isomers, e.g., OOS and OSO. *The difference between both fats is statistically significant ($p<0.05$). **The difference between both fats is statistically significant ($p<0.05$) and the TAG weight fraction is >3% in one or both milk fats.

Early retention-time TAGs containing capronic acid (BuCoP, CoMP and CoPP) were found in lower concentrations in BMF compared to CMF. Whereas BMF contained more TAGs presenting butyric acid. The latter finding is in agreement with previous literature (Ménard et al., 2010). In addition to the identified TAGs, the amount of unknown matters (including the non-identified peak number 3) were 11.28% and 14.29 % for BMF and CMF,

respectively. This portion most likely comprises DAGs and other TAGs in smaller amount, which could not be identified with the current separation and identification procedures (Lopez et al., 2006; Zhou et al., 2014).

3.4.2 Thermal characterisation of BMF and CMF

DSC cooling and heating thermograms for CMF and BMF are shown in **Figure 3.3**. The thermograms of the cooling step (**Figure 3.3** A, B, C) show that both BMF and CMF exhibited two exothermic peaks, which corresponded to the crystallisation of α-2L and α-3L polymorphs, respectively (Lopez, 2018). It was found that onset nucleation temperatures were higher, when the cooling rate decreased (as summarized in **Table 3.3**). For instance, at 10 °C/min cooling rate, the α-2L nucleated at 17.4 °C and 15.6 °C for BMF and CMF, respectively. Whereas, at 0.5 °C/min cooling rate, the nucleation started at 19.1 °C and 17.9 °C. These results are readily understood, since slower cooling rates offer more time for nuclei of critical size to form, thus nucleation processes are expected to be observed at lower degrees of undercooling compared to faster cooling rates.

It is interesting to note, that the onset nucleation of BMF occurred at a higher temperature than that of CMF at all three cooling rates (**Table 3.3**). In descending order of cooling rates (10, 2 and 0.5 °C/min), the BMF α-2L nucleated at 17.4, 18.7, and 19.9 °C, whilst the CMF α-2L nucleated at 15.6 °C, 16.6 and 17.9, respectively. Similarly, the onset nucleation of BMF α-3L also occurred at higher temperature than CMF. BMF α-3L nucleation was observed at 13.4, 14.9 and 13.7 °C (versus 10.4, 11.7 and 11.9 °C in CMF) for 10, 2 and 0.5 °C/min cooling rate. These findings are consistent with the chromatographic measurements. The higher nucleation temperature in BMF is attributed to higher content of fully saturated TAGs. These molecules, especially the long-chained PPP, PPS and SPS have the highest melting point among all other TAGs present in milk fat.

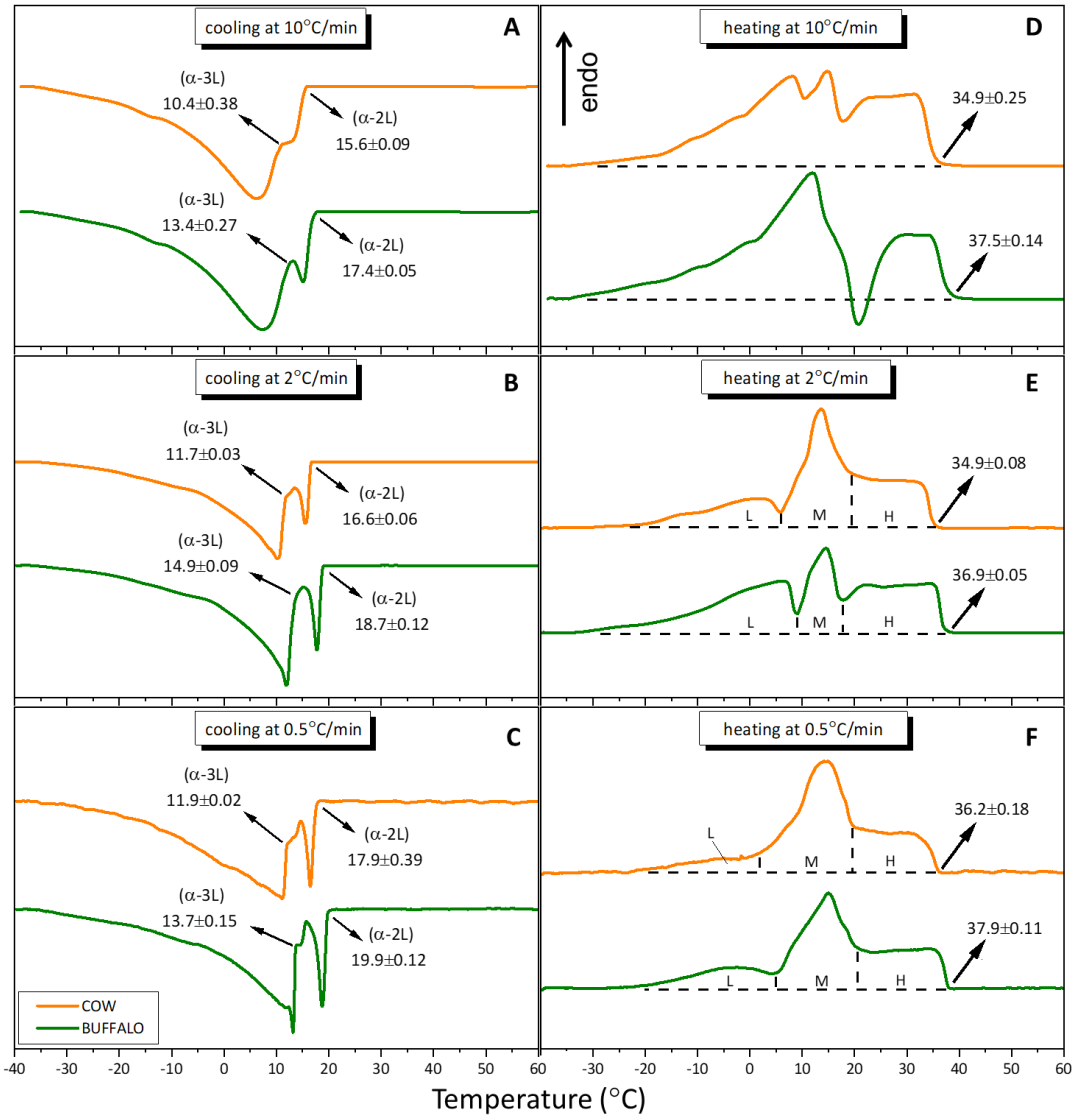

Figure 3.3 Thermograms of buffalo milk fat and cow milk fat on cooling (A, B, C) and on subsequent heating scans (D, E, F). Both, cooling and heating scans were carried out in the temperature interval of 60 °C to -40 °C. The applied scan-rates were 10, 2 and 0.5 °C/min, respectively. Arrows indicate associating crystallisation and melting events. L, M, and H indicate three distinguished melting fractions, see Table 3.4.

Figure 3.3 (D, E, F) show the BMF and CMF thermograms of the subsequent heating step after cooling. CMF typically displays three overlapping endothermic peaks, possibly as a result of three groups of TAGs that melt consecutively, namely the low-melting, middle-melting and high-melting fractions (Deffense, 1993; Grotenhuis et al., 1999). A previous study suggests that the presence of this peaks is a combined effect of the melting of each fraction and polymorphic transformations. Lopez et al. (2007) reported the structural evolution of sub-α ↔ α → β' → liquid on the heating of milk fat

globules at 2 °C/min after cooling at 1 °C/min. The current work is in agreement with the previous studies, where CMF exhibited three endothermic clustered peak-regions at all three different heating rates (10, 2 and 0.5 °C/min). In contrast, BMF showed three endothermic peak-regions only for the 2 and 0.5 °C/min heating rate. At 10 °C/min, we observed two endothermic and one exothermic peak. The position and shape of the endothermic peaks depends on the cooling rate, as different rates can result in different crystal polymorphs being formed (Van Aken et al., 1999; Lopez, 2018). It is also plausible that the exothermic peak represents a polymorphic transformation, as such transformations during the melting process are influenced by the heating rate (Lopez et al., 2007). Nonetheless, the current result indicates that BMF forms distinctly different polymorphs, when applying a 10 °C/min cooling and heating rate.

Table 3.3 Onset of nucleation and end of melting temperature of buffalo milk fat and cow milk fat at different rates.

Event		**Rate (°C/min)**		
		0.5	**2**	**10**
Onset of α-2L (°C)	BMF	19.9±0.12	18.7±0.12	17.4±0.05
	CMF	17.9±0.39	16.6±0.06	15.6±0.09
	p-value	0.006	0.002	0.004
Onset of α-3L (°C)	BMF	13.7±0.15	14.9±0.09	13.4±0.27
	CMF	11.9±0.02	11.7±0.03	10.4±0.38
	p-value	0.002	<0.001	0.005
End of Melting (°C)	BMF	37.9±0.11	36.9±0.05	37.5±0.14
	CMF	36.2±0.18	34.9±0.08	34.9±0.25
	p-value	0.04	0.005	0.06

BMF: buffalo milk fat; CMF: cow milk fat; values presented as mean ± SD, $n = 4$.

BMF shows an about 2 °C higher melting point compared to CMF (**Table 3.3**). The BMF melted completely at 37.5, 36.9, and 37.9 °C (versus 34.9, 34.9, and 36.2 °C in CMF) for 10, 2, and 0.5 °C/min heating rate, respectively. This result is explained by the fact that BMF has a significantly higher amount of fully saturated TAGs compared to CMF. Another aspect influencing the thermal stability concerns the polymorphic form, where more stable polymorphs (such as β’ and β) have higher melting points than the metastable α polymorphs. In

this respect, the 0.5 °C/min scan rate displayed the highest melting points for both milk fats, because the preceding slower cooling ramps lead to the formation of more stable polymorphs, whereas higher cooling rates tend to produce mainly metastable polymorphs.

We further measured the area under the endothermic peaks recorded at 2 and 0.5 °C/min heating rate for both, BMF and CMF. These values are largely related to the enthalpy of fusion of each melting fraction in the milk fat, and therefore, to their relative concentrations (**Table 3.4**). There are significant differences between the estimated BMF and CMF relative melting fractions. At both heating rates, BMF was found to be higher in the low- and high-melting fractions, whilst CMF was found higher in the middle-melting fraction. As mentioned previously, the endothermic profile is largely influenced by the cooling/heating rate, thus the difference in estimated melting/enthalpy fraction contribution at 2 and 0.5 °C/min heating rate was expected. A more distinct difference was found at 2 °C/min heating rate, where BMF low-, middle- and high- melting enthalpy fractions were 41.1, 22.2, and 36.7 % compared to 22.8, 48.7 and 28.5 % in CMF, respectively.

Table 3.4 Milk fat fractions' relative concentration of buffalo milk fat and cow milk fat.

Heating rate (°C/min)	MP fraction	Enthalpy Fraction (%) mean±SD, *n=4*		
		BMF	CMF	*p*
2	low	41.1 ±0.4	22.8 ± 0.6	<0.001
	middle	22.2 ± 0.2	48.7 ± 1.7	<0.001
	high	36.7 ± 0.5	28.5 ± 1.5	<0.001
0.5	low	18.8 ± 0.4	13.3 ± 1.2	0.001
	middle	50.0 ± 0.8	58.7 ± 1.3	<0.001
	high	31.2 ± 1.1	28.0 ± 0.3	0.011

MP: melting point, BMF: buffalo milk fat; CMF: cow milk fat.

Nevertheless, the BMF and CMF enthalpy fractions comparison was consistent for both heating rates, with BMF displaying greater low- and higher-melting fractions. The most plausible explanation for this trend lies their difference in TAG composition. As shown in **Figure 3.2**, the chromatographic data are consistent with the DSC thermal analysis.

3.4.3 Nanostructural analysis of the two α- and two β'-polymorphs in BMF and CMF

The nanostructural polymorphs of BMF and CMF upon crystallisation were evaluated. After a quenching step from 60 °C with cooling rate of 2 °C/min, the evolution of the small- and wide-angle X-ray scattering patterns of both milk fats were observed, while holding the samples isothermally at -10 °C for 5 hours (**Figure 3.4**).

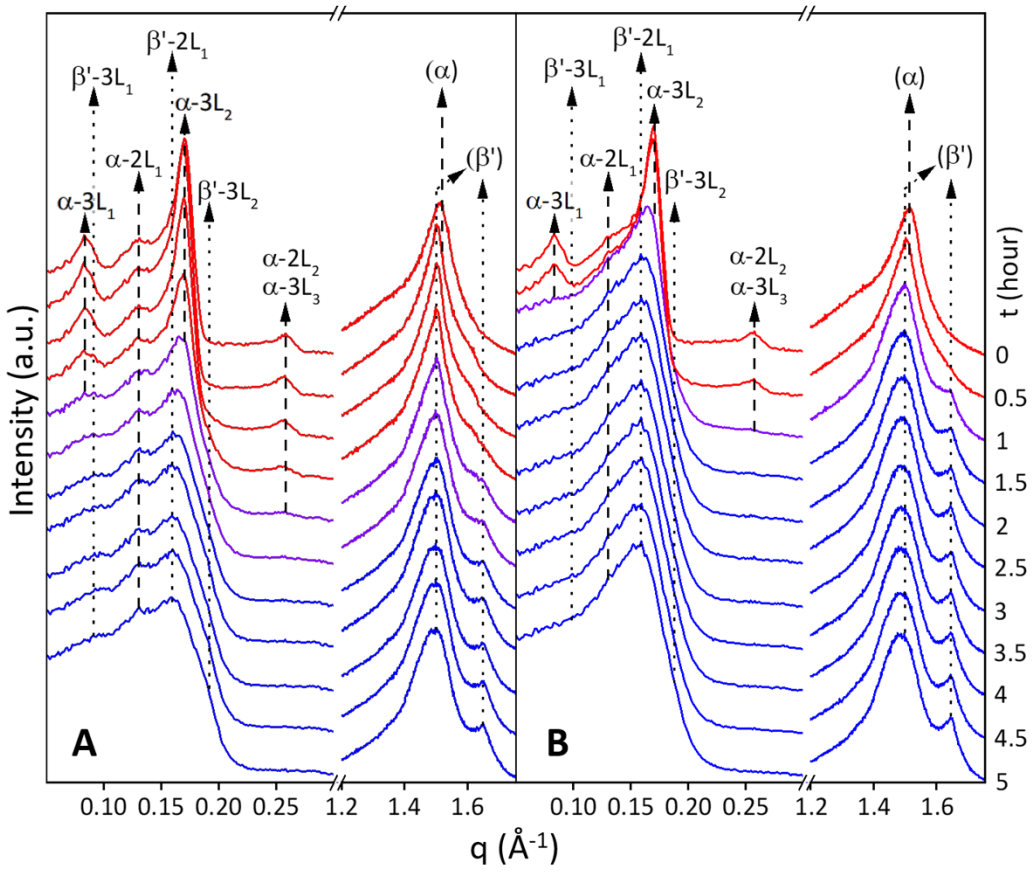

Figure 3.4 X-ray diffraction patterns of (A) buffalo milk fat and (B) cow milk fat in isothermal condition at -10 °C for 5 hours after cooling from 60 °C at -2 °C/min. Red lines/dashed arrows: α-polymorph, blue lines/dotted arrows: β'-polymorph, purple lines: polymorphic transition.

At the beginning of the isothermal hold (*t* = 0 hour), both BMF and CMF exhibited a crystal structure with hexagonal chain packing (α-polymorph), as shown by the presence of a single short spacing of 4.15 Å. Concomitantly, as apparent from the SAXS patterns, two crystal lattices with distinct stacking organisations with *d*-spacing of 48.4 Å (α-2L) and 72.8 Å (α-3L) were observed. The α-3L displayed stronger scattering intensity than the α-2L

polymorph. Lopez et al. (2006) reported similar finding, where the α-polymorph was observed, when CMF was cooled with 1 °C/min rate, displaying three different crystalline phases, i.e., the α-2L (47 Å), α-2L (42 Å) and α-3L (72 Å) polymorph. Note, the α-2L (42 Å) was not identified in our study. Finally, the α-2L and α-3L polymorphs start to transform after 1.5 hours into their corresponding β'-2L and β'-3L polymorphs (**Figure 3.4**), which we will discuss in further detail later on.

The similar *d*-spacing of BMF and CMF can be attributed to the similarity in TAG species, albeit differences in their relative concentrations. The *d*-spacing in TAG crystals, either in 2L or 3L stacking configuration, is dictated by the carbon chain length of the contributing TAGs and the possible tilt angles of the hydrocarbon chain with respect to the stacking direction. The α-2L phase is commonly accepted to have a hydrocarbon chain tilt angle of 0° due to their free chain rotational mode, as reflected in the hexagonal chain packing and as confirmed for pure TAG samples with known hydrocarbon chain length (Mykhaylyk and Hamley, 2004). Therefore, since BMF has a similar *d*-spacing in the α-2L-phase as CMF we can conclude that their average chain-length compositions is alike in this polymorphic phase. Further, it is possible to estimate the average number of carbons, N_C, per hydrocarbon chain in the α-2L-phase. Since the average C-C bond length projected on the hydrocarbon chain of is known to be 1.27 Å (Nagle and Tristram-Nagle, 2000) and the glycerol backbone extension in stacking direction is about 8 Å (Ladd Parada et al., 2018), we obtain:

$$d = 2\,(N_C\ 1.27\text{Å}) + 8\text{Å} \quad \text{or} \quad N_C = (d - 8\text{Å})/2.54\ \text{Å}$$

Eq. (3.2)

Figure 3.5 shows the electron density profiles (EDPs) of BMF of the α-2L, α-3L, β'-2L and β'-3L polymorphs as observed at -10 °C. For all 3L-polymorphs, the overall *d*-spacing can be further decomposed into a saturated-rich bilayer chain region, d_S, and into an unsaturated-rich chain region, d_U, in which the chains pack in an interdigitated fashion. Hence, in the 3L-phase the overall lattice spacing $d = d_S + d_U$.

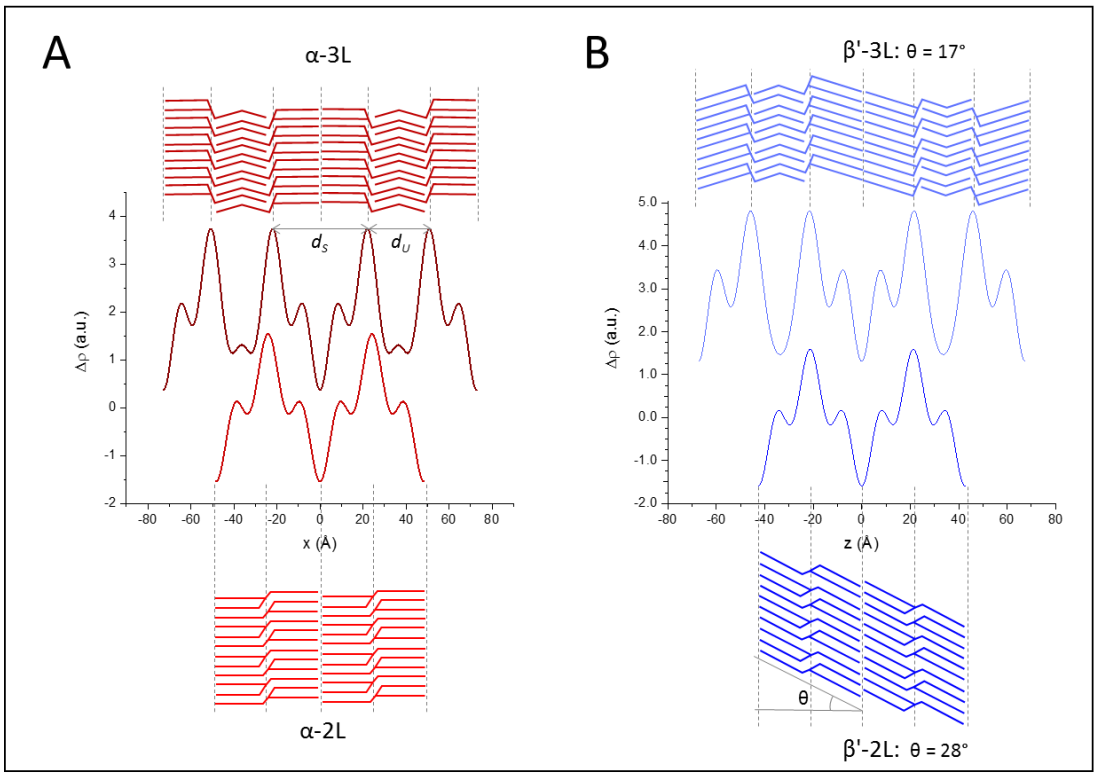

Figure 3.5 Electron density profiles (EDPs) of buffalo milk fat at -10 °C. (A) The α-2L and α-3L polymorphs with *d*-spacings of 48.4 and 72.8 Å (d_S = 44.3 Å), respectively. (B) The β'-2L and β'-3L polymorphs with *d*-spacings of 42.6 and 67.4 Å (d_S = 42.3 Å), respectively. Further details on the determination of the EDPs are given in the Supporting Information Appendix A in **Figure A.2** and **A.3** as well as in **Table A.2**.

Following the chain length concept for the α-2L form, N_C can also be estimated from d_S following **Eq. 3.2**, but the tilt angle of chains needs to be considered beforehand. For the unsaturated-rich chain region, d_U, we can also formulate a rough estimate for N_C:

$$N_C \geq (d_U - 8\text{Å})/1.27\text{ Å},$$

Eq. (3.3)

where again, 1.27 Å refers to projected the C-C bond length and the glycerol backbone extension is considered to be 8 Å. However, due to expected fatty acid with cis double bonds in this region, which give rise to kinked acyl chains, the **Eq. 3.3** only gives a lower bound estimate for N_C.

Confirming the DSC thermograms, the α-2L phase consistently nucleates before the α-3L crystalline form in cooling (cp. **Figure 3.3** and **3.6**). Therefore, we suppose that both crystals are formed from two different TAG fractions, with the α-2L containing TAG with relatively higher melting points. Using Eq. 1, the α-2L (48.4 Å) structure has been estimated to contain about 15.9 carbon

atoms in average. This is slightly lower than what was found by Lopez et al. (2006), who estimated for the similar α-2L species 16.7 carbon atoms on average. As the α-2L polymorph is nucleating at relatively higher temperature, it is reasonable to predict that this structure is constituted mostly of saturated fatty acids which have higher melting point than its unsaturated counterpart. In fact, the average number of 16 carbon atoms corresponds perfectly to palmitic (C16:0) fatty acids or to combinations of for instance myristic (C14:0) and stearic (18:0). TAGs such as MPP, PPP, SPS, and PPS might therefore part of in this α-2L structure.

Using a similar approach as for the α-2L polymorph, the saturated bilayer region of BMF α-3L (d_S =44.3 Å; **Figure 3.5A**) was found to have an average lipid length of 14.3 carbon atoms. We assumed again a zero-chain tilt angle also for this α-phase. Considering the diverse population of TAGs in milk fat, we estimated that the saturated region in the 3L structure is likely to comprise of a wider range of saturated fatty acids, such as lauric (12:0), myristic (14:0) and palmitic (16:0). In contrast, the estimated d_U thickness was 28.5 Å, which corresponds to chains with $N_C \geq 16$ carbon atoms as calculated by **Eq. 3.3**. Because this region of the lamella contains mainly unsaturated fatty acids, the number of carbon atoms estimated can only be associated with sufficiently long unsaturated chains present in milk fat such as oleic (18:1) and linoleic (18:2) acids. Thus, we expect that the α-3L structure is formed by several TAGs consisting of both saturated and unsaturated fatty acids such as PML, PMO, POO, OMO, PLO, etc. This can also explain the lower nucleation temperature. Further evidence is indicated by the bigger peak-fraction area in the crystallisation thermogram of α-3L compared to α-2L (**Figure 3.3** A, B, C), which shows a higher portion of TAGs involved in the second crystallisation event.

It is worth pointing out, that the electron density profile (EDP) of the α-3L phase in BMF is different from other published α-3L phases, such as for SOS (Mykhaylyk and Hamley, 2004). While the 3L-α polymorph of BMF clearly displays a perfect hexagonal chain packing as known for all α polymorphs, the long spacings and corresponding amplitudes, F_h, are strikingly similar to the 3L-γ polymorph of SOS (Mykhaylyk and Hamley, 2004) (see **Table A.3** in the Appendix A). In contrast, the electron density profile of the 3L-α polymorph of SOS is clearly different to the 3L-α polymorph of BMF. In summary, the 3L-α polymorph of BMF displays common α-phase packing of chains combined with commonly known γ-phase stacking of TAGs.

Figure 3.4 also displays a polymorphic transformation from the metastable α-polymorph into the more stable β'-polymorph. This is confirmed by the disappearance of the α-$3L_1$ peak at q = 0.083 $Å^{-1}$ (75 Å), as well as the vanishing of the overlapping α-$2L_2$ and α-$3L_3$ peaks at q = 0.258 $Å^{-1}$ (24 Å) (we note, however, that this concerns mainly the α-$3L_3$ intensity, because the α-$2L_2$ reflection is very weak in intensity) (Ladd Parada et al., 2018). Furthermore, in the wide angle regime, the appearance of the β'-polymorph was clearly indicated by the presence of an additional, β'-phase characteristic peak at q = 1.649 $Å^{-1}$ (3.81 Å). These polymorphic transitions are further supported by determined fraction curves of the β'-2L and β'-3L phases formations (**Figure A.4,** Appendix A). While both β'-phases start to appear simultaneously, only the α-3L → β'-3L turnover is completed within the experimental window of 5 hours, whereas the α-2L → β'-2L transformation remains incomplete, with reference to our preferred interpretation of having distinct TAG compositions in the 2L and 3L polymorphs, respectively. Nonetheless, the 3L transitional route being completed, whereas the 2L form show only an incomplete turnover is readily understood. 3L phases are energetically favoured in condensing their chain packing during the α- to β-phase transition, because they are less prone to packing frustration. Note, saturated and unsaturated lipids are neatly phase-separated in the 3L-stacking geometry and hence increasing the packing density in the d_S-regime is easier to achieve than in the 2L-phases, where the unsaturated and saturated lipids are irrevocably coexisting in the bilayer region.

The polymorphic transformation from the α to the β' form took place at different times for BMF and CMF. During the isothermal hold at -10 °C, the β'-polymorph in CMF appeared at t = 1 hour, whereas BMF took a further half an hour to develop the β'-polymorph. This indicates slower α to β' polymorph transformation kinetics in BMF, when compared to CMF.

Importantly, we observe the formation of both, the β'-phase with 2L and 3L stacking architecture. However, their lattice spacings are considerable smaller, due to their denser fatty acid chain packing, which is always accompanied by a chain tilt in order to match the molecular areas at the polar/apolar interface. Hence, the 3L-form has a d-spacing of 67 Å and a 2L-form of 39 Å, which compares to d-spacings of 72.8 Å and 48.4 Å of the α-polymorphs. Note, we observed the same β'-2L crystal species with d-spacing of 41 and 43 Å in our thermokinetic experiments (shown in **Figure 3.6** and **Figure 3.7**). Lopez et al. (2006) reported a similar finding, where the 2L form (d = 41 Å) has been associated with a β'-polymorph, whilst the 3L form was

tentatively identified as the α or β'-polymorph. In the current study, the appearance of the long-spacing peaks in the small angle regime coincided with the appearance of the β'-polymorph peaks in wide angle. Therefore, we concluded that both the 2L (39 Å) and 3L (67 Å) forms are associated with the β'-polymorph.

As mentioned above, the 2L- and 3L-form of the α polymorphs (hexagonal packing) are most likely characterised by different TAG compositions, since the former has a higher melting point. Thus, interpreting the polymorphic transformation from α to β'-polymorph to occur within the same stacking configurations, i.e., α-2L (48.4 Å) → β'-2L (39 Å) and α-3L (72.8 Å) → β'-3L (67 Å) remains to make good sense. This finding was also confirmed in a melting experiment (**Figure 3.7**), which shows that the β'-3L has lower melting temperature than the β'-2L.

The shorter *d*-spacing of the β'-polymorph indicates a more dense packing in this form compared to the α-polymorph. Assuming that both α-crystals do not have a chain tilt, the tilt angles for the β'-2L and β'-3L were estimated to be 28° and 17°, respectively. Corresponding schemes of the EDPs of β'-2L and β'-3L are presented in **Figure 3.5** B.

3.4.4 Nucleation Kinetics

The nucleation kinetics of BMF and CMF were evaluated using three different cooling rates, i.e., 4, 2, and 0.5 °C/min, respectively. The milk fats were fully melted at 60 °C before being subjected to a cooling ramp down to -10 °C. The temperature resolved X-ray diffraction patterns are shown in **Figure 3.6**.

When applying a cooling rate of 4 °C/min (**Figure 3.6** A and D), both BMF and CMF developed a crystalline structure with a peak at q = 0.131 $Å^{-1}$ (48 Å), at temperatures of 12 and 8 °C, respectively. These structures match the 2L form α-polymorph with hexagonally packed hydrocarbon chains, as indicated by a single strong peak in wide angle at q = 1.510 $Å^{-1}$ (4.16 Å). Subsequently, four distinct peaks were observed in the small angle regime; the strongest one at q = 0.170 $Å^{-1}$ (37 Å). These peaks were identified to belong to the α-3L form with *d*-spacing of 72.8 Å. This structure was observed at 4 and 0 °C for BMF and CMF, respectively.

With a cooling rate of 2 °C/min (**Figure 3.6** B and E), similar trends to the faster cooling were observed. The α-2L crystalline species (48 Å) was nucleated first, at temperatures of 14 and 12 °C for BMF and CMF, respectively. A second crystal lattice associated with the hexagonal packing

α-polymorph and 3L stacking form (α-3L) nucleated subsequently, evidenced by the appearance of its 4 orders of diffraction peaks in the small angle regime. The BMF α-3L nucleated at a temperature of 8 °C, while CMF nucleated at 6 °C.

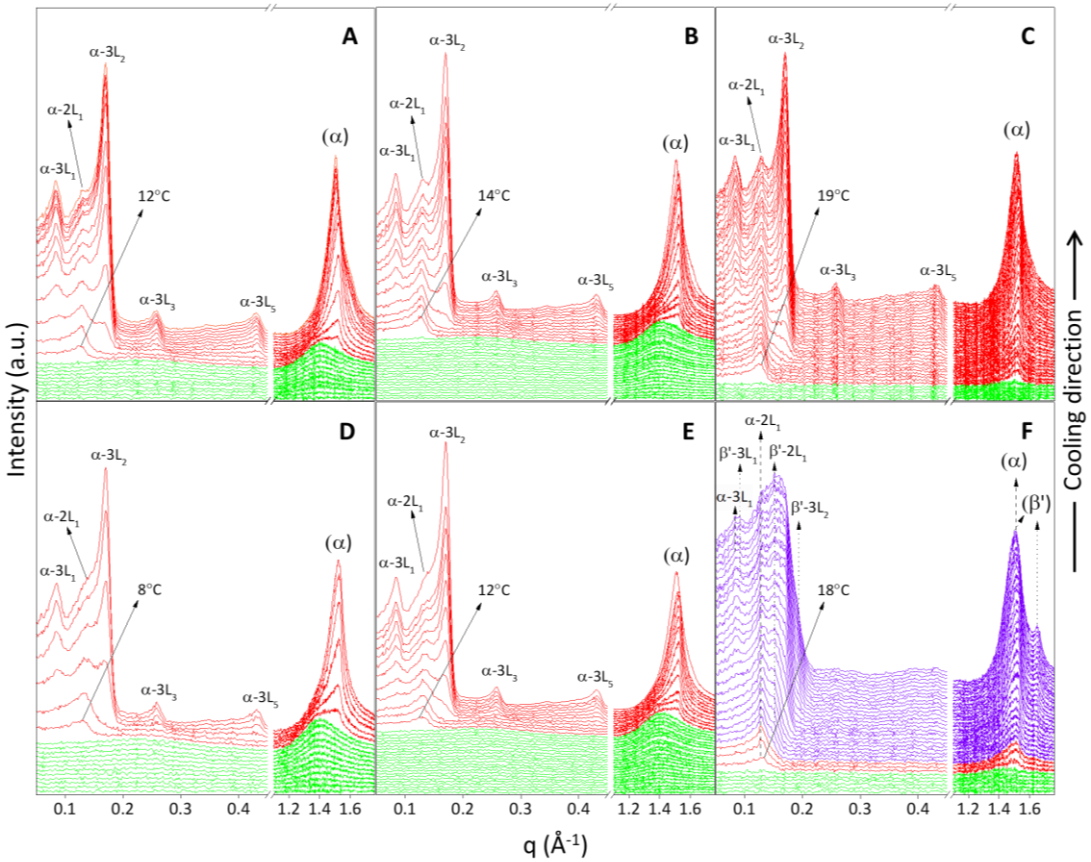

Figure 3.6 Temperature-resolved X-ray diffraction patterns recorded at small and wide angles on cooling from 60 °C to -10 °C. (A) buffalo milk fat (BMF) on cooling 4 °C/min (B) BMF on cooling 2 °C/min (C) BMF on cooling -0.5 °C/min (D) cow milk fat (CMF) on cooling 4 °C/min (E) CMF on cooling 2 °C/min (F) CMF on cooling 0.5 °C/min. (C) and (F) are presented only from 25 °C to -10 °C for clarity. Green lines: liquid phase, red lines: α-polymorph, purple lines: α- and β'- polymorph.

The results from crystallisation experiments at 4 and 2 °C/min cooling rate showed that the α-2L consistently nucleated before the α-3L crystalline form. This is due to the aforementioned evidences that the α-2L most likely comprises long chain saturated TAGs, such as SPS and PPS; the α-3L crystal is instead made of a combination of medium to long saturated FAs and unsaturated FAs (oleic or linoleic acids). SPS and PPS are the TAGs with highest melting points among all TAG species in milk fat, thus providing the highest thermodynamic driving force for nucleation during the cooling profiles. For this same reason, we were expecting that the BMF α-2L would nucleate at higher temperature, when compared to CMF.

The X-ray scattering data are in agreement with the thermal analysis results, which showed higher nucleation temperatures in BMF than CMF for both exothermic peaks associated with the α-2L and α-3L crystal lattices (**Figure 3.3, Table 3.3**). However, the crystallisation events were not observed at the exact same temperatures. For instance, at 2 °C/min cooling rate, the nucleation temperatures for the α-2L were 18.7 and 16.6 °C for BMF and CMF, respectively. Whereas, the nucleation temperatures recorded in the X-ray scattering experiment for the same cooling rate were 14 and 12 °C for BMF and CMF, respectively. It should be noted that the amount of sample and the geometry of the sample holder of the DSC and X-ray equipment were different, which could be the reason for this discrepancy.

Different behaviours of BMF and CMF were observed using a cooling rate of 0.5 °C/min (**Figure 3.6** C and F). In BMF, two crystal lattices associated with the α-2L (48.5 Å) and α-3L (72.8 Å) structures nucleated at temperatures of 19 and 12 °C. The same trend is observed in our thermal analysis, where lower cooling rates resulted in higher nucleation temperatures. Despite the difference in nucleation temperatures, with all applied methods we observed a consistent crystallisation behaviour at all three cooling rates for BMF.

On the other hand, CMF behaved differently from BMF at the lowest cooling rate of 0.5 °C/min. In fact, this sample developed at least four different crystal lattices. The α-2L (48 Å) crystalline nucleated at a temperature of 18 °C. Subsequently, starting from around 15 °C, three additional crystal structures were observed. The exact nucleation temperatures of these other crystal structures were hard to pinpoint due to various superimposed diffraction peaks during the phase formations. However, we could identify each nucleated form. The first one was a 3L crystalline structure associated with the hexagonal packing α-polymorph, as indicated by peak at q = 0.087 $Å^{-1}$ (d-spacing of 72 Å). Another 3L crystal form with d-spacing of 67 Å could be identified (note, here we used the intense second order peak at q = 0.190 $Å^{-1}$ for determining the lattice spacing). This specific crystal lattice was found in neither of the other cooling rates for CMF, nor for any cooling rate used for BMF. We associate this structure with the orthorhombic packing of a β'-polymorph, as evidenced by the presence of the 3.8 Å peak in wide angle. The last identified crystal lattice, observable at q = 0.153 $Å^{-1}$ (41 Å), also corresponds to a β'-polymorph with 2L lamellar stacking.

The formation of a β'-polymorph in CMF has been reported in previous studies using anhydrous CMF, where different polymorphic crystalline forms were observed as the function of different cooling rates. Our study is in agreement

with Grotenhuis et al. (1999) who found that α-crystallisation was favoured for cooling rates ≥ 1.67 °C/min with no β′-polymorph observed. Whereas, the β′-crystallisation was observed for cooling rates ≤ 1°C/min. Another study by Lopez et al. (2005) did not find a β'-polymorph up to cooling rates of 1°C/min, whilst observed the β′-crystallisation at a cooling rate of 0.1 °C/min. It is worth noticing that both Grotenhuis et al. (1999) and Lopez et al. (2005) used different sample holder and sample volumes compared to the current study. Both factors can affect the kinetics of nucleation and crystal growth; therefore, while a similar behaviour among this study and previous ones can be observed, the actual cooling rates at which different polymorphs can appear might be different.

It is worth noting that BMF has similar TAG species to CMF but still failed to produce the β' form when a slow cooling rate of 0.5 °C/min was applied. A crystallisation study involving olein- and stearin-rich fractions of anhydrous CMF (Lopez et al., 2006) showed that when these fractions were subjected to a cooling rate of 1°C/min, the olein-rich fraction favoured the crystallisation of the pure α-form, whilst the stearin-rich sample produced both α- and β'-polymorphs. The study indicated that crystallisation of the β' crystal structure is more likely to occur in the presence of saturated or higher-melting TAGs, such as given in the stearin-rich fraction. Therefore, the failure in producing the β'-polymorph, is somewhat contradicting the fact that BMF contains a higher amount of saturated TAGs compared to CMF. One possible explanation is that BMF has a higher olein fraction as well, when compared to CMF; thus offsetting the effect of a higher saturated TAG content. We estimated the amount of olein and stearin in CMF and BMF by looking at the TAG composition. Our results in **Figure 3.2** show that BMF has a higher content of high-molecular weight TAGs (associated to stearin) and low-molecular weight TAGs (associated to olein) compared to CMF. The total weight fraction for the high-molecular weight TAG was 18.1%, whilst for the low-molecular weight TAG it was 48.8%. Therefore, we can estimate a higher olein content in BMF, which could explain the absence of the β'-polymorph for slow cooling rates (**Figure 3.6** C) and slower kinetics of α- to β'-transition under isothermal condition (**Figure 3.4**). Nevertheless, further studies are needed to confirm this conjecture.

3.4.5 Kinetics of melting and β-polymorph identification

Figure 3.7 shows the X-ray diffraction patterns on heating at 2 °C/min of frozen samples of BMF and CMF. An orthorhombic lateral packing of the β'-

polymorph was dominant in both milk fats, as shown by the presence of two peaks in the wide angle, i.e., referring to the short spacings of 4.2 and 3.81 Å. Two crystal lattices corresponding to a 2L and a 3L lamellar stacking conformation with *d*-spacing of 42.9 and 64.2 Å were observed. Furthermore, we observed an additional crystal lattice in the small angle regime of BMF, with *d*-spacing of 53 Å. We identified this crystal lattice as a 3L stacking structure. This identification is in agreement with Lopez et al. (2005), where a crystal lattice with *d*-spacing of 54 Å was observed in anhydrous CMF conditioned at 4 °C for 5 days.

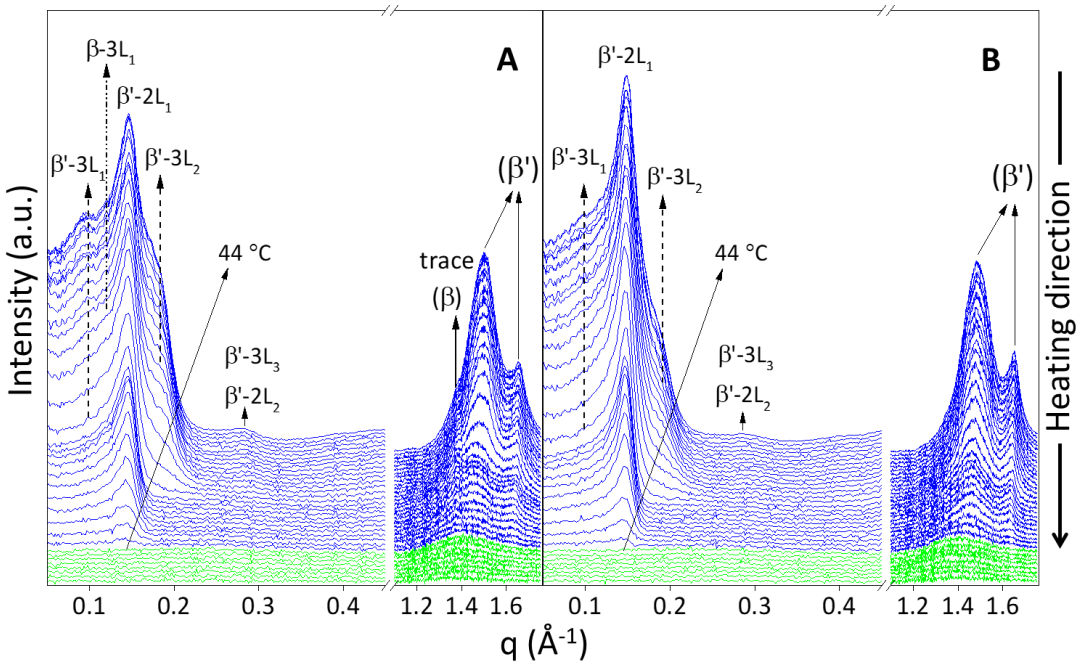

Figure 3.7 Temperature-resolved X-ray diffraction patterns of (A) buffalo milk fat and (B) cow milk fat heating from -10 to 60°C at 2 °C/min after being frozen for 3 weeks. Green lines: liquid phase, blue lines: β'- polymorph.

Lopez et al. (2005) did not associate this 3L structure with any specific polymorph type. However, in the current study, we can infer that it is a triclinic packing corresponding to a β-polymorph. As shown in the wide angle regime (**Figure 3.7** A), the appearance of the 3L form in BMF was accompanied by a peak at q = 1.376 Å^{-1} (4.6 Å), which corresponds to the most intense β-polymorph short spacing. Similar spacings, both concerning small and wide angle regimes, were not found in CMF (**Figure 3.7** B). At freezer temperature, BMF has more liquid oil portion due to its higher low melting point TAGs than that of CMF. The presence of liquid oil allows better diffusion of the milk fat TAGs to form more stable β-crystals, as also reported by Wright et al. (2005).

The *d*-spacing of the β-3L (53 Å) observed here is very small compared to a well-known β-crystals of SOS which is 64.5 Å (Mykhaylyk and Hamley, 2004). In order to shed some light on this structure, we simulated the EDP of the β-3L (see **Figure A.5** in the Appendix A). Since the *d*-spacing was the only experimental observable parameter, the simulated EDP based on two rigorous assumptions. Firstly, the saturated bilayer was assumed to comprise 16 carbon atoms saturated fatty acid in average. Note, palmitic acid is the most abundant FA in BMF (Ménard et al., 2010; Abd El-Salam and El-Shibiny, 2011). Secondly, the chain tilt angle for the β-phase was assumed to be 36° as confirmed in literature for SOS (Mykhaylyk and Hamley, 2004). Other SOS-rich samples (Gregersen et al., 2016) display chain tilt angles of 33° and 36° for the β'-3L and β-3L polymorph, respectively. Thus, we limited possible chain tilts in the β-3L polymorph in BMF to vary from 33 to 36°, and consequently find d_S to vary in the range of 39-41 Å from which d_U values from 12-14 Å follow. The monolayer unsaturated chain region is very thin, with an average chain length of about 4 carbon atoms (**Eq. 3.3**). Milk fat is abundant in short chain fatty acids such as butyric (C4) and caproic (C6) acids. Hence, it is very tempting to come to the conclusion that this β-3L (53 Å) crystal lattice comprises of the TAGs containing short fatty acids being present in the d_U regions, and thus entirely different from those contributing to α-3L and β'-3L polymorphs. This tentative conclusion also aligns well with the fact that BMF has a higher content of butyric-containing TAGs (**Figure 3.2**), which might explain the appearance of the β-3L in BMF but not in CMF. The summary of all polymorphs and the associating crystal lattices found in this work is given in **Table 3.5**.

Table 3.5 Summary of all polymorphs of buffalo milk fat and cow milk fat.

Structure	*d*-spacing (Å)	d_S (Å)	d_U (Å)	Contributing TAG
α-2L	48-49	-	-	Long chain saturated TAG (e.g., PPP, PPS and SPS)
α-3L	72-73	44.3	28.5	TAG containing medium-long saturated FAs and long chain mono/poly-unsaturated FAs (e.g., PLaO, PCO, PPO)
β'-2L	39-43	-	-	Proposed compositional similarity to α-2L

Structure	*d*-spacing (Å)	d_S (Å)	d_U (Å)	Contributing TAG
β'-3L	64-67	42.3	25.1	Proposed compositional similarity to α-3L
β-3L	53	39-41	12-14	Proposed: TAG containing short chain FAs (e.g., BuPS, BuPP, CoMP)

On heating at 2 °C/min, the peak intensity in the small angle regime decreased and finally reached a constant value, indicating the melt of the crystals (**Figure 3.7**). The β'-3L crystal disappeared at around 22 °C and the β'-2L final melting temperature was around 44 °C. There was no observable difference in melting temperatures for each polymorphs of BMF and CMF. Finally, while the β-3L (53 Å) peak was subtle and the intensity too poor to pinpoint its exact melting point, we clearly observed that the wide angle 4.6 Å (β) peak persisted until 44 °C.

3.4.6 Crystal microstructure

Micrographs of BMF and CMF upon cooling at 2 and 0.5 °C/min are presented in Figure 8. In general, both milk fats showed a higher rate of nucleation, but slower crystal growth at the faster cooling rate. Faster cooling rates induce nucleation at higher levels of undercooling, thus generating a larger number of nuclei. Moreover, as the cooling was continued further to -10°C, the nuclei growth was hindered not only by their dense population but also by the increasing viscosity of the sample, which impairs crystal growth (Himawan et al., 2006).

At a cooling rate of 2 °C/min (**Figure 3.8** A and B), the BMF and CMF samples both show characteristics clusters of needle-like crystals (spherulites) of different average equivalent diameter (around 7 μm for BMF and of 6 μm for CMF). The faster nucleation rate for CMF in this cooling conditions, highlighted by the presence of a larger number of clusters, might be due to the lower content of low melting TAGs compared to BMF, which nucleate slower than the mid- and high-melting TAGs. This behaviour is in accordance with what found by Ramel and Marangoni (2016) on ternary mixtures of high-, mid- and low-melting fraction of milk fat.

A slower cooling rate of 0.5 °C/min (**Figure 3.8** C and D) showed less clusters of larger size for both, BMF and CMF. The BMF spherulites were around 19.5 μm in diameter, while the CMF had an average diameter of 25.3 μm and displayed a dendritic/snow-flake morphology. These results show a difference in the growth and nucleation rates at slow cooling rates between BMF and CMF; however, the reason for this behaviour is still unclear and requires further investigation.

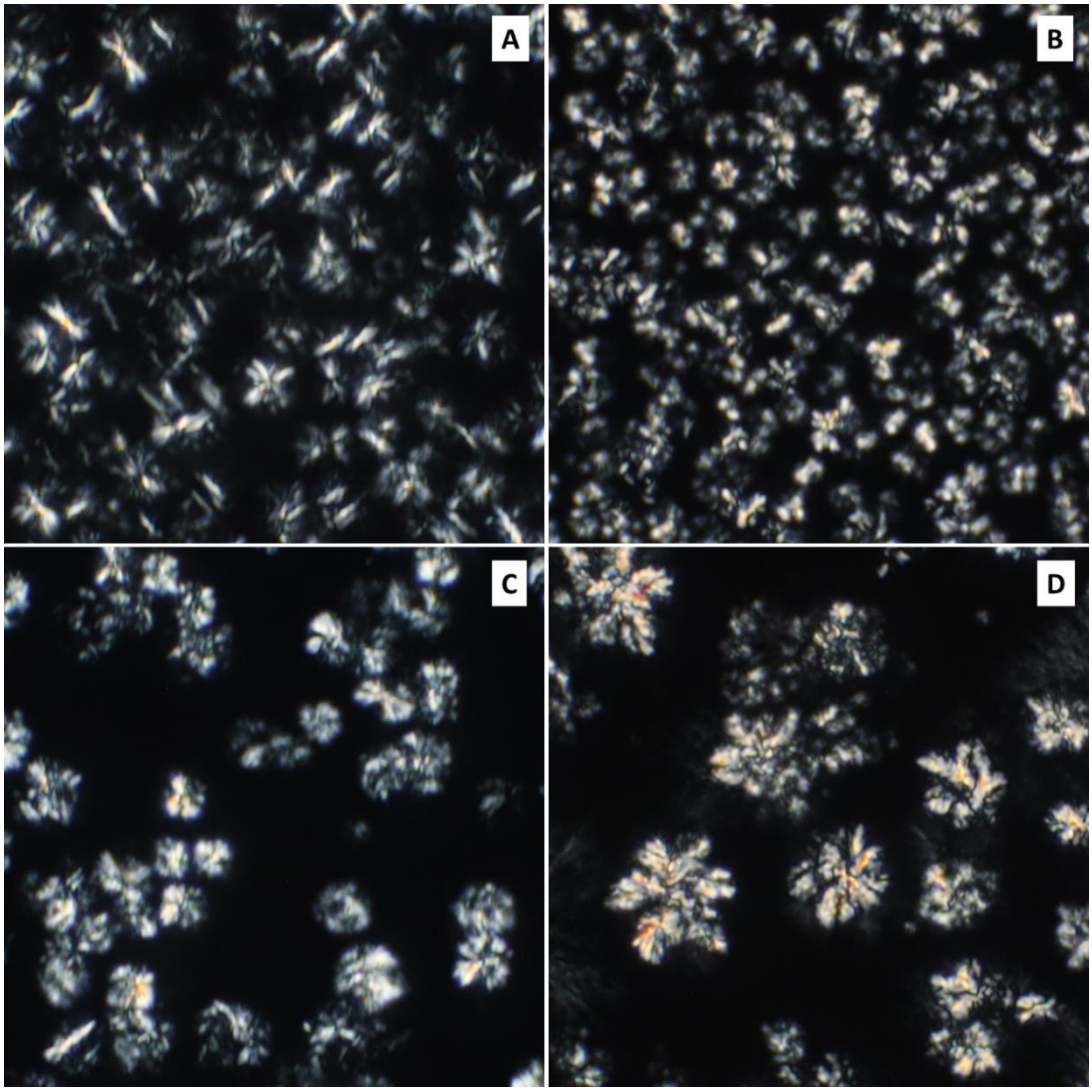

Figure 3.8 Polarised light micrographs taken at 15°C of (A) buffalo milk fat (BMF), (B) cow milk fat (CMF) on cooling at 2°C/min and (C) BMF, (D) CMF on cooling at 0.5°C/min from melt at 60°C. Dimensions on each image correspond to 200x200 microns.

3.5 Conclusions

For the first time, the BMF crystallisation has been detailed in great depths, combining mass-spectroscopy and calorimetry data with nano- as well as microstructural studies. In particular, the extensive small- and wide angle X-ray scattering experiments have revealed the unique dynamic and polymorphic behaviour of BMF. While BMF has similar TAG species as CMF, 20 out of 37 identified TAGs differ significantly in their quantities. Although the nucleation temperatures of BMF are higher, the formation of β'-polymorph in BMF takes longer time than in CMF under isothermal conditions (hold at -10 °C). Similarly, BMF nucleates only α-polymorphs during slow cooling rates, while CMF forms both, α- and β'-polymorph. The delay of the β'-polymorph formation is potentially caused by the higher portion of olein-fraction or low molecular weight TAGs in BMF, while the higher nucleation and melting point temperatures in BMF are a consequence of the bigger portion of saturated TAGs. We further provided evidence for a specific segregation in the milk fat crystallisation process. The polymorphic transformations seem to occur within the same lamellar structures, and hence driven by the same TAG groups, i.e., leading to two parallel transitions: α-2L → β'-2L and α-3L → β'-3L. This is supported by our detailed nanostructural analysis as well as by the higher nucleation and melting temperatures of α-2L and β'-2L, respectively, which match the characteristic TAG groups consisting of mainly saturated species. Furthermore, we proposed a novel interpretation of the three chain length β-polymorph (*d*-spacing 53 Å), which is likely to be formed by asymmetrical TAGs containing butyric acids. In addition to the difference in nanostructure, BMF also displayed different microstructure than CMF (spherulites *vs.* snowflake like crystals). As such, this study provides profound insight into the crystallisation behaviour of different milk fats as influenced by its TAG compositional difference.

3.6 References

Abd El-Salam, M.H. and El-Shibiny, S. 2011. A comprehensive review on the composition and properties of buffalo milk. *Dairy Science & Technology*. **91**(6), pp.663-699.

Amara-Dali, W. Ben, Karray, N., Lesieur, P. and Ollivon, M. 2005. Anhydrous goat's milk fat: Thermal and structural behavior. 1. Crystalline forms

obtained by slow cooling. *Journal of Agricultural and Food Chemistry*. **53**(26), pp.10018-10025.

Amara-Dali, W. Ben, Lesieur, P., Artzner, F., Karray, N., Attia, H. and Ollivon, M. 2007. Anhydrous goat's milk fat: Thermal and structural behaviors studied by coupled differential scanning calorimetry and X-ray diffraction. 2. Influence of cooling rate. *Journal of Agricultural and Food Chemistry*. **55**(12), pp.4741-4751.

Angelis, M. De and Gobbetti, M. 2011. Pasta-Filata Cheeses: Traditional Pasta-Filata Cheese *In*: J. W. Fuquay, P. F. Fox and P. L. H. McSweeney, eds. *Encyclopedia of Dairy Sciences: Second Edition*. Oxford: Academic Press, 1:745-752.

Arumughan, C. and Narayanan, K.M. 1982. Triacylglycerol composition of buffalo milk fat. *Journal of Dairy Research*. **49**(1), pp.81-85.

Campos, R., Narine, S.S. and Marangoni, A.G. 2002. Effect of cooling rate on the structure and mechanical properties of milk fat and lard. *Food Research International*. **35**(10), pp.971-981.

D'Souza, V., deMan, J.M. and deMan, L. 1990. Short spacings and polymorphic forms of natural and commercial solid fats: A review. *Journal of the American Oil Chemists' Society*. **67**(11), pp.835-843.

Deffense, E. 1993. Milk fat fractionation today: A review. *Journal of the American Oil Chemists' Society*. **70**(12), pp.1193-1201.

FAO 2022. FAOSTAT Statistical Database. [Accessed 27 January 2023]. Available from: https://www.fao.org/faostat/en/#data/QCL. Ganguli, N.C. and Jain, M.K. 1973. Ghee: Its Chemistry, Processing and Technology. *Journal of Dairy Science*. **56**(1), pp.19-25.

Gantner, V., Mijić, P., Baban, M., Škrtić, Z. and Turalija, A. 2015. The overall and fat composition of milk of various species. *Mljekarstvo*. **65**(4), pp.223-231.

Gastaldi, D., Medana, C., Giancotti, V., Aigotti, R., Dal Bello, F. and Baiocchi, C. 2011. HPLC-APCI analysis of triacylglycerols in milk fat from different sources. *European Journal of Lipid Science and Technology*. **113**(2), pp.197-207.

Gregersen, S.B., Povey, M.J.W., Andersen, M.D., Hammershøj, M., Rappolt, M., Sadeghpour, A. and Wiking, L. 2016. Acoustic properties of crystallized fat: Relation between polymorphic form, microstructure,

fracturing behavior, and sound intensity. *European Journal of Lipid Science and Technology*. **118**(9), pp.1257-1270.

Grotenhuis, E. Ten, Van Aken, G.A., Van Malssen, K.F. and Schenk, H. 1999. Polymorphism of milk fat studied by differential scanning calorimetry and real-time X-ray powder diffraction. *JAOCS, Journal of the American Oil Chemists' Society*. **76**(9), pp.1031-1039.

Himawan, C., Starov, V.M. and Stapley, A.G.F. 2006. Thermodynamic and kinetic aspects of fat crystallization. *Advances in Colloid and Interface Science*. **122**(1-3), pp.3-33.

Idziak, S.H.J. 2018. Powder X-ray Diffraction of Triglycerides in the Study of Polymorphism *In*: A. G. Marangoni, ed. *Structure-Function Analysis of Edible Fats Second Edition*. AOAC Press, pp.73-99.

Karray, N., Lopez, C., Lesieur, P. and Ollivon, M. 2004. Dromedary milk fat: thermal and structural properties 1. Crystalline forms obtained by slow cooling. *Le Lait*. **84**(4), pp.399-416.

Karray, N., Lopez, C., Lesieur, P. and Ollivon, M. 2005. Dromedary milk fat: thermal and structural properties 2. Influence of cooling rate. *Le Lait*. **85**(6), pp.433-451.

Ladd Parada, M., Sadeghpour, A., Vieira, J., Povey, M. and Rappolt, M. 2018. Global Small-Angle X-ray Scattering Data Analysis of Triacylglycerols in the α-Phase (Part II). *Journal of Physical Chemistry B*. **122**(45), pp.10330-10336.

Larsen, M.K., Andersen, K.K., Kaufmann, N. and Wiking, L. 2014. Seasonal variation in the composition and melting behavior of milk fat. *Journal of Dairy Science*. **97**(8), pp.4703-4712.

Li, N.Y.D., Perutková, Š., Iglič, A. and Rappolt, M. 2017. My first electron density map: A beginner's guide to small angle X-ray diffraction. *Elektrotehniski Vestnik/Electrotechnical Review*. **84**(3), pp.69-75.

Lopez, C. 2018. Crystallization Properties of Milk Fats *In*: K. Sato, ed. *Crystallization of Lipids: Fundamentals and Applications in Food, Cosmetics and Pharmaceuticals*. Hoboken, NJ: Wiley Blackwell, pp.283-321.

Lopez, C., Bourgaux, C., Lesieur, P. and Ollivon, M. 2007. Coupling of time-resolved synchrotron X-ray diffraction and DSC to elucidate the crystallisation properties and polymorphism of triglycerides in milk fat globules. *Le Lait*. **87**(4-5), pp.459-480.

Lopez, C., Bourgaux, C., Lesieur, P., Riaublanc, A. and Ollivon, M. 2006. Milk fat and primary fractions obtained by dry fractionation. 1. Chemical composition and crystallisation properties. *Chemistry and Physics of Lipids*. **144**(1), pp.17-33.

Lopez, C., Lesieur, P., Bourgaux, C. and Ollivon, M. 2005. Thermal and structural behavior of anhydrous milk fat. 3. Influence of cooling rate. *Journal of Dairy Science*. **88**(2), pp.511-526.

Marangoni, A.G. and Lencki, R.W. 1998. Ternary Phase Behavior of Milk Fat Fractions. *Journal of Agricultural and Food Chemistry*. **46**(10), pp.3879-3884.

Martini, S. and Marangoni, A.G. 2007. Microstructure of Dairy Fat Products *In*: A. Tamime, ed. *Structure of Dairy Products*. Oxford: Blackwell Publishing Ltd, pp.72-103.

Mazzanti, G., Guthrie, S.E., Sirota, E.B., Marangoni, A.G. and Idziak, S.H.J. 2004. Effect of minor components and temperature profiles on polymorphism in milk fat. *Crystal Growth and Design*. **4**(6), pp.1303-1309.

Mazzanti, G., Marangoni, A.G. and Idziak, S.H.J. 2009. Synchrotron study on crystallization kinetics of milk fat under shear flow. *Food Research International*. **42**(5-6), pp.682-694.

Ménard, O., Ahmad, S., Rousseau, F., Briard-Bion, V., Gaucheron, F. and Lopez, C. 2010. Buffalo vs. cow milk fat globules: Size distribution, zeta-potential, compositions in total fatty acids and in polar lipids from the milk fat globule membrane. *Food Chemistry*. **120**(2), pp.544-551.

Mottram, H.R. and Evershed, R.P. 2001. Elucidation of the composition of bovine milk fat triacylglycerols using high-performance liquid chromatography-atmospheric pressure chemical ionisation mass spectrometry. *Journal of Chromatography A*. **926**(2), pp.239-253.

Murtaza, M.A., Pandya, A.J. and Khan, M.H.M. 2017. Buffalo milk: Buffalo milk utilization for dairy products *In*: Y. W. Park, G. F. W. Haenlein and W. L. Wendorff, eds. *Handbook of Milk of Non-Bovine Mammals: Second Edition*. Oxford, UK: Wiley Blackwell, pp.284-342.

Mykhaylyk, O.O. and Hamley, I.W. 2004. The packing of triacylglycerols from SAXS measurements: Application to the structure of 1,3-distearoyl-2-oleoyl-sn-glycerol crystal phases. *Journal of Physical Chemistry B*. **108**(23), pp.8069-8083.

Nagle, J.F. and Tristram-Nagle, S. 2000. Structure of lipid bilayers. *Biochimica et Biophysica Acta - Reviews on Biomembranes*. **1469**(3), pp.159-195.

Norman Dyson 1998. *Chromatographic Integration Methods* second. (R. M. Smith, ed.). Cambridge: The Royal Society of Chemistry.

Penchev, P., Ilieva, Y., Ivanova, T. and Kalev, R. 2016. Fatty acid composition of buffalo and bovine milk as affected by roughage source - silage versus hay. *Emirates Journal of Food and Agriculture*. **28**(4), p.1.

Ramel, P.R. and Marangoni, A.G. 2016. Engineering the microstructure of milk fat by blending binary and ternary mixtures of its fractions. *RSC Advances*. **6**(47), pp.41189-41194.

Ramel, P.R. and Marangoni, A.G. 2017. Insights into the mechanism of the formation of the most stable crystal polymorph of milk fat in model protein matrices. *Journal of Dairy Science*. **100**(9), pp.6930-6937.

Sato, K. 2001. Molecular Aspects in Fat Polymorphism *In*: N. Widlak, R. Hartel and S. Narine, eds. *Crystallization and Solidification Properties of Lipids*. Champaign, Illinois, Illinois: AOCS Press, pp.1-17.

Shi, Y., Smith, C.M. and Hartel, R.W. 2001. Compositional effects on milk fat crystallization. *Journal of Dairy Science*. **84**(11), pp.2392-2401.

Smiddy, M.A., Huppertz, T. and van Ruth, S.M. 2012. Triacylglycerol and melting profiles of milk fat from several species. *International Dairy Journal*. **24**(2), pp.64-69.

Ten-Doménech, I., Beltrán-Iturat, E., Herrero-Martínez, J.M., Sancho-Llopis, J.V. and Simó-Alfonso, E.F. 2015. Triacylglycerol Analysis in Human Milk and Other Mammalian Species: Small-Scale Sample Preparation, Characterisation, and Statistical Classification Using HPLC-ELSD Profiles. *Journal of Agricultural and Food Chemistry*. **63**(24), pp.5761-5770.

Tzompa-Sosa, D.A., Meurs, P.P. and van Valenberg, H.J.F. 2018. Triacylglycerol Profile of Summer and Winter Bovine Milk Fat and the Feasibility of Triacylglycerol Fragmentation. *European Journal of Lipid Science and Technology*. **120**(3), p.1700291.

Tzompa-Sosa, D.A., Ramel, P.R., Van Valenberg, H.J.F. and Van Aken, G.A. 2016. Formation of β Polymorphs in Milk Fats with Large Differences in Triacylglycerol Profiles. *Journal of Agricultural and Food Chemistry*. **64**(20), pp.4152-4157.

Van-Aken, G., Ten Grotenhuis, E., Van Langevelde, A.J. and Schenk, H. 1999. Composition and crystallization of milk fat fractions. *JAOCS, Journal of the American Oil Chemists' Society*. **76**(11), pp.1323-1331.

Van-Aken, G. and Visser, K.A. 2000. Firmness and crystallization of milk fat in relation to processing conditions. *Journal of Dairy Science*. **83**(9), pp.1919-1932.

Wright, A.J., Batte, H.D. and Marangoni, A.G. 2005. Effects of canola oil dilution on anhydrous milk fat crystallization and fractionation behavior. *Journal of Dairy Science*. **88**(6), pp.1955-1965.

Wright, A.J., Hartel, R.W., Narine, S.S. and Marangoni, A.G. 2000. Effect of minor components on milk fat crystallization. *JAOCS, Journal of the American Oil Chemists' Society*. **77**(5), pp.463-475.

Wright, A.J., McGauley, S.E., Narine, S.S., Willis, W.M., Lencki, R.W. and Marangoni, A.G. 2000. Solvent effects on the crystallization behavior of milk fat fractions. *Journal of Agricultural and Food Chemistry*. **48**(4), pp.1033-1040.

Zeb, A. and Murkovic, M. 2010. Analysis of triacylglycerols in refined edible oils by isocratic HPLC-ESI-MS. *European Journal of Lipid Science and Technology*. **112**, pp.844-851.

Zhou, L., Tang, Q., Wasim Iqbal, M., Xia, Z., Huang, F., Li, L., Liang, M., Lin, B., Qin, G. and Zou, C. 2018. A comparison of milk protein, fat, lactose, total solids and amino acid profiles of three different buffalo breeds in Guangxi, China. *Italian Journal of Animal Science*. **17**(4), pp.873-878.

Zhou, Q., Gao, B., Zhang, X., Xu, Y., Shi, H. and Yu, L. 2014. Chemical profiling of triacylglycerols and diacylglycerols in cow milk fat by ultra-performance convergence chromatography combined with a quadrupole time-of-flight mass spectrometry. *Food Chemistry*. **143**, pp.199-204.

Chapter 4 Polymorphism of a Highly Asymmetrical Triacylglycerol in Milk Fat: 1-butyryl 2-stearoyl 3-palmitoyl-glycerol

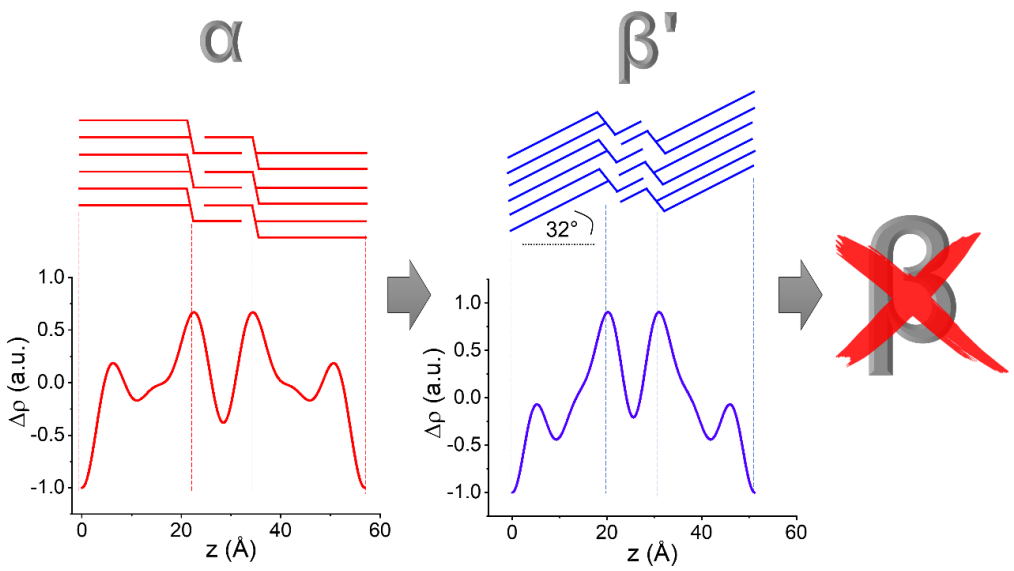

4.1 Abstract

Milk fat has more than 200 triacylglycerols (TAGs) which play a pivotal role in its crystallisation behaviour. Asymmetrical TAGs containing short butyryl chains contribute to a significant portion of milk fat TAGs. This work aims to elucidate the crystallisation behaviour of the milk fat asymmetrical TAGs by employing the pure compound of 1-butyryl 2-stearoyl 3-palmitoyl-glycerol (BuSP). The structural evolution of BuSP after being cooled down to 20 °C from the melt, is evaluated by small- and wide-angle X-ray scattering (SAXS and WAXS) and differential scanning calorimetry (DSC). The temporal structural observation shows that BuSP crystallizes into α-form with short and long spacing of 4.10 Å and 56.9 Å, respectively, during the first hour of isothermal hold at 20 °C. The polymorphic transformation of α to β' phase occurred after 4 hours of isothermal hold and the β' to α-form fraction ratio was about 70:30 at the end of the isothermal experiment (18h). Pure β'-form X-ray patterns are obtained from the BuSP powder with short spacing of 4.33, 4.14 and 3.80 Å, whilst the long spacing of 51.2 Å depicts a three-chain length lamellar structure with a tilt angle of 32°. Corresponding DSC measurements display that BuSP crystallizes from melt at 29.1 °C, whereas the melting of α and β'-form were recorded at 30.3 and 47.8 °C, respectively. With the absence of β-form, the β'-polymorph is the most stable observed form in BuSP. This

work exemplary explains the crystallisation behaviour of the asymmetrical milk fat TAGs and thus provides new insight into its role in the overall milk fat crystallisation.

Key words: Polymorphism, butyric acid, milk fat, asymmetrical triacylglycerol, crystallisation.

4.2 Introduction

Milk fat is one of the most complex fats found in nature. More than 200 different triacylglycerol (TAG) species have been reported (Gresti et al., 1993) to make up 98% of the total composition of milk fat(Jensen et al., 1991). Additionally, milk fat contains some minor components such as sterols, phospholipids, free fatty acids, mono- and di-acylglycerols (Walstra et al., 2005). The wide array of TAGs in milk fat contains 13 major fatty acids, whose contribution to the total composition are each higher than 1% (w/w). Nine fatty acids are saturated ($C_{4:0}$, $C_{6:0}$, $C_{8:0}$, $C_{10:0}$, $C_{12:0}$, $C_{14:0}$, $C_{15:0}$, $C_{16:0}$, and $C_{18:0}$), whereas four are unsaturated ($C_{14:1}$, $C_{16:1}$, $C_{18:1}$, and $C_{18:2}$) (Gresti et al., 1993). In addition to its large number of TAGs, milk fat TAGs composition is known to be influenced by a number of factors such as breed, stage of lactations, seasons and geographical location where milking species are grown as well as the type of feed (Grummer, 1991; Palmquist et al., 1993; Soyeurt et al., 2006; Stoop et al., 2009; Huppertz et al., 2009; Maurice-Van Eijndhoven et al., 2011; Tzompa-Sosa et al., 2018). Nevertheless, the compositional differences in milk fat among different milking species, for instance cow *vs* buffalo *vs* goat, are greater than that of inter-species variation (Ménard et al., 2010; Smiddy et al., 2012; Gantner et al., 2015). As an example, in our previous study we found that 20 out of 37 identified TAGs differ significantly in their proportion between cow and buffalo milk fat (Pratama et al., 2021).

Because of its complex nature, milk fats exhibit a broad melting range and complex crystallisation behaviour, with multiple crystal structures forming (Grotenhuis et al., 1999; Amara-Dali et al., 2005; Tomaszewska-Gras, 2013; Lopez, 2018; Arita-Merino et al., 2022). In fact, at least five different molecular chain packing arrangements are known, corresponding to α, γ (sub-α), β'-1, β'-2, and β packing configuration. On the other hand, numerous stacking architectures have been observed, which fall into two main lamellar stacking types. First, double-chain length (2L) structures with *d*-spacing ranging from 39 to 48 Å, and triple-chain length (3L) structures with *d*-spacing between 53

to 73 Å (Lopez, 2018; Pratama et al., 2021). Moreover, the polymorphic behaviour during milk fat crystallisation is strongly influenced by processing factors such as cooling rate, isothermal holding time, and the presence of shear (Grotenhuis et al., 1999; Campos et al., 2002; Lopez, Bourgaux, Lesieur, Bernadou, et al., 2002; Mazzanti et al., 2004; Mazzanti et al., 2009).

The structure of milk fat crystals is essential as it directly affects the physical properties of fat-based dairy products, such as their melting characteristics, mouthfeel, stability and spreadability (Martini and Marangoni, 2007). The chain packing information that denote the polymorph type are commonly obtained from wide-angle X-ray scattering (WAXS) measurements. In addition, measurements in the small angle X-ray scattering (SAXS) regime provide the lamellar thickness of the 2L and 3L stacking repeat, which in turn allows to approximately identify which types of TAGs contribute to a given polymorph structure. Thus, an accurate identification of the chain packing with its accompanying stacking type (2L or 3L) allows pinpointing the TAGs that are prevalent in a specific crystal structure. Finally, the identification of TAGs self-assembled structures is important to understand how milk fat crystallises and offers great opportunities for controlling and further tailoring milk fat processing. For example, by manipulating the proportions of TAGs in order to obtain the polymorph and kinetics of nucleation and growth that suits a specific dairy product best.

In single polymorphic TAG samples, it is straightforward to associate the lamellar stackings to the given chain packing type. However, in mixtures of polymorphic forms, the association of different lamellar thicknesses to its corresponding chain packing can be tricky. As an illustration, a straightforward association of the 2L (46 Å) and a 3L (72 Å) lamellar structures with a hexagonal chain packing could be unanimously accepted, because they were observed in a pure α-system, when the milk fat was cooled at -3 °C/min rate (Lopez, Bourgaux, Lesieur, Bernadou, et al., 2002). Our previous study also observed the same finding with 48.4 and 72.8 Å stacking distance, corresponding to α-polymorph after cooling at -2 °C/min rate (Pratama et al., 2021). Similarly, a very unstable γ-form was the only observed structure upon rapid quenching of milk fat to -8 °C. Thus, also here the two stacking configurations with a 70 and 47 Å lattice spacing (3L and 2L) could be readily attributed to the same packing type, a γ-phase (Lopez et al., 2005).

On the other hand, association of the lamellar structures with β'- and β-polymorphic packing in milk fat are not as straight forward. These polymorphs are rarely observed in their pure form in milk fat, but often coexist with each

other or with the metastable α-phase. For example, Lopez et al (Lopez, Bourgaux, Lesieur, Bernadou, et al., 2002) attributed a lattice structure with *d*-spacing of 40-41.5 Å to a β'-polymorph with a 2L architecture. While a crystal structure with *d*-spacing of 67 Å was attributed to a 3L stacking structure, it could only be tentatively assigned to a β'-form due to the coexistence with a α-polymorph. In our studies, we recently confirmed that the long spacing 67 Å corresponds to β'-phase after conducting a long isothermal experiment diminishing most of the α-phase, and additionally, being able to determine the electron density profile of the β'-form (Pratama et al., 2021). The correct phase identification is even more difficult concerning the β-polymorph. Indeed its existence in milk fat is still a subject of ongoing debate. Some studies did not observe the β-form at all (Grotenhuis et al., 1999; Mazzanti et al., 2009), whilst other studies reported the presence of this polymorph as trace and or in coexistence with other crystal structures (Lopez, Bourgaux, Lesieur, Bernadou, et al., 2002; Mazzanti et al., 2004; Tzompa-Sosa et al., 2016; Pratama et al., 2021). Indeed, the full understanding of this triclinic system and its corresponding lamellar configurations in milk fat is still lacking.

Having summarised most of the key lamellar thicknesses of milk fat crystals above, one repeat distance of particular interest has a *d*-spacing of 53 Å. The nature of this particular structure of milk fat is still fairly unclear, unlike those of the 3L structures of 67-73 Å that are associated with long chain milk TAGs, containing unsaturated fatty acid(s) or the 2L structures of 39-48 Å that are associated with long chain fully saturated TAGs (Lopez, 2018; Pratama et al., 2021). We observed this 53 Å lamellar structure in our previous study (Pratama et al., 2021) and speculated that it may correspond to a β-crystal polymorph. In fact, a similar lattice spacing (54 Å) is also reported by Lopez et al. (Lopez, Bourgaux, Lesieur, Bernadou, et al., 2002), despite no polymorph type association has been made. However, both studies agree that at 53-54 Å length, the stacking type should be that of a triple-layered chain structure. This unknown polymorph has a very short d-spacing for a 3L structure, especially when compared to the well-known α-3L (72 Å) and β'-3L (67 Å). Therefore, we estimated that this stacking configuration can only be a result of asymmetrical TAGs containing the very short butyric ($C_{4:0}$) to caproic ($C_{6:0}$) fatty acid (Pratama et al., 2021). It is worth noticing that a TAG is considered to be asymmetrical, when it has a solitary fatty acid at the *sn*-1 or *sn*-3 position with an acyl chain length differing more than two carbon atoms as compared to the other two fatty acids (Sato, 2001).

In its free fatty acid form, butyric acid (IUPAC name: butanoic acid) (Jensen, 2002) is volatile and thus contributes to specific sensorial properties of dairy products. It is among key odorants in cream and it is described as having a cheese-like aroma (Pionnier and Hugelshofer, 2006). However, the presence of butyric acid in milk fat is mainly in the form of a TAG. In a recent study, we found that butyryl containing TAGs account for 13 out of 37 molecules identified in milk fat (Pratama et al., 2021), whereas another study reported that this fatty acid appears in 14 out of 56 identified TAGs (Lopez et al., 2006). Moreover, Gresti et al. (1993) reported that three major TAGs in milk fat are all butyryl containing TAGs, namely butyryl-palmitoyl-oleoyl-glycerol, butyryl-dipalmitoyl-glycerol, and butyryl-myristoyl-palmytoyl-glycerol. Thus, butyryl containing asymmetrical TAGs represent a quite significant portion of the milk fat composition. However, despite its high proportion, little information is available on how this group of asymmetrical TAGs contribute to the overall phase behaviour or to the polymorphism of milk fat. The asymmetrical TAGs cannot generally form the most stable triclinic β-crystal in a mixture with other symmetric TAGs due to the severe packing constraints (Sato, 2001). Therefore, researchers commonly link a high amount of asymmetrical TAGs to the lack of β-polymorph observed in milk fat (Grotenhuis et al., 1999).

Among many short-chain butyric containing TAGs in milk fat, 1-butyryl 2-palmitoyl 3-stearoyl-glycerol (BuPS) is present in concentrations of 3.9% and 4.6% (w/w) in cow milk fat and buffalo milk fat, respectively (Pratama et al., 2021). We note, that this percentage also accounts for possible positional isomers, for instance 1-butyryl 2-stearoyl 3-palmitoyl-glycerol (BuSP). However, it can be expected that, due to the small length difference of the palmitic ($C_{16:0}$) and stearic acid ($C_{18:0}$) chains that positional isomers (*sn*-2 and *sn*-3) have little effect on the overall structural arrangement in the crystals. On that account, the present study on BuSP, is greatly representative for the general behaviour of asymmetrical TAGs in milk fat. Indeed, this work aims to provide an in-depth evaluation to the polymorphism of the butyric containing asymmetrical TAGs in milk fat, and thus provides insights into their role in the bigger scheme of complex milk fat polymorphism. This is achieved by a crystallographic investigation of a pure butyryl containing TAG compound, applying small- and wide-angle X-ray scattering as well as differential scanning calorimetry. Further, the mechanism of the structural rearrangement i.e., from pre-nucleation clustering to tilt angle modification of different crystal polymorphic types is evaluated by their electron density profiles.

4.3 Material and Methods

4.3.1 Materials

The 1-butyryl 2-stearoyl 3-palmitoyl-*rac*-glycerol sample (CAS number 152914-63-1) was obtained from Cayman Chemical (Michigan, USA) in the form of powder with a purity of ≥ 98%. The sample was received in a temperature-controlled package and then immediately stored in a freezer (*ca*. -18 °C) until the day of experiment.

4.3.2 Small- and wide-angle X-Ray scattering measurements

The powder sample was directly filled into a 2 mm outer diameter (1.56 mm inner diameter) thick glass capillary (Virtex, Herlev Denmark) without any further preparation. The capillary was subsequently sealed with two-component epoxy glue and a polycarbonate plug. The crystal structure measurements were conducted at the Diamond-Leeds Small Angle X-ray Scattering (DL-SAXS) Facility, situated at Diamond Light Source Ltd., Didcot, United Kingdom. The SAXS instrument, a Xeuss 3.0 from Xenocs SAS (Grenoble, France), was equipped with a molybdenum source and coupled with an Eiger2 R 1 M detector from Dectris AG (Baden-Dätwill, Switzerland). Measurements were carried out at a sample to detector distance of 275 mm, resulting in a q ($4\pi \sin\theta/\lambda$) range of 0.08 - 2.2 $Å^{-1}$ which covered the regime of interest. A Peltier sample stage (Xenocs SAS, Grenoble France) was used to control the sample temperature with an accuracy of 0.1 °C.

Acquisition of the sample scattering patterns of the original powder were acquired at 20 °C for 30 minutes. Subsequently, the powder was melted at 60 °C and held at such temperature for 15 minutes. The diffraction patterns of the molten samples were acquired at the same temperature for 15 minutes. The sample was then quenched to 20 °C and underwent an isothermal hold for 18 hours. X-ray scattering patterns were recorded every 15 minutes during the holding time. The data reduction was carried out in DAWN 2.24 programme (Basham et al., 2015) (this concerns (i) the calibration of the q-axis, (ii) the radial integration of the 2D-intensity images and (iii) the background subtraction of the empty capillary). Further, the data analysis and presentation of data was carried out with Origin 2019b (OriginLab, Massachusetts, USA). For peak fittings Pearson VII distributions were used. The d-spacings were obtained from linear interpolation of all recorded peak positions ($d(h) = 2\pi/q(h)$).

4.3.3 Chain tilt angle estimations

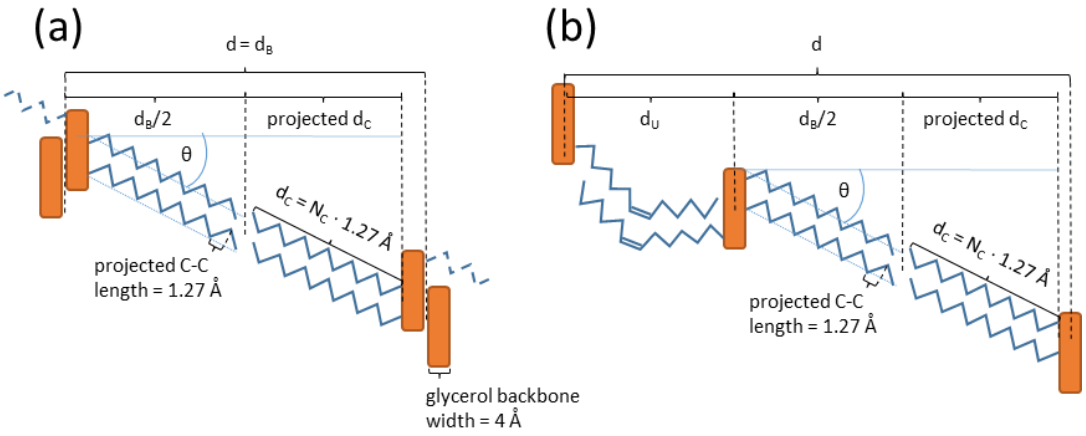

Figure 4.1 Tilt angle estimation given for 2L-polymorphs (a) and 3L-polymoprhs (b). Hydrocarbon chain are colour-coded in blue and the glycerol backbones in orange. The overall thickness in 2L-layers is given by the bilayer thickness (d_B), while in 3L-layers by the sum of the bilayer and monolayer thickness ($d = d_B + d_M$).

The given estimations for the tilt angle of the hydrocarbon chains in the 2L- and 3L-phases of TAGs is based on two experimental findings. First, the projected bond-length (C-C) along the hydrocarbon chains is known to be 1.27 Å(Nagle and Tristram-Nagle, 2000) and the extension of 1 glycerol backbone in stacking direction is about 4 Å(Ladd Parada et al., 2018) (Figure 1). With these hypotheses, the chain tilt angle in 2L-phases can be expressed as:

$$\boldsymbol{\theta_{2L} = cos^{-1}\left(\frac{projected\ d_C}{d_C}\right) = cos^{-1}\left(\frac{0.5\ d_B - 4\text{Å}}{N_C\ 1.27\text{Å}}\right)}$$

Eq. (4.1)

Similarly, for 3L-phases it can be represented as:

$$\boldsymbol{\theta_{3L} = cos^{-1}\left(\frac{projected\ d_C}{d_C}\right) = cos^{-1}\left(\frac{0.5\ d_B - 2\text{Å}}{N_C\ 1.27\text{Å}}\right)}$$

Eq. (4.2)

It is worth noticing that the estimate for the longitudinal glycerol backbone extension was drawn from data on cacao butter in the 2L-α phase and

depending on the glycerols backbone orientation in other TAG-phases this value might easily be off by 0.5 to 1 Å.

4.3.4 Calculation of the area per chain

The calculation of the area per chain, A_C, is given by the hexagonal sub-cell in the α-phase and by orthorhombic sub-cell in the β'-phase. In the hexagonal packing, the area per chain is given by:

$$A_{C(\alpha)} = \frac{2}{\sqrt{3}} d_{10}^2$$

Eq. (4.3)

where d_{10} is the d-spacing of the only diffraction peak recorded at about q_{10} = 1.53 Å^{-1}. The area per lipid chain in the β'-phase given by (Marsh, 2012):

$$A_{C(\beta')} = \frac{d_{20} d_{11}}{\sqrt{1 - \left(\frac{d_{11}}{2d_{20}}\right)^2}}$$

Eq. (4.4)

where d_{20} is the corresponding d spacing for the medium-intense peak at about q_{20} = 1.64 Å^{-1} and d_{11} is the corresponding d spacing of the strong peak at about q_{11} = 1.51 Å^{-1} (Van Langevelde et al., 2000).

4.3.5 Electron density calculation for the molten phase

Electron density profiles of the molten phase is employed to evaluate the pre-nucleation clustering event of the BuSP. The broad peak at small angle scattering regime in the molten phase was simulated using an electron density model developed based on Gaussian distributions. Details of the model development have been described elsewhere (Sadeghpour et al., 2018). Briefly, the electron density profile comprises of three Gaussian distributions; the first one describing the glycerol backbone of self-assembled triglycerides and positioned at the centre of the profile. The second Gaussian distribution is off-centred at either sides of glycerol headgroup region representing the hydrocarbon methylene groups. A third Gaussian distribution with lower height attributed to the loosely attached triglycerides forming a shell around the core of the assembly. The simulated scattering profile could be obtained by squared Fourier transform of the electron density and then applying a Lorentzian correction. The positions, broadness as well as the height of

Gaussian distributions could be optimised by comparing the simulated and experimental scattering profiles. We have applied a particle swarm optimisation approach to obtain the best fitting parameters in our model.

4.3.6 Electron density profiles (EDP)

EDP determinations of BuSP α- and β'-polymorph were carried out using a standard Fourier transform procedure (Li et al., 2017; Ladd Parada et al., 2018). Concisely, the Braggs peak intensities were obtained from the fitted area, which were then Lorentz corrected. The Lorentzian correction of the recorded intensities, *I(h)*, for a point focus set-up, as used in this study, is h^2, where *h* is the Miller index (diffraction order), i.e., all fitted intensities (I_h) were multiplied with h^2 (for further reading on the Lorentz correction, see Li *et al*. (2017)). Subsequently, the amplitude values (F_h) were obtained from the square root of the corrected intensities ($\sqrt{I_h}\ h$). In case of centrosymmetric EDPs, the Fourier transform is obtained by the summation of cosine terms only:

$$\Delta\rho(z) = \sum_{h=1}^{h_{max}} \alpha_h F_h cos\left(\frac{2\pi z h}{d}\right)$$

Eq. (4.5)

where $\Delta\rho$ is the electron density contrast, α_h the phases (note, α_h is fixed to -1 for h = 1), and *d* denotes the lattice spacing. The phases α_h for h = 2 to 6 were taken from literature to be -1, +1, -1, -1 and -1 (Mykhaylyk and Hamley, 2004).

4.3.7 Differential scanning calorimetry (DSC) measurements

Heat flow measurements were carried out with a TA instrument DSC Q-20 (Elstree, UK). An 8 ± 0.01 mg BuSP powder sample was readily inserted into an aluminium T-zero pan (TA instruments, Elstree, UK) and hermetically sealed. The heat flow of sample was calculated as the net heat flow difference between the sample-containing pan and an empty reference pan.

The applied thermal procedure consisted in three subsequent heating and cooling ramps. The heating rate was 5 °C/min, whereas the cooling rate was -10 °C/min for the entire experiment. First, the sample powder was equilibrated at 20 °C before being heated to 65 °C. The sample was held at this temperature for 2 minutes before subjected to a cooling back to 20 °C.

Afterward, the temperature was kept constant for 1 hour followed by a heating ramp to 65 °C to re-melt the sample. Similarly, a 2 minutes hold was applied before the sample was brought to 20 °C. Last, an isothermal hold for 18 hours was carried out before the final melting ramp to 65 °C. All experiments were conducted in triplicate. Data were processed using TA Instruments Universal Analysis 2000 version 4.5A and plotted in Origin 2019b (OriginLab, Massachusetts, USA).

4.4 Results and Discussion

4.4.1 Crystallisation kinetics during isothermal hold

The temporal evolution of BuSP X-ray diffraction patterns during the isothermal hold at 20°C is presented in **Figure 4.2a**. The crystallisation from the molten BuSP occurred immediately after the isothermal target temperature was reached. A crystal structure corresponding to a hexagonal packing was observed during the first hour of isothermal hold, with a stacking distance of 57 Å. On further observation with longer isothermal hold, a polymorphic transformation from the metastable α- to the more stable β'-polymorph took place. Most notable indications are the decaying intensities of the 4^{th} and 6^{th} order peaks of the α-phase, whilst all the β'-peaks are rising in intensity as clearly noticeable by its 4^{th} order peak at q = 0.48 $Å^{-1}$. The polymorph transformation can be observed also in the wide-angle region, where the short spacing peak at q_{20} = 1.64 $Å^{-1}$ (d_{20} = 3.84 Å) grows in intensity. Note, together with the q_{11}-peak at 1.51 $Å^{-1}$ (d_{11} = 4.15 Å) the q_{20} peak defines the orthorhombic sub-cell of the β'-polymorph chain packing (Van Langevelde et al., 2000) (**Eq. 4.4**).

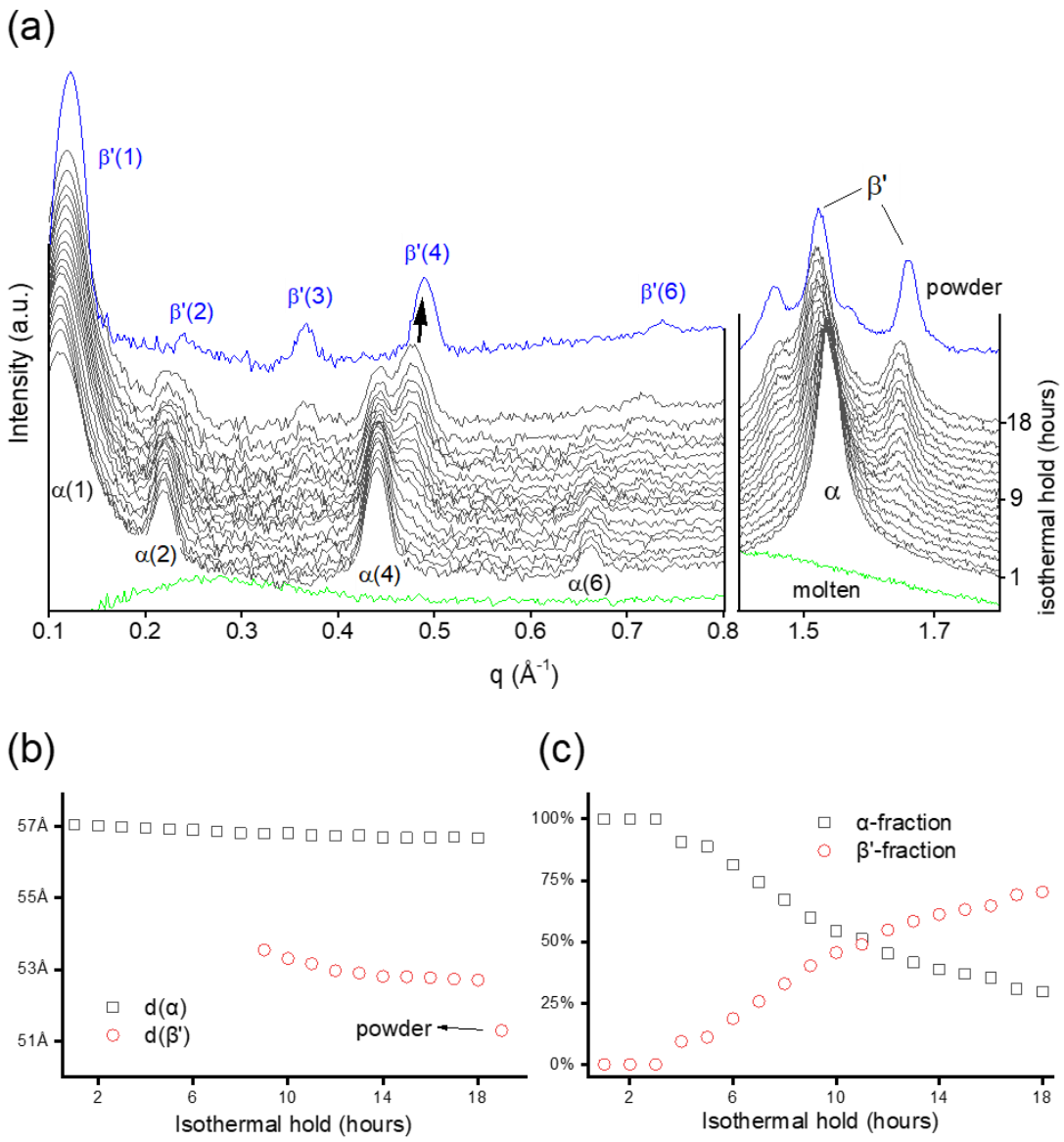

Figure 4.2 (a) Evolution of BuSP structure at 20°C during an isothermal hold for 18 hours as observed by small- and wide-angle X-ray scattering. Note, for each non-zero diffraction peak the corresponding Miller index is given in brackets. (b) D-spacing of the α- and β'- polymorph. (c) Estimated crystalline fractions of the α- and β'- polymorph over the isothermal hold time.

Figure 4.2b shows the time evolution of the lamellar repeat distances of both the α- and β'-polymorph. Note, that in the coexistence regime, these stacking distances were estimated from the relatively strong and well-resolved 4th order peaks. The strongest first order peaks positions were not considered in this analysis, as they are widely overlapping. The lamellar thickness of the α-form was observed to decrease only slightly from 57.0 Å to 56.7 Å at the end of the isothermal hold. The β'-polymorph peaks were observed firstly after 3 hours of the isothermal hold (see **Figure 4.2a** - WAXS). However, the first reliable

4th order peak in the SAXS region could only be clearly obtained from the 9th hour onwards, which displayed a lamellar thickness of 53.5 Å. The *d*-spacing of the β'-form decreased to 52.7 Å at the end of the isothermal hold. Further comparison of this value to the X-ray diffraction of the powder sample shows that the β'-crystal eventually evolves to an even more compact structure, with a *d*-spacing of 51.2 Å.

Figure 4.2c shows a binary transformation from the α- to the β'-polymorph. To estimate the polymorphs fractions as a function of time, we used the intensity of the q_{20} peak of the orthorhombic sub-cell (see **Figure 4.2a** - WAXS). The highest intensity of the q_{20} peak from the powder sample was set as 100% of β'-fraction, whereas the pure α-system at isothermal t = 1 hour represents 100% of the α-fraction. As a result, at the end of the isothermal hold (18h), we estimate the BuSP crystalline material consisted of around 70% β'-form and 30% α-form. Additional conversions of molten TAGs to the crystalline phases has not been considered. Indeed, the α- to β'- polymorphic conversion is accompanied by continuous increase in the solid fat content (SFC). Estimations from the wide angle X-ray patterns (Arita-Merino et al., 2020) show that the SFC increases from 47 to 76 % from t = 1 to t = 18 hours of isothermal hold. Details on SFC estimations are presented in the Supporting Information (Appendix B) **Figure B.1**.

The kinetics of the BuSP α- to β'-crystal transformation is slow, if we compare it with that of milk fat. In our previous study, the α-polymorph in milk fat had already disappeared after 5 hours of isothermal hold at -10 °C (Pratama et al., 2021). Note, in this study we employ a higher isothermal hold temperature (20°C), which should promote an even faster polymorph transformation towards the β'-crystal (Grotenhuis et al., 1999), as this temperature is closer to the melting point of the α-phase. It was also reported that milk fat can directly crystallize into the β'-form after quenching to 25 °C (Bayard et al., 2022), which demonstrates its favourable pathway to stabilise in the orthorhombic packing of the hydrocarbon chains. Hence, the slower temporal evolution of BuSP in this study supports the notion that asymmetric TAGs may play a significant role in delaying the polymorphic transformation from α- to β'-crystal in milk fat. We note, that this view is also in agreement with our previous findings (Pratama et al., 2021), where the buffalo milk fat which has higher butyryl containing TAGs than cow milk fat, exhibits slower α to β' polymorph transformation at cooling rate of -0.5 °C/min.

4.4.2 Polymorphism of BuSP

For obtaining a better understanding on the nanostructure of the different polymorphs of BuSP, selected X-ray diffraction patterns are presented in more detail in **Figure 4.3**. For BuSP heated to 60 °C, **Figure 4.3a** shows two broad scattering peaks corresponding to a characteristic length of 22.6 and 4.43 Å, respectively. The first diffuse peak arises from the clustering of molten TAG molecules (Ladd Parada et al., 2018) and the second diffuse peak stems from the short-range interchain correlation peak position (Spaar and Salditt, 2003). Concerning the clustering behaviour we have recently presented a 'core-shell cluster' model to elucidate this phenomenon (Sadeghpour et al., 2018). The model describes the TAGs being arranged in a 'back to back' fashion in its core, whilst an outer layer of TAGs is only loosely attached to it. Employing the model, we have fitted the molten BuSP scattering patterns with this three Gaussian model (Sadeghpour et al., 2018), obtaining very a similar cluster model (**Figure 4.4**) as determined for cocoa butter (CB) (Sadeghpour et al., 2018).

Briefly, the overall BuSP cluster size (**Figure 4.4b**) is of 46 Å, leading to a fluid 'bilayer' thickness of 23 Å, which compares to a determined chain length of palmitic and stearic acids of 13-14 Å (Pabst et al., 2004). Note, the term 'bilayer' is not used strictly here. First, our model cannot pinpoint whether the TAG clusters have a planar or rod-like geometry, and further the second loosely attached TAGs layer coverage is only about 8%. Further, considering the extension of the glycerol backbones to occupy about 6 Å per 'bilayer' (a full glycerol backbone extension in the core, 4 Å, and half at the outer layer, 2 Å), we can conclude that the core and second layer interdigitate up to about 9 Å. At this stage it remains speculative, but this observed interdigitation might be caused by fatty acyls not only orienting outwards from the centre of the core, but also reaching into the opposite side of the cluster and hence creating a void deeper inside the core, which gets occupied by the second layer TAGs. This would apply for TAGs being in the tuning fork (Tf) and chair conformation (Ch), while the trident (Tr) TAGs would not cause any interdigitation effect in this picture. As already assumed in our original paper on TAG cluster formation (Sadeghpour et al., 2018), the propeller (Pr) TAGs would fit best into the clusters at the edges, i.e., into the highly curved areas of the TAG cluster. In this respect, it is instructive to know, that the probability of finding a TAG in a specific conformation in the fluid phase was recently simulated to follow the order of Tr (50-56%) > Ch (28-34%) > Pr (11-14%) > Tf (1-6%) (Golodnizky et al., 2022), allowing for the proposed TAG cluster formation.

Finally, since the BuSP and CB (Sadeghpour et al., 2018) clusters analysis have shown practically identical structural extension, we do believe that the butyric acid plays only a minor role in the fluid cluster formation.

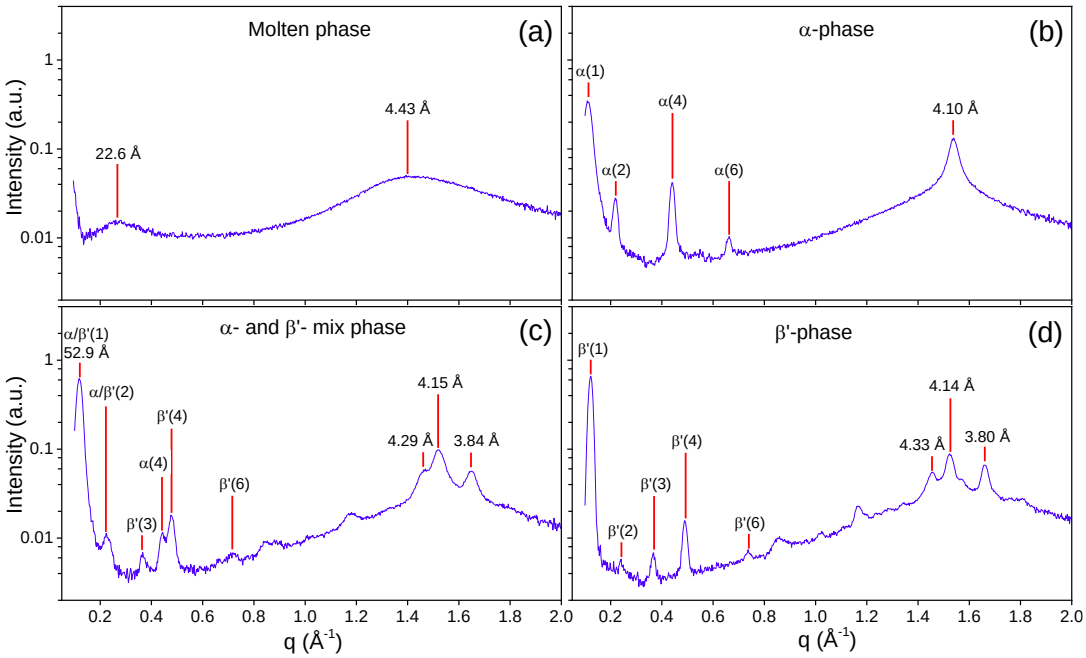

Figure 4.3 X-ray diffraction patterns of 1-butyryl 2-stearoyl 3-palmitoyl-glycerol at different phases: (a) molten, sample heated at 60°C for 15 minutes (b) α-phase, molten sample quenched to 20°C and held for 1 hour (c) mix of α- and β'-phase, molten sample quenched to 20°C and held for 18 hours and (d) β'-phase, direct observation on powder sample.

Returning to our overview graph, the X-ray scattering pattern of the BuSP α-polymorph is shown in **Figure 4.3b**. The single peak at wide angle with short spacing of 4.10 Å corresponds to a hexagonal lateral packing of the hydrocarbon chains, whereas in the small-angle regime, diffraction peaks covering the first six orders arise from the 3L stacking structure with a *d*-spacing of 56.9 Å. Here, the calculated *d*-spacing accuracy is slightly improved from the incorporation of all peaks, as compared to **Figure 4.2b**, where only the 4th order peak was considered.

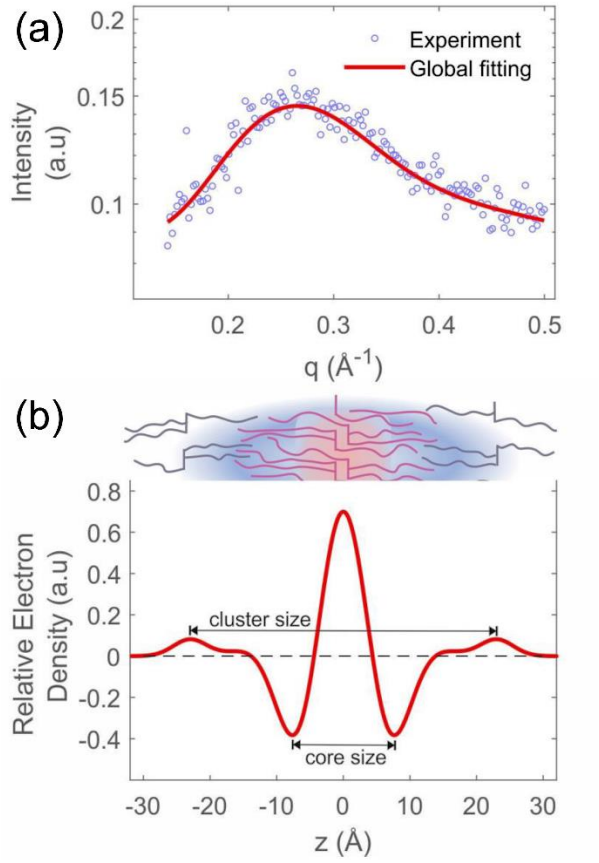

Figure 4.4 a) The global fitting (line) of the SAXS pattern from BuSP in the molten phase (open circles) bases on the structural TAG cluster model presented below. b) The electron density profile demonstrates the BuSP assembly in a core-shell cluster model. The outmost peaks represent loosely attached BuSPs to the cluster core.

Figure 4.3c shows the diffraction pattern of BuSP displaying the coexistence of the α- and β'-polymorphs, which was taken after 18 hours of isothermal hold. The presence of the β'-form is clearly indicated by the q_{20} peak at 2π/3.84 Å^{-1}. At this specific isothermal time, the α-polymorph has decreased significantly, but not entirely vanished. This can be seen from the less-intense 4th order peak (q = 0.441 Å^{-1}) of the α-phase, which is coexisting with the more intense 4th order peak (q = 0.477 Å^{-1}) of the β'-phase. Noteworthy, the position of the overlapping 1st order peaks corresponds to 52.9 Å. This long spacing is very close to the *d*-spacing of the ambiguous 3L structure (53 Å) previously observed in milk fat (Lopez et al., 2002; Pratama et al., 2021). Thus, it is tempting to conclude that this 53 Å spacing most-likely stems from the mixed α- and β'-phases of butyryl-containing TAGs. This conjecture is also in accordance with the fact that BuSP exhibits relatively slow polymorphic transformation kinetics compared to milk fat in general.

The X-ray scattering pattern of the pure β'-polymorph of BuSP was obtained from the powder sample (**Figure 4.3d**). Note, no traces of the α-polymorph were detected here. Again, we were able to record the first six order peaks in the small-angle regime, with a non-zero 3rd order peak being unique as it was not recorded in the α-form (**Figure 4.3b**). Taking all peaks into consideration, the longitudinal *d*-spacing is 51.2 Å. In the wide-angle regime three dominant peaks are apparent, i.e., referring to the short spacings of 4.33, 4.14, and 3.80 Å, with the second peak having the strongest intensity. In agreement to literature (Mykhaylyk and Hamley, 2004; Ghazani and Marangoni, 2019) this diffraction pattern is attributed to the form IV of the β' polymorph in cocoa butter. We note, while the characteristic three diffraction peak positions vary only little among different form IV polymorph structures (Ghazani and Marangoni, 2019), the intensity profiles do display differences. For instance for cocoa butter samples the 4.33 and 4.14 related peaks are the most intense, while other samples such SOS and POP-rich sample display a similar intensity profile as BuSP (Mykhaylyk and Hamley, 2004). Using the **Eq. 4.3** and **4.4**, we have calculated the area per chains, A_C, in the pure α phase and the pure β' phase. Clearly A_C decays from 19.4 to 18.8 Å^2, which is in good agreement to other reported hydrocarbon chain packings (Ruocco and Shipley, 1982; Li et al., 2022).

We note that our BuSP powder sample was received in a temperature-controlled package and it was then kept in the freezer for more than one month before measurement. Therefore, we argue that the sample should be the most stable crystal form of this asymmetrical TAG. On that note, the current results show that our previous hypothesis (Pratama et al., 2021) on asymmetrical TAGs being linked to a β-polymorph appearance in milk fat can no longer be upheld. An intense peak corresponding to the short spacing of 4.6 Å is the main indication for a triclinic chain packing as found in the β-polymorph (D'Souza et al., 1990). However, this peak was not observed in our experiments (**Figure 4.3d**). BuSP instead seems to be stable in an orthorhombic packing configuration and is unlikely to transform into a triclinic-based structure.

The inhibition of the β-polymorph formation in BuSP may stem from the density of butyryl chain packing in the monolayer regime being too low as compared to common oleic acid monolayers arrangement, for instance in stearoyl-oleoyl-stearoyl-glycerol (SOS). Indeed the EDPs of BuSP (**Figure 4.5**) do display relatively lower densities, when compared to monolayer regime of SOS in the stable β phase (Mykhaylyk and Hamley, 2004). As detailed in

Figure 4.6b, we estimate a loose interdigitation of butyryl chains in the monolayer regime causing a reduction of Van der Waals forces, which in turn does not allow a denser packing in the bilayer region (β-polymorph). This evaluation is in accordance with the earlier work of Kodali et al. (1984) who studied the polymorphism of 1,2-dipalmitoyl-3-acyl-*sn*-glycerols, with the *sn*-3 acyl substituted by 2-16 even numbered saturated fatty acyl chains (PP2-PP16). The current results show similar behaviour with 1,2-dipalmitoyl-3-hexanoyl-glycerols (PP6), where the compound is most stable in β'-form with 3L lamellar architecture, but not with PP4 (reported 2L-stacking). We speculate the difference in BuSP may arise from methyl end stacking interaction, i.e., stearoyl-palmitoyl *vs* palmitoyl-palmitoyl, which influences the chain length organization (Sato, 2001). Remarkably, Goto et al. (1992) observed a 3L stacking even in PP2 (single crystals), which agrees with the current finding. However, it is worth to note that the current observed behaviour of BuSP is from a racemic compound. Whereas the optically active version of the BuSP might show different crystallisation behaviour as seen in other asymmetrical triacylglycerol (Mizobe et al., 2013). Nevertheless, this work provides further support to the view that the asymmetrical TAGs are typically stable in the β'-polymorph (Sato, 2001). Consequently, the high proportion of these TAGs in milk fat could be a contributing factor to the β'-polymorph being predominant in milk fat crystals (Grotenhuis et al., 1999). A summary of the BuSP α- and β'-polymorph X-ray crystallographic parameters are presented in **Table 4.1**.

Table 4.1 Summary of d-spacing, small angle peaks intensity and short spacings of BuSP polymorphs.

Poly-morph	***d*-spacing (Å)**	**Intensity of small angle peaks**						**Short spacings (Å)**		
		1	2	3	4	5	6			
α	56.9	vs	w	-	m	-	vw	-	4.10 (vs)	-
β'	51.2	vs	vw	w	m	-	vw	4.33 (m)	4.14 (s)	3.80 (s)

vs: very strong, s: strong, m: medium, w: weak, vw: very weak

4.4.3 Electron density profiles (EDPs) and the structural evolution of the β'-polymorph

EDPs are a useful tool to further obtain fine-structural information from X-ray scattering data (Li et al., 2017). For instance, the maxima in the EDPs represents the highest electron density, which in the case of TAGs, is given by the carbonyl groups in the glycerol backbone. Accordingly, one can utilize the peak-to-peak distance in the EDPs to obtain the inner structure of the TAG lamellae, such as the bilayer and monolayer thickness. Further, by knowing the bilayer thickness, one can work out the tilt angle and estimate the number of its contributing carbons in the chain (Pratama et al., 2021) (see **Figure 4.1** as well as **Eq. 4.1** and **4.2**).

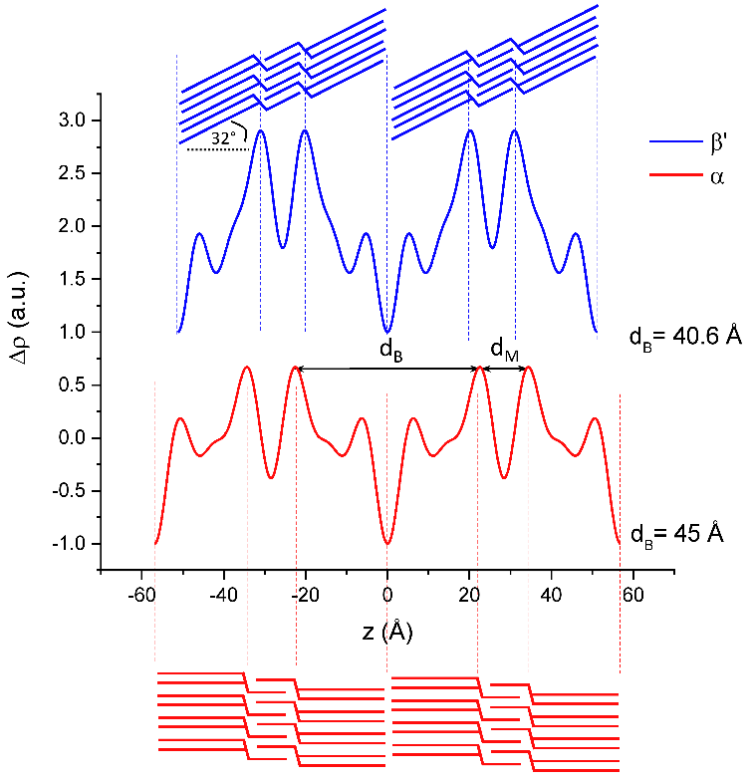

Figure 4.5 Electron density profiles (EDPs) of 1-butyryl 2-palmitoyl 3-stearoyl-glycerol (BuSP) determined from X-ray diffraction patterns presented in Figure 4.2. The α-polymorph has a d-spacings of 56.9 Å (d_B = 45 Å) and the β'-polymorph a d-spacings of 51.2 Å (d_B = 40.6 Å). d_B =bilayer thickness, d_M = monolayer thickness.

Figure 4.5 shows the EDPs of α- and β'-polymorph of BuSP, whose structural parameters are given in **Table 4.2**. It is clearly displayed that the BuSP crystals are organized as 3L architectures, as shown by two maxima corresponding to two separated glycerol backbones regions. By contrast, a 2L

structure would only manifests a single maxima per unit cell stemming from the back-to-back arrangements of glycerol backbones. The shorter distance between maxima in **Figure 4.5** indicates that the monolayer region can only be occupied by the short chain butyryl, whereas the longer stearoyl and palmitoyl chain aggregate in the bilayer region. It is worth noticing that all three alkyl chains of BuSP are saturated fatty acid, thus we assume all three to be in their all-trans conformation. The EDPs are constructed from four and five non-zero diffraction peaks for the α- and β'-polymorph, respectively. Nevertheless, we recorded in both cases diffraction peaks up to the 6th Bragg's order. While the resolution of the EDPs should scale roughly with half of the smallest recorded lattice spacing (i.e., about 5 Å), the precision finding the maxima in the EDP at this given resolution is expected to be below 1 Å (Rappolt, 2010). The bilayer thickness determined from the β'-polymorph EDP (**Figure 4.5**) is 40.6 Å, whilst the number of contributing carbons for BuSP is taken as an average of that of stearic and palmitic acid (N_C = 17). The β'-form tilt angle for a 3L structure was calculated using **Eq. 4.2** as introduced in the Materials and Methods section. Hence, the calculated tilt angle of the BuSP β'-polymorph is about 32°. Previously reported chain tilt for the most stable β-form of stearoyl-oleoyl-stearoyl-glycerol was 36° (Mykhaylyk and Hamley, 2004). Therefore, the current result is in excellent agreement with the common knowledge that the β' structure has a looser chain packing than the β, and consequently it displays a smaller tilt angle.

Table 4.2 Structural parameters used for the calculation of the BuSP electron density profiles.

h	α-polymorph			β'-polymorph		
	q (Å^{-1})	**I_h (a.u.)**	**$\alpha_h F_h$ (a.u.)**	**q (Å^{-1})**	**I_h (a.u.)**	**$\alpha_h F_h$ (a.u.)**
1	0.1104	1.000	-1.00	0.1219	1.000	-1.00
2	0.2189	0.042	-0.41	0.2454	0.004	-0.12
3	-	-	+0.00	0.3660	0.008	+0.27
4	0.4405	0.090	-1.20	0.4899	0.026	-0.64
5	-	-	-0.00	-	-	-0.00
6	0.6619	0.011	-0.62	0.7368	0.004	-0.36

The hexagonally packed α-polymorph chains are freely rotating around their long-axis, thus the chain packing tilt is expected to be about 0°. This is further confirmed from the EDP-deduced chain length d_C, which we estimated to be equal to $d_B/2$ - 2Å (see **Figure 4.1**), i.e., 45/2 - 2 Å = 20.5 Å. This compares well to an all-trans chain with 17 carbons: $d_C = 17 \cdot 1.27$ Å = 21.6 Å. Note that the deviation is within the errors and might be caused by both the given uncertainty on the longitudinal glycerol backbone extension of 4 Å and the positional error of the EDP maxima.

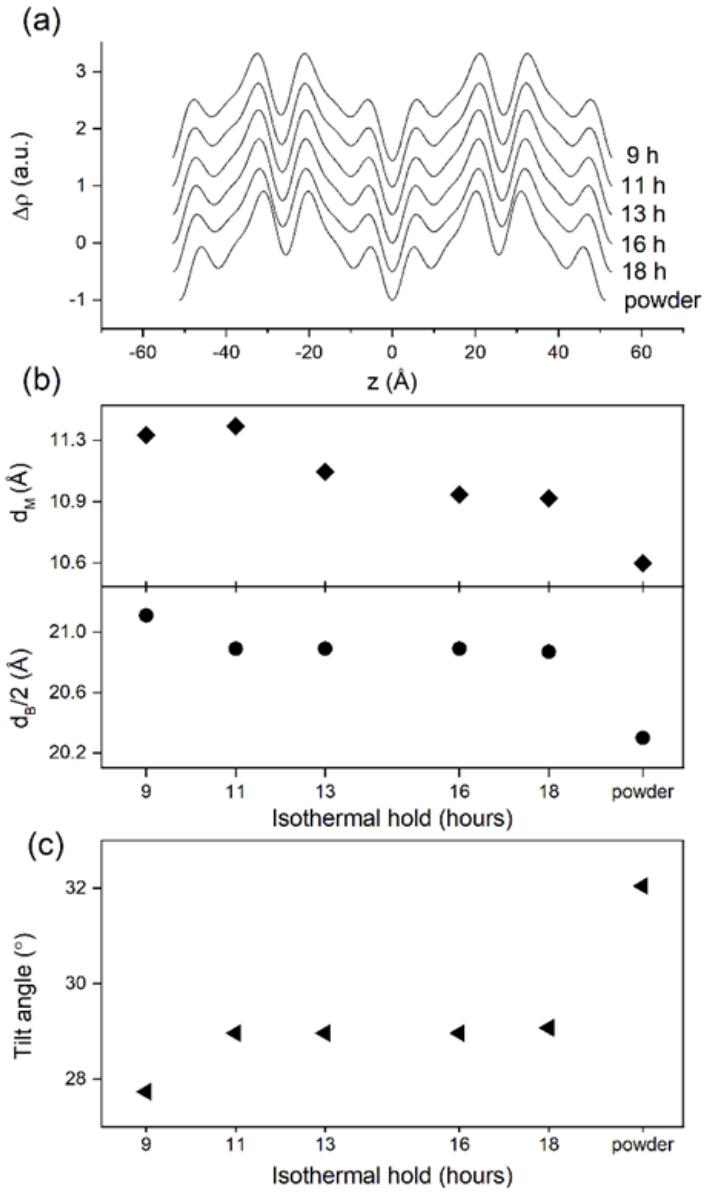

Figure 4.6 (a) Evolution of electron density profiles (EDPs) of 1-butyryl 2-palmitoyl 3-stearoyl-glycerol (BuSP) β'-polymorph at different isothermal hold. (b) The evolution of bilayer and monolayer thickness of the BuSP β'-polymorph at different isothermal hold. (c) The evolution of the tilt angle of the BuSP β'-polymorph at different isothermal hold.

Chain packing tilt is a consequence of the conformational rearrangement of the TAG molecules towards a more compact structure during a polymorphic transformation. In this respect, one observes for instance an increasing chain tilt from the metastable β' to the stable β polymorph. However, a tilt angle evolution is also observed during finer structural rearrangements within a phase. For instance, during the condensation process from initial β'-polymorph formation towards the final and stable organization of this packing, as already indicated by the shrinking of its *d*-spacing (**Figure 4.2b**). **Figure 4.6a** and **4.6c** display a series of EDPs and the corresponding tilt angle evolution of BuSP β'-crystal as a function of elapsed time.

It is worth noticing that the determination of EDPs, when the α- and β'- crystal coexist (**Figure 4.3c**), required an intensity correction procedure because of the strongly overlapping 1^{st} and 2^{nd} order peaks. For this reason, the fitted areas of both peaks were corrected by the corresponding fraction of the β'-polymorph (**Figure 4.2c**). In conclusion, we can associate the shortening *d*-spacing of β'-form (**Figure 4.2b**) with an increasing chain packing tilt (**Figure 4.6c**). At t = 9 hours, the β'-crystal is observed with an estimated chain tilt of 27.7° (**Figure 4.6c**). The crystal becomes more compact and its lamellae condenses with longer isothermal hold. At the end of the experiment (t = 18 hours), the tilt angle increases to 29.1°. Taking the BuSP powder as the final β'-polymorph architecture, we can infer that this packing readjustment will continue until the final chain tilt 32° is reached.

Figure 4.6b shows the evolution of the bilayer and monolayer thickness of the β'-form as a function of time. It is worth noting that not only the bilayer but also the monolayer thickness decreases during the longer isothermal hold. This shows that the more compact β'-stacking (**Figure 4.6b**) is not only reflected in increasing chain tilts, but it is also due to changes in the monolayer region. In fact, the monolayer thickness, d_M, changes from 11.3, 11.0 to 10.6 Å for t = 9 h, t = 18 h and t > 30 days, respectively. A plausible explanation for this would be that the degree of interdigitation augments with time in this region, and hence it also contributes to the condensing of the β' polymorph. Indeed, the estimated all-trans chains length, d_C, of butyryl is only 5.1 Å ($N_C \cdot 1.27$ Å = 4 · 1.27 Å), while the monolayer region accommodates spaces of 6.6 to 7.3 Å (d_M - 4 Å). Nevertheless, even though the trends in d_M are significant, absolute errors 0.5 to 1.0 Å have still to be considered.

4.4.4 Thermal characterisation of BuSP

Thermograms of BuSP subjected to different thermal treatments are presented in **Figure 4.7**. Four experimental setups were carried out to complement the X-ray scattering observation. The first one is to observe the crystallisation temperature of BuSP from its melt (**Figure 4.7a**). When subjected to -10°C/min cooling rate, the onset of the exothermic peak shows that BuSP melt has a nucleation point of 29.1 ± 0.03 °C. As a comparison, cow and buffalo milk fat show nucleation point at 15.6 and 17.4 °C, respectively, at the same cooling rate (Pratama et al., 2021). Therefore, BuSP is among the higher melting point TAGs in milk fat, most likely due to its fully saturated chains. Nonetheless, it melts at lower temperatures than fully saturated long chain TAGs, such as tripalmitin that reaches 66 °C (Lutton, 1950).

In order to produce the α-polymorph, the second thermal treatment was an isothermal hold for 1 hour at 20°C following crystallisation. Upon heating at 5°C/min rate, the thermogram exhibits two endothermic and one exothermic peaks (**Figure 4.7b**). The first endothermic corresponds to the melting of BuSP α-polymorph, with onset point of 30.3 ± 0.03 °C. This is followed by an exothermic dip that corresponds to a polymorphic crystallisation α → β' polymorph. Hence, the second endothermic peak could be attributed to the melting of the β'-phase with the onset point at 45.9 ± 0.1 °C.

Figure 4.7c shows the thermogram of BuSP melting after long isothermal hold (18h) as the third thermal treatment. From X-ray measurements (**Figure 4.2**), we have observed a significant, but not complete, α → β' polymorphic transformation with this treatment. The thermogram shows the incomplete transformation as indicated by a small hump at about 32 °C, corresponding to traces of α-form melting. In comparison to the 1 hour isothermal hold, a deep valley corresponding to an exothermic event (e.g., a polymorphic transformation) is not observable. In turn, one endothermic peak is observed, which corresponds to the β'-polymorph melting. The peak onset is 46.0 ± 0.16 °C, which is quite similar to that of 1 hour isothermal hold. It is interesting to compare both onset points with the last thermal treatment, a direct melting of BuSP powder at heating rate of 5°C/min (**Figure 4.7d**). The powder melting displays an onset point at 47.8 °C, which is about 1.6 °C higher than the isothermally treated samples. Correlating this with the above observations from X-ray scattering data, we can associate the higher melting point as the result of a more stable and compact structure, albeit the same crystal packing

architecture of a β'-polymorph is present. It is worth noticing that the powder could be melt only once due to sample limitation.

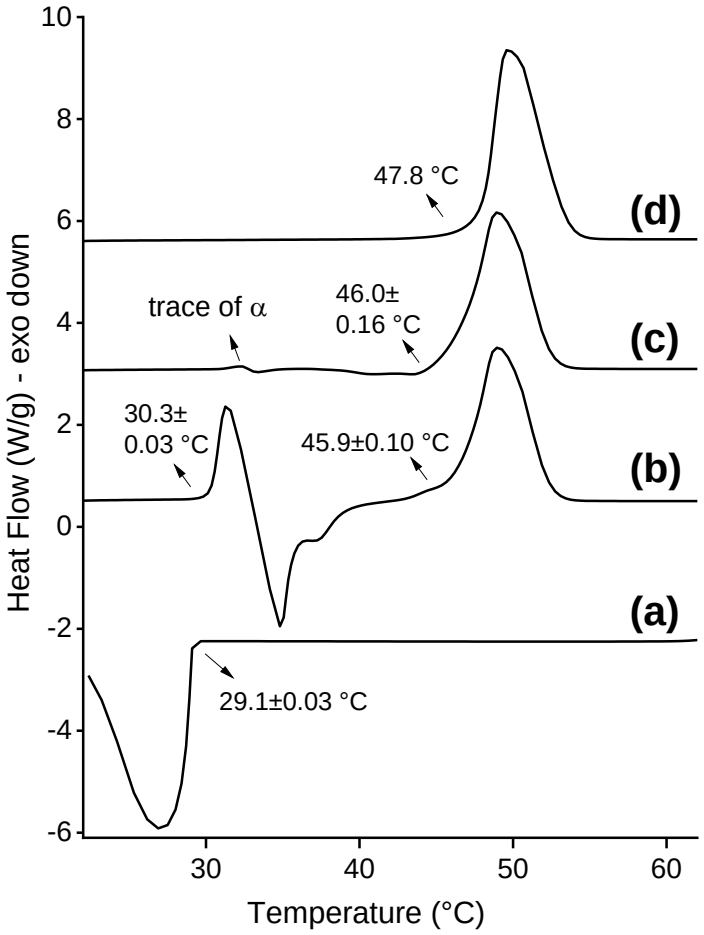

Figure 4.7 Thermogram of BuSP at different thermal conditions: (a) Melt cooling from 65 to 20 °C at 10 °C/min rate, (b) molten sample is equilibrated at 20 °C for 1 hour before heated to 65°C at 5 °C/min rate, (c) molten sample is equilibrated at 20°C for 18 hours before heated to 65 °C at 5 °C/min rate, and (d) powder sample is heated to 65°C at 5 °C/min rate.

4.5 Conclusions

The polymorphism of asymmetrical TAGs in milk fat, as represented by BuSP, was studied here for the first time. BuSP shows only α and β'- polymorphs with *d*-spacing of 56.9 and 51.2 Å, respectively. The most stable β-polymorph is not observed, even after months, possibly due to a relatively lower fatty acyl density in the monolayer regime, prohibiting a denser bilayer packing as needed for the formation of the β phase.

BuSP also displays relatively slower polymorphic transition from the α to β' phase, when compared to milk fat. The most condensed structure was

observed in the pure β'-phase after being kept for more than one month at -18 °C, with a tilt angle of 32° and monolayer thickness of 10.6 Å. Melting point observations using differential scanning calorimetry confirms that this most compact structure. Finally, the modelled molten phase structure shows that the butyryl chains do not play a significant role in in the clustering of TAGs, but its architecture is mainly dominated by the stearic and palmitic fatty as and their distribution into tuning, chair, trident and propeller conformations.

This specific polymorphism of BuSP gives valuable insights into the crystallisation behaviour of butyryl containing TAGs in milk fat, and further, how the behaviour of these asymmetrical TAGs plays a role in the overall milk fat crystallisation. At the higher crystallisation temperature, asymmetrical TAGs containing unsaturated fatty acyl chain may likely be part of the liquid fraction due to their lower nucleation point. Moreover, because of its slow polymorphic transformation, it is plausible to predict that a high concentration of asymmetrical TAGs might delay the polymorphic transformation from the α to β' phase in milk fat crystallisation. Lastly, the asymmetrical TAGs do not tend to form the β polymorph, which could be a major factor to the common absence of the β polymorph in milk fat.

4.6 References

Amara-Dali, W. Ben, Karray, N., Lesieur, P. and Ollivon, M. 2005. Anhydrous goat's milk fat: Thermal and structural behavior. 1. Crystalline forms obtained by slow cooling. *Journal of Agricultural and Food Chemistry*. **53**(26), pp.10018-10025.

Arita-Merino, N., te Nijenhuis, L., van Valenberg, H. and Scholten, E. 2022. Multiple phase transitions and microstructural rearrangements shape milk fat crystal networks. *Journal of Colloid and Interface Science*. **607**, pp.1050-1060.

Arita-Merino, N., Van Valenberg, H., Gilbert, E.P. and Scholten, E. 2020. Quantitative Phase Analysis of Complex Fats during Crystallization. *Crystal Growth and Design*. **20**(8), pp.5193-5202.

Basham, M., Filik, J., Wharmby, M.T., Chang, P.C.Y., El Kassaby, B., Gerring, M., Aishima, J., Levik, K., Pulford, B.C.A., Sikharulidze, I., Sneddon, D., Webber, M., Dhesi, S.S., Maccherozzi, F., Svensson, O., Brockhauser, S., Náray, G. and Ashton, A.W. 2015. Data Analysis WorkbeNch (DAWN). *Journal of Synchrotron Radiation*. **22**, pp.853-858.

Bayard, M., Kauffmann, B., Vauvre, J.M., Leal-Calderon, F. and Cansell, M. 2022. Isothermal crystallization of anhydrous milk fat in presence of free fatty acids and their esters: From nanostructure to textural properties. *Food Chemistry*. **366**(June 2021), p.130533.

Campos, R., Narine, S.S. and Marangoni, A.G. 2002. Effect of cooling rate on the structure and mechanical properties of milk fat and lard. *Food Research International*. **35**(10), pp.971-981.

D'Souza, V., deMan, J.M. and deMan, L. 1990. Short spacings and polymorphic forms of natural and commercial solid fats: A review. *Journal of the American Oil Chemists' Society*. **67**(11), pp.835-843.

Gantner, V., Mijić, P., Baban, M., Škrtić, Z. and Turalija, A. 2015. The overall and fat composition of milk of various species. *Mljekarstvo*. **65**(4), pp.223-231.

Ghazani, S.M. and Marangoni, A.G. 2019. The Stability and Nature of the Form IV Polymorph of Cocoa Butter Is Dictated by 1-Palmitoyl-2-Oleoyl-3-Stearoyl-Glycerol. *Crystal Growth and Design*. **19**(3), pp.1488-1493.

Golodnizky, D., Shmidov, Y., Bitton, R., Bernardes, C.E.S. and Davidovich-Pinhas, M. 2022. Isotropic liquid state of triacylglycerols. *Journal of Molecular Liquids*. **353**, p.118703.

Goto, M., Kodali, D.R., Small, D.M., Honda, K., Kozawa, K. and Uchida, T. 1992. Single crystal structure of a mixed-chain triacylglycerol: 1,2-Dipalmitoyl-3-acetyl-sn-glycerol. *Proceedings of the National Academy of Sciences of the United States of America*. **89**(17), pp.8083-8086.

Gresti, J., Bugaut, M., Maniongui, C. and Bezard, J. 1993. Composition of Molecular Species of Triacylglycerols in Bovine Milk Fat. *Journal of Dairy Science*. **76**(7), pp.1850-1869.

Grotenhuis, E. Ten, Van Aken, G.A., Van Malssen, K.F. and Schenk, H. 1999. Polymorphism of milk fat studied by differential scanning calorimetry and real-time X-ray powder diffraction. *JAOCS, Journal of the American Oil Chemists' Society*. **76**(9), pp.1031-1039.

Grummer, R.R. 1991. Effect of Feed on the Composition of Milk Fat. *Journal of Dairy Science*. **74**(9), pp.3244-3257.

Huppertz, T., Kelly, A.L. and Fox, P.F. 2009. Milk Lipids - Composition, Origin and Properties *In*: A. Y. Tamime, ed. *Dairy Fats and Related Products*. Chichester, UK: Blackwell Publishing Ltd, pp.1-27.

Jensen, R.G. 2002. The composition of bovine milk lipids: January 1995 to December 2000. *Journal of dairy science*. **85**(2), pp.295-350.

Jensen, R.G., Ferris, A.M. and Lammi-Keefe, C.J. 1991. The Composition of Milk Fat. *Journal of Dairy Science*. **74**(9), pp.3228-3243.

Kodali, D.R., Atkinson, D., Redgrave, T.G. and Small, D.M. 1984. Synthesis and polymorphism of 1,2-dipalmitoyl-3-acyl- sn-glycerols. *Journal of the American Oil Chemists Society*. **61**(6), pp.1078-1084.

Ladd Parada, M., Sadeghpour, A., Vieira, J., Povey, M. and Rappolt, M. 2018. Global Small-Angle X-ray Scattering Data Analysis of Triacylglycerols in the α-Phase (Part II). *Journal of Physical Chemistry B*. **122**(45), pp.10330-10336.

Van Langevelde, A., Van Malssen, K., Driessen, R., Goubitz, K., Hollander, F., Peschar, R., Zwart, P. and Schenk, H. 2000. Structure of CnCn+2Cn-type (n = even) β′-triacylglycerols. *Acta Crystallographica Section B: Structural Science*. **56**(6), pp.1103-1111.

Li, N.Y.D., Moore, D.J., Thompson, M.A., Welfare, E. and Rappolt, M. 2022. Influence of humectants on the thermotropic behaviour and nanostructure of fully hydrated lecithin bilayers. *Chemistry and Physics of Lipids*. **243**, p.105165.

Li, N.Y.D., Perutková, Š., Iglič, A. and Rappolt, M. 2017. My first electron density map: A beginner's guide to small angle X-ray diffraction. *Elektrotehniski Vestnik/Electrotechnical Review*. **84**(3), pp.69-75.

Lopez, C. 2018. Crystallization Properties of Milk Fats *In*: K. Sato, ed. *Crystallization of Lipids: Fundamentals and Applications in Food, Cosmetics and Pharmaceuticals*. Hoboken, NJ: Wiley Blackwell, pp.283-321.

Lopez, C., Bourgaux, C., Lesieur, P., Bernadou, S., Keller, G. and Ollivon, M. 2002. Thermal and structural behavior of milk fat 3. Influence of cooling rate and droplet size on cream crystallization. *Journal of Colloid and Interface Science*. **254**(1), pp.64-78.

Lopez, C., Bourgaux, C., Lesieur, P., Riaublanc, A. and Ollivon, M. 2006. Milk fat and primary fractions obtained by dry fractionation. 1. Chemical composition and crystallisation properties. *Chemistry and Physics of Lipids*. **144**(1), pp.17-33.

Lopez, C., Lesieur, P., Bourgaux, C. and Ollivon, M. 2005. Thermal and structural behavior of anhydrous milk fat. 3. Influence of cooling rate. *Journal of Dairy Science*. **88**(2), pp.511-526.

Lutton, E.S. 1950. Review of the polymorphism of saturated even glycerides. *JAOCS, Journal of the American Oil Chemists' Society*. **27**(7), pp.276-281.

Marsh, D. 2012. Lateral order in gel, subgel and crystalline phases of lipid membranes: Wide-angle X-ray scattering. *Chemistry and Physics of Lipids*. **165**(1), pp.59-76.

Martini, S. and Marangoni, A.G. 2007. Microstructure of Dairy Fat Products *In*: A. Tamime, ed. *Structure of Dairy Product*s. Oxford: Blackwell Publishing Ltd, pp.72-103.

Maurice-Van Eijndhoven, M.H.T., Hiemstra, S.J. and Calus, M.P.L. 2011. Short communication: Milk fat composition of 4 cattle breeds in the Netherlands. *Journal of Dairy Science*. **94**(2), pp.1021-1025.

Mazzanti, G., Guthrie, S.E., Sirota, E.B., Marangoni, A.G. and Idziak, S.H.J. 2004. Effect of minor components and temperature profiles on polymorphism in milk fat. *Crystal Growth and Design*. **4**(6), pp.1303-1309.

Mazzanti, G., Marangoni, A.G. and Idziak, S.H.J. 2009. Synchrotron study on crystallization kinetics of milk fat under shear flow. *Food Research International*. **42**(5-6), pp.682-694.

Ménard, O., Ahmad, S., Rousseau, F., Briard-Bion, V., Gaucheron, F. and Lopez, C. 2010. Buffalo vs. cow milk fat globules: Size distribution, zeta-potential, compositions in total fatty acids and in polar lipids from the milk fat globule membrane. *Food Chemistry*. **120**(2), pp.544-551.

Mizobe, H., Tanaka, T., Hatakeyama, N., Nagai, T., Ichioka, K., Hondoh, H., Ueno, S. and Sato, K. 2013. Structures and Binary Mixing Characteristics of Enantiomers of 1-Oleoyl-2,3-dipalmitoyl-sn-glycerol (S-OPP) and 1,2-Dipalmitoyl-3-oleoyl-sn- glycerol (R-PPO). *JAOCS, Journal of the American Oil Chemists' Society*. **90**(12), pp.1809-1817.

Mykhaylyk, O.O. and Hamley, I.W. 2004. The packing of triacylglycerols from SAXS measurements: Application to the structure of 1,3-distearoyl-2-oleoyl-sn-glycerol crystal phases. *Journal of Physical Chemistry B*. **108**(23), pp.8069-8083.

Nagle, J.F. and Tristram-Nagle, S. 2000. Structure of lipid bilayers. *Biochimica et Biophysica Acta - Reviews on Biomembranes*. **1469**(3), pp.159-195.

Pabst, G., Amenitsch, H., Kharakoz, D.P., Laggner, P. and Rappolt, M. 2004. Structure and fluctuations of phosphatidylcholines in the vicinity of the main phase transition. *Physical Review E - Statistical Physics, Plasmas, Fluids, and Related Interdisciplinary Topics*. **70**(2), p.9.

Palmquist, D.L., Denise Beaulieu, A. and Barbano, D.M. 1993. Feed and Animal Factors Influencing Milk Fat Composition. *Journal of Dairy Science*. **76**(6), pp.1753-1771.

Pionnier, E. and Hugelshofer, D. 2006. Characterisation of key odorant compounds in creams from different origins with distinct flavours. *Developments in Food Science*. **43**(C), pp.233-236.

Pratama, Y., Simone, E. and Rappolt, M. 2021. The Unique Crystallization Behavior of Buffalo Milk Fat. *Crystal Growth and Design*. **21**(4), pp.2113-2127.

Rappolt, M. 2010. Bilayer thickness estimations with 'poor' diffraction data. *Journal of Applied Physics*. **107**, p.084701.

Ruocco, M.J. and Shipley, G.G. 1982. Characterisation of the sub-transition of hydrated dipalmitoylphosphatidylcholine bilayers. Kinetic, hydration and structural study. *Biochimica et Biophysica Acta (BBA) - Biomembranes*. **691**(2), pp.309-320.

Sadeghpour, A., Ladd Parada, M., Vieira, J.J., Povey, M., Rappolt, M., Parada, M.L., Vieira, J.J., Povey, M. and Rappolt, M. 2018. Global Small-Angle X-ray Scattering Data Analysis of Triacylglycerols in the Molten State (Part I). *J. Phys. Chem. B*. **122**(45), pp.10320-10329.

Sato, K. 2001. Molecular Aspects in Fat Polymorphism *In*: N. Widlak, R. Hartel and S. Narine, eds. *Crystallization and Solidification Properties of Lipids*. Champaign, Illinois, Illinois: AOCS Press, pp.1-17.

Smiddy, M.A., Huppertz, T. and van Ruth, S.M. 2012. Triacylglycerol and melting profiles of milk fat from several species. *International Dairy Journal*. **24**(2), pp.64-69.

Soyeurt, H., Dardenne, P., Gillon, A., Croquet, C., Vanderick, S., Mayeres, P., Bertozzi, C. and Gengler, N. 2006. Variation in Fatty Acid Contents of Milk and Milk Fat Within and Across Breeds. *Journal of Dairy Science*. **89**(12), pp.4858-4865.

Spaar, A. and Salditt, T. 2003. Short Range Order of Hydrocarbon Chains in Fluid Phospholipid Bilayers Studied by X-Ray Diffraction from Highly Oriented Membranes. *Biophysical Journal*. **85**(3), p.1576.

Stoop, W.M., Bovenhuis, H., Heck, J.M.L. and van Arendonk, J.A.M. 2009. Effect of lactation stage and energy status on milk fat composition of Holstein-Friesian cows. *Journal of Dairy Science*. **92**(4), pp.1469-1478.

Tomaszewska-Gras, J. 2013. Melting and crystallization DSC profiles of milk fat depending on selected factors. *Journal of Thermal Analysis and Calorimetry*. **113**(1), pp.199-208.

Tzompa-Sosa, D.A., Meurs, P.P. and van Valenberg, H.J.F. 2018. Triacylglycerol Profile of Summer and Winter Bovine Milk Fat and the Feasibility of Triacylglycerol Fragmentation. *European Journal of Lipid Science and Technology*. **120**(3), p.1700291.

Tzompa-Sosa, D.A., Ramel, P.R., Van Valenberg, H.J.F. and Van Aken, G.A. 2016. Formation of β Polymorphs in Milk Fats with Large Differences in Triacylglycerol Profiles. *Journal of Agricultural and Food Chemistry*. **64**(20), pp.4152-4157.

Walstra, P., Wouters, J.T.M. and Geurts, T.J. 2005. *Dairy science and technology, second edition*. Boca Raton, FL: CRC Press.

Chapter 5 Decoding the Role of Triacylglycerol Composition in the Milk Fat Crystallisation Behaviour: a Study using Buffalo Milk Fat Fractions

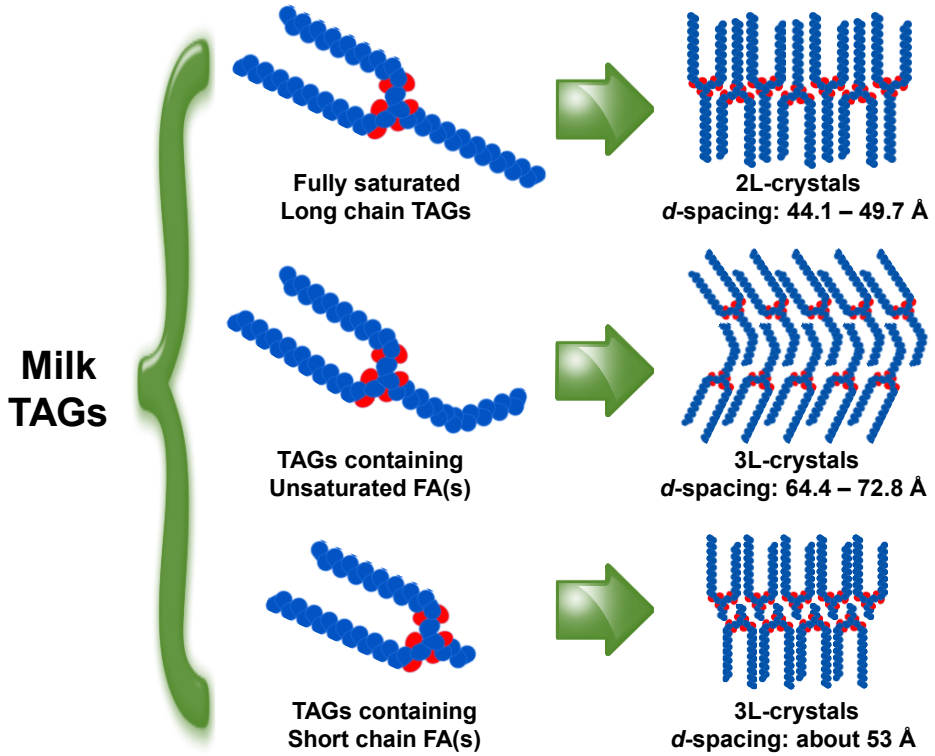

5.1 Abstract

The role of triacylglycerols (TAGs) composition in milk fat crystallisation is evaluated from a new perspective by correlating the crystal structures and their predicted TAG contributors. Four different TAG groups, defined by their fatty acid (FA) chain length and saturation are proposed to explain the crystallisation behaviour of different milk fat samples, namely TAGs containing (i) fully saturated long chain FAs, (ii) single unsaturated long-chain FA and (iii) multi unsaturated long-chain FAs, as well as (iv) short-chain FAs. Samples containing different TAGs proportions were obtained from two-step dry fractionation of buffalo milk fat. Liquid chromatography and mass spectrometry (LCMS) was employed to determine the TAGs composition. The crystallisation characteristics were evaluated using small-angle X-ray scattering (SAXS), differential scanning calorimetry (DSC) and polarised light microscopy. The results confirm that fully saturated long chain TAGs are responsible for the formation of high melting point 2L-crystals (*d*-spacing: 44.1-49.7 Å), whilst the low melting point 3L-crystals (64.4 - 72.8 Å) are mainly contributed by long chain TAGs containing unsaturated fatty acids. Further,

the crystallisation inhibiting effect of asymmetrical TAGs, containing short chain fatty acid (C4-6) is evident. As a final point, effects of the four TAG groups, each given with specific composition, were examined closely also with respect to their influence on the nucleation and polymorphic transformation kinetics of milk fat crystals.

Keywords:

Milk fat, buffalo milk, crystallisation, fractionation, triacylglycerol.

5.2 Introduction

Milk fat is one of the most important natural fats in the food industry. The annual processed milk fat (as butter and ghee) is estimated in around 12.5 million tonnes globally in 2020 (FAO, 2022b). The milk fat is not only limited to manufacturing of dairy products such as butter, cheese and cream, but also widely used in confectionary like chocolate and candy. The presence of milk fat crystals in the food system affects their overall quality and textural properties, for example, in the stabilisation of whipped cream (Nguyen et al., 2015), the hardness of butter (Rønholt et al., 2013) and the bloom formation in confectionary products (Schmelzer and Hartel, 2001). However, the crystallisation behaviour of milk fat is still far from being fully understood. The main reason lies in its very large variety of triacylglycerols (TAGs), with more than 200 species amounting to >98% of total milk fat composition (Jensen et al., 1991; Gresti et al., 1993). Adding to this complexity, the composition of milk fat TAGs can greatly vary due to many factors such as milking species (Abd El-Salam and El-Shibiny, 2011; Smiddy et al., 2012; Gantner et al., 2015; Pratama et al., 2021), animal breed (Soyeurt et al., 2006; Maurice-Van Eijndhoven et al., 2011), type of feed (Grummer, 1991; Palmquist et al., 1993), season (Romano et al., 2011; Larsen et al., 2014; Tzompa-Sosa et al., 2018), and geographical factors (Shi et al., 2001). Milk fat also does not have any particular dominant TAG species as compared to other important fat commodities, such as cocoa butter and palm oil/fat. For instance, cocoa butter has three dominant triacylglycerols, namely POP, POS and SOS (note: P-palmitic, O-oleic, S-stearic) that account for about 80% of its total composition, which are the main drivers of crystallisation (Loisel et al., 1998). Whereas in palm oil, there are only two dominant TAGs, namely POP (28%) and POO (24%) (Omar et al., 2015).

Due to the complex TAGs composition, milk fat typically shows three broad endothermic peaks on differential scanning calorimetry (DSC) measurements (Grotenhuis et al., 1999; Tomaszewska-Gras, 2013). This led to the notion that milk fat consists of three separate TAG groups based on their melting point, which are commonly named high, medium and low melting fractions (HMF, MMF, LMF) (Timms, 1980; Deffense, 1993; Grotenhuis et al., 1999; Shi et al., 2001). Even though this interpretation is broadly accepted, there is no standardized definition for these three fractions, as the endothermic peak positions and relative areas are largely influenced by the thermal history of the sample before applying the heating scan. In fact, using different cooling rates can promote the formation of different fat polymorphs, with different melting points (Tomaszewska-Gras, 2013). Nonetheless, researchers have attempted to separate these fractions according to their melting ranges. Several fractionation techniques including dry and solvent methods with at least two steps of crystallisation have been put forward (Timms, 1980; Deffense, 1993; Campos et al., 2003; Romano et al., 2011).

In-situ combined DSC-SAXS studies have shown that the typical endothermic pattern is also influenced by polymorphic changes that might occur during DSC heating scans. The local minimum separating the first and second endothermic peak is actually influenced by an exothermic dip that corresponds to the polymorphic transformation from the α to β' polymorph (Lopez et al., 2001; Lopez et al., 2005). Having pointed this out, it is more accurate to view the typical three endothermic peaks as superimposed events of (1) melting of the different TAG groups and (2) polymorphic transformations, including the melting of metastable structures and recrystallisation of more stable crystals followed by their subsequent final melting. Consequently, a quantification of the composition of different milk fat fractions using DSC alone cannot be accurate.

Having reviewed the existing studies on milk fat fractionation, many researchers focused on understanding and testing the different properties of each fraction, with the purpose of using them as ingredients for different food systems. Indeed, different physical properties, such as melting range, rheology and mechanical properties are a direct consequence of TAG compositional changes after fractionation. However, a more fundamental question needs to be addressed. That is, how varying TAGs composition affect the phase and crystallisation behaviour of milk fat. The effect of TAGs composition on polymorphism is crucial, as different polymorphs of the same compound may present very different physical properties; secondly, the TAGs composition can also affect the kinetics of crystallization and polymorphic

transformations. Both aspects are important for the design of manufacturing processes as well as for the stability of the final food material. As an example, a recent study (Lopez et al., 2006) showed that a one-step dry fractionation at 21 °C generated a high melting solid fraction with the tendency to crystallise into the β' phase, whereas the low melting liquid fraction remained in the α form, when a cooling rate -1 °C/min was applied. It is worth noting that at least five different molecular packing arrangements have been reported for milk fat, including γ, α, β'-1, β'-2 and β structures, and their lamellar stacking repeat distances have been reported to be within a range of 39 to 73 Å, with either a 2 chain length (2L) or 3 chain length (3L) architecture (Lopez, 2018; Pratama et al., 2021).

Further attempts to elucidate the effect of varying milk fat TAGs composition on the physical properties of the resulting material have been carried out by mixing milk fat (H, M, L) melting fractions in different proportions. Marangoni and Lencki (1998) studied the phase behaviour of different ternary mixture of the three milk fractions and observed mostly monotectic behaviour. Only at zero degrees, a eutectic transition was observed. The same group also investigated, how the different proportions of each fraction affected the microstructure of the formed milk fat crystals (Ramel and Marangoni, 2016), and further examined the kinetics of the polymorphic transformations (Cisneros et al., 2006). The HMF is characterised by rod or needle-like shaped crystal microstructure and showed a slower α → β' transformation compared to HMF/LMF mixture. It is worth mentioning that the effect of TAGs composition on the crystallization behaviour of milk fat has also been demonstrated by our recent study. Cow and buffalo milk fat, which have different ratios of the HMF, MMF and LMF exhibited different kinetics in the formation of the β' crystals at the slow cooling rate of -0.5 °C/min (Pratama et al., 2021). The buffalo milk fat, which has higher HMF and LMF proportion compared to cow milk fat, showed a slower β' formation.

Despite the wide literature on milk fat and milk fat fractions crystallisation, the concrete role of the TAGs composition in milk fat crystallisation remains unclear. We argue that using the HMF, MMF and LMF fractions and their ratios as sole argumentative basis for explaining the crystallisation behaviour of milk fat is not sufficient. This is supported by two reasons: (1) as abovementioned, there is no clear-cut definition for these fractions and how to quantify them. Researchers have come up with different fractionation methods, which result in different TAGs composition; (2) fractionation cannot perfectly separate the different melting groups. For instance, TAGs that belong to the HMF (fully saturated TAGs) are also observed in the low melting

fraction and *vice versa* (Dimick et al., 1996; Van Aken et al., 1999; Lopez et al., 2006). This inclusion is likely due to co-crystallisation during fractionation, which results in mixed crystals (Deffense, 1993), as well as the physical entrapment of low melting TAGs inside the crystalline network developed during crystallisation (Che Man et al., 1999).

With the limitations of the HMF, MMF and LMF framework to explain the milk fat crystallisation behaviour being put forward, we propose in the current study to elucidate the role of TAGs in milk fat crystallisation by grouping them by their molecular properties, such as chain length and saturation level. This approach is motivated by findings from previous studies (Lopez et al., 2006; Pratama et al., 2021; Pratama et al., 2022) on the crystallization of milk fat and how the different forming TAGs distribute in the existing polymorphs, depending on their molecular structure. It is possible to identify what TAGs are prevalent in a specific solid phase by determining not only their lattice spacing, but also their underlying electron density profile. Subsequently, this allows also to estimate the hydrocarbon chain tilt as well as the packing density, i.e., the area per chain, of the different polymorphs (Pratama et al., 2022).

The four different TAG groups, containing (i) fully saturated long chain FAs, (ii) single unsaturated long-chain FA and (iii) multi unsaturated long-chain FAs as well as (iv) short-chain FAs, have been identified as dominant types of TAGs in three different polymorphs and the molten TAG fraction, respectively. First, previous studies suggest that 2L-α crystals with lamellar stacking distance of about 47-48 Å are likely to be dominantly composed of fully saturated TAGs, such as PPP and PPS (Lopez et al., 2006; Pratama et al., 2021). Second, 3L-α crystals with *d*-spacing of 71-73 Å are predicted to be rich in TAGs containing both saturated and unsaturated fatty acids such as PMO and POO (note: M-myristic) (Pratama et al., 2021). Third, a 3L structure with *d*-spacing of 53-54 Å is composed mainly by asymmetrical TAGs containing short chain C4 to C6 fatty acids such as BuPS and BuPO (note: Bu-butyric) (Pratama et al., 2021). The presence of these types of TAGs is significant in milk fat, and their particular crystallisation behaviour has been reported (Pratama et al., 2022).

This ‘chemical grouping’ of TAGs approach is particularly suitable for dry fractioned buffalo milk fat. This type of milk fat has high quantities of fully saturated TAGs as well as short-chain fatty acids containing TAGs, when compared to cow milk fat (Pratama et al., 2021). Since all four groups are given in significant quantities, it is possible to separate them more effectively

by fractionation, and in turn, allows a good evaluation of their role in milk fat crystallisation. Nevertheless, the presented experimental results are also relevant to other fat mixtures with similar TAGs composition (Pratama et al., 2021). To the best of our knowledge, this work is the first to report on the crystallisation behaviour TAGs mixtures obtained by dry fractionation of buffalo milk fat, and ultimately, will have an impact on the growing use of buffalo milk in industry, as it recently has become the second most produced milk globally (FAO, 2022b). More importantly, the current approach's focus on TAG chemical structure, is universally applicable. For instance, it can be adapted in the endeavours to substitute milk fat with that of plant-based origin.

5.3 Materials and Methods

5.3.1 Milk Fat Preparation and Fractionation

Buffalo butter samples with fat content ≥ 82% in weight were purchased from La Marchesa (Terevola, Italy). Moisture and other milk solids were removed from butter by heat clarification, following the method described in our previous work (Pratama et al., 2021). Briefly, 250 grams of butter were heated to 110 °C and kept at this temperature for 20 minutes at 100 rpm stirring with a magnetic stirrer (IKA RCT Basic, IKA-Werke GmbH & Co, Staufen, Germany). The coagulated milk solids were then vacuum filtered with a Buchner funnel and Whatman No. 1 filter paper. The resulting buffalo milk fat sample contains ≥ 99.5% fat content as confirmed by applying the Soxhlet extraction.

Milk fat fraction samples were obtained from two-step dry fractionation. In the first step, the milk fat sample was brought to melt at 70 °C for 15 mins, before being transferred into a 100 ml jacketed cylinder connected to a Tamson TLC2 cooling circulator (PM Tamson Instruments, Bleiswijk, The Netherlands). Crystallisation was then conducted at 35 °C for 24 hours, under 200 rpm stirring (IKA RW 11 Lab Egg overhead stirrer, IKA-Werke GmbH & Co, Staufen, Germany). The resulted slurry was then centrifuged at 10.000 RCF for 30 mins at the corresponding crystallisation temperature (35 °C) in an Avanti J-30I centrifuge (Beckman Coulter, Indianapolis, United States). The liquid fraction was carefully separated using a pipette. In order to purify the solid from the residual liquid phase, the solid fraction in the centrifuge tube was washed with 5 ml petroleum ether (Alfa Aesar, Heysham, United Kingdom), followed by the same washing with 5 ml isobutanol (Fluorochem, Hadfield, United Kingdom), for three cycles in total (Yao et al., 2020). The tube

was then left to dry for 24 hours to remove the residual organic solvent. The solid fraction from the first crystallisation step is henceforth called the “Stearin” fraction. The second step fractionation used the liquid material pipetted from the first fractionation step. The same procedure for the first step was applied (i.e., melting, crystallisation, centrifugation and washing). The only difference was the crystallisation and centrifugation temperature, which was 25 °C. The resulting liquid fraction from the second step fractionation is henceforth referred as the “Olein” fraction, whereas the solid one is referred to as “Mid” fraction. Fractionation was conducted in three repeats. The terms Stearin, Mid and Olein fractions are used here to avoid confusion with high, medium, low melting fractions used in literature.

5.3.2 Yield Calculation

To account for the loss of liquid during the washing step, the yield of fractionation was calculated using the solid fraction as the basis. For every fractionation step, the solid and liquid fraction yield (%) are calculated as below

$$\boldsymbol{Solid\ fraction}\ (\%) = \frac{\boldsymbol{Solid\ weight}}{\boldsymbol{Initial\ weight}} \cdot \mathbf{100}$$

Eq. (5.1)

$$\boldsymbol{Liquid\ fraction}\ (\%) = \mathbf{100} - \boldsymbol{Solid\ fraction}\ (\%)$$

Eq. (5.2)

5.3.3 Liquid Chromatography and Mass Spectrometry (LMCS) Measurements

The TAGs composition of milk fat and milk fat fractions were evaluated according to the Zeb and Murkovich procedure (Zeb and Murkovic, 2010) in a Shimadzu LCMS 2020 (Japan) with a separation column Phenomenex Luna 3u C18(2) 100A LC Column 150 x 3.0 mm. The detailed procedure is described in our previous work (Pratama et al., 2021). Measurements were performed in triplicates and the collected data were processed in the LabSolutions software (version 5.97) to obtain chromatograms and mass spectra. Further chromatograms peak fittings, integration and plotting were carried out using OriginPro 2019b. Prior to fitting, the solvent contribution was removed. Peak fitting and integration followed the ‘*peak analyzer*’ routine; briefly, the baseline was defined as a straight line from two ends each side of

the peak and the position of the peaks were identified by the local maximum method. The total peak number and positions were cross referenced to the mass spectra obtained from the LabSolutions software. This allowed the exclusion of the unidentified peaks from the analysis.

5.3.4 X-ray Scattering Measurements and Analysis

X-ray scattering measurements were conducted with a SAXSpace benchtop small and wide X-ray scattering instrument (Anton Paar GmbH, Graz, Austria). The wavelength, λ, was 0.154 nm, produced by a Cu-anode at 40 kV and 50 mA. The instrument is equipped with a TCstage 150 (Anton Paar GmbH, Graz, Austria) to provide a temperature-controlled sample environment with accuracy ± 0.1 °C. The sample to detector distance (SDD) was 130 mm, which covers the small and wide-angle regime with a q-range from 0.01 to 1.76 $Å^{-1}$ ($q = 4\pi \sin(\theta)/\lambda$). A Mythen micro-strip detector (Dectris Ltd, Baden, Switzerland) was used to record the 1D scattering patterns.

Samples of milk fat and its fractions were molten at >60 °C prior to filling (about 100 µL) into quartz capillary tubes (1.5 mm outside diameter), obtained from Capillary Tube Supplies Ltd. (Cornwall, United Kingdom). The capillaries were then sealed with wax. Measurements were carried out following three thermal procedures (**Figure 5.1**), where the samples were brought to melt at 60 °C for 10 minutes to erase the crystal memory and then cooled to -10 °C at three different rates (-5, -2, and -0.5 °C/min). At the end of the cooling scan, the samples were kept at constant temperature for 5 minutes before being heated back to 60 °C at a rate of 2 °C/min. Scattering patterns were collected every minute with a 30 s exposure time.

The SAXSTreat program was used to correct the position of the primary beam and the SAXSQuant program was employed to normalise the scattering pattern intensities by their transmission, and further used, to subtract the scattering contribution of the empty capillary. Both software packages are supplied by Anton Paar GmbH (Graz, Austria). Further data processing was carried out using OriginPro 2019b. This includes the further subtraction of the scattering contribution from the residual molten sample, peak fittings and plotting. In the case of multiple Bragg's peak per polymorph, the strongest peak was used to determine the crystallisation evolution.

5.3.5 Differential Scanning Calorimetry (DSC) Measurements

Heat flow measurements were conducted using a DSC Q-20 (TA Instruments, Elstree-UK). About 15 mg of sample was placed in a sealed Tzero aluminium pan (TA Instruments, Elstree-UK) and subjected to three thermal procedures alike the ones for the X-ray measurements (**Figure 5.1**). Measurements were done in three repeats. Collected data were processed with the TA Instruments Universal Analysis software (Version 4.5A) and plotted in Origin Pro 2019b.

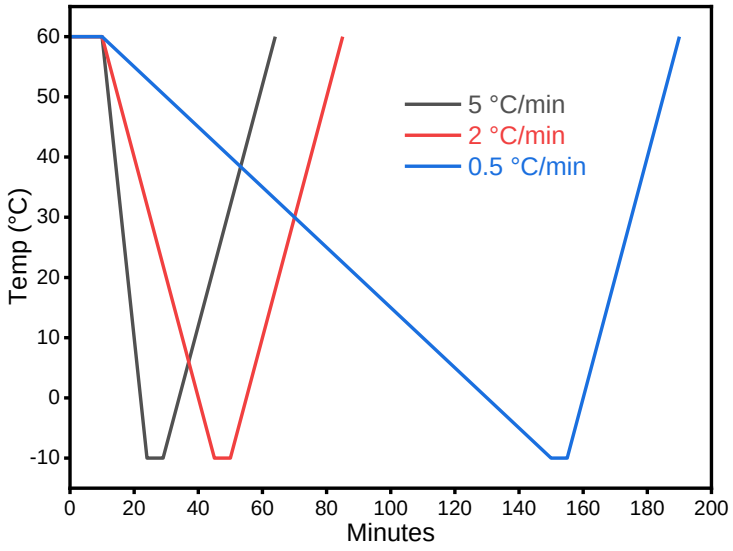

Figure 5.1 Schematic of thermal procedures applied to SAXS and DSC for milk fat samples characterisation

5.3.6 Polarised Light Microscopy (PLM) Measurements

The microstructures of milk fat crystals were observed in a polarised light microscope (Leitz Dialux, Wetzlar, Germany). The lens was a Nikon M Plan 40x ELWD and the digital images were captured using a Canon EOS 7D Mark II (Canon, Japan) camera, providing a 5472 x 3072 pixels resolution. 50 µL of molten sample was placed in a Linkam CSS 450 hot stage (Linkam Instruments, Tadworth-UK), with the gap set at 100 µm. Two thermal procedures were used and the stage temperature was controlled with the Linksys 32 data capture programme (Linkam Instruments, Tadworth-UK). All samples were exposed to 60 °C for 10 minutes, in order to erase the crystal memory and then they were subjected to a cooling ramp of -5 °C/min down to 0°C. The Stearin fraction was also slowly cooled at -0.5 °C/min after the same melting procedure. ImageJ 1.53a software (NIH, USA) was used for image processing. All captured images were scaled using a 1 mm graticule image, which was taken in the same microscopy set up. Image contrasts were enhanced for publication purpose.

5.4 Results and Discussion

5.4.1 TAGs Composition of Milk Fat Fraction Samples

The current dry fractionation procedure resulted in three fractions, i.e., the Stearin, Mid and Olein fractions with an extraction yield of 33.8 ± 3.7 %, 23.6 ± 1.7 % and 42.6 ± 2.9 %, respectively. The two-step fractionation at 35 and 25 °C gave different results compared to the existing literature. Van-Aken et al. (1999) reported the yield of Stearin fraction (>30°C) to be 24 % and the Olein fraction (<24°C) to be 37 %, leaving the Mid fraction (24-30°C) portion to be 39 %. Comparatively, the Stearin portion we found was bigger than estimated by Van-Aken et al. (1999), even though the current fractionation was carried out at a higher crystallisation temperature (35 °C *vs* 30 °C in Van-Aken et al. (1999)). On the other hand, the current Mid fraction yield is lower than in the previously reported study (Van Aken et al., 1999) albeit covering a broader temperature range of 25-35 °C. The Olein portion of both studies is nearly the same. It is worth noticing that the crystallisation temperatures are just slightly different (25 *vs* 24°C), so the slightly lower Olein yield from Van-Aken et al. (1999) might be comparable to the current result, if the experiments would have been both carried out at 25 °C. The major differences in yields most likely come from the fact that a different type of milk fat was used (current: buffalo, Van-Aken et al. (1999): cow). We note that the difference in the milk fraction yield confirms our previous report (Pratama et al., 2021), which showed a higher percentage of high melting and low melting point TAGs in buffalo milk fat, when compared to cow milk fat. Whereas the middle melting point TAGs percentage is found to be lower in buffalo milk fat.

Table 5.1 shows the TAGs composition of the three different Stearin, Mid and Olein fractions and of the buffalo milk fat in total (henceforth, termed Whole Fat to differentiate it from the other fractions). 37 different TAG species have been successfully identified. Based on the different crystallisation behaviour of different types of TAGs (as mentioned earlier), we grouped these 37 TAGs into four categories, i.e., TAGs with (i) only saturated fatty acid (all-SFA), (ii) TAGs containing single unsaturated FA (single-UFA), (iii) TAGs containing multi unsaturated FA (multi-UFA) and (iv) short chain fatty acid ($N_C \leq 6$) containing TAGs (short-FA) to explain the effects of varying TAGs composition on milk fat crystallisation behaviour. The contribution of each group to the composition of each fraction is presented in **Figure 5.2,** whereas chromatogram examples from highly different Stearin and Olein fractions are given in **Figure C.1** (Appendix C).

Table 5.1 Triacylglycerol composition of milk fractions (shown as mean ± SD).

Compound	RT	Whole Fat	Stearin	Mid	Olein
Short chain FA-containing TAGs (short-FA)					
Bu-Co-P	2.87	1.57±0.26	1.62±0.59	1.29±0.21	1.33±0.09
Bu-C-M	3.30	1.08±0.04	0.88±0.05	0.94±0.02	1.10±0.03
Bu-C-P	3.73	1.92±0.07	1.73±0.07	2.04±0.24	1.98±0.04
Bu-La-P	4.33	1.74±0.67	1.70±0.17	2.53±0.26	2.06±0.01
Bu-La-O	4.57	1.19±0.39	1.01±0.39	1.79±0.39	1.42±0.10
Bu-M-P	5.20	5.67±0.96	5.39±0.88	5.01±0.29	6.18±0.11
Bu-M-O	5.30	3.50±0.70	2.84±0.74	3.53±0.78	3.17±0.49
Bu-P-L	5.47	3.83±1.03	3.63±0.23	3.38±0.92	4.94±0.43
Co-M-P	6.13	1.72±0.41	1.88±0.31	1.93±0.32	2.51±0.18
Bu-P-P	6.27	6.07±0.44	5.11±0.42	5.02±0.55	6.17±0.08
Bu-P-O	6.40	7.61±0.60	6.82±0.36	7.37±0.45	7.79±0.01
Bu-O-O	6.60	4.28±0.28	3.24±0.80	3.32±0.30	5.34±0.04
Co-P-P	7.37	3.25±0.16	2.77±0.36	2.74±0.06	3.69±0.04
Bu-P-S	7.60	5.79±0.00	5.47±0.64	5.58±0.43	6.66±0.45
Bu-S-O	7.83	4.16±0.30	3.36±0.58	3.65±0.13	4.32±0.04
Co-S-P	9.07	2.36±0.08	2.07±0.16	2.13±0.14	2.49±0.07
Sub Total		**55.8±0.6**	**49.5±0.7**	**52.3±1.3**	**61.2±0.8**
TAGs containing single unsaturated FA chain (single-UFA)					
P-Cy-O	9.37	2.60±0.29	2.72±0.58	2.61±0.30	3.20±0.63
P-La-O	13.93	1.83±0.02	1.93±0.27	1.79±0.04	1.88±0.00
P-M-L	14.43	1.08±0.30	1.15±0.36	1.16±0.32	1.24±0.18
P-M-O	17.50	2.93±0.37	2.75±0.15	3.06±0.14	2.83±0.06
O-P-P	22.00	3.65±0.23	3.60±0.46	3.90±0.20	3.32±0.24
S-P-O	27.83	2.30±0.04	2.63±0.19	2.69±0.20	1.97±0.04
S-S-O	35.27	0.66±0.24	0.80±0.23	0.82±0.20	0.52±0.01
Sub Total		**15.0±0.7**	**15.6±0.6**	**16.0±0.6**	**15.0±0.6**
TAGs containing multi unsaturated FA chains (multi-UFA)					
C-O-O	11.60	0.87±0.14	1.15±0.43	1.00±0.36	0.74±0.01
O-M-O	18.03	1.95±0.04	1.86±0.11	1.98±0.20	2.07±0.25
O-P-L	18.90	1.38±0.64	1.59±0.45	1.38±0.09	0.97±0.07
P-O-O	22.83	2.81±0.30	3.17±0.10	3.03±0.15	3.22±0.18
O-O-O	23.73	1.34±0.27	1.21±0.04	1.21±0.08	1.28±0.15
O-O-S	28.90	1.18±0.29	1.29±0.37	1.29±0.29	1.08±0.03
Sub Total		**9.5±0.6**	**10.3±0.9**	**9.9±0.7**	**9.4±0.6**
TAGs with long fully saturated FA (all-SFA)					
P-P-Cy	8.83	1.09±0.05	1.03±0.16	1.04±0.09	1.24±0.16
P-P-C	10.87	1.42±0.09	1.39±0.24	1.61±0.05	1.16±0.02
La-P-P	13.43	1.41±0.05	1.76±0.08	2.04±0.09	0.91±0.02
M-P-P	16.80	1.82±0.14	2.80±0.08	2.79±0.25	0.68±0.00

Compound	RT	Whole Fat	Stearin	Mid	Olein
P-P-P	21.13	1.76±0.26	3.47±0.24	2.32±0.15	0.34±0.05
P-P-S	26.80	1.34±0.09	2.90±0.36	1.36±0.08	0.02±0.02
S-P-S	33.97	0.78±0.21	1.76±0.41	0.71±0.17	0.04±0.04
Sub Total		**9.6±0.4**	**15.1±0.3**	**11.9±0.1**	**4.4±0.2**
Unidentified		10.1	9.5	9.9	10.1
Grand total		100	100	100	100

RT: retention-time; TAG: triacylglycerol; SD: standard deviation; Bu: butyric (C4), Co: caproic (C6), Cy: caprylic (C8), C: capric (C10), La: lauric (C12), M: myristic (C14), P: palmitic (C16), S: stearic (C18), O: oleic (C18:1), L: linoleic (C18:2) fatty acid.

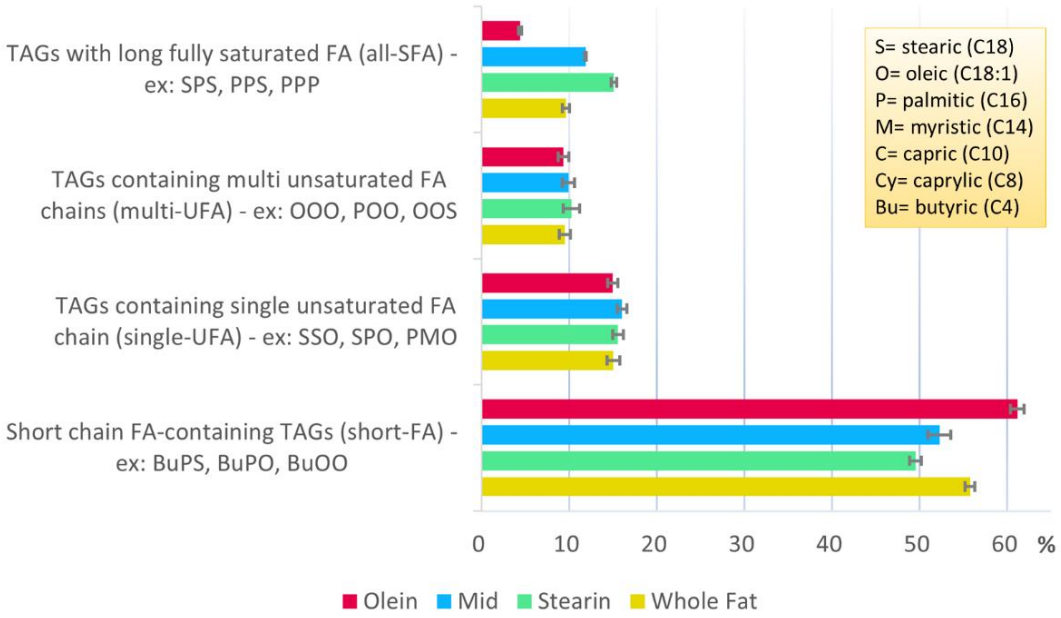

Figure 5.2 Distribution of four different TAG groups in milk fat and milk fat fraction samples.

The Whole Fat consists of 55.8, 15.0, 9.5 and 9.6 % w/w of short-FA, single-UFA, multi-UFA and all-SFA, respectively. All-SFA TAGs are present in decreasing order from 15.1 to 4.4 % in the Stearin to Olein fractions. This is expected because the all-SFA have higher melting points compared to the other TAGs; thus, they can be separated with high yield at higher fractionation temperature. On the other hand, the presence of unsaturation in the TAG molecules decreases the melting point significantly. As an example, the fully saturated PPP has a melting point of 63-67 °C, whilst the monounsaturated POP and polyunsaturated OPO melt at ranges of 33-35 °C and 19-21 °C, respectively (MacRidachis et al., 2021). Therefore, it is expected that the concentration of both single-UFA and multi-UFA groups should increase (as

opposite to all-SFA), following the order of fractionation (Stearin < Mid < Olein). However, the current results show that there is no clear trend in single-UFA and multi-UFA concentration over the three fractions. The single-UFA were found in the range of 15-16 % for all three fractions, whereas the multi-UFA were in a 9-10% range. A likely explanation for this is that single-UFA and multi-UFA co-crystallise and/or are entrapped in agglomerates of crystals during crystallisation, since unsaturated TAGs are equally present even at high crystallisation temperatures.

The short-FAs instead show a clear increasing trend following the order of the fractionation, with the highest amount of this TAGs group contained in Olein (61.2 %) and the lowest in Stearin (49.5 %). This demonstrates the tendency of short-FA to remain in the liquid fraction, which implies a lower incorporation of this TAGs group into the solid crystals formed during fractionation. In our recent work, we hypothesized that that the TAGs containing unsaturated short-FA remain part of the liquid during crystallization, due to their low nucleation point (Pratama et al., 2022). However, as 49.5 % of short-FA coming from the whole milk fat remained were found in the Stearin fraction, a significant level of co-crystallisation and entrapment is clearly also taking place.

Having overviewed the composition of the four TAG groups in **Figure 5.2**, it is apparent that the applied dry fractionation technique is not able to completely separate the TAGs according to their theoretical melting points or justify fully the so-called HMF-MMF-LMF fraction notation. Indeed, all four TAG groups are still observed in the resulting fractions, only in different quantity. These results are beneficial for our approach to evaluate the effect of different types of TAGs on milk fat crystallisation.

5.4.2 Crystallisation Behaviour of the Different Milk Fat Fractions

The small- and wide-angle X-ray scattering (SAXS and WAXS) patterns of the four milk fat samples with distinctly different TAG compositions are shown in **Figure 5.3**. Applying three different cooling ramps, the plots show four different crystal structures at the end of the temperature profile (at -10 °C), i.e., α-2L (46-49.7 Å), β'-2L (44.1 Å), α-3L (72.8 Å), and β'-3L (64.4 Å) polymorphs, where values in the brackets indicate the *d*-spacings.

The α-2L crystals (peak at $q \tilde{=} 0.13$ Å^{-1}) shown with the highest intensity in the Stearin fraction and appeared at cooling rates of -5 and -2 °C/min. Whereas this polymorph was not visible in Olein at -2 and -0.5 °C/min, it was observed

at the higher rate of -5 °C/min. Since the Stearin and Olein fractions contain all-SFA at the highest and the lowest level, respectively (**Figure 5.2**), these results confirm that the α-2L crystals are more likely to form in the presence of all-SFA (Lopez et al., 2006; Pratama et al., 2021). It is worth noting that the *d*-spacing of the α-2L stacking varied among the samples. Stearin, Mid, Olein fractions and Whole Fat *d*-spacings were 49.7 Å, 48.3 Å, 46.0 Å and 48.0 Å, respectively. Because the crystals formed are made of different TAGs with similar chain length of the fatty acids (mixed crystal) (Breitschuh and Windhab, 1998), the resulting *d*-spacing is dictated by the proportion of such contributing TAGs. For instance, the Stearin fraction contains the highest amount of SPS, PPS and PPP (**Table 5.2**), which display a greater *d*-spacing compared to other all-SFA (e.g., LaPP and MPP), hence the Stearin fraction displays highest α-2L *d*-spacing. In contrast, Olein contains the lowest amount of those three TAGs, which results in a shorter *d*-spacing.

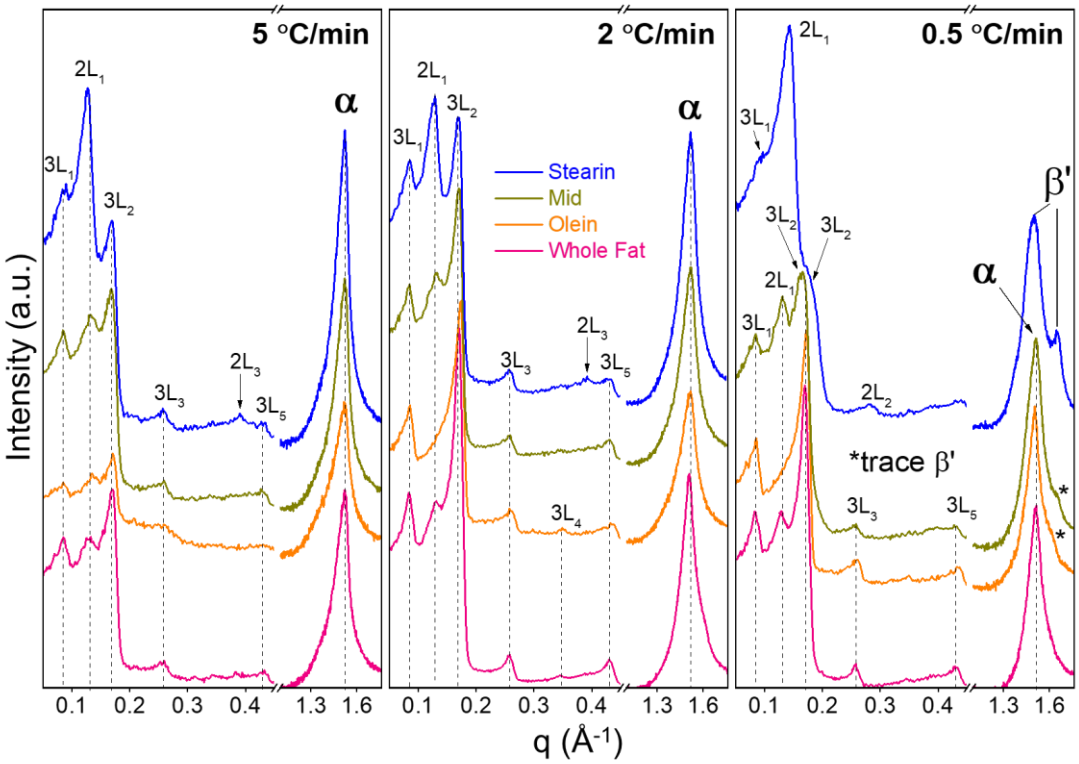

Figure 5.3 X-ray scattering patterns of milk fat samples at -10°C after cooling at different rates from melt. The patterns have been subtracted by its molten fat contributions to induce better clarity.

Another interesting result is the presence of the α-2L phase in the Olein fraction at high cooling rate of -5 °C/min, where the same crystal form is not observed at lower cooling rates. Certainly, the Olein fraction still contains a

small amount of all-SFA (about 4 %, **Table 5.1**). We speculate, that this little amount of TAGs needs higher undercooling for nucleation. Secondly, at higher undercooling conditions the clustering of all-SFA occurs at higher rate, inducing a partial segregation in the mixture. This segregation allows the all-SFA to have a critical mass to form the α-2L crystal. On the other hand, the all-SFA are able to diffuse in the bulk of the sample at lower cooling rates and thus could not form this structure.

In contrast to the clear trend observed in the α-2L crystals, the α-3L structures (strongest 2nd order peak at q = 0.17 Å^{-1}) are shown in all samples at all cooling rates applied. We note, that the maximum intensity of this second order peak does not vary much among the different fractions, especially at -2 °C/min. Studies have shown that the α-3L phase nucleates at lower temperature than the α-2L phase (Lopez, 2018; Pratama et al., 2021), indicating that the crystals are most likely made of TAG groups with lower melting points. Therefore, the α-3L phase is expected to appear more abundantly in the reverse order of the fractionation temperature (i.e., Stearin < Mid < Olein). The current results, however, do not reflect this trend. This is consistent with relatively similar concentrations of single- and multi-UFA in all samples (**Figure 5.2**). Thus, it is likely that the 3L architecture in milk fat is formed of TAGs containing at least one unsaturated fatty acid (Lopez et al., 2006; Pratama et al., 2021). The kinked fatty acid chain is likely to arrange in the monolayer regime of the lamellae; whereas, the bilayer contains predominantly the saturated chains (Pratama et al., 2021).

The present results prove the suitability of our ‘chemical grouping’ of TAGs approach, whilst at the same time giving evidence of the limitation of the HMF-MMF-LMF grouping for explaining the milk fat crystallisation behaviour. As mentioned above, the three melting fractions viewpoint is difficult to rationalize, simply because there is no clear categorization of which TAGs are included in each fraction. On top of that, it is hard to achieve a ‘clean’ fractionation of the different melting TAGs due to co-crystallization and molecular entrapment.

The crystal structure associated with asymmetric TAGs (containing short-FA) given by the β’-3L form with *d*-spacing around 53 Å, which was analysed in detail in our previous work (Pratama et al., 2022), was not observed in the current set of experiments. A possible explanation is that this polymorph has a relatively slow nucleation rate. Our previous experiments showed that this form is observable in buffalo milk fat after being frozen at ca. -18 °C for 3 weeks (Pratama et al., 2021). Whereas in cream and anhydrous milk fat, this

structure is apparent after tempering at 4 °C for 60 h (Lopez, Bourgaux, Lesieur and Ollivon, 2002). Therefore, it is not surprising that greater portions of short-FA remain liquid and accumulate also in the liquid Olein fraction during fractionation (**Figure 5.2**).

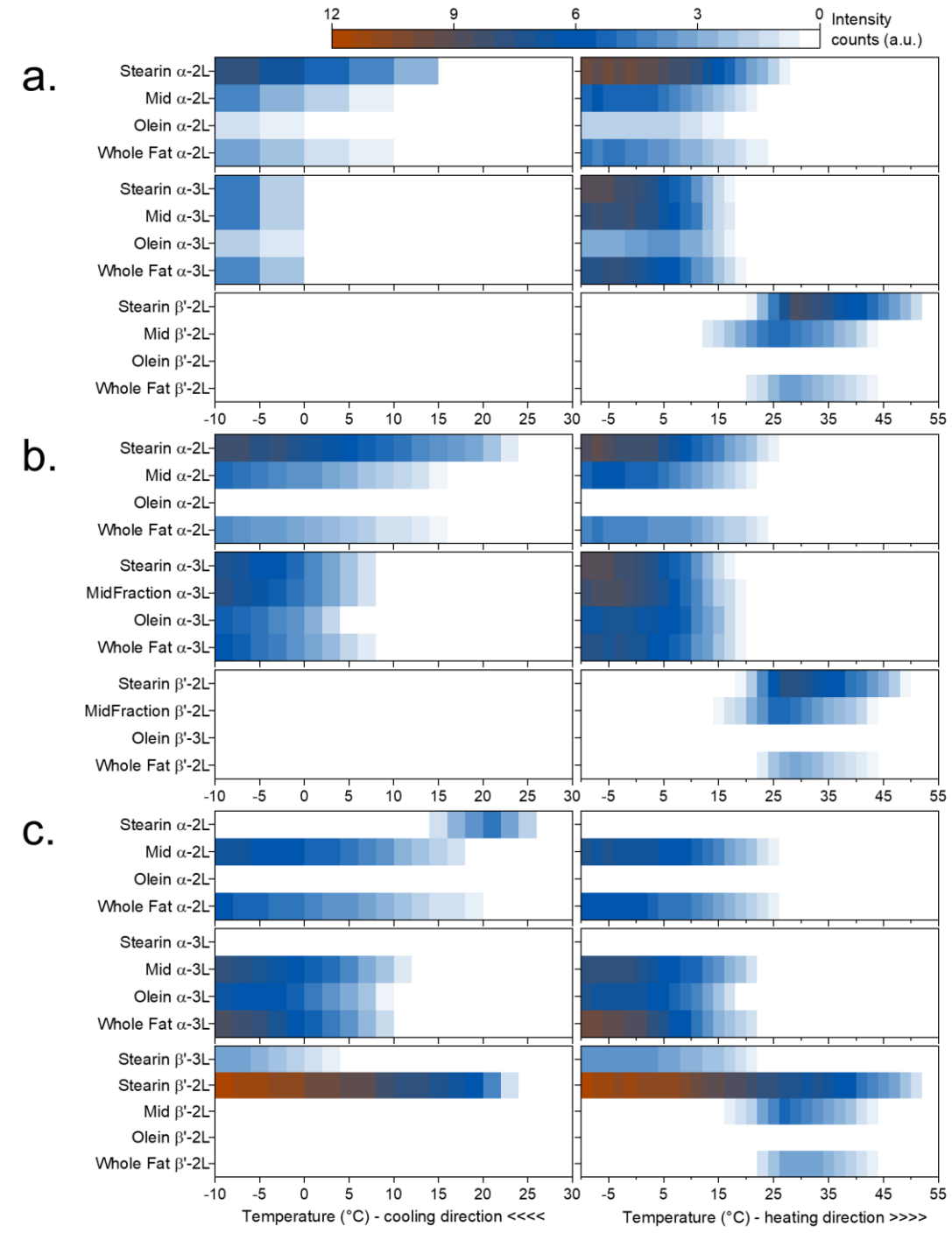

Figure 5.4 Overview of crystal intensity evolution at different cooling rates: (a) -5, (b) -2 and (c) -0.5 °C/min which followed by subsequent heating at 2°C/min.

5.4.3 Kinetics and Evolution of Crystal Formation as Affected by Different TAG Compositions

The phase evolution overview of all four milk fat samples and with the three different applied thermal procedures is presented in **Figure 5.4.** All detailed X-ray intensity trends can be found in the Appendix C, **Figure C.2** and **C.3.** The twelve different experiments are further grouped based on three different characteristic crystallisation pathways observed. The first pathway (**Figure 5.5**) shows a phase evolution, where only the α-polymorphs are observed during the cooling and heating ramps. This pattern is for instance observable in the Olein fraction at all the three different cooling rates (-5, -2 and -0.5 °C/min). Due to its low all-SFA content, the X-ray measurements confirm that the main crystalline form is in the 3L stacking architecture. This crystal structure nucleated during the cooling profile and subsequently melted upon heating without any polymorphic transformation. The thermogram (**Figure 5.5**, bottom panels) agrees broadly with the X-ray observation as only one major exothermic (12.0 °C) and one endothermic (17.1 °C) peak are present during cooling and heating, respectively. However, an additional small exothermic event (12.5 °C) is observed in the DSC cooling regime, which can be associated with the nucleation of α-2L crystals. Correspondingly, a small endothermic peak (16 °C) was also observed during heating, which can be associated with the melting of the same crystal structure. Most likely, the all-SFA TAGs in the Olein fraction (about 4% as shown in **Table 5.1**) is responsible for these thermogram results. However, these additional subtle peaks were not captured in the SAXS measurements (**Figure 5.5**, top panels).

Differences in SAXS and DSC measurements can be explained considering the difference in the amount of sample used and the different sample holder geometry, which results in slightly different heat exchange efficiency albeit applying the same thermal procedure. It is worth noting that in general, the SAXS experiments reveal a thermal lag when compared to DSC measurements (i.e., displaying lower nucleation and higher melting points) due to a less efficient heat transfer of the SAXS setup (capillaries heated from both ends) compared to the DSC pans. For example, the onset of α-3L nucleation is shown at 9 and 12.0 °C for SAXS and DSC, respectively (**Figure 5.5**).

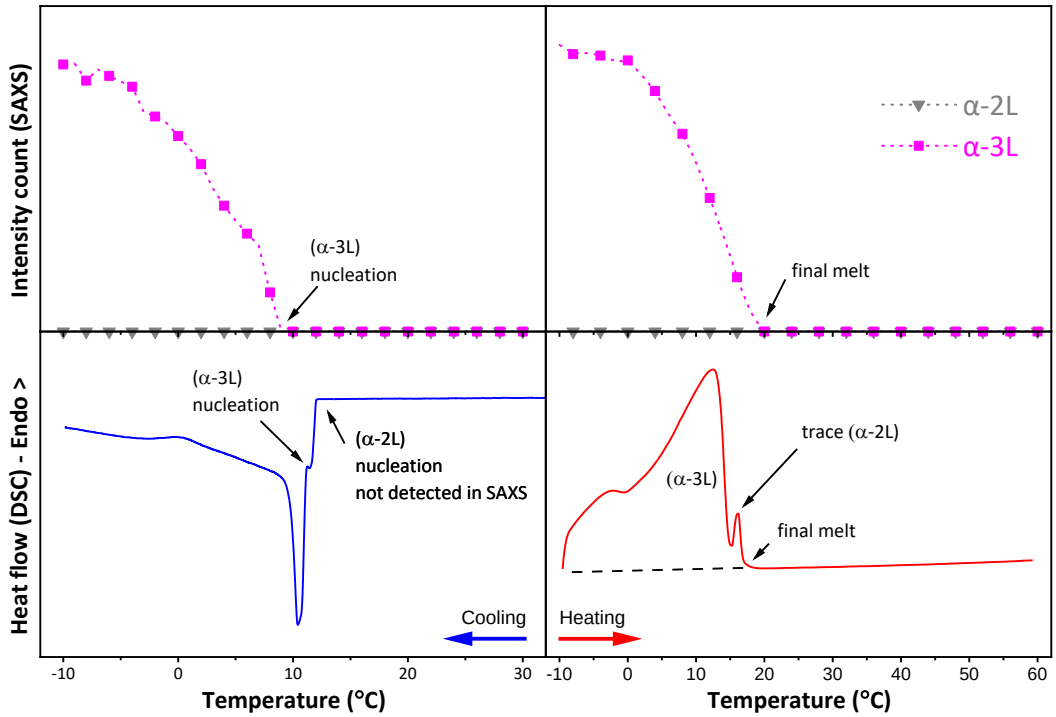

Figure 5.5 Phase evolution pathway one: The β'-phase is absence on cooling and heating. Shown result, Olein fraction cooled from melt at -0.5 °C/min to -10 °C, followed by subsequent heating at 2 °C/min to 60 °C.

The second pathway (**Figure 5.6**) exhibits the formation of an α-polymorph during cooling and a polymorphic transformation from α to β' form upon subsequent heating. This crystallisation pathway is the most common among the three observed scenarios, and it was found in eight out of twelve experiments, i.e., Mid fraction and Whole Fat for all cooling rates, the Stearin fraction at -5 and -2 °C/min rate (**Figure 5.4, Figure C.2 and C.3**). The formation of α-phase upon cooling is indicated by two nucleation events, as observed on both SAXS and DSC measurements. The first, which occurs at higher temperature (between 18-25 °C depending on the cooling rate, **Table 5.2**), can be attributed to the formation of α-2L crystals, whereas the second nucleation event at lower temperature (13-15 °C, **Table 5.2**) is attributed to the appearance of α-3L crystals. It is worth noticing that the final amount of the crystals of each polymorphic form nucleated depended on the TAGs composition. For instance, **Figure 5.4b** shows the Stearin fraction, which contains more all-SFA and has consequently more α-2L crystals at -10 °C, when compared to the Mid fraction that instead showed more of the α-3L crystals. Correspondingly, two main exothermic events are recorded in DSC, attributed to the α-2L (19.1 °C) and α-3L (14.0 °C) nucleation, respectively (**Figure 5.6**, **Table 5.2**).

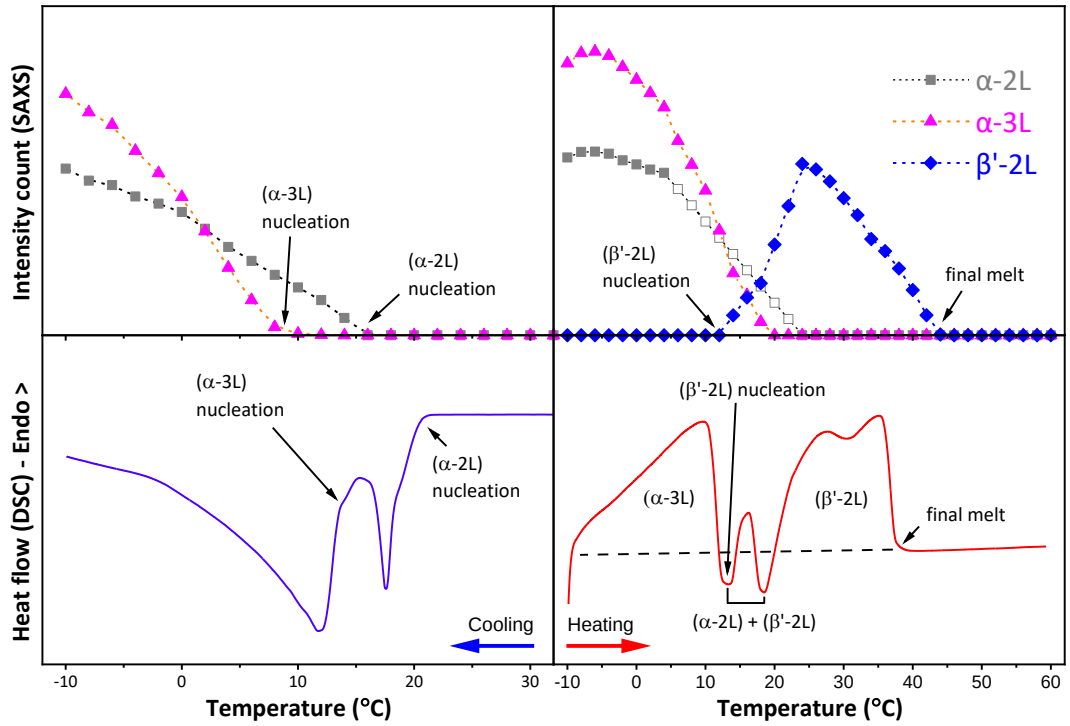

Figure 5.6 Phase evolution pathway two: The β'-phase appears during heating treatment. For instance, the Mid fraction cooled from melt at -2 °C/min to -10 °C, followed by subsequent heating at 2 °C/min to 60 °C displays this pathway. The hollow squares indicate estimated data points derived from the wide-angle X-ray scattering data.

Upon heating, the Bragg peaks corresponding to the two α crystal structures showed a slight increase in intensity, followed by a decrease until their complete disappearance at 20-25 °C. The evolution of the amount of the α-2L form over time, is hard to quantify from the intensity of the main Bragg peak in the SAXS regime (q = 0.13 Å^{-1}), because it overlaps with a newly arising peak associated with the more stable β'-2L phase (q = 0.14 Å^{-1}, d-spacing= 44.1 Å), forming during heating at about 13-15 °C. Therefore, some intensity data points (**Figure 5.6**, hollow squares) were estimated from the trend of disappearance of the α-peak in the wide-angle region (q = 1.52 Å^{-1}). It is likely that this transformation is melt-mediated, because the formation of the 2L-β' phase occurs concomitantly to the melting of the α-crystals (Sato, 2018b).

The DSC thermogram (**Figure 5.6**, bottom panels) shows the three typical broad endothermic peaks of milk fat melting. By correlating these thermal events with the X-ray pattern evolution, we can associate the first peak to the melting of the α-3L crystals. The following minimum is an exothermic dip that is associated to the formation of the β'-2L crystals (see also the blue line in the SAXS panel of **Figure 5.6**). Hence, the second thermal peak is probably

the result of the α-2L melting and β'-2L nucleation. Finally, the last endothermic peak corresponds to the melting of the β'-2L structure. The current interpretation is in agreement with an *in-situ* DSC-SAXS study in cream crystallisation previously performed (Lopez, Bourgaux, Lesieur, Bernadou, et al., 2002). **Table 5.2** summarises the temperatures of the important thermal events for all samples at different cooling rates.

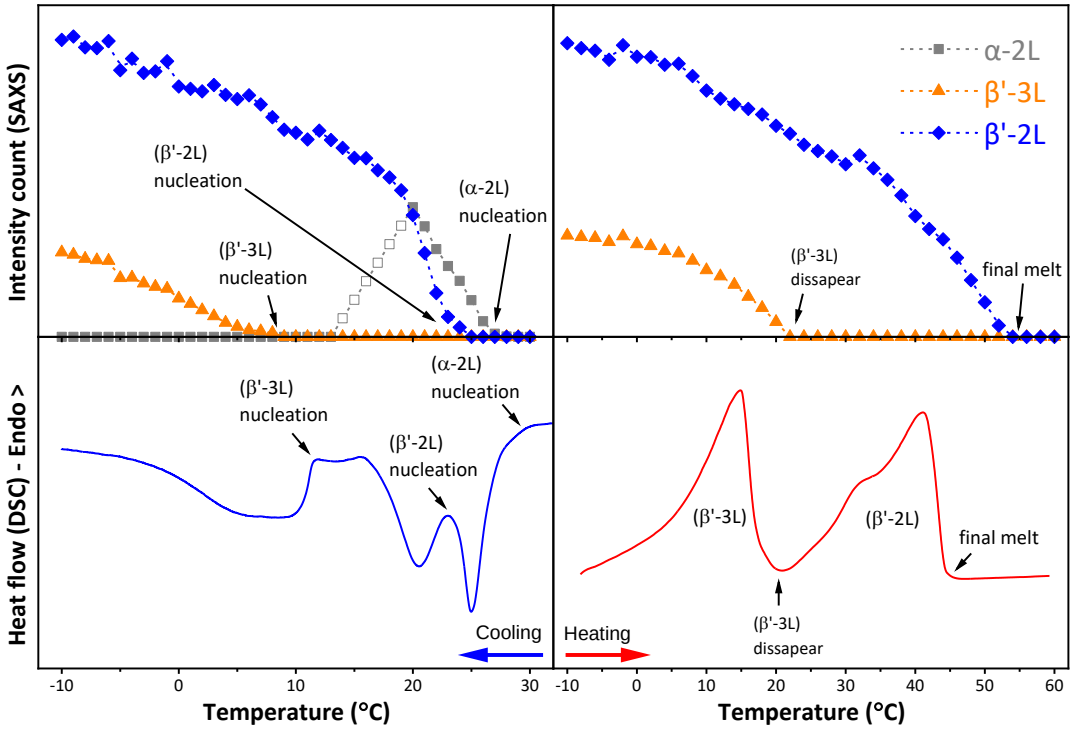

Figure 5.7 Phase evolution pathway three: The β'-phase appears during cooling treatment. Only the Stearin fraction cooled from melt at -0.5 °C/min to -10 °C, followed by subsequent heating at 2 °C/min to 60 °C displays this pathway. The hollow squares indicate estimated data points derived from the wide-angle X-ray scattering data.

The last crystallisation pathway is only observed for the Stearin fraction at a cooling rate of -0.5 °C/min (**Figure 5.7**). This pathway is different from the other more common two, because the formation of the β'-polymorph is observed during the cooling process rather than during subsequent heating stage. There are three nucleation events observable from the SAXS patterns: the first one at around 26 °C, corresponding to the α-2L crystal structure formation. However, this form is short-lived as observed from the decreasing in intensity of its characteristic wide-angle peak at q = 1.52 $Å^{-1}$. Similarly to the heating process shown in **Figure 5.6**, the decrease trend in X-ray intensities here are estimated from the characteristic WAXS peak intensity of the α-

polymorph (hollow squares), due to the overlapping of the main α-2L and β'-2L peaks in the SAXS regime. The two following nucleation events at around 23 and 8 °C are associated with the formation of the β'-2L and β'-3L polymorphs, in this order.

Three nucleation events can also be observed from the thermograms, where three exothermic peaks are present with onsets at 27.0, 24.0 and 11.8 °C (**Table 5.2**). It is worth noting, that without the accompanying X-ray scattering data, these three exothermic events can be easily wrongly interpreted, especially when relying on the melting fractions concept (HMF, MMF, LMF). However, by combining both techniques we can be certain that a polymorphic transformation is taking place, indicated by the disappearing α-peak in the wide-angle region. Moreover, the presence of two exothermic peaks during cooling ramp, related to the same 2L-stacking (α-2L and β'-2L), suggests that a polymorphic transformation has taken place from the α-2L to the β'-2L phase (Sato, 2018b). This aligns with our previous interpretation that the α → β' transformation occurs within the same stacking configuration in milk fat (Pratama et al., 2021).

Following the SAXS pattern in **Figure 5.7**, no α-3L crystals were observed upon cooling as the 3L structure directly nucleated into a β'-phase. In contrast, at higher cooling rates of -2 and -5 °C/min (**Figure 5.6**), Stearin also crystallised in the α-3L form. According to the Ostwald's rule of stages, TAGs normally nucleate into the less stable form (α-phase) given appropriate undercooling, which can be kinetically favoured, and then transform into a more stable polymorph (e.g., the β'-phase) (Himawan et al., 2006). However, the slow cooling rate of -0.5 °C/min provided low undercooling, which can override this rule (Himawan et al., 2006) and result in the direct nucleation of a more stable form (β'-3L in this case). It is worth noting that this same cooling rate did not produce β'-3L in other milk fat fraction samples (Appendix C, **Figure C.2**). We attribute this to the high amount of short-FA TAGs in the other samples, which hinder the α → β' transformation.

In contrast to the second pathway, there are no polymorphic transformation occurring during the subsequent heating stage (cp. **Figure 5.6** and **5.7**). Instead, two separate DSC endothermic peaks are observable, which are linked to the melting of the two crystal forms of β'-3L and β'-2L. It is worth pointing out that the Stearin fraction cooled at -5 and -2 °C/min showed three melting peaks in its thermogram, whereas the -0.5 °C/min rate showed only two melting events. This provides further evidence that the thermal

characteristics of milk fat are largely affected by the TAG composition as well as the processing conditions that precede the heating scan.

5.4.4 Effect of the Cooling Rate on the Thermal Properties of Different Milk Fat Samples

One of the objectives of testing the same heating rate of 2 °C/min for all samples was to evaluate if the different preceding cooling rates can affect the melting range of the different fractions. This depends on the type of polymorphs present, their crystallinity and the TAGs composition. As can be seen in **Table 5.2**, the melting range of the milk fat fractions are largely different. Stearin fraction have the highest, whereas Olein fraction display the lowest melting points among all samples. This trend can be easily understood as being the result of varying amounts of high melting TAGs (all-SFA). Furthermore, the effect of the cooling rate on the melting range was investigated. Whole Fat, Stearin and Mid fraction samples cooled at -0.5 °C/min showed about 0.6-1.1 °C higher final melting points (see notation on **Figure 5.5, 5.6, 5.7**) than the same sample cooled at -5 °C/min. This trend is in accordance with our previous study on buffalo and cow milk fat (Pratama et al., 2021), where slow cooling resulted in higher melting points. Noting that the three samples display the β'-2L phase at the end of melting process, one can attribute the enhanced melting point as a result of (i) higher amount of β'-2L crystalline material formed during a slower cooling process and (ii) the difference in β'-2L crystal packing density as affected by the crystallisation time. Indeed, we previously observed a similar phenomenon with a pure milk fat asymmetrical TAG (1-butyryl 2-stearoyl 3-palmitoyl-glycerol), that a long isothermal hold allowed the β'-crystal packing to become denser. As a consequence, the strength of Van der Waals interactions between hydrocarbon chains can increase and lead to a higher melting temperature (Pratama et al., 2022).

With a similar argument, we can also explain, why the melting point of the Olein fraction is not much affected by the cooling rate, with the -5 and -0.5 °C/min rates, giving the same final melting temperature of 17.1 °C. The Olein fraction did not form β' crystals upon heating, and stayed in the hexagonal packing of the α-polymorph. We note that the chain packing in the α-form is characterised by the hydrocarbon chains undergoing free rotations along their long axis, and in turn not allowing the chain packing to become significantly denser with time, i.e., the Van der Waals interactions remain practically constant in this case. Hence, different crystallisation times (more or less time

at high undercooling) do not have a significant effect on the melting temperatures.

Table 5.2 DSC thermogram events compilation.

Sample	Cooling rate (°C/min)	Cooling				Heating	
		α-2L	α-3L	β'-2L	β'-3L	β'-2L nucleation	Final melt
Whole Fat	5	18.7±0.6	15.3±0.5	-	-	13.5±0.1	37.9±0.4
	2	19.3±0.5	13.9±0.4	-	-	14.0±0.1	37.8±0.2
	0.5	25.0±0.9	14.2±0.4			13.7±0.4	38.4±0.3
Stearin	5	25.0±0.4	13.6±0.6	-	-	13.5±0.5	43.5±0.6
	2	25.6±0.5	13.6±0.7	-	-	13.1±0.1	43.7±0.5
	0.5	27.0±0.2	-	24.0±0.9	11.8±0.4	21.0±0.3*	44.3±0.1
Mid	5	18.4±1.0	13.3±1.2	-	-	12.1±0.6	37.8±0.5
	2	19.1±0.4	14.0±0.6	-	-	12.8±0.2	37.8±0.5
	0.5	21.2±0.7	14.5±0.6	-	-	12.7±0.3	38.9±0.5
Olein	5	-	11.3±0.5	-	-	-	17.1±0.3
	2	-	11.5±0.6	-	-	-	17.4±0.7
	0.5	-	12.0±0.9	-	-	-	17.1±0.4

*melting of β'-3L

Another interesting observation concerns the similar melting properties of the Mid fraction and the Whole Fat sample. Indeed, the Mid fraction is the result of the Whole Fat sample being separated from most of its 'higher' and 'lower' melting TAGs. One could think that, upon removal of the high melting TAGs, the Mid fraction would have a lower melting point. However, due to co-crystallization and entrapment during fractionation, the Mid fraction has actually a TAG composition that is close to the original Whole Fat sample (**Figure 5.2**), and thus sustains their similar thermal and melting properties.

5.4.5 Microstructure of Different Milk Fat Fractions

The microstructure of milk fat crystals is of interest as it influences food quality attributes, such as mouthfeel. For instance, large crystal size has been associated with an unpleasant grainy texture in butter. Here, we report the microstructure of the milk fat fractions with different TAGs composition, as they are cooled from melt at -5 °C/min (**Figure 5.8**). The amount of the high melting all-SFA in the sample played a significant role in the nucleation temperature, as can be seen in **Table 5.2**, where Stearin α-2L nucleated at higher temperatures than the Whole Fat and Mid fraction. Micrographs

(**Figure 5.8**) show that Stearin fraction samples nucleated at temperatures above 25 °C, whereas Whole Fat and Mid fraction samples presented their first nucleation events at about 20 °C. Lastly, the Olein fraction, which has the lowest all-SFA content nucleated only below 15 °C.

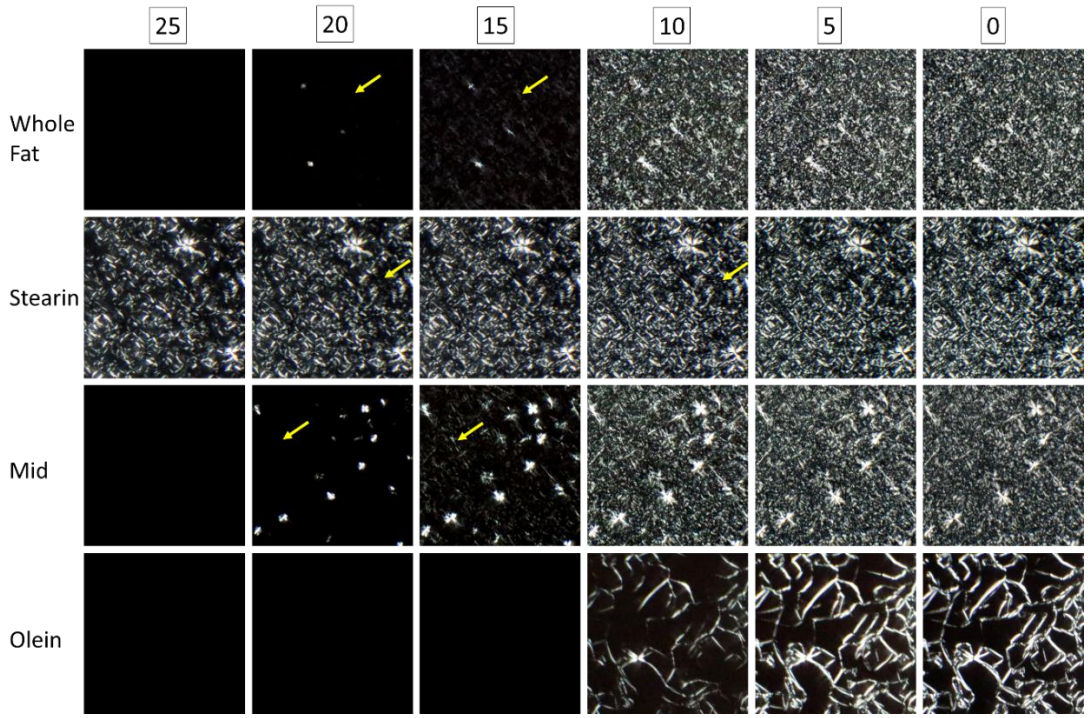

Figure 5.8 Crystal microstructure of milk fat samples during the cooling scan from the melt at -5 °C/min. Captured images are presented from 25 to 0 °C at 5 °C interval. Each side corresponds to 200 μm. Yellow arrows indicate the formation of new crystals in the void (second nucleation).

Supported by our SAXS and DSC findings, we are interested to deliver best interpretations of the PLM images. For instance, the two nucleation events, which correspond to the appearance of α-2L and α-3L crystals, are clearly observed in the Whole Fat and Mid fraction samples. The nucleation of the α-2L polymorph is evident, when large bright crystal clusters appeared at 20 °C, whereas the second nucleation event (α-3L) is observed from the appearance of smaller crystal agglomerates that filled out the molten sample at 15 °C, and grew brighter as the cooling proceeded. More α-2L crystal clusters can be observed in the Mid fraction than in the Whole Fat sample, which is linked to its higher amount of all-SFA that corresponds to the α-2L crystals (**Table 5.2**, **Figure 5.2**). The second nucleation event in the Stearin fraction is harder to observe due to the high concentration of all-SFA TAGs that results in higher amount of α-2L nuclei. However, focusing on the area indicated by the yellow arrow (**Figure 5.8**, second row), we can see the formation of new crystal nuclei at 15 °C. In contrast, only one nucleation event is visible in the Olein fraction,

with the formation of streaky crystal clusters at 10 °C, corresponding to the α-3L polymorph. These microscopy evaluations are in accordance with the results obtained from SAXS and DSC measurements, despite differences in the measurement set ups affecting the exact temperature values of the crystallization events.

One particular experiment of interest concerned the cooling of the Stearin fraction at -0.5 °C/min. In fact, this experiment did display three nucleation events (**Figure 5.7**). **Figure 5.9** shows the microstructures formed upon slow cooling, and we can confirm three separate events also at the micro-scale level. The first nucleation event is observed at 29.5 °C, which corresponds to the appearance of α-2L crystals. The nuclei are less in number but grow bigger, compared to the -5 °C/min cooling rate (nucleation seen at 25 °C, **Figure 5.8**). The same trend was observed in buffalo and cow whole milk fat upon slow and fast cooling (Pratama et al., 2021). The second nucleation event is visible with the appearance of a corona of small crystals surrounding the existing agglomerates, at about 20 °C. This structure corresponds to the formation of β'-2L crystals, recorded in DSC at 24.0 °C (**Table 5.2**). It is worth noting, that according to the SAXS measurements, the α-crystal intensity diminishes when the β'-2L nucleates (**Figure 5.7**). However, the micrographs do not indicate that the initial nuclei of α-2L disappeared, when the corona was formed. A possible explanation is that the α-2L nuclei transform into β'-2L under solid state transformation, emphasizing the lack of melting of the metastable phase. This transformation type is contrasting to melt-mediated ones, where the α-2L melts before the formation of β'-2L phase during heating process (**Figure 5.6**). Indeed, the continuous slow cooling process kept the temperature below the melting point of α-2L crystals, which in turn provides a suitable condition for this solid state polymorphic transition (Sato, 2018b). However, PLM provides lower resolution compared to SAXS and DSC techniques, so that some nano-scale changes (for example, α-crystals melting and β'-crystals forming concomitantly) might not be visible. Finally, the third nucleation event can be seen with the formation of elongated crystal agglomerates, which appeared at about 10 °C. This event corresponds to the formation of the β'-3L polymorph, which was recorded at 11.8 °C in the DSC measurements (**Table 5.2**).

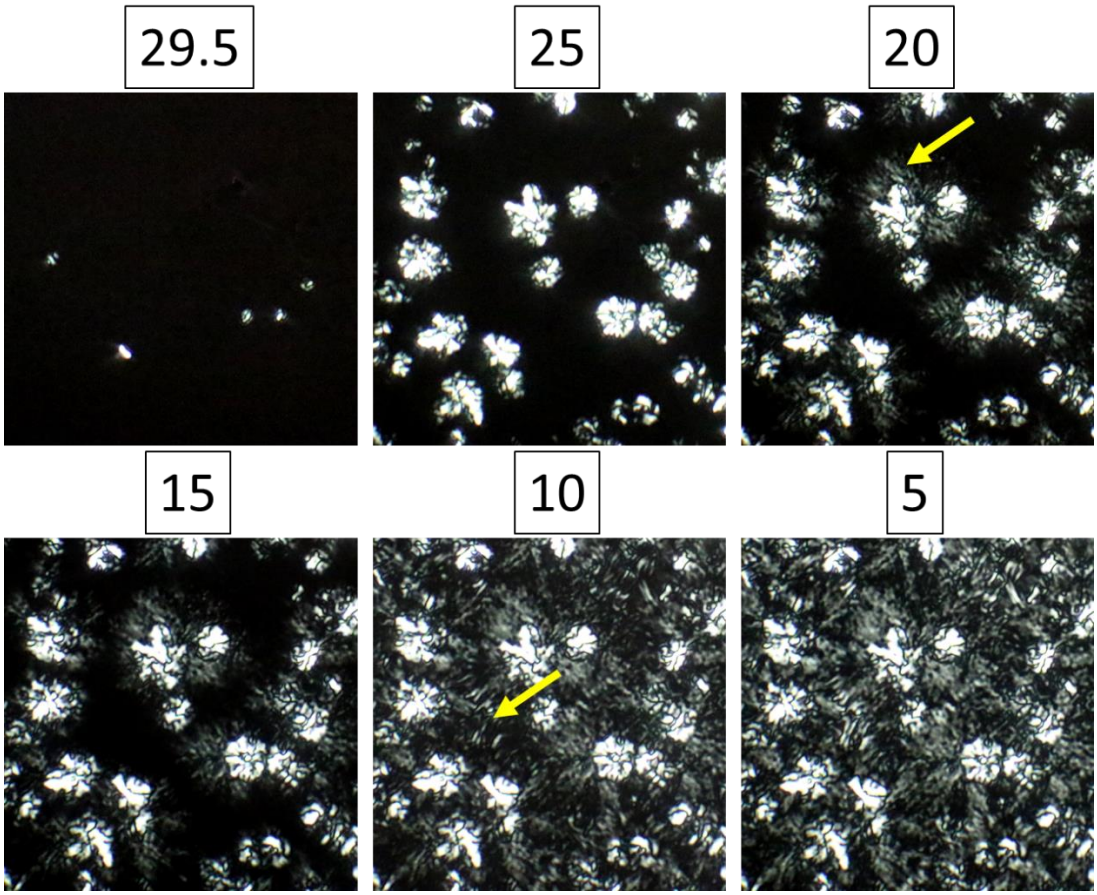

Figure 5.9 Crystal microstructure formation in the Stearin fraction on cooling from melt at -0.5 °C/min. Captured images are presented from 25 to 0 °C at 5 °C interval. Each image side corresponds to 200 µm. Yellow arrows indicate the formation of new crystals in the void (second and third nucleation).

5.5 Conclusion and Outlook

We have shown that 2L-stacked crystals are formed mainly in fractions rich in all-SFA TAGs, whereas the 3L form is mainly related to the presence of single and multi-UFA TAGs. The short-FA TAGs are not easily incorporated in the solid crystals and are found in higher quantity in the liquid fraction. Furthermore, this type of TAGs does contribute to delayed polymorphic transformations. In this study, we once more confirmed the main contribution of each TAG groups to the different crystalline forms in milk fat, and discussed how they interact as a mixture in determining the crystallisation kinetics. Here, the TAGs composition or specifically the TAG groups ratios play a significant role in crystallization. For instance, the Stearin fraction forms the β'-polymorph during slow cooling, due a relatively small proportion of short-FA TAGs that can impede the α to β' phase transformation. The opposite effect applies to the Olein fraction, which is unable to form the β' phase under the given

experimental conditions, because of its higher content of short-FA TAGs. However, the crystallisation kinetics of the Whole Fat and Mid fraction samples behave very similarly despite some compositional differences. This suggests that in order to induce a significant change in the kinetics of polymorphic transformations, compositional differences need to be quite significant, as given in the Stearin and Olein fractions.

With respect to future TAGs composition design-focussed studies, Bayard et al. (2022) found that the addition of 1% tristearin had little effect to the nanostructure of milk fat crystals. In contradiction, our past study (Pratama et al., 2021) found that TAGs composition differences in buffalo and cow milk fat, albeit not as substantial as the Stearin and Olein fractions with respect to the Mid fraction or Whole Fat sample, are sufficient to induce a difference in the type and ratio of different polymorphs at the end of a slow cooling profile. Nonetheless, due to the complexity of milk fat TAGs, it is virtually impossible to mimic changes in its composition using a model system approach, as for cocoa butter with its three main TAGs only (Ghazani and Marangoni, 2021). The use of actual fat or fat fractions is thus the only practical option for fine-tuning the crystallisation behaviour of milk fat products. For this purpose, we argue that a robust and accurate compositional analysis technique is very important. To date many chromatographic studies published on the milk fat TAGs composition, (Gresti et al., 1993; Lopez et al., 2006; Zhou et al., 2014; Lopez, 2018) reported as low as 17 (Amanda J. Wright, McGauley, et al., 2000) to more than 3000 (Liu et al., 2020) TAG species with varying concentration. This highly affects the interpretation of the obtained compositional results, especially regarding the TAG groups ratios. A better understanding of the interaction effects between all-SFA, single and multi-UFA as well as short-FA TAG groups will allow us to predict the possible crystallisation pathways and kinetics, and even further, to design compositional modification strategies in order to achieve specific milk fat crystallisation characteristics.

5.6 References

Abd El-Salam, M.H. and El-Shibiny, S. 2011. A comprehensive review on the composition and properties of buffalo milk. *Dairy Science & Technology*. **91**(6), pp.663-699.

Bayard, M., Kauffmann, B., Vauvre, J.M., Leal-Calderon, F. and Cansell, M. 2022. Isothermal crystallization of anhydrous milk fat in presence of free

fatty acids and their esters: From nanostructure to textural properties. *Food Chemistry*. **366**(June 2021), p.130533.

Breitschuh, B. and Windhab, E.J. 1998. Parameters influencing cocrystallization and polymorphism in milk fat. *Journal of the American Oil Chemists' Society 1998 75:8*. **75**(8), pp.897-904.

Campos, R.J., Litwinenko, J.W. and Marangoni, A.G. 2003. Fractionation of milk fat by short-path distillation. *Journal of Dairy Science*. **86**(3), pp.735-745.

Che Man, Y.B., Haryati, T., Ghazali, H.M. and Asbi, B.A. 1999. Composition and Thermal Profile of Crude Palm Oil and Its Products. *JAOCS, Journal of the American Oil Chemists' Society*. **76**(2), pp.237-242.

Cisneros, A., Mazzanti, G., Campos, R. and Marangoni, A.G. 2006. Polymorphic transformation in mixtures of high- and low-melting fractions of milk fat. *Journal of Agricultural and Food Chemistry*. **54**(16), pp.6030-6033.

Deffense, E. 1993. Milk fat fractionation today: A review. *Journal of the American Oil Chemists' Society*. **70**(12), pp.1193-1201.

Dimick, P.S., Reddy, S.Y. and Ziegler, G.R. 1996. Chemical and thermal characteristics of milk-fat fractions isolated by a melt crystallization. *JAOCS, Journal of the American Oil Chemists' Society*. **73**(12), pp.1647-1652.

FAO 2022. FAOSTAT Statistical Database. [Accessed 27 January 2023]. Available from: https://www.fao.org/faostat/en/#data/QCL.

Gantner, V., Mijić, P., Baban, M., Škrtić, Z. and Turalija, A. 2015. The overall and fat composition of milk of various species. *Mljekarstvo*. **65**(4), pp.223-231.

Ghazani, S.M. and Marangoni, A.G. 2021. Molecular Origins of Polymorphism in Cocoa Butter. *Annual Review of Food Science and Technology*. **12**, pp.567-590.

Gresti, J., Bugaut, M., Maniongui, C. and Bezard, J. 1993. Composition of Molecular Species of Triacylglycerols in Bovine Milk Fat. *Journal of Dairy Science*. **76**(7), pp.1850-1869.

Grotenhuis, E. Ten, Van Aken, G.A., Van Malssen, K.F. and Schenk, H. 1999. Polymorphism of milk fat studied by differential scanning calorimetry and

real-time X-ray powder diffraction. *JAOCS, Journal of the American Oil Chemists' Society*. **76**(9), pp.1031-1039.

Grummer, R.R. 1991. Effect of Feed on the Composition of Milk Fat. *Journal of Dairy Science*. **74**(9), pp.3244-3257.

Himawan, C., Starov, V.M. and Stapley, A.G.F. 2006. Thermodynamic and kinetic aspects of fat crystallization. *Advances in Colloid and Interface Science*. **122**(1-3), pp.3-33.

Jensen, R.G., Ferris, A.M. and Lammi-Keefe, C.J. 1991. The Composition of Milk Fat. *Journal of Dairy Science*. **74**(9), pp.3228-3243.

Larsen, M.K., Andersen, K.K., Kaufmann, N. and Wiking, L. 2014. Seasonal variation in the composition and melting behavior of milk fat. *Journal of Dairy Science*. **97**(8), pp.4703-4712.

Liu, Z., Li, C., Pryce, J. and Rochfort, S. 2020. Comprehensive Characterisation of Bovine Milk Lipids: Triglycerides. *ACS Omega*. **5**(21), pp.12573-12582.

Loisel, C., Keller, G., Lecq, G., Bourgaux, C. and Ollivon, M. 1998. Phase transitions and polymorphism of cocoa butter. *JAOCS, Journal of the American Oil Chemists' Society*. **75**(4), pp.425-439.

Lopez, C. 2018. Crystallization Properties of Milk Fats *In*: K. Sato, ed. *Crystallization of Lipids: Fundamentals and Applications in Food, Cosmetics and Pharmaceuticals*. Hoboken, NJ: Wiley Blackwell, pp.283-321.

Lopez, C., Bourgaux, C., Lesieur, P., Bernadou, S., Keller, G. and Ollivon, M. 2002. Thermal and structural behavior of milk fat 3. Influence of cooling rate and droplet size on cream crystallization. *Journal of Colloid and Interface Science*. **254**(1), pp.64-78.

Lopez, C., Bourgaux, C., Lesieur, P. and Ollivon, M. 2002. Crystalline structures formed in cream and anhydrous milk fat at 4 °C. *Lait*. **82**(3), pp.317-335.

Lopez, C., Bourgaux, C., Lesieur, P., Riaublanc, A. and Ollivon, M. 2006. Milk fat and primary fractions obtained by dry fractionation. 1. Chemical composition and crystallisation properties. *Chemistry and Physics of Lipids*. **144**(1), pp.17-33.

Lopez, C., Lavigne, F., Lesieur, P., Bourgaux, C. and Ollivon, M. 2001. Thermal and structural behavior of milk fat. 1. Unstable species of anhydrous milk fat. *Journal of Dairy Science*. **84**(4), pp.756-766.

Lopez, C., Lesieur, P., Bourgaux, C. and Ollivon, M. 2005. Thermal and structural behavior of anhydrous milk fat. 3. Influence of cooling rate. *Journal of Dairy Science*. **88**(2), pp.511-526.

Macridachis, J., Bayés-García, L. and Calvet, T. 2021. Mixing Phase Behavior of Tripalmitin and Oleic-Rich Molecular Compound-Forming Triacylglycerols. *Cite This: Ind. Eng. Chem. Res*. **60**, pp.5374-5384.

Marangoni, A.G. and Lencki, R.W. 1998. Ternary Phase Behavior of Milk Fat Fractions. *Journal of Agricultural and Food Chemistry*. **46**(10), pp.3879-3884.

Maurice-Van Eijndhoven, M.H.T., Hiemstra, S.J. and Calus, M.P.L. 2011. Short communication: Milk fat composition of 4 cattle breeds in the Netherlands. *Journal of Dairy Science*. **94**(2), pp.1021-1025.

Nguyen, V., Duong, C.T.M. and Vu, V. 2015. Effect of thermal treatment on physical properties and stability of whipping and whipped cream. *Journal of Food Engineering*. **163**, pp.32-36.

Omar, Z., Hishamuddin, E., Sahri, M.M., Fauzi, S.H.M., Dian, N.L.H.M., Ramli, M.R. and Rashid, N.A. 2015. Palm Oil Crystallisation: A Review. *Journal of Oil Palm Research*. **27**(2), pp.97-106.

Palmquist, D.L., Denise Beaulieu, A. and Barbano, D.M. 1993. Feed and Animal Factors Influencing Milk Fat Composition. *Journal of Dairy Science*. **76**(6), pp.1753-1771.

Pratama, Y., Burholt, S., Baker, D.L., Sadeghpour, A., Simone, E. and Rappolt, M. 2022. Polymorphism of a Highly Asymmetrical Triacylglycerol in Milk Fat: 1-Butyryl 2-Stearoyl 3-Palmitoyl-glycerol. *Crystal Growth and Design*. **22**(10), pp.6120-6130.

Pratama, Y., Simone, E. and Rappolt, M. 2021. The Unique Crystallization Behavior of Buffalo Milk Fat. *Crystal Growth and Design*. **21**(4), pp.2113-2127.

Ramel, P.R. and Marangoni, A.G. 2016. Engineering the microstructure of milk fat by blending binary and ternary mixtures of its fractions. *RSC Advances*. **6**(47), pp.41189-41194.

Romano, R., Giordano, A., Chianese, L., Addeo, F. and Musso, S.S. 2011. Triacylglycerols, fatty acids and conjugated linoleic acids in Italian Mozzarella di Bufala Campana cheese. *Journal of Food Composition and Analysis*. **24**(2), pp.244-249.

Rønholt, S., Mortensen, K. and Knudsen, J.C. 2013. The Effective Factors on the Structure of Butter and Other Milk Fat-Based Products. *Comprehensive Reviews in Food Science and Food Safety*. **12**(5), pp.468-482.

Sato, K. 2018. Polymorphism of Lipid Crystals *In*: K. Sato, ed. *Crystallization of Lipids: Fundamentals and Applications in Food, Cosmetics and Pharmaceuticals*. Hoboken, NJ: Wiley Blackwell, pp.17-60.

Schmelzer, J.M. and Hartel, R.W. 2001. Interactions of Milk Fat and Milk Fat Fractions with Confectionery Fats. *Journal of Dairy Science*. **84**(2), pp.332-344.

Shi, Y., Smith, C.M. and Hartel, R.W. 2001. Compositional effects on milk fat crystallization. *Journal of Dairy Science*. **84**(11), pp.2392-2401.

Smiddy, M.A., Huppertz, T. and van Ruth, S.M. 2012. Triacylglycerol and melting profiles of milk fat from several species. *International Dairy Journal*. **24**(2), pp.64-69.

Soyeurt, H., Dardenne, P., Gillon, A., Croquet, C., Vanderick, S., Mayeres, P., Bertozzi, C. and Gengler, N. 2006. Variation in Fatty Acid Contents of Milk and Milk Fat Within and Across Breeds. *Journal of Dairy Science*. **89**(12), pp.4858-4865.

Timms, R.E. 1980. The phase behaviour and polymorphism of milk fat, milf fat fractions and fully hardened milk fat. *The Australian Journal of Dairy Technology*. **35**, pp.47-52.

Tomaszewska-Gras, J. 2013. Melting and crystallization DSC profiles of milk fat depending on selected factors. *Journal of Thermal Analysis and Calorimetry*. **113**(1), pp.199-208.

Tzompa-Sosa, D.A., Meurs, P.P. and van Valenberg, H.J.F. 2018. Triacylglycerol Profile of Summer and Winter Bovine Milk Fat and the Feasibility of Triacylglycerol Fragmentation. *European Journal of Lipid Science and Technology*. **120**(3), p.1700291.

Van-Aken, G., Ten Grotenhuis, E., Van Langevelde, A.J. and Schenk, H. 1999. Composition and crystallization of milk fat fractions. *JAOCS, Journal of the American Oil Chemists' Society*. **76**(11), pp.1323-1331.

Wright, A.J., McGauley, S.E., Narine, S.S., Willis, W.M., Lencki, R.W. and Marangoni, A.G. 2000. Solvent effects on the crystallization behavior of milk fat fractions. *Journal of Agricultural and Food Chemistry*. **48**(4), pp.1033-1040.

Yao, Y., Liu, W., Zhang, D., Li, R., Zhou, H., Li, C. and Wang, S. 2020. Dynamic changes in the triacylglycerol composition and crystallization behavior of cocoa butter. *LWT*. **129**, p.109490.

Zeb, A. and Murkovic, M. 2010. Analysis of triacylglycerols in refined edible oils by isocratic HPLC-ESI-MS. *European Journal of Lipid Science and Technology*. **112**, pp.844-851.

Zhou, Q., Gao, B., Zhang, X., Xu, Y., Shi, H. and Yu, L. 2014. Chemical profiling of triacylglycerols and diacylglycerols in cow milk fat by ultra-performance convergence chromatography combined with a quadrupole time-of-flight mass spectrometry. *Food Chemistry*. **143**, pp.199-204.

Chapter 6 General Discussion and Conclusions

The significant increase in the production of buffalo milk for the last decades indicate the growing interest to this milk and its derivatives. Buffalo milk has been utilised widely in primary dairy products such as fresh milk, milk powder, butter, cheese, ghee, cream (Asif et al., 2022; Mejares et al., 2022), ice cream (Atallah et al., 2022) and yoghurt (Junaid et al., 2023). It also finds application in other product such as in chocolate (de Jesus Silva et al., 2022). Not to mention that buffalo milk has also been employed in many cultural or traditional food products such as Dadih from Indonesia (Arnold et al., 2021), Kajmak from Serbia (Becskei et al., 2020), Rasomalai from Bangladesh (Asif et al., 2021), and Paneer from India (Masud et al., 2007). Without doubt, however, the most important product of buffalo milk is buffalo mozzarella cheese which is popular in Italy as *mozzarella di bufala campana.* It has also obtained the protected designation of origin status from European Union since 1996 (Angelis and Gobbetti, 2011).

The buffalo based products are generally considered to be higher in quality than the similar products from cow milk origin, and thus priced more expensively (Murtaza et al., 2017b). For milk fat-based products like butter, cream and cheese, the product quality attributes are largely influenced by the fat composition, such as the fatty acid and TAGs profiles. The composition plays a pivotal role in the crystallisation behaviour of fat, determining the structure and physical characteristic of the products. Previous studies have shown that buffalo milk has a higher quantity of milk fat and significantly different fatty acid composition than cow milk. However, our knowledge on how these differences translate into different attributes of buffalo milk fat-based products are relatively poor.

Therefore, this thesis has focused on two main aspects: first, the ***evaluation of the crystallisation behaviour of buffalo milk fat*** and its direct derivatives, i.e., buffalo milk fat fractions. This evaluation is also carried out by direct comparison to cow milk fat, enabling better insights on the effects of the different fat composition. The first highlight of this thesis is important for the growing buffalo milk industry as it can be used to design improved buffalo milk-based products. The second aspect analysed in the thesis is of a more fundamental nature, as it provides a ***link between milk fat composition and crystallisation behaviour***. Milk fat consists of more than 200 TAGs and its composition can vary greatly depending on many factors (as described in **Chapter 2**). However, this variation effects to the crystallisation behaviour are

still not well understood. Previous studies often discuss the issue in a realistic scenario but narrow context, for instance the comparison of summer and winter milk fat (Larsen et al., 2014), different breed or different feeds (Shi et al., 2001). Not to mention that there are groups of TAGs that are abundant in milk fat, the asymmetrical ones, whose role in crystallisation has never been addressed properly. Thus, the current thesis offers a new and universal approach in understanding the role of different TAGs in the crystallisation behaviour of milk fat.

6.1 Highlighting the differences in buffalo and cow milk fat crystallisation behaviour

Prior to the comparative study of buffalo and cow milk fat crystallisation behaviour, it is important to evaluate the difference in their fat composition. Several studies have reported the fatty acid compositional differences between the two milk fat, emphasising the higher quantity of saturated fatty acids and a lower quantity of mono-unsaturated fatty acids in buffalo milk fat compared to that of cow milk fat (Ménard et al., 2010; Abd El-Salam and El-Shibiny, 2011; Murtaza et al., 2017b). However, the majority of milk fat is in the form of TAGs (>95%) with free fatty acids, mono- and di-acylglycerols considered as minor components (Huppertz et al., 2009). Thus, fat crystallisation can be best explained from its TAGs composition, as the configuration of the fatty acids in the TAG molecule dictates how it crystallises. Therefore, the present thesis has provided the TAGs compositional difference between buffalo and cow milk fat (**Chapter 3**), where the former was found to have higher amount of high melting and low melting TAGs. Whereas, the middle melting TAGs were found higher in cow milk fat.

Building on these results, we can explain the main differences in the buffalo and cow milk fat crystallisation behaviour; which have been evaluated using SAXS, DSC and PLM (**Chapter 3**). The higher amount of high melting TAGs in buffalo milk fat corresponds to its higher nucleation and melting temperatures. However, it is interesting that the faster nucleation in buffalo milk fat was followed by a slower α → β' polymorphic transformation as shown when applying a slow cooling rate (-0.5 °C/min). This phenomenon is attributed to the higher proportion of low melting TAGs in buffalo milk fat. The β' polymorph is functional, and the preferred form in food products such as margarine and butter (Hondoh et al., 2018). Therefore, its delayed formation in buffalo milk fat constitutes an important knowledge for buffalo milk industries.

6.2 Unravelling the mystery of the short (53 Å) three layered crystal structure in milk fat

There are two dominant milk fat crystal forms observed in the present thesis, namely 2L form (*d*-spacing 42.6 (β') - 48.4 (α) Å) and 3L form (*d*-spacing 67.4 (β') - 72.8 (α) Å). Using electron density profiles (EDPs) determination, the prevalent TAGs contributors of those two forms could be estimated (**Chapter 3**). The 2L structure is mainly related to long chain saturated TAGs (e.g., PPP, PPS and SPS), whereas the 3L structure is characterised by TAGs containing medium-long saturated FAs and long chain mono/poly-unsaturated FAs (e.g., PLaO, PCO, PPO) (note: P-palmitic, S-stearic, O-oleic, La-lauric, C-capric). This interpretation is in accordance with Lopez et al. (2006).

An additional crystal structure was observed from milk fat sample which have been kept at -18 °C for 3 weeks. The buffalo milk fat exhibited a subtle peak at wide angle region q = 1.376 $Å^{-1}$ (4.6 Å) which is characteristic of a β-polymorph. This structure was characterised by a stacking architecture with a *d*-spacing of 53 Å in the small angle regime, in addition to the two main structures mentioned above. Both 4.6 and 53 Å *d*-spacings were not observed in cow milk fat (**Figure 3.7**). The unknown form is probably a β-3L crystal structure with a short d-spacing of 53 Å. This short 3L architecture is rarely reported in milk crystallisation studies. Only one study, to the best of our knowledge, reported a similar structure with a long spacing of 54 Å in cream and anhydrous (cow) milk fat after isothermal hold at 4 °C for 60 hours (Lopez, Bourgaux, Lesieur and Ollivon, 2002). However, the origin of this structure was unclear. **Chapter 3** has attempted to elucidate the nature of this form by simulating an electron density profile that attributed the short 3L architecture to crystals originating from TAGs containing short chain fatty acids such as butyric (C4) and caproic (C6).

In order to confirm the simulation result, pure 1-butyryl 2-stearoyl 3-palmitoyl-glycerol (BuSP) was procured for crystallisation studies. As it can be seen in **Chapter 4**, we observed the *d*-spacing of BuSP crystal were 56.9 and 51.2 Å for the α and β' polymorph, respectively. Whereas during the polymorphic transformation, the mixture of α/β' form exhibited an overlapping strongest 1st order peak corresponding to a d-spacing of 52.9 Å. This value is very close to the *d*-spacing of the short 3L (53 Å) polymorph observed in the buffalo milk fat kept at freezing temperature for long time. Therefore, these findings validate the previous conjecture on the simulated EDPs, that this 3L stacking architecture is most likely formed by the TAGs containing short fatty acids. It is worth noting that BuSP was not observed in its most stable β-form, and only

observed in the β' even after very long (> 1 month) storage in a freezer. Therefore, the previous association of the 3L (53 Å) as a β polymorph might need to be revisited. Indeed, an association between stacking and its chain packing structure is proven to be difficult in a complex system with multiple structures coexisting concurrently such as in milk fat.

6.3 The role of asymmetrical TAGs in the milk fat crystallisation

Asymmetrical TAGs have been defined as TAGs with combination of UUS or SSU, in which the solitary unsaturated (U) or saturated (S) fatty acid resides on either the *sn*-1 or *sn*-3 position or triglycerides with acyl chain length differences greater than two carbon atoms (Sato, 2001). It has been estimated that the amount of asymmetrical TAGs in milk fat is quite significant, owing to the relatively high content of butyric acid (Gresti et al., 1993; Lopez, 2018; Pratama et al., 2021). This characteristic is possibly unique to milk fat, as compared to the fatty acid composition of cocoa butter (Lipp and Anklam, 1998), animal fats (Haas, 2005) as well as vegetable oils/fats (Gunstone, 2011), which do not contain, or contain in a very small amount butyric acid. Butyric acid is also important flavour contributor in dairy products, for instance giving characteristic cheese aroma (Pionnier and Hugelshofer, 2006).

In milk fat crystallisation, the asymmetrical TAGs are considered to play an important role in the formation of β' crystals, whilst the β form is either not observed or only apparent in small quantity (Grotenhuis et al., 1999; Tzompa-Sosa et al., 2016). Therefore, considering the unique nature of this group of TAGs and its abundant quantity in milk fat, it is essential to evaluate the role of asymmetrical TAGs in milk fat crystallisation. The current thesis used BuSP as a model for asymmetrical TAGs, in order to explain the role of this particular group in the crystallisation of the more complex milk fat. In **Chapter 4** I have shown that the BuSP has a relatively slow polymorphic transformation α → β' and could not form the most stable β form under the given conditions. These findings further support the view that milk fat has the tendency to be quasi-stable in the β' polymorph, because of the higher content of these asymmetrical TAGs. Moreover, it is plausible that the presence of BuSP or the asymmetrical TAGs in general, do delay the overall milk fat polymorphic transformation. This is in accordance to the observed slower α → β' transformation in buffalo milk fat, as it contains higher amounts of asymmetrical TAGs when compared to cow milk fat (**Chapter 3**).

6.4 A new approach in the analysis of the role of TAGs in the crystallisation of milk fat

In **Chapter 3** the main TAGs contributors of two dominant crystal forms in milk fat have been investigated, namely (1) fully saturated TAGs, composing the 2L crystals (42.6 - 48.4 Å) and (2) long chain TAGs containing unsaturated FA(s), forming the 3L structures (67.4 - 72.8 Å). With the role of asymmetrical TAGs in milk fat crystallisation being clarified in this thesis (**Chapter 4**), it is now viable to interpret the crystallisation of complex milk fat with its >200 TAGs in a more simplified manner. By categorising the milk fat TAGs based on their chemical properties, such as fatty acid chain length and saturation, their combined effects to milk fat crystallisation can be explained. In the current thesis four different TAGs groups were identified, namely (a) fully saturated TAGs (b) long chain TAGs containing one unsaturated FA (c) long chain TAGs containing multiple unsaturated FAs, and (d) TAGs containing short chain FA. The behaviour of each TAGs group was examined to check how they dictate the milk fat crystallisation behaviour (**Chapter 5**). Commonly three classes of milk fat TAGs are identified, based on their different melting points, with the objective to explain milk fat crystallisation behaviour (Timms, 1980; Deffense, 1993; Marangoni and Lencki, 1998; Grotenhuis et al., 1999; Campos et al., 2003).

The proposed new method, termed as ‘chemical grouping’ approach, was exercised using fat samples with different TAGs proportion, which were obtained from two step dry-fractionated buffalo milk fat. This approach has also technological relevance to the buffalo milk industry. The results confirmed that 2L crystal structures (long spacing about 48 Å) were more abundant in samples containing higher fully saturated TAGs. Whereas, the 3L structures (long spacing about 72 Å) were observed at around the same intensity for all employed samples, which can be attributed to the fact that long chain TAGs containing unsaturated FA(s) were present in similar quantity in all three fractions. The current dry fractionation protocol could not effectively separate the long chain TAGs containing different amounts of unsaturated FA chain, most likely due to the formation of mixed crystals incorporating these TAGs. Hence, both TAGs groups, with single or multiple unsaturated chains, are contributing to the formation of the 3L structures.

On the other hand, the short (53 Å) 3L crystal structures associated with asymmetrical TAGs were not observed in the experiments. It was evident, however, that the polymorphic transformation was absent or retarded in the samples containing high amount of this TAG group. Correspondingly, faster

transformation kinetics were observed in the sample containing least amount of asymmetrical TAGs. Therefore, the overall results confirmed the suitability of the chemical grouping approach to understand the role of TAGs in milk fat crystallisation behaviour.

6.5 Potential impacts on macro scale food properties

Section **2.2** has pointed out that the sensory and textural properties at the macro level of milk fat based is strongly influenced by its nano-scale characteristics. One very important attribute is the polymorphism of fat crystals, which with the increasing stability from α → β' → β phases. In this order, more stable and the higher melting products can be obtained.

This thesis has focused mainly on the nano-scale characteristics of milk fat during various crystallisation processes. In some cases, we have now better understanding on the role of TAGs in the crystallisation, which ideally allows one to predict or to tailor the process. Specifically, it has been shown that the formation of β' crystals is heightened by higher all-SFA and lower short-FA composition. The β' form is functional in dairy and fat products in general, as it is associated with stability, smooth texture and good spreadability (Sato, 2018). Therefore, industry can utilise the newly acquired knowledge in the endeavour of process optimisation.

One particular example, the variability of butter hardness due to seasonal effects is a known problem in milk industry. The milk fat composition varies because of the different feed during summer and winter months, hence the different texture. Common efforts to standardise the butter rheological properties include selection of churning temperatures, application of secondary mechanical treatment and addition of liquid milk fat fraction (Staniewski et al., 2021). Now, the proposed chemical grouping approach can be used to address the problem with a new perspective. For instance, by searching the ideal ratio of each TAG groups, ideal butter crystals and texture can be obtained, addressing a new strategy for industry to modify the varying milk fat composition due to seasonal effects. Nonetheless, it is worth noting that rheological properties are not solely dictated by the polymorphism. The amount of solid fat at a given temperature also plays important role. Therefore, any TAG composition alteration in crystallisation studies must also consider its effect to the overall solid fat content.

6.6 Conclusions

Buffalo milk fat has a higher nucleation and melting point than that of cow milk fat, whilst exhibiting a slower polymorphic α → β' transformation. This phenomenon is attributed to the significantly different proportions of some TAGs between the two milk fats, albeit the similarity in TAGs species. Specifically, buffalo milk fat contains higher amounts of high-melting and low melting TAGs, as well as lower amounts of medium-melting TAGs. The slower polymorphic transformation in buffalo milk fat was found to be related to the higher amount of asymmetrical TAGs in buffalo milk fat, particularly the TAGs containing the very short butyric/caproic acid. This conjecture has been confirmed in the detailed analysis on a pure asymmetrical TAG (1-butyryl 2-stearoyl 3-palmitoyl-glycerol) which showed an incomplete α → β' transformation (about 30:70 ratio) even after 18 h isothermal hold at 20 °C upon cooling from melt. Further, the structure of the triple layered crystal structures of this asymmetrical TAG have been examined in great detail, where the *d*-spacing of α and β'-polymorph were found to be 56.9 and 51.2 Å, respectively. The most stable triclinic packing β-polymorph was not detected during the experiment, agreeing well with the existing knowledge that asymmetrical TAGs are quasi-stable in the orthorhombic packing β'-form. These findings support the view that asymmetrical TAGs are responsible for milk fats predominantly displaying β'-polymorph crystals.

This thesis has put forward a new approach in the analysis of TAGs composition effects towards milk fat crystallisation. The chemical grouping approach used here has successfully demonstrated the prevalence of long chained all-SFA TAGs to the high melting double layered crystals (*d*-spacing: 44.1-49.7 Å). Whereas, the low melting triple layered structures (64.4 - 72.8 Å) are formed prevalently by long chained TAGs containing unsaturated fatty acids. The role of asymmetrical TAGs in the polymorphic transformation have been further assessed. For instance, in the sample containing the least amount of these TAGs, i.e., the Stearin fraction, both 2L and 3L β'-structures were observed during a slow cooling profile. On the other hand, only the α-form was observed in the sample containing the highest amount of asymmetrical TAGs, i.e., in the Olein fraction. These results showcase the practicability of the new chemical grouping method in explaining the different kinetics of milk fat crystallisation based on the TAGs composition. Hence, it could become a useful tool to design modification of the milk fat TAGs, for instance, to obtain specific product/processing attributes.

6.7 Future Directions

This thesis has investigated the crystallisation behaviour of buffalo milk fat and in relation to its milk TAGs composition, developing a new approach that can be applied to other natural fat systems. However, there are several future research directions stemming from this work, as summarised below:

- Applying the proposed chemical grouping approach to evaluate the effects of different TAGs composition on the crystallisation kinetics of edible fats in different processing conditions, for example, at different isothermal temperatures or in the presence of mechanical agitation. Specific interest could be invested to understand how these variables (composition and processing factors) can enhance the formation of the most stable β-polymorph in milk fat. It is worth noting that the presence of this β-form in milk fat has become a subject of ongoing debate (Tzompa-Sosa et al., 2016).
- Follow-up research is also necessary for the evaluation of milk fat TAGs composition modification to produce products with tailored made properties. The TAGs composition could be modified to promote or inhibit specific crystallisation processes and engineering the resulting milk fat crystal structures.
- For the buffalo milk industry, it is important to ‘scale up’ the crystallisation process and verify that the findings presented in this thesis are applicable at industrial scale. Additionally, it would be important how the results of this thesis translate into more complex food products such as emulsified milk systems. Further, real samples using fresh buffalo milk, cream or butter should be evaluated focusing on their crystallisation properties. For a more technological relevance, the research can be aimed to understand how/why buffalo mozzarella is of unique quality compared to its bovine counterpart.
- Buffalo milk fat shows higher melting point than cow milk fat. This implies its suitability for products intended for a warmer climate. Therefore, further research is required to design crystallisation processes for products such as ‘heat resistant butter’, which could be suitable for use in tropical climate.
- Finally, the demand for more sustainable food production, including also the vegan diet trend have significantly increased over the past years. This translates into the demand of animal-based milk fat replacement by vegetable-based fat. Thus, future endeavours must be aimed to develop (1) milk fat replacers/substitutes, which can be used for partial substitution of the milk fat, or further (2) milk fat equivalents, which resemble milk fat in both physical and chemical characteristics. This is a more challenging task,

for instance, as compared to the replacement of other important natural fat such as cocoa butter, due to the higher complexity of the milk fat composition.

6.8 References

Abd El-Salam, M.H. and El-Shibiny, S. 2011. A comprehensive review on the composition and properties of buffalo milk. *Dairy Science & Technology*. **91**(6), pp.663-699.

Angelis, M. De and Gobbetti, M. 2011. Pasta-Filata Cheeses: Traditional Pasta-Filata Cheese *In*: J. W. Fuquay, P. F. Fox and P. L. H. McSweeney, eds. *Encyclopedia of Dairy Sciences: Second Edition*. Oxford: Academic Press, 1:745-752.

Arnold, M., Rajagukguk, Y.V., Gramza-Michałowska, A., Kandylis, P., Solieri, L., Garde-Cerdan, T., Bartkiene, E. and Rocculi, P. 2021. Characterisation of Dadih: Traditional Fermented Buffalo Milk of Minangkabau. *Beverages 2021, Vol. 7, Page 60*. **7**(3), p.60.

Asif, A.H.M., Deb, G.K., Habib, M.R., Harun-ur-Rashid, M., Sarker, M.A.H., Shahjadee, U.F., Lisa, S.A., Ahmed, S., Ekeberg, D., Vargas-Bello-Pérez, E. and Islam, M.A. 2021. Variations in fatty acid and amino acid profiles of doi and rasomalai made from buffalo milk. *Journal of Advanced Veterinary and Animal Research*. **8**(3), p.511.

Asif, A.H.M., Sarker, M.A.H., Deb, G.K., Habib, M.R., Arefin, S., Bari, M.S., Islam, M.Z., Rashid, M.H.U., Siddiki, M.S.R., Shahjadee, U.F., Lisa, S.A., Ahmed, S. and Islam, M.A. 2022. Fatty acid and amino acid profiles of cheese, butter, and ghee made from buffalo milk. *Journal of Advanced Veterinary and Animal Research*. **9**(1), p.144.

Atallah, A.A., Morsy, O.M., Abbas, W. and Khater, E.S.G. 2022. Microstructural, Physicochemical, Microbiological, and Organoleptic Characteristics of Sugar- and Fat-Free Ice Cream from Buffalo Milk. *Foods 2022, Vol. 11, Page 490*. **11**(3), p.490.

Becskei, Z., Savić, M., Ćirković, D., Rašeta, M., Puvača, N., Pajić, M., Dordević, S. and Paskaš, S. 2020. Assessment of Water Buffalo Milk and Traditional Milk Products in a Sustainable Production System. *Sustainability 2020, Vol. 12, Page 6616*. **12**(16), p.6616.

Campos, R.J., Litwinenko, J.W. and Marangoni, A.G. 2003. Fractionation of milk fat by short-path distillation. *Journal of Dairy Science*. **86**(3), pp.735-745.

Deffense, E. 1993. Milk fat fractionation today: A review. *Journal of the American Oil Chemists' Society*. **70**(12), pp.1193-1201.

Gresti, J., Bugaut, M., Maniongui, C. and Bezard, J. 1993. Composition of Molecular Species of Triacylglycerols in Bovine Milk Fat. *Journal of Dairy Science*. **76**(7), pp.1850-1869.

Grotenhuis, E. Ten, Van Aken, G.A., Van Malssen, K.F. and Schenk, H. 1999. Polymorphism of milk fat studied by differential scanning calorimetry and real-time X-ray powder diffraction. *JAOCS, Journal of the American Oil Chemists' Society*. **76**(9), pp.1031-1039.

Gunstone, F.D. (ed.). 2011. *Vegetable Oils in Food Technology: Composition, Properties and Uses, Second Edition*. West Sussex: Wiley Blackwell.

Haas, M.J. 2005. Animal Fats *In*: F. Shahidi, ed. *Bailey's Industrial Oil and Fat Products*. Hoboken, NJ: John Wiley & Sons, Inc.

Hondoh, H., Ueno, S. and Sato, K. 2018. Fundamental Aspects of Crystallization of Lipids *In*: K. Sato, ed. *Crystallization of Lipids: Fundamentals and Applications in Food, Cosmetics and Pharmaceuticals*. Hoboken, NJ: Wiley Blackwell, pp.105-141.

Huppertz, T., Kelly, A.L. and Fox, P.F. 2009. Milk Lipids - Composition, Origin and Properties *In*: A. Y. Tamime, ed. *Dairy Fats and Related Products*. Chichester, UK: Blackwell Publishing Ltd, pp.1-27.

de Jesus Silva, G., Gonçalves, B.H.R.F., Conceição, D.G., de Jesus, J.C., Vidigal, M.C.T.R., Simiqueli, A.A., Bonomo, R.C.F. and Ferrão, S.P.B. 2022. Microstructural and rheological behavior of buffalo milk chocolates. *Journal of Food Science and Technology*. **59**(2), pp.572-582.

Junaid, M., Inayat, S., Gulzar, N., Khalique, A., Shahzad, F., Irshad, I. and Imran, M. 2023. Physical, chemical, microbial, and sensory evaluation and fatty acid profiling of value-added drinking yogurt (laban) under various storage conditions. *Journal of Dairy Science*. **106**(1), pp.39-46.

Larsen, M.K., Andersen, K.K., Kaufmann, N. and Wiking, L. 2014. Seasonal variation in the composition and melting behavior of milk fat. *Journal of Dairy Science*. **97**(8), pp.4703-4712.

Lipp, M. and Anklam, E. 1998. Review of cocoa butter and alternative fats for use in chocolate - Part A. Compositional data. *Food Chemistry*. **62**(1), pp.73-97.

Lopez, C. 2018. Crystallization Properties of Milk Fats *In*: K. Sato, ed. *Crystallization of Lipids: Fundamentals and Applications in Food, Cosmetics and Pharmaceuticals*. Hoboken, NJ: Wiley Blackwell, pp.283-321.

Lopez, C., Bourgaux, C., Lesieur, P. and Ollivon, M. 2002. Crystalline structures formed in cream and anhydrous milk fat at 4 °C. *Lait*. **82**(3), pp.317-335.

Lopez, C., Bourgaux, C., Lesieur, P., Riaublanc, A. and Ollivon, M. 2006. Milk fat and primary fractions obtained by dry fractionation. 1. Chemical composition and crystallisation properties. *Chemistry and Physics of Lipids*. **144**(1), pp.17-33.

Marangoni, A.G. and Lencki, R.W. 1998. Ternary Phase Behavior of Milk Fat Fractions. *Journal of Agricultural and Food Chemistry*. **46**(10), pp.3879-3884.

Masud, T., Shehla, S. and Khurram, M. 2007. Paneer (white cheese) from buffalo milk. *Biotechnology and Biotechnological Equipment*. **21**(4), pp.451-452.

Mejares, C.T., Huppertz, T. and Chandrapala, J. 2022. Thermal processing of buffalo milk - A review. *International Dairy Journal*. **129**, p.105311.

Ménard, O., Ahmad, S., Rousseau, F., Briard-Bion, V., Gaucheron, F. and Lopez, C. 2010. Buffalo vs. cow milk fat globules: Size distribution, zeta-potential, compositions in total fatty acids and in polar lipids from the milk fat globule membrane. *Food Chemistry*. **120**(2), pp.544-551.

Murtaza, M.A., Pandya, A.J. and Khan, M.H.M. 2017. Buffalo milk: Buffalo milk utilization for dairy products *In*: Y. W. Park, G. F. W. Haenlein and W. L. Wendorff, eds. *Handbook of Milk of Non-Bovine Mammals: Second Edition*. Oxford, UK: Wiley Blackwell, pp.284-342.

Pionnier, E. and Hugelshofer, D. 2006. Characterisation of key odorant compounds in creams from different origins with distinct flavours. *Developments in Food Science*. **43**(C), pp.233-236.

Pratama, Y., Simone, E. and Rappolt, M. 2021. The Unique Crystallization Behavior of Buffalo Milk Fat. *Crystal Growth and Design*. **21**(4), pp.2113-2127.

Sato, K. 2018. Introduction: Relationships of Structures, Properties, and Functionality *In*: K. Sato, ed. *Crystallization of Lipids: Fundamentals and Applications in Food, Cosmetics and Pharmaceuticals*. Hoboken, NJ: Wiley Blackwell, pp.1–15.

Sato, K. 2001. Molecular Aspects in Fat Polymorphism *In*: N. Widlak, R. Hartel and S. Narine, eds. *Crystallization and Solidification Properties of Lipids*. Champaign, Illinois, Illinois: AOCS Press, pp.1-17.

Shi, Y., Smith, C.M. and Hartel, R.W. 2001. Compositional effects on milk fat crystallization. *Journal of Dairy Science*. **84**(11), pp.2392-2401.

Staniewski, B. et al. 2021. The effect of triacylglycerol and fatty acid composition on the rheological properties of butter. *International Dairy Journal*. **114**, p.104913.

Timms, R.E. 1980. The phase behaviour and polymorphism of milk fat, milf fat fractions and fully hardened milk fat. *The Australian Journal of Dairy Technology*. **35**, pp.47-52.

Tzompa-Sosa, D.A., Ramel, P.R., Van Valenberg, H.J.F. and Van Aken, G.A. 2016. Formation of β Polymorphs in Milk Fats with Large Differences in Triacylglycerol Profiles. *Journal of Agricultural and Food Chemistry*. **64**(20), pp.4152-4157.

Appendix A
Supporting Information for Chapter 3

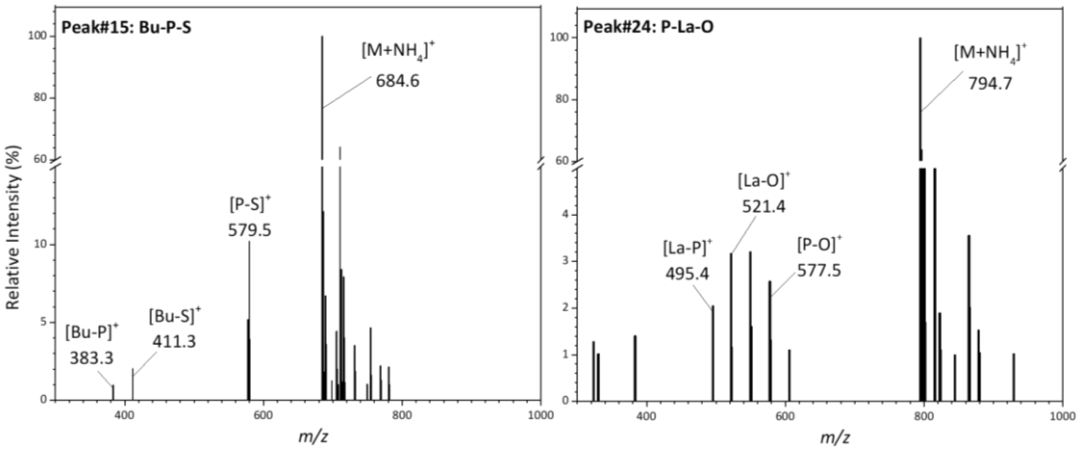

Figure A.1 Identification of selected peaks from Figure 3.1 (peak number is indicated in the figure) based on its mass spectra. $[M+NH_4]^+$ indicates molecular mass of triacylglycerols (TAG) with the addition of ammonium ion as adduct, fragments' molecular mass refer to diacylglycerols (DAG) ions where Bu: butyric (C4), La: lauric (C12), P: palmitic (C16), S: stearic (C18), O: oleic (C18:1). Complete identification refers to **Table A.1**.

The identification of TAG was achieved by mass spectra analysis (Zeb and Murkovic, 2010). For example, the peak number **15** was identified as 1(3)-butyryl-2-palmitoyl-1(3)-stearoyl glycerol (BuPS), where the main mass spectrum value (m/z) 684.6 corresponded to the total molecular weight of this TAG (667.1) plus the molecular weight of the ammonium fragment (18). The presence of BuPS DAG fragment ions, i.e. 1-palmitoyl-2-stearoyl-sn-glycerol [P-S]+ (m/z 579.5), 1-butyryl-2-stearoyl-sn-glycerol [Bu-S]+ (m/z 411.3), and 1-butyryl-2- palmitoyl -sn-glycerol [Bu-P]+ (m/z 383.3) also confirmed that this chromatographic peak was indeed the BuPS TAG. Similarly, peak number **24** was identified as 1(3)-palmitoyl-2-lauroyl-1(3)-oleoyl glycerol (P-La-O) as its molecular weight is 777.2 and in addition with ammonium adduct corresponds to the main m/z spectra 794.7. It is worth noticing that the intensity of the fragment ions was not very strong, in some cases less than 10% of main m/z intensity. Thus, we find the similar spectra profiles in the work of Zhou et al. (2014) as particularly useful. Moreover, the peak number 30 was unambiguously identified as tripalmitoyl glycerol (PPP) by comparing its retention time with that of the TAG mixture standard.

Table A.1 Peak identification according to TAG molecular mass and its DAG fragments.

Peak No	RT (min)	TAG Structure	[M+ NH4]+	[DAG]+ fragments (m/z)		
1	2.8	Bu-Co-P	516.4	[Bu-Co]+ 243.2	[Co-P]+ 411.3	[Bu-P]+ 383.3
2	3.2	Bu-C-M	544.5	[Bu-M]+ 355.3	[M-C]+ 439.4	[Bu-C]+ 299.2
3	3.4	n/i	750.5	-	-	-
4	3.8	Bu-C-P	572.5	[Bu-C]+ 299.2	[C-P]+ 467.4	[Bu-P]+ 383.3
5	4.4	Bu-La-P	600.5	[Bu-La]+ 327.2	[La-P]+ 495.4	[Bu-P]+ 383.3
6	4.5	Bu-La-O	626.5	[Bu-C]+ 299.2	[C-O]+ 493.4	[Bu-O]+ 309.3
7	5.2	Bu-M-P	628.5	[Bu-M]+ 355.3	[M-P]+ 523.5	[Bu-P]+ 383.3
8	5.3	Bu-M-O	654.5	[Bu-M]+ 355.3	[M-O]+ 549.5	[Bu-O]+ 409.3
9	5.6	Bu-P-L	680.5	[Bu-P]+ 383.3	[Bu-L]+ 369.6	[P-L]+ 537.9
10	6.1	Co-M-P	656.6	[Co-M]+ 383.3	[M-P]+ 523.5	[Co-P]+ 411.3
11	6.3	Bu-P-P	656.6	[Bu-P]+ 383.3	[P-P]+ 551.5	-
12	6.5	Bu-P-O	682.6	[Bu-P]+ 383.3	[P-O]+ 577.5	[Bu-O]+409.3
13	6.7	Bu-O-O	708.6	[Bu-O]+ 409.3	[O-O]+ 603.5	-
14	7.5	Co-P-P	684.6	[Co-P]+ 411.3	[P-P]+ 551.5	-
15	7.7	Bu-P-S	684.6	[Bu-P]+ 383.3	[P-S]+ 579.5	[Bu-S]+ 411.3
16	7.9	Bu-S-O	710.6	[Bu-S]+ 411.3	[S-O]+ 605.6	[Bu-O]+ 409.3
17	8.9	P-P-Cy	712.6	[P-P]+ 551.5	[Cy-P]+ 439.4	-
18	9.2	Co-S-P	712.6	[Co-S]+ 439.4	[P-S]+ 579.5	[Co-P]+ 411.3
19	9.5	P-Cy-O	738.7	[Cy-P]+ 439.4	[Cy-O]+ 465.4	[P-O]+577.5

Peak No	RT (min)	TAG Structure	[M+ NH4]+	[DAG]+ fragments (m/z)		
20	11.0	P-P-C	740.7	[P-P]+ 551.5	[P-C]+ 467.4	-
21	11.4	P-C-O	766.7	[P-C]+ 467.4	[P-O]+ 577.5	[C-O]+ 493.4
22	11.8	C-O-O	792.7	[C-O]+ 493.4	[O-O]+ 603.5	-
23	13.7	La-P-P	768.7	[La-P]+ 495.4	[P-P]+ 551.5	-
24	14.2	P-La-O	794.7	[La-P]+ 495.4	[P-O]+ 577.5	[La-O]+ 521.5
25	14.7	P-M-L	820.7	[M-L]+ 521.5	[P-L]+ 575.5	[M-P]+ 523.5
26	17.1	M-P-P	796.7	[M-P]+ 523.5	[P-P]+ 551.5	-
27	17.7	P-M-O	822.7	[M-P]+ 523.5	[P-O]+ 577.5	[M-O]+ 549.5
28	18.4	O-M-O	848.7	[M-O]+ 549.5	[O-O]+ 603.5	-
29	19.4	O-P-L	874.7	[P-O]+ 577.5	[P-L]+ 575.5	[O-L]+ 601.5
30	21.6	P-P-P	824.7	[P-P]+ 551.5	-	-
31	22.4	O-P-P	850.7	[P-P]+ 551.5	[P-O]+ 577.5	-
32	23.2	P-O-O	876.8	[P-O]+ 577.5	[O-O]+ 603.5	-
33	24.2	O-O-O	902.7	[O-O]+ 603.5	-	-
34	27.3	P-P-S	852.8	[P-P]+ 551.5	[P-S]+ 579.5	-
35	28.4	S-P-O	878.8	[P-S]+ 579.5	[P-O]+ 577.5	-
36	29.6	O-O-S	904.8	[O-O]+ 603.5	[S-O]+ 605.6	-
37	34.8	S-P-S	880.8	[P-S]+ 579.5	[S-S]+ 607.6	-
38	36.3	S-S-O	906.8	[S-S]+ 607.6	[S-O]+ 605.6	-

RT: retention time; TAG: triacyclglycerols; DAG: diacylglycerols; $[M+NH4]^+$: molecular mass of TAG + ammonium ion; Bu: butyric (C4), Co: caproic (C6), Cy: caprylic (C8), C: capric (C10), La: lauric (C12), M: myristic (C14), P: palmitic (C16), S: stearic (C18), O: oleic (C18:1), L: linoleic (C18:2) fatty acid.

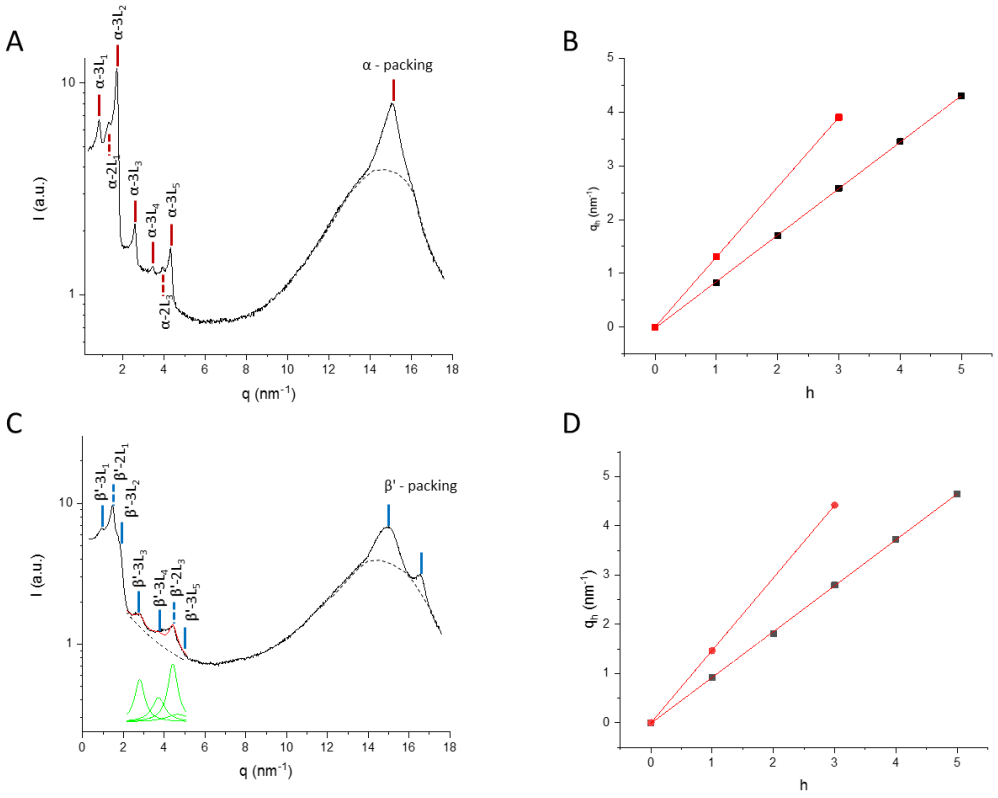

Figure A.2 BMF diffraction patterns at -10 °C and indexing. A) Small- and wide-angle X-ray scattering of two co-existing α-polymorphs. B) From indexing of all recorded orders follows d = 48.4 Å for the 2L-form and d = 72.8 Å for the 3L-form. C) Small- and wide-angle X-ray scattering of two co-existing β'-polymorphs. D) From indexing of all recorded orders follows d = 42.6 Å for the 2L-form and d = 67.4 Å for the 3L-form.

Data analysis: As described in the Materials and Methods all analysed pattern were transmission corrected and the scattering contribution of the capillary was subtracted. All peaks were then fitted with Lorentz distribution and additionally fitting the diffuse scattering contributions with second degree polynomials (see dashed lines in **Figure A.2**). For the 2L-phases the first three orders were recorded, while for the 3L-pahse we were able to record the fits five order reflections. Most critical were the fits of the 4th and 5th order reflections in the β'-3L phase (see Lorentz fits in **Figure A.2** C - green lines). Note, for these two Bragg peaks the peak positions were fixed according to the lattice spacing and their FWHMs were estimated (not fitted) from the FWHM trend given by the first three fitted diffraction peaks (h = 1-3). In order to understand the influence of uncertainties of F_4 and F_5 onto the resulting

EDP, further evaluations were carried out (cf. **Figure A.3**). All resulting amplitudes together with their phases are summarised in **Tables A.2** and **A.3**.

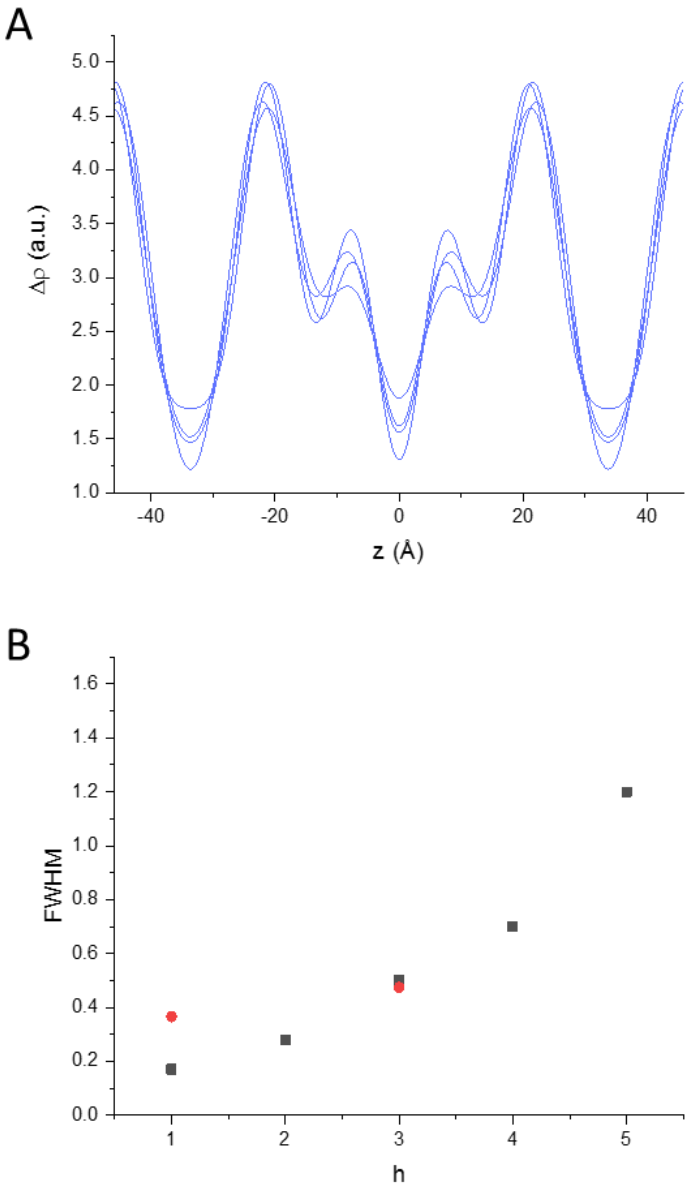

Figure A.3 Analysing the error of glycerol backbone positioning in the EDPs of the β'-3L phase at -10°C. As seen in the diffraction pattern in the small angle regime (Figure A.2 C) the fourth and fifth order Bragg-reflections of the β'-3L phase are not well resolved, but overlap with the third order of the β'-2L phase. A) Thus, the fourth and forth order amplitudes, Fh, were varied from 0.3 to 0.6 and 0.25 to 0.5, respectively. From the resulting electron diffraction pattern, we get the bilayer thickness, dS, to vary from 41.8 to 44.2 Å. B) Note, to reduce the fitting uncertainties a constraint was employed onto the FWHM as a function of diffraction order, h. Satisfying the lattice disorder of second kind only monotonous increasing FWHM(h) were allowed.

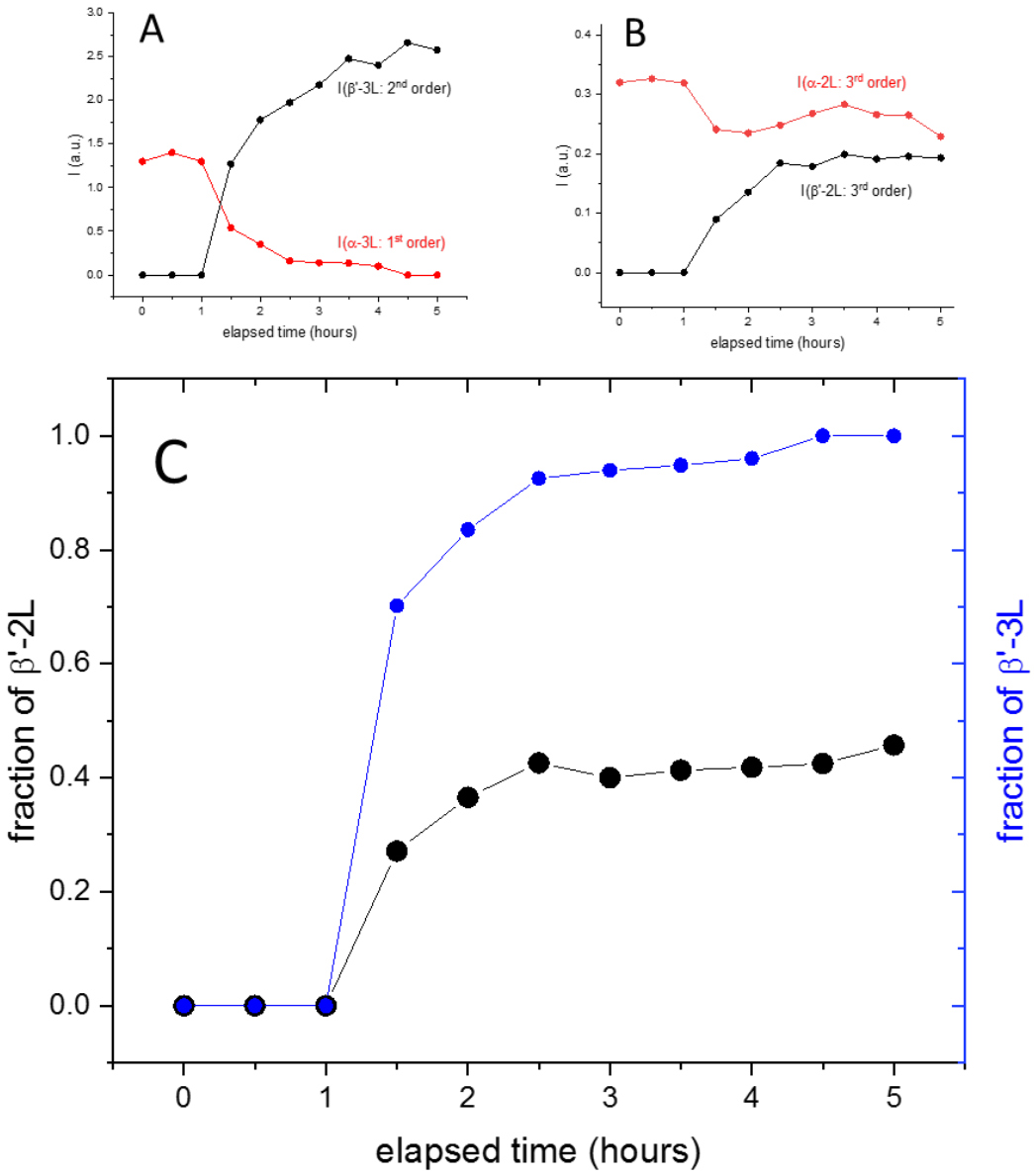

Figure A.4 The α-3L to β' 3L and α-2L to β' 2L and transitions. A) Intensity of the 1st order diffraction peak of the α-3L phase (red circles) and 2nd order diffraction peak of the β'-3L phase (black circles) as function of elapsed time. B) Intensity of the 3rd order diffraction peak of the α-2L phase (red circles) and 3rd order diffraction peak of the β'-2L phase (black circles) as function of elapsed time. C) Fraction of the β'-2L (black circles) and β'-3L phase (blue circles) as function of elapsed time. The fractions were calculated as I(β')/[I(α)+I(β')]. Note, we have chosen the strongest reflections of each phase, where possible, and only weaker reflections, when they were nicely isolated in the diffraction pattern. All intensity data refer to the diffraction pattern presented in **Figure 3.4**.

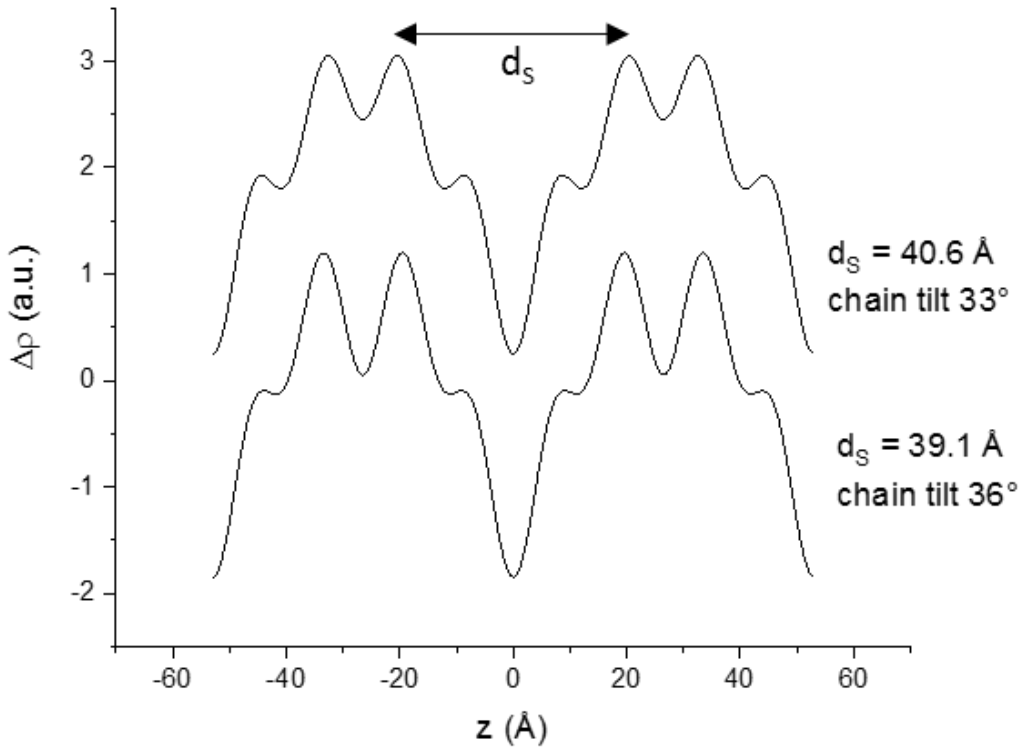

Figure A.5 Simulation of the electron density profile (EDP) of the 3L-β phase.

To obtain a first idea about the possible electron density profile of the observed 3L-β phase (d = 53 Å), two assumptions were made. First, we assumed the chain tilt in the bilayer region to be comparable to literature data,(Mykhaylyk and Hamley, 2004) that is, ideally a chain tilt of 36° is assumed (see bottom EDP). In a second simulation, a slightly looser chain packing with 33° tilt was assumed (upper EDP). The second important assumption was to expect in the bilayer region mainly longer saturated chains (palmitic and stearic fatty acids) as we observed for the 2L-α and 2L-β' polymorphs, i.e., $d_S = d(\text{2L-}\alpha)\cos(36°)$ and $d_S = d(\text{2L-}\alpha)\cos(33°)$, respectively. Finally, EDPs were simulated with variation of the amplitudes F_2, F_3 and F_4, until the predicted d_S-value was obtained. Noteworthy, **d_U with values in the range of 12 to 14 Å is rather small** (note, $d = d_S + d_U$). Note, best values for F_2, F_3 and F_4 were -0.45, +0.05 and -0.45 (chain tilt 36°) and -0.25, +0.10 and -0.40 (chain tilt 33°), respectively. Note F_1 was fixed -1.00.

Table A.2 Structural parameters of the 2L-α, 3L-α, 2L-β' and 3L-β' polymorphs at -10 °C.

	2L-α[a]	**3L-α[b]**	**2L-β'[c]**	**3L-β'[d]**
h	F_h	F_h	F_h	F_h
1	-1.00	-0.24	-1.00	-0.18
2	-	-1.00	-	-1.00
3	-0.54	+0.37	-0.59	+0.60
4	-	-0.16	-	-0.61
5	-	-0.60	-	-0.50

[a] d = 48.4 Å; [b] d = 72.8 Å; [c] d = 42.6 Å; [d] d = 67.4 Å.

Table A.3 Amplitudes of the SOS α-3L and γ-3L phases compared to the α-3L ones of BMF.

	3L-α (SOS)[a]	**3L-γ (SOS)[b]**	**3L-α (BMF)[c]**
h	F_h	F_h	F_h
1	-0.84	-0.07	-0.24
2	-1.00	-1.00	-1.00
3	+0.12	+0.41	+0.37
4	-0.43	-0.11	-0.16
5	-	-0.69	-0.60

[a] d = 55.6 Å; [b] d = 74.8 Å; [c] d = 72.8 Å.

Remark: Although the recorded diffraction pattern in the wide-angle region of the 3L-α polymorph of BMF clearly displays the chain packing of a α-phase (perfect hexagonal chain packing with free chain-rotation), the long spacings and corresponding amplitudes, F_h, are strikingly similar to the 3L-γ polymorph of SOS (Mykhaylyk and Hamley, 2004). In contrast, the electron density profile of the 3L-α polymorph of SOS is clearly different to the 3L-α polymorph of BMF.

References

Mykhaylyk, O.O. and Hamley, I.W. 2004. The packing of triacylglycerols from SAXS measurements: Application to the structure of 1,3-distearoyl-2-oleoyl-sn-glycerol crystal phases. *Journal of Physical Chemistry B*. **108**(23), pp.8069-8083.

Zeb, A. and Murkovic, M. 2010. Analysis of triacylglycerols in refined edible oils by isocratic HPLC-ESI-MS. *European Journal of Lipid Science and Technology*. **112**, pp.844-851.

Zhou, Q., Gao, B., Zhang, X., Xu, Y., Shi, H. and Yu, L. 2014. Chemical profiling of triacylglycerols and diacylglycerols in cow milk fat by ultra-performance convergence chromatography combined with a quadrupole time-of-flight mass spectrometry. *Food Chemistry*. **143**, pp.199-204.

Appendix B
Supporting Information for Chapter 4

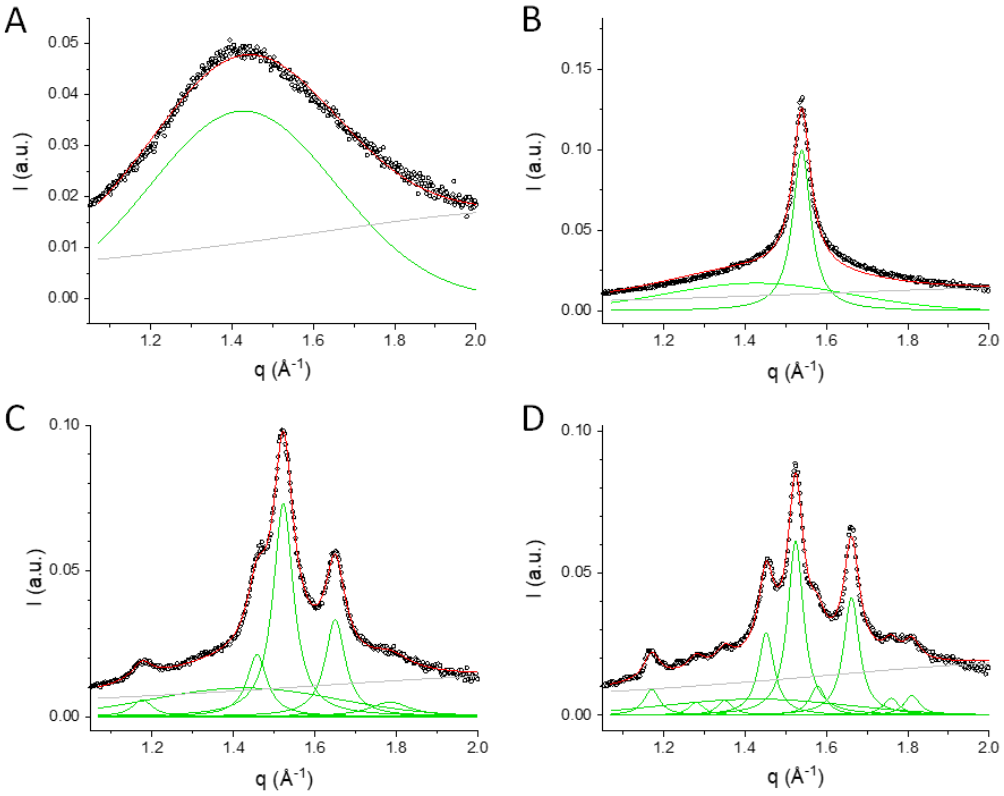

Figure B.1 Solid Fat Content (SFC) estimation using the WAXS data.

This analysis does follow the ideas outlined in the reference (Arita-Merino et al., 2020). (A) 1-butyryl 2-stearoyl 3-palmitoyl-glycerol (BuSP) sample at 60 °C before cooling down to 20 °C. Here the **SFC = 0%**. (B) After one hour of isothermal hold at 20 °C the α-phase forms. The **SFC = 46%**. (C) After 18 hours the newly formed β'-phase still coexists with the α-phase. The **SFC = 76%**. The BuSP sample that was stored before X-ray measurements at -18 °C for 720 hours (1 month) displays solely the β'-phase. The **SFC = 80%**. Grey lines indicate background scattering, the green lines display all diffraction peaks as well as the diffuse scattering of the fluid phase. The red lines display the fitted data curves. Note, the background scattering is the same in all patterns, and moreover, the fluid phase diffuse scattering was fixed in its width and position. IMPORTANT NOTE: Applying the method of the Elke Scholten group using Pearson VII functions for all scattering contributions (Arita-Merino et al., 2020), we did fix the shape of the diffuse scattering to a Gaussian shape (m = 100) and that of the diffraction peaks to a Lorentzian shape (m = 1),

which is the expected peak shape for smectic liquid crystalline phases. We note, that not fixing the shape of the peaks can lead to artificial results, such as overestimating or underestimating peak areas due to different tailing off behaviour of differently shaped peaks.

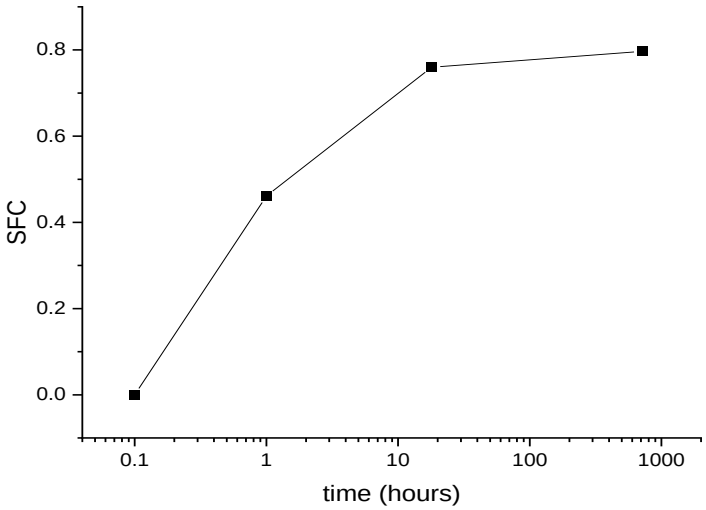

Figure B.2 Temporal development of the SFC in BuSP.

References

Arita-Merino, N., Van Valenberg, H., Gilbert, E.P. and Scholten, E. 2020. Quantitative Phase Analysis of Complex Fats during Crystallization. *Crystal Growth and Design*. **20**(8), pp.5193-5202.

Appendix C
Supporting Information for Chapter 5

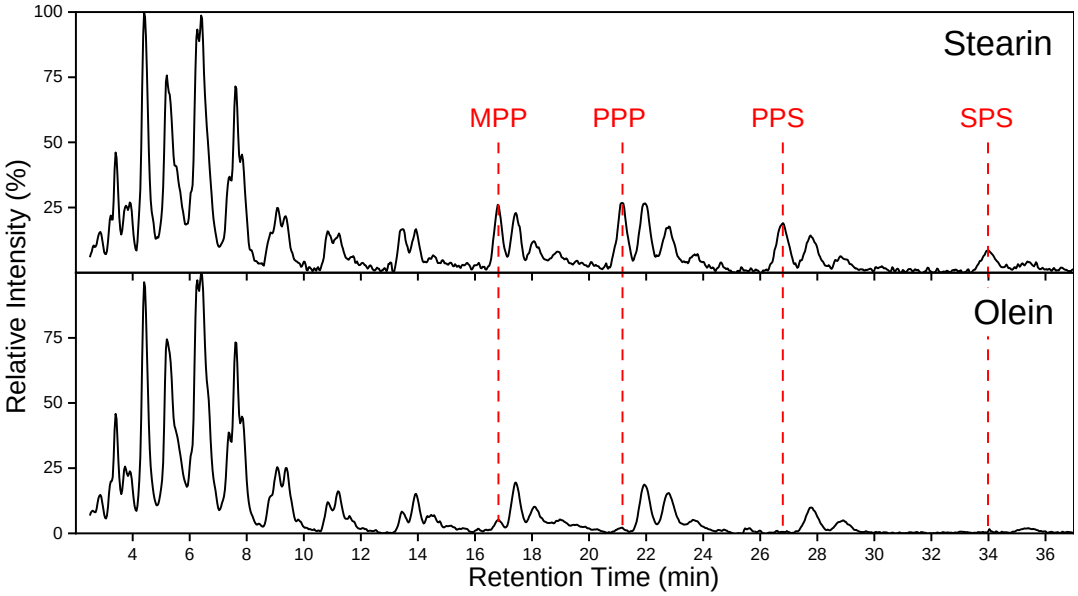

Figure C.1 Chromatogram of Stearin and Olein fraction with focus on long chained fully saturated TAGs peaks (i.e., MPP, PPP, PPS and SPS). M: myristic (C14), P: palmitic (C16), S: stearic (C18).

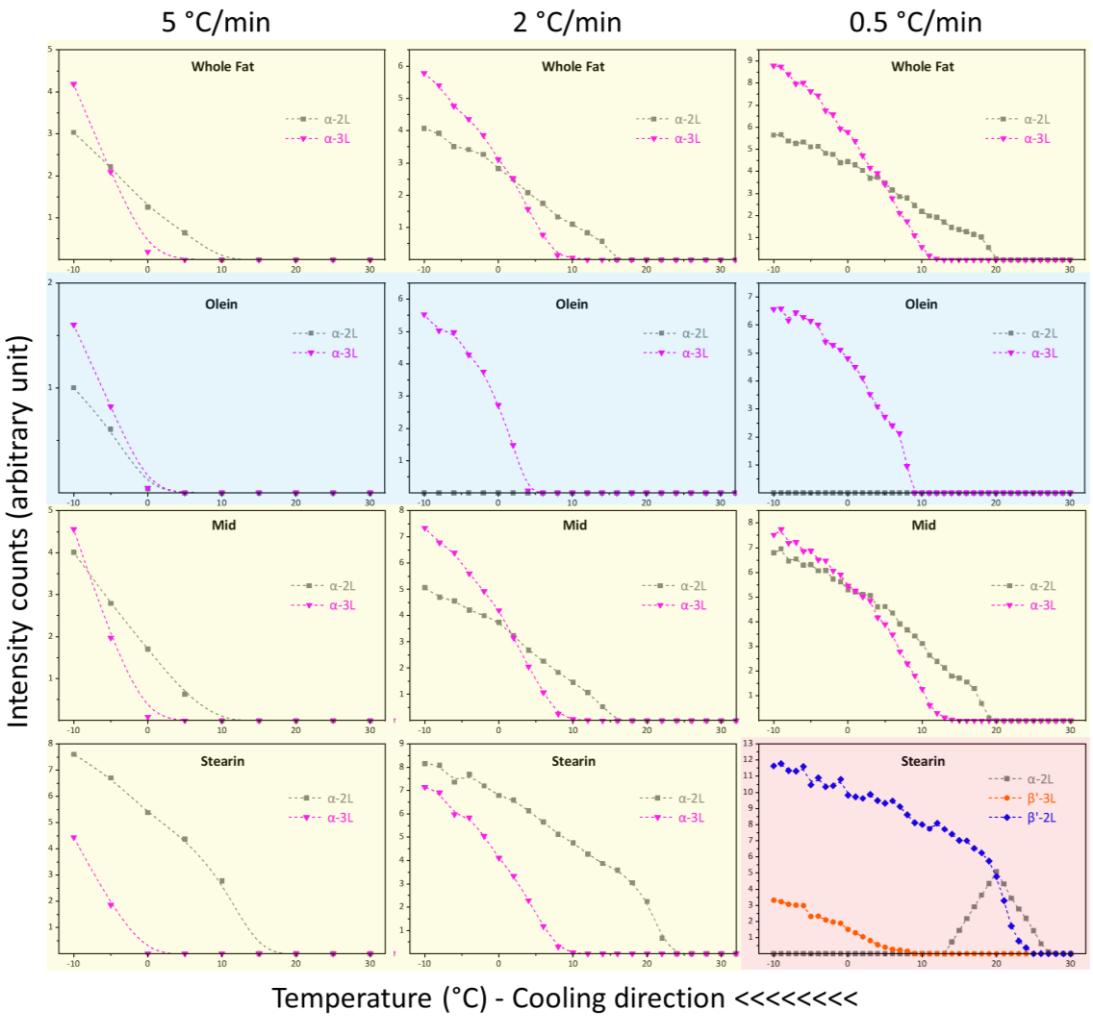

Figure C.2 The X-ray scattering intensity evolution of milk fat samples at different cooling rates (i.e., -5, -2 and -0.5 °C/min). Colour coding: blue, yellow and red correspond to crystallisation behaviour pathway 1, 2 and 3, respectively.

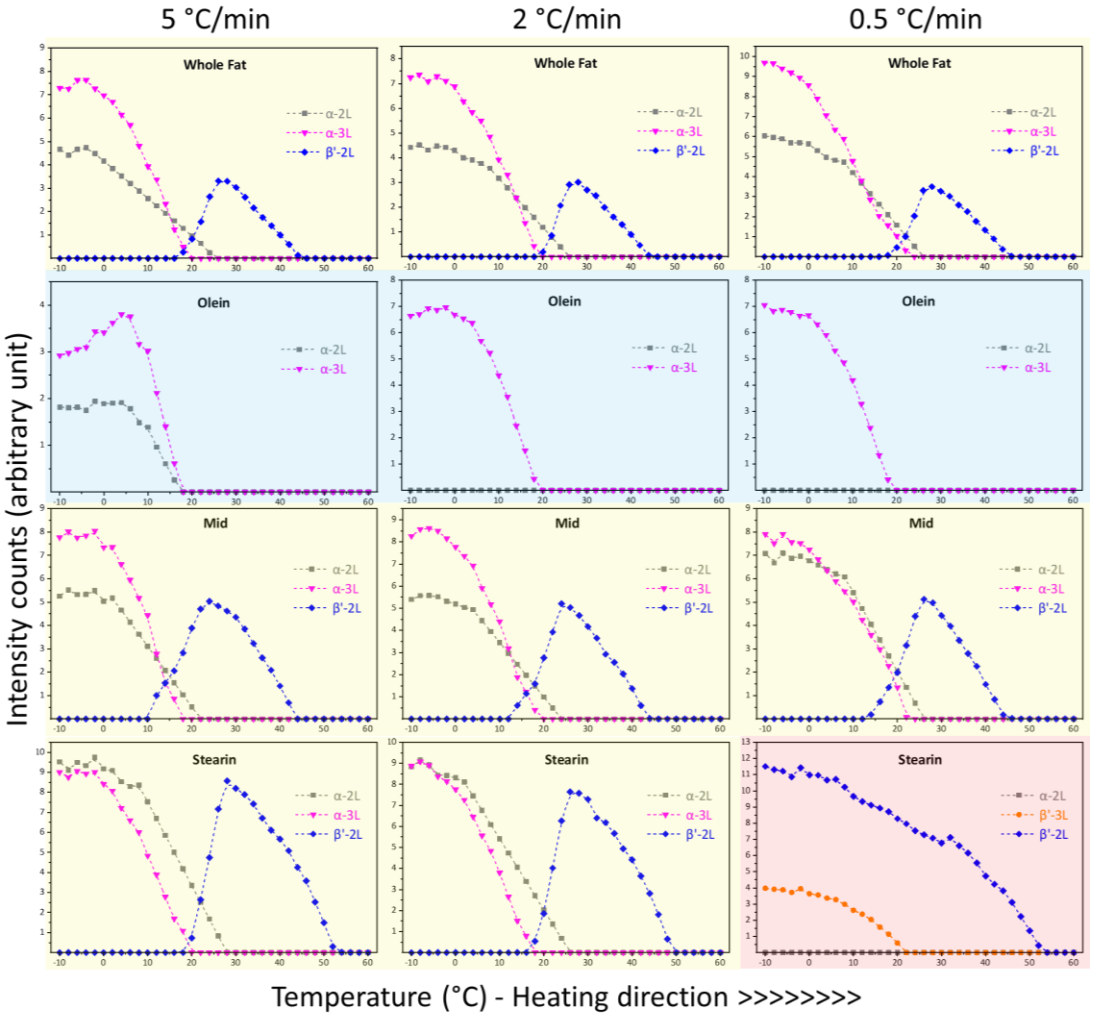

Figure C.3 The X-ray scattering intensity evolution of milk fat samples on heating at 2 °C/min after being crystallised at different cooling rates (i.e., -5, -2 and -0.5 °C/min). Colour coding: blue, yellow and red correspond to crystallisation behaviour pathway 1, 2 and 3, respectively.